Core-Shell Oxidative Aromatization Catalysts for Single Step Liquefaction of Distributed Shale Gas

Final Technical Report
10/15/2024

Award - DE-FE0031869

SUBMITTED BY
NC State University
RM2-009, Engineering Building I, 911 Partners Way,
Raleigh, NC 27695

PRINCIPAL INVESTIGATOR
Fanxing Li
919-515-7328
fli5@ncsu.edu

PROJECT PARTNERS
West Virginia University
Lehigh University
Susteon Inc.
Shell

SUBMITTED TO
U.S. Department of Energy
National Energy Technology Laboratory

Acknowledgment: This material is based upon work supported by the Department of Energy under Award Number DE-FE0031869.

Contents

Executive Summary

The objective of this project was to design and demonstrate a core-shell structured multifunctional catalyst to convert the light (dry) components of shale gas into liquid aromatic compounds (primarily benzene and toluene) in a single step. Operated in a modular oxidative aromatization system (OAS) under a cyclic redox scheme, the novel catalyst and process can significantly improve the value and transportability of distributed shale gas. Since the project started, each quarter addressed a different set of tasks related to the completion of the milestone detailed in the project award. The yearly summaries of these tasks are summarized below:

Q1-Q4:

- Conducted project planning and literature search.
- Investigated a number of SHC redox catalysts using thermogravimetric analysis and fixed-bed reactor experiments.
- Initiated process modeling towards generating two process models for the methane DHA base case and OAS process.
- Developed DHA catalysts capable of producing >500 g/kg-cat-hr aromatics at 80% or greater aromatics selectivity at 700°C.

Q5-Q8:

- Developed alternative approaches with sequential bed configurations to enhance the aromatic yields based on OCM+DHA
- Improved the zeolite synthesis efficiency by using the microwave-assisted technique and investigated the synthesis conditions on the zeolite yield, crystalline structure and morphology
- Constructed a set of Aspen Plus process models with significant energy savings for OAS as compared to the base case non-oxidative DHA.
- Adapted conventional hydrothermal method to be applicable to the microwave synthesizer unit for more efficient catalyst synthesis.
- Studied the structure of the OCM catalyst and the dispersion of the carbonate in the redox reactions and in methane flow with Raman Spectroscopy.

Q9-Q12:

- Scaled up the catalyst synthesis with the microwave synthesis method. Based on its performance, procedural characterizations and catalytic performance testing were further conducted for the new microwave synthesized catalysts with the newly-developed product analysis procedure.
- Developed the reaction system setup for the C2-DHA or OCM+DHA reaction product and achieved a better product collection-analysis method for the aromatic products with an improved carbon balance. The product from the OCM reaction exhibited complicated effects on the DHA catalyst.
- Conducted additional OCM catalyst characterization using Near Ambient Pressure X-ray Photoelectron Spectroscopy and *in situ* Raman characterization
- Validated the significant energy savings for OAS as compared to the base case non-oxidative DHA. Successfully set up the simulation model for the OCM+DHA+SHC reaction system based on the updated experimental results from NCSU.

Q13-End of project:

- Synthesized new zeolite catalysts by the microwave method, conducted characterizations (XRD, SEM, and TEM) and catalytic behavior testing.
- Explored the "wet" C_2H_6 and C_2H_4 DHA reactions with using steam co-feed. A subsequent reduction as the regeneration step can regenerate the DHA catalyst and recover 99% activity of the fresh performance.
- Achieved a 15.3% single-pass aromatic yield from methane by rationally combining the OCM and DHA at different temperatures.
- Conducted a 105-hour stability test with an improved regeneration procedure, with an average aromatic yield of 13.8%.
- Developed new catalyst and achieved a record-high 23.2% yield.

Background and Technical Approach

Although conventional, indirect gas-to-liquids (GTL) technologies can convert light hydrocarbons into liquid fuels and chemicals, they face significant challenges in high capital cost and low overall efficiency due to complex unit operations including reforming, air separation (for CH_4 partial oxidation), syngas conditioning, Fischer-Tropsch (F-T), and product refining and upgrading. The process complexity dictates that indirect GTL is only economically viable for centralized liquid fuel production (>10,000 bbl/day) due to economy of scale. Although the extensive attempts on modularization of methane reforming and F-T synthesis in "microchannel reactors" have led to significant progress to improve the reactor throughput and reduce the overall process footprint,[1, 2] these "small-scale" GTL technologies have yet to demonstrate economic feasibility at scales commensurate with distributed shale gas production/processing sites (150–500 BOE/day). Therefore, the complexity of indirect GTL severely limits its small-scale applications. As shown in Figure 1, conversion of C1/C2 to aromatics increases their volume-based energy density by 500 to 1000 times, significantly reducing the transportation costs while adding ~ $6.6/MM Btu in value. Converting rejected C1/C2 alone will result in $5 billion/year value creation.

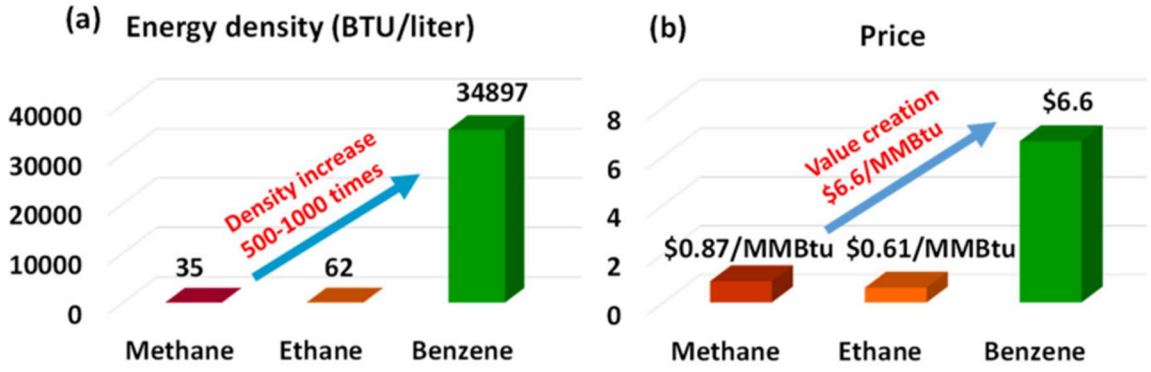

Figure 1. (a) Volume based energy density comparison of benzene and C1/C2. (b) Comparison of OAS feedstock and product values (Appalachian basin prices were used,13 value creation was calculated based on converting 1 MMBtu C1/C2 to 0.49 MMBtu aromatics assuming 80% carbon efficiency and aromatic products were sold at a fuel oil price of $2/gallon[3]).

This proposal aims to design and demonstrate a core-shell structured multifunctional catalyst (Figure 2a) to convert the light (dry) components of shale gas into liquid aromatic compounds (primarily benzene and toluene). Operated in a modular oxidative aromatization system (OAS) under a cyclic redox scheme (Figure 2b), the novel catalyst and process can significantly improve the value and transportability of distributed shale gas. Therefore, OAS represents a disruptive

technology that can greatly benefit the US oil, gas, and chemical industries while reducing the energy consumptions and CO_2 emissions.

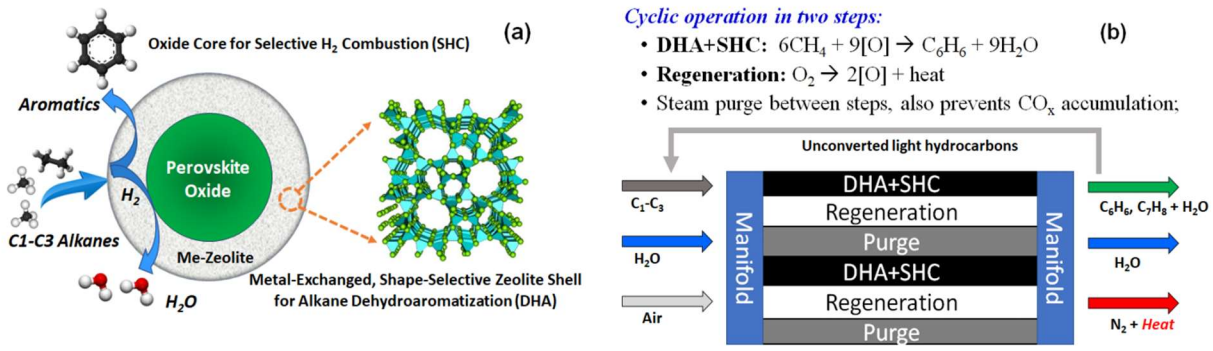

Figure 2. Schematic of (a) the SHC@DHA redox catalyst; (b) the modular OAS reactor. ~5% of unconverted gas is purged/combusted in a gas engine (not shown).

Direct conversion of methane into chemicals and fuels is potentially simpler. However, none of the direct methane conversion processes, including DHA[4], have shown commercial feasibility due to their limited product selectivity and yields. Key challenges of methane DHA include equilibrium limitations (low aromatics yield), coke formation (low catalyst stability), and high reaction endothermicity. The proposed concept, which combines an SHC redox catalyst and a DHA catalyst, has excellent potential to be disruptive since it addresses all the key challenges for conventional and emerging methane activation approaches (Table 1). OAS also draws a comparison with the recently published electrochemical membrane based DHA approach[5]. The advantages of OAS reside in its simplicity (does not consume electricity) and robustness (does not rely on membrane)[5, 6]. Compared to the electrochemical membrane approach, which demonstrated ~20% increase in peak aromatics yield than a conventional DHA packed bed, our preliminary data indicated >25% increase in cumulative aromatics yield (>200% increase in instantaneous yield) using the proposed DHA+SHC concept. The DHA and SHC catalysts are also fully regenerable through repeated reduction-oxidation cycles[1, 7]. The proposed project will develop scalable and tunable synthesis methods for core-shell structured DHA@SHC catalysts to achieve high methane conversion, high product selectivity, autothermal operation, and simplified product separation (simple condensation and gas recycling). In addition to DHA, high temperature non-oxidative methane coupling can also produce aromatic products. However, the highly

endothermic reactions (>600 kJ/mol benzene) require very high operating temperature (~1100 °C) in order to obtain ~15% aromatic yield[8]. Since extensive gas separation is not practical for distributed applications, it would be very challenging to obtain a reasonable carbon to liquids yield.

Table 1. Comparisons of conventional GTL and emerging methane activation technologies

	GTL	Oxidative Coupling	1-Step Methanol	Non-oxidative Coupling	DHA	**OAS (DHA+SHC)**
Key unit operations*	>4	≥2	> 2	>2	2	**1**
Liquid Product?	Yes	No	Yes	Yes	Yes	**Yes**
Single pass yield	High	<25%	<5%	15%	<12%	**>40%⁺**
Endo/Exo-thermicity	~	Highly Exothermic		*Highly Endothermic*		**Autothermal⁼**
Carbon efficiency	<80%	Low	Low	Low	Low	**>90%⁺**
Catalyst stability	High	n/a	High	High	Low	**n/a#**

Only includes major process steps, e.g. air separation, reforming, F-T synthesis, product refining. + Technical target to be demonstrated. Current SHC performance indicates 75% single-pass equilibrium yield can be achieved; =Exothermicity is tunable depends on fraction of H2 combusted; # Catalyst stability will be demonstrated in this project, preliminary data indicate satisfactory stability.

The OAS concept capitalizes on the recent breakthroughs in molecular level understandings of alkane dehydroaromatization (DHA) and redox-based selective hydrogen combustion (SHC) catalysts. Conventional DHA, catalyzed by zeolite supported metal or metal carbides, suffers from severe challenges including: a. low aromatic yields due to equilibrium limitations; b. coke formation and catalyst deactivation; and c. high reaction endothermicity. The catalyst design (Figure 2a) and packed bed reactor system for OAS (Figure 2b), specifically address these limitations. For instance, the SHC@DHA core-shell redox catalyst not only aromatizes C1-C3 hydrocarbons with its DHA shell but also selectively combusts the H_2 byproducts to H_2O with the active lattice oxygen ([O] or O^{2-}) in its SHC core. The concurrent H_2 oxidation significantly enhances the equilibrium yield of aromatics (from 8% to 75% for CH_4 to C_6H_6 at 650 °C). Meanwhile, the water produced is forced to diffuse through the DHA shell to inhibit coking. OAS operates under a cyclic redox mode to replenish the O^{2-} in the SHC core without negatively affecting the active sites in the shell. Cyclic regeneration and the ability to inhibit coking ensures high catalyst stability and process robustness compared to membrane-based approaches.[9] Unlike conventional DHA, which is very endothermic (+722 kJ/mol @600°C), the combined DHA-SHC reaction is exothermic (-1,500 kJ/mol), allowing autothermal cyclic operation in a compact, parallel fixed bed system similar to the well-established Houdry process. Oxidative removal of H_2

from DHA allows the light alkane/alkenes to be recycled to near extinction, yielding up to 90% aromatics on a carbon basis. Besides the "methane DHA + SHC strategy" for H_2 combustion and increased benzene yield, we have also adopted an alternative strategy with the OCM (oxidative couple of methane) and DHA (dehydroaromatization). This alternative strategy will apply redox catalyst for OCM reaction and the zeolite catalyst for the DHA reaction. The OCM bed will partially convert methane into C_2H_6 and C_2H_4 with nearly 30% yield with the active lattice oxygen ([O] or O^{2-}) in the redox catalyst. Then DHA bed contains will convert the as-formed C_2H_6 and C_2H_4 from the 1st-layer OCM bed into benzene and H_2. This strategy can also utilize the hydrogen combustion during the OCM reaction and thus it will be autothermal process. Besides, the H_2 oxidation during the OCM reaction significantly enhances the equilibrium towards aromatics formation. Meanwhile, the water produced is forced to diffuse through the DHA shell to inhibit coking.[7] And the existence of water instead of gaseous H_2 will also reduce the cost of separation for the hydrocarbons.

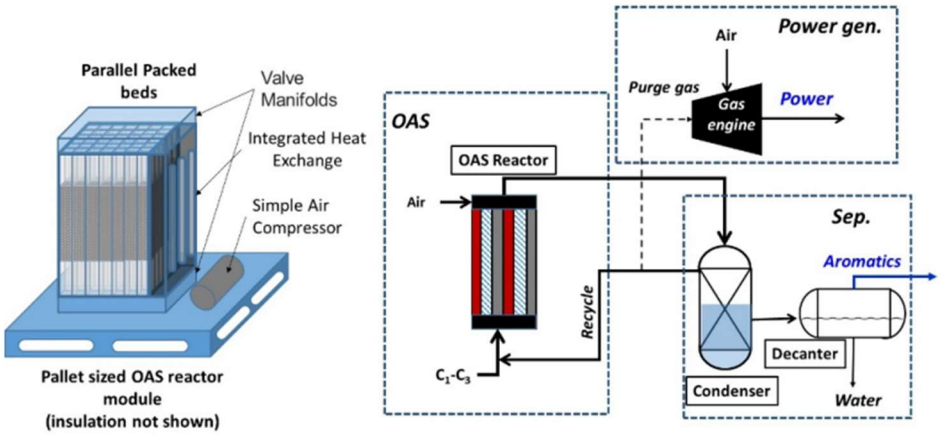

Figure 3. Schematic illustration of the OAS reactor module (Left) and simplified flow diagram of the OAS system (Right).

As such, OAS produces high-value liquid aromatics from low-value dry shale gas: converting flared and rejected C1 and C2 alone will lead to >$5 billion/year value creation. The proposed approach is disruptive and uniquely suited for distributed shale gas conversion since it significantly simplifies state-of-the-art (SoTA) GTL scheme: 1. Simplified feedstock preparation: The SHC-DHA redox catalyst will simultaneously convert C1-C3 components in shale gas. The active lattice

oxygen in the redox catalyst also inhibits poisoning effects by low levels of shale gas contaminants such as H_2S, CO_2, and NH_3. As such, feedstock preparation for OAS can be greatly simplified with a crude acid gas removal (AGR) step (e.g. caustic wash) followed by compression and NGL condensation. 2. Increased single pass yield and productivity: existing DHA is limited by thermodynamics with 8% single pass CH_4 conversion at 650 °C. Selective combustion of hydrogen in OAS significantly shifts the equilibrium of Reaction 1 to 75% CH_4 conversion within a single pass. Heat integration for OAS is also greatly simplified due to the exothermicity of the overall reaction; 3. Simplified product separation and recycle scheme: SHC in OAS results in an easy-to-separate product slate consisting of liquids (aromatics and water) and gas (gaseous alkanes and alkenes with small amount of CO_x and unconverted H_2). Simple cooling, condensation, and decantation will produce liquid aromatics, water, and gases. The gases can be directly recycled after CO_2 removal (with the upstream AGR system) since all the remaining gaseous products will ultimately be converted into aromatics, water, or CO_2.[7] 4. High flexibility: The simple process scheme and modular OAS reactor design significantly reduces the capital investment and operating cost. Moreover, its high turndown ratio and numbered-up design can accommodate fluctuations in feedstock supply. As a net producer of power and water, the modular system is not only self-sustainable but also produces valuable byproducts for the shale gas/oil production site. 5. High robustness: The cyclic process periodically regenerates the catalysts. Compared to a membrane based approach[5], the proposed redox process is cheaper and more robust.

In this project, a 0.2 liter/day modular test unit will be used to demonstrate the OAS technology. Successful completion of the project will result in optimized OAS redox catalysts with superior aromatics yield (>20% per-pass) and stability (>5% deactivation over 100 hours redox cycle). The project team is composed of leading experts in redox catalyst/process design (PI Li at NCSU), alkane aromatization (Co-PI Wachs at Lehigh and Co-PI Hu at WVU), and new technology development and commercialization (Susteon Co-PI Gupta). Supported by industrial collaborator (Shell), foundation (Kenan Institute), and promising preliminary data, the team is well-positioned to demonstrate and commercialize this promising technology.

Key Tasks Performed

Task 1: Project Management and Planning

Task 1 focuses on effective project management. A technology maturation plan and a baseline techno-economic assessment report will also be developed and submitted to DOE, during the early stage of the project.

Subtask 1.1 – *Project Management Plan*:

The Recipient shall manage and direct the project in accordance with a Project Management Plan to meet all technical, schedule and budget objectives and requirements. The Recipient will coordinate activities in order to effectively accomplish the work. The Recipient will ensure that project plans, results, and decisions are appropriately documented, and project reporting and briefing requirements are satisfied.

Task 2: Catalyst Screening

Subtask 2.1: SHC Redox Catalyst Synthesis and Screening

Studies conducted at NCSU have focused on establishing the activity, selectivity, stability, and operating ranges of redox-based selective hydrogen combustion (SHC) catalysts. Perovskite oxide-based redox catalysts in particular (e.g. $CaMnO_3$, $SrMnO_3$) have exhibited an ability to rapidly and selectively combust H_2 to H_2O with active lattice oxygen ([O] or O^{2-}) in the temperature range from 600 °C to 700 °C.[10] The addition of alkali-based molten salt promoters, such as Na_2WO_4 or Na_2MoO_4[11], has been shown to markedly improve the selectivity towards H_2 combustion from multi-component gas mixtures, notably in the presence of ethylene, a key intermediate species in both methane and ethane dehydroaromatization (DHA). the most promising SHC redox catalyst was tested via thermogravimetric analysis (TGA), and hydrogen combustion activity was calculated for each material at 650°C (for ethane DHA), 700°C (for methane DHA), or both. In a typical TGA experiment, 15 to 30 mg of redox catalyst was loaded into a quartz crucible in a hanging basket configuration (SETARAM Setsys Evolution), with gas flowing downward over the crucible and sample. The sample temperature was controlled by the TGA furnace. After heating to reaction temperature under inert (He, 200 mL/min), the gas environment was cycled between reducing (P_{H2} = 0.1) and oxidizing atmospheres (P_{O2} = 0.1), typically with 20 min reduction and oxidation steps, separated by a 10 min purge step. Each sample was cycled three or more times at each condition to ensure redox stability and repeatability of performance, and multiple temperatures were tested sequentially. Raw data of sample mass (mg) vs. time (s) were differentiated into a mass rate of oxygen removal (mmol O / mg-cat-s) and further manipulated to give a hydrogen combustion activity (mol H_2/kg cat-hr). It is worth noting that while P_{H2} = 0.1 may be a realistic mean hydrogen partial pressure in the DHA application, P_{H2} may also be substantially higher, which would give a higher combustion rate due to the near-unity reaction order of H_2 combustion.[10] The calculated H_2 combustion rates for 7 promising perovskite oxide-based redox catalysts are provided in Table 2. Four of the seven SHC redox catalysts demonstrate a hydrogen combustion rate exceeding 200 mol H_2/kg cat-hr, which is one of the two key criteria for Milestone 2.1, while an additional two redox catalysts gave greater than 100 mol H_2/kg cat-hr activity at 700°C. However, existing reaction data for all of these redox

catalysts for applications such as n-hexane oxidative cracking (which also involves heavy C6+ hydrocarbons in mixture with H_2) give a good approximation for the H_2 selectivity which can be expected from the redox catalysts in the DHA setting. Table 1 thus provides literature data and related unpublished data on H_2 selectivity for the redox catalysts in previous applications, with citations available in the footnotes of the table.

Table 2. Summary of redox catalyst development and progress towards Milestone 2.1 (achieving redox catalysts with hydrogen combustion activity of 200 mol H_2/kg cat-hr and H_2 selectivity of at least 80% at 700°C.

Redox Catalyst	H_2 Combustion Rate (mol H_2/kg-cat-hr)[a]		H_2 Selectivity (%)[b]	
	650°C	*700°C*	*650°C*	*700°C*
$Na_2WO_4/SrMnO_3$	237	248	85	84
$CaMnO_3$	492	557	35	--
$Na_2WO_4/CaMnO_3$	92	127	99	95
$CaMn_{0.9}Fe_{0.1}O_3$	316	334	77	77
$Na_2WO_4/CaMn_{0.9}Fe_{0.1}O_3$	54	--	87	90
$CaMn_{0.9}Ti_{0.1}O_3$	280	292	--	low
$Na_2MoO_4/CaMn_{0.9}Ti_{0.1}O_3$	--	156	--	90

a.) Calculated H_2 combustion activity/rates are derived from thermogravimetric analysis (TGA) experiments using P_{H2} = 0.1. Actual rates may be higher if P_{H2} exceeds 0.1 in a DHA setting. b.) Estimates for H_2 selectivity are preliminary and based on previous work. Selectivity values for $Na_2WO_4/SrMnO_3$, $CaMnO_3$, and $Na_2WO_4/CaMnO_3$ are from reference[10]and indicate selectivity to H_2 during n-hexane oxidative cracking, which involves C6 hydrocarbons similar to the DHA application. Selectivity values for $CaMn_{0.9}Fe_{0.1}O_3$ and $Na_2WO_4/CaMn_{0.9}Fe_{0.1}O_3$ are from reference [12] reported for the ethane oxidative dehydrogenation (ODH), involving fewer heavy hydrocarbons, leading to higher selectivity values even for $CaMn_{0.9}Fe_{0.1}O_3$. Selectivity values for H_2 combustion by $CaMn_{0.9}Ti_{0.1}O_3$ and $Na_2MoO_4/CaMn_{0.9}Ti_{0.1}O_3$ are not directly available; however, the addition of Na_2MoO_4 to $CaMn_{0.9}Ti_{0.1}O_3$ enables olefin selectivity of 88% from ethane ODH (reference [11]), which generally indicates high H_2 combustion selectivity.

Of the four redox catalysts demonstrating a hydrogen combustion rate exceeding 200 mol H_2/kg cat-hr, one ($Na_2WO_4/SrMnO_3$) also gave a high H_2 selectivity (84% at 700°C) and meets the two key criteria given in Milestone 2.1. A second redox catalyst, $CaMn_{0.9}Fe_{0.1}O_3$, nearly meets these criteria (334 mol H_2/kg cat-hr, 77% selectivity at 700°C), and a further two redox catalysts ($Na_2WO_4/CaMnO_3$ and $Na_2MoO_4/CaMn_{0.9}Ti_{0.1}O_3$) give 90% or higher H_2 selectivity and activity greater than 120 mol H_2/kg cat-hr. We anticipate that through further optimization of the redox catalyst design and promoter levels, we will shortly obtain four or more SHC redox catalysts with > 80% H_2 selectivity and appropriate activity in fulfillment of Milestone 2.1.

Accordingly, in order to obtain the most conservative estimate of hydrogen combustion selectivity in the OAS context, an H_2:C_6H_6 ratio of 1:1 was utilized for all experiments in this report to mimic the most H_2-depleted conditions that may be encountered in the process. Thus, all selectivity values provided are conservative. A series of redox catalysts were first screened using equimolar co-feed H_2/C_6H_6 temperature-programmed reaction (TPR) experiments, from T = 450°C to 750°C, to determine the temperature range of activity for each material as well as its approximate reducibility and oxygen capacity. TPR experiments also provided an early sense of the SHC selectivity of the redox catalysts in the presence of both hydrogen and benzene. Figure 4 shows the TPR results of six candidate redox catalysts, with H_2 consumption on the y-axis.

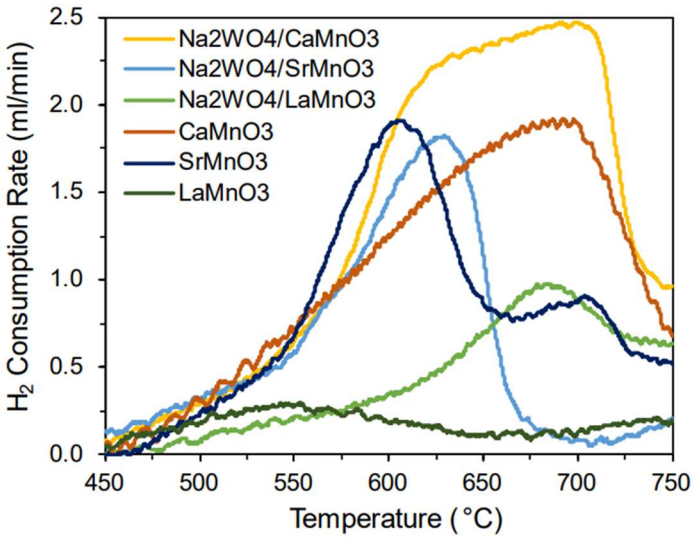

Figure 4. Co-feed H_2/C_6H_6 TPR results for six redox catalyst materials, to screen the activity and selectivity for hydrogen combustion (SHC) in the oxidative aromatization setting.

The candidate materials were unpromoted and 20 wt.% Na_2WO_4-promoted variants of the $CaMnO_3$, $SrMnO_3$, and $LaMnO_3$ perovskite oxides, selected based on earlier experimental results. As shown in Figure 4, all six materials begin to donate lattice oxygen around T = 500°C, with the Ca and Sr-based materials experiencing significant increases in activity near 550°C. $SrMnO_3$ shows early combustion peaks which indicate that its available oxygen capacity is depleted at this point. $CaMnO_3$ possesses the highest oxygen capacity (approx. 10wt.%), followed by Na_2WO_4/$CaMnO_3$ (approx. 8 wt.%), and then the $SrMnO_3$ materials, and lastly the $LaMnO_3$-based redox catalysts. Based on the initial screening, $LaMnO_3$ and Na_2WO_4/$LaMnO_3$ may possess insufficient oxygen capacity to be carried forward as a candidate, as evidenced by the small area

under the TPR curve as compared to the other materials. Finally, the presence of Na_2WO_4 is shown to shift the peak temperatures of both SrMnO3 and LaMnO3, meaning that the material is slightly less reducible and likely more selective to hydrogen combustion. This change is insignificant for $CaMnO_3$.

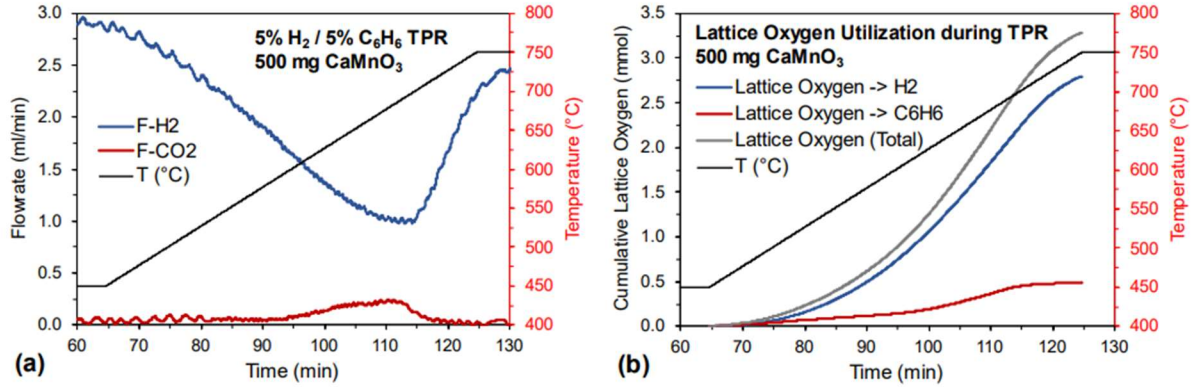

Figure 5. H_2/C_6H_6 co-feed TPR results for $CaMnO_3$. (a) Flowrates of H_2 and CO_2 vs. temperature program; (b) lattice oxygen utilization towards H_2 combustion, C_6H_6 combustion, and in total.

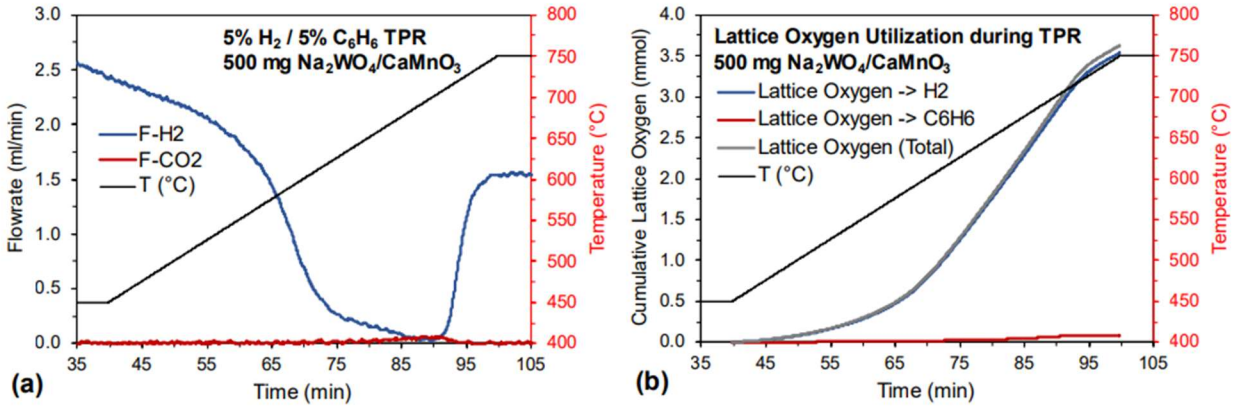

Figure 6. H_2/C_6H_6 co-feed TPR results for $Na_2WO_4/CaMnO_3$. (a) Flowrates of H_2 and CO_2 vs. T program; (b) lattice oxygen utilization towards H_2 combustion, C_6H_6 combustion, and in total.

Examining the $CaMnO_3$ system in more detail, Figure 5 shows the (a) H_2 and CO_2 flowrates and (b) lattice oxygen utilization and distribution for the $CaMnO_3$ system. Figure. 6 illustrates the analogous results for $Na_2WO_4/CaMnO_3$. In these SHC results, H_2 combustion may be directly

measured by assessing the decrease in H_2 flowrate (F-H_2, ml/min) as compared to the baseline at 2.5 ml/min, whereas non-selective C_6H_6 combustion can be indirectly calculated by the product flowrate of CO_2. By comparing the TPR results of both materials, it can be clearly seen that Na_2WO_4 increases the selectivity of the lattice oxygen to nearly 100% for H2 combustion, while not harming the total activity of the material (the ending oxygen utilization values are comparable, Figure 5b and 6b). The detailed TPR results for $SrMnO_3$ and Na_2WO_4/$SrMnO_3$, and $LaMnO_3$ and Na_2WO_4/$LaMnO_3$, which are not included here for brevity, also demonstrate that Na_2WO_4 promotion improves the lattice oxygen selectivity of the perovskite oxides while minimally affecting the overall utilization. Based on the TPR screening, the CaMnO3 and SrMnO3 systems were carried forward to the next stage of evaluation. Temperature-programmed experiments are useful for initial screening, but for a more realistic assessment of the redox catalyst SHC activity and selectivity at the operating conditions of the OAS concept, isothermal redox cycle experiments were conducted next. In a typical SHC experiment, a 45-min redox cycle was implemented, consisting of a 15-minute reduction and 10- min oxidation, separated by two 10-min purge steps. During the reduction step, which represents both the DHA reaction itself (6 CH_4 ◊ C_6H_6 + 9 H_2) as well as the SHC reaction, the equimolar ratio of hydrogen and benzene was used again; 2.5 ml/min H_2 and 3.0 ml/min C_6H_6 (roughly 5% H_2 and 6% C_6H_6, balance Ar). The oxidation used 5.0 ml/min O_2 in 25 ml/min Ar. The key markers to trace during the experiment were the H2 flowrate and the CO_2 flowrate, both of which were estimated using a downstream quadrupole mass spectrometer (QMS) calibrated for these gases. The benzene flowrate could not be reliably observed using MS. Instead, the flowrate was calibrated by sending a set duration of flow (typically 20-30 min) through a dodecane solvent trap to remove the benzene. The resulting liquid volume of dodecane and benzene was vaporized in a GC, and the standard volume of dodecane was used to calculate the liquid and then the gas volume of benzene which entered the trap throughout the duration. The first pane of Figure 7, Figure 7a, shows the outlet trace of a blank redox cycle when no catalyst is present; instead, an inert Al_2O_3 packing material was used in the quartz microreactor. The reduction, purge, and regeneration steps are labeled and last 15, 10, and 10 minutes, respectively. All other parts of Figure 5 show the results of a redox catalyst and temperature combination, wherein 500 mg of redox catalyst is centered in the quartz microreactor and held at a temperature of either 650°C or 700°C.

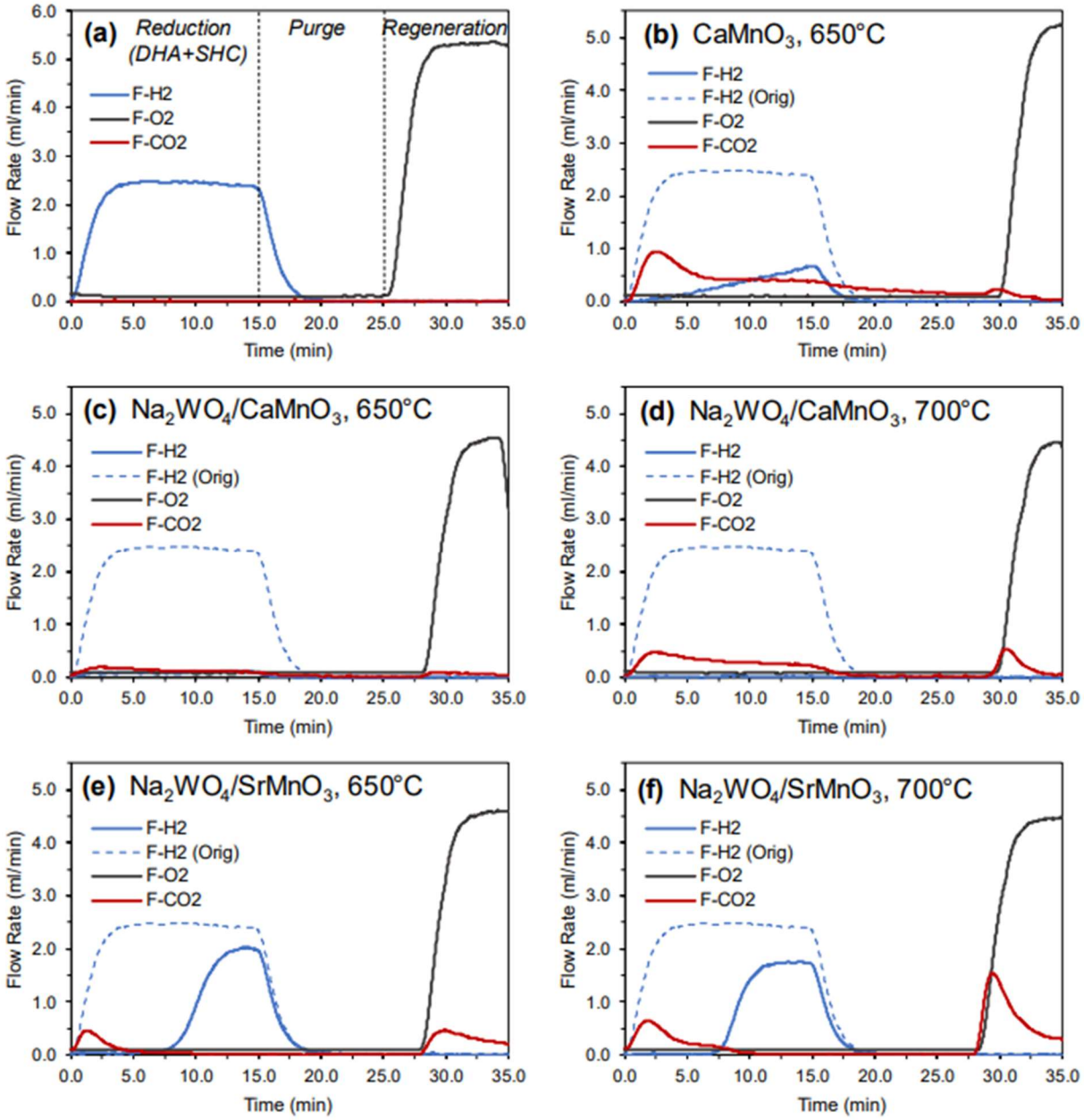

Figure 7. Selective hydrogen combustion (SHC) experiments in the oxidative aromatization setting using co-feed H_2/C_6H_6 over a selection of redox catalyst materials. (a) Blank experiment over Al_2O_3 to demonstrate MS gas traces and cycle duration; (b) $CaMnO_3$; (c-d) 20 wt.% Na2WO4/CaMnO3; (e-f) 20 wt.% $Na_2WO_4/SrMnO_3$. Conditions: T = 650°C or 700°C, 500 mg redox catalyst. Reduction flow: 2.5 ml/min H_2, 3.0 ml/min C_6H_6, 47.5 ml/min Ar, 15 min. Oxidation flow: 5 ml/min O_2, 25 ml/min Ar, 10 min. Purge flow: 25 ml/min Ar, 10 min (X2). Total cycle duration: 45 min.

Figure 7b shows the SHC performance of $CaMnO_3$ at 650°C via the H_2 and CO_2 flowrates; the dotted-line curve shows the H_2 from the blank experiment for reference, with the area between the two H_2 curves (dotted and solid) representing the amount of H_2 combusted by the redox catalyst. As can be seen, $CaMnO_3$ successfully combusts nearly all of H_2 present in the first 5 minutes, and continues to remove over 70% of the H_2 throughout the entire 15 min reduction step. Throughout this duration, CO_2 is also produced, particularly at the beginning of the reduction, reflecting the non-selective combustion of benzene. The slowly decreasing CO_2 over time demonstrates that as oxygen is removed from the redox catalyst, the oxygen that remains becomes more selective to H_2 combustion, as H_2 is a more effective reducing agent. From Figure 7c and 7d, which show the results of $Na_2WO_4/CaMnO_3$ at 650°C and 700°C, respectively, we can see that the addition of Na_2WO_4 once again improves the selectivity of the redox catalyst towards H_2 combustion. Nearly 100% of the H_2 is removed via combustion in both experiments, evidenced by the F-H_2 curve near zero. At 650°C in Figure 7c, in significant contrast with $CaMnO_3$ from Figure 5a, almost no CO_2 is present, reflecting the high selectivity of the promoted material for H_2 combustion in the presence of benzene, even at a 1:1 feed ratio. At 700°C, some CO_2 is formed due to the lower stability and higher reactivity of the benzene molecule at higher temperature. However, we note that this redox catalyst and all of the others would be more selective for a reactant mixture with H2:C6H6 ratio higher than 1:1, e.g. 3:1 or 6:1. For the $Na_2WO_4/SrMnO_3$ redox catalyst, pictured in Figure 7e and 7f at 650°C and 700°C, there are two key differences as compared to $Na_2WO_4/CaMnO_3$. First, the oxygen capacity is lower, and as a result, the H2 curve begins to return to near the baseline after 7 to 8 minutes of reaction, signaling the depletion of the lattice oxygen. The CO_2 curve also disappears at this time marker. Second, there is substantial CO_2 formation during the regeneration step. There are two potential explanations: (i) some CO_2 formed from non-selective oxidation of benzene during the reduction step is strongly adsorbed to the more basic $Na_2WO_4/SrMnO_3$ surface and is desorbed during regeneration; (ii) there is increased coking during the reduction step for this material, and the CO_2 indicates the coke burn-off in oxygen. In either case, the carbon must come from benzene, and the presence of this CO_2 should be included in the carbon balance as an undesired product. Higher H_2 gas content may improve upon this carbonate or coke formation issue for $Na_2WO_4/SrMnO_3$. The results of the experiments depicted in Figure 7 are summarized in Table 3 in terms of calculated metrics including total H_2 combustion and SHC selectivity. Total H_2 combustion in mmol is taken as the area between the blank H_2 curve

and the observed H_2 from each experiment. Selectivity is calculated as the quotient of the lattice oxygen going towards H_2 combustion (mmol) divided by the total lattice oxygen in mmol leaving either as H_2O or CO_2. CO is not a significant product as verified via GC. Two redox catalysts are shown to possess selectivity at or exceeding 80% for SHC in the presence of benzene, at both 650°C and 700°C. However, these are low-end estimates. The "lattice oxygen distribution" metric is used here for SHC selectivity and is the most conservative metric for selectivity, as the combustion of 1 mmol of H_2 requires 1 mmol of lattice oxygen ([O]), whereas the combustion of benzene leads to 6 mmol CO_2 (as well as 3 mmol H_2O, not included in the calculation). For example, if 1 molecule of benzene were lost to over-oxidation for every 9 molecules of H_2 combusted, the selectivity based on this conservative definition would equal 9 / (9+6), or 60%. Even the $Na_2WO_4/SrMnO_3$ redox catalyst exceeds this threshold, and most of the materials far exceed 60% selectivity, indicating that despite the equimolar feed ratio, the redox catalysts are favoring H_2 combustion over C_6H_6 combustion in a 10-to-1 margin or more.

Table 3. Summary of SHC redox catalyst performance in the experiments of Figure 7, in terms of H_2 combustion and selectivity in the presence of equimolar H_2:C_6H_6.

Sample	T (°C)	Total H_2 Combustion	Selectivity w/o Coke	Selectivity w/ Coke
$CaMnO_3$	650	1.40 mmol	70.4%	N/A
$Na_2WO_4/CaMnO_3$	650	1.55 mmol	89.7%	N/A
$Na_2WO_4/CaMnO_3$	700	1.60 mmol	79.6%	75.1%
$Na_2WO_4/SrMnO_3$	650	1.16 mmol	90.2%	76.9%
$Na_2WO_4/SrMnO_3$	700	1.15 mmol	82.5%	60.6%

We conclude this section by noting two important points. (i) The selectivity, while high for these tests, is likely to grow higher when an H_2:C_6H_6 ratio of greater than 1:1 is used, and such a ratio would be more realistic for the average DHA experiment with methane (H_2:C_6H_6 = 9:1 production) and ethane (H_2:C_6H_6 = 6:1 production). A ratio of 1:1 may exist in an OAS reactor bed when SHC has removed most of the H_2, although a ratio of H_2:C_6H_6 = 3:1 may be a more reasonable estimate for the average ratio across the entire OAS reactor bed. The amount of redox catalyst can be optimized to maintain a desirable H_2:C_6H_6 ratio. (ii) In these experiments, relatively little H_2 was used in order to force harsh conditions, and nearly all of the H_2 present is combusted. This

combustion rate amounts to 13.4 mol H_2/kg-cat-hr. The redox catalysts are capable of much higher H_2 combustion rates meeting or exceeding 200 mol H_2/kg-cat-hr.

Subtask 2.2: Redox catalyst characterization, Mechanistic, Kinetics, and optimization

Given the importance of SHC redox catalyst for the OAS process, the dehydrated molecular structures of α-Al_2O_3 supported 20% Na_2WO_4 and 20% $Na_2W_2O_7$ were characterized using in situ Raman spectroscopy. To dehydrate the catalysts, both were heated to 450°C under 30cc of 10%O_2/Ar and calcined for 30 minutes before being cooled down to 120°C to ensure no rehydration takes place. The dehydrated Raman spectra for the 20%Na_2WO_4/α-Al_2O_3 catalyst (Figure 8a) exhibited sharp crystalline vibrations associated with α-Al_2O_3 and Na_2WO_4, along with a more disordered broad peak at ~250 cm-1 associated with θ-Al_2O_3. Conversely, the dehydrated Raman spectra for the 20%$Na_2W_2O_7$/α-Al_2O_3 catalyst (Figure 8b) showed only crystalline $Na_2W_2O_7$ signals. The lack of the α-Al_2O_3 peaks is probably related to the more efficient scattering by the $Na_2W_2O_7$ layer covering the surface compared to the bulk α-Al_2O_3 phase. Combined, these results demonstrate how altering the tungsten content in the catalyst enables the tuning of the sodium tungstate phase that is formed on the α-Al_2O_3 surface.

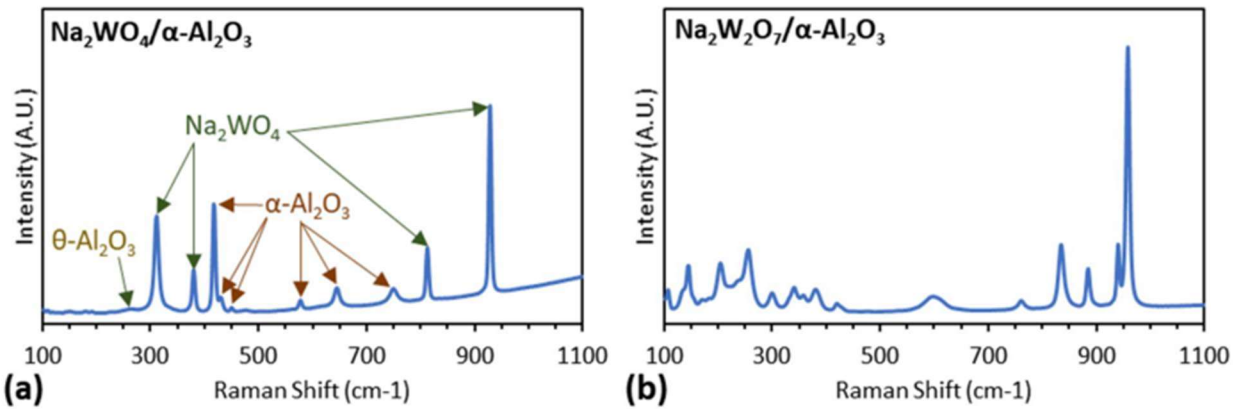

Figure 8. In situ Raman spectra acquired at 120°C after dehydration at 450°C under a flow of 30cc 10%O_2/Ar of: (a) 20%Na_2WO_4/α-Al_2O_3 and (b) 20%$Na_2W_2O_7$/α-Al_2O_3.

Since SHC can still be relevant component down the road, $Na_4Mg(WO_4)_3$ impregnated catalysts were investigated for their stability on the Al_2O_3 and $MnMg_6O_8$ supports relative to the previously investigated Na_2WO_4 and $Na_2W_2O_7$ impregnated catalysts. Due to the inhomogeneity of

$Na_4Mg(WO_4)_3$ both as a bulk surface compound, 121 spatially resolved spectra were acquired of each sample. The dehydrated, bulk $Na_4Mg(WO_4)_3$ was composed mostly of a $Na_aMg_bW_cO_d$ solid solution which is likely to be close in composition to the stoichiometric $Na_4Mg(WO_4)_3$ phase, but also exhibited significant Na_2WO_4 and $MgWO_4$ and minor $Na_2W_2O_7$ crystallite contributions (Figure 9a). The impregnation of $Na_4Mg(WO_4)_3$ on the oxide supports affects the crystallite composition, with the type of support affecting the composition in a different way. Impregnation on the Al_2O_3 generates a spectrum with major contributions from Na_2WO_4, $Na_aMg_bW_cO_d$, $Na_2W_2O_7$ and $MgWO_4$ phases (Figure 9b). Conversely, the 20% $Na_4Mg(WO_4)_3$ loaded Mg_6MnO_8 sample exhibits no $Na_2W_2O_7$ vibrations at all, and has similar Na_2WO_4 and $Na_aMg_bW_cO_d$ as well as major $MgWO_4$ contributions (Figure 9c). Increasing the loading further to 33% on the Mg_6MnO_8 support leads to an increase in the $Na_aMg_bW_cO_d$ and decrease in the Na_2WO_4 signals relative to the 20% loaded sample (Figure 9d). It is worth mentioning that no $MnWO_4$ was detected on either of the Mg_6MnO_8 supported samples, indicating that the addition of Mg to the loaded tungstate stabilizes the tungstate species relative to previously investigated Mg-free tungstates, thereby preventing the formation of $MnWO_4$. Comparing all four samples in Figure 9e, it is clear the spatial inhomogeneity of the bulk $Na_4Mg(WO_4)_3$ sample is further complicated by the changes in tungstate composition due to support interactions during the synthesis of the supported catalysts.

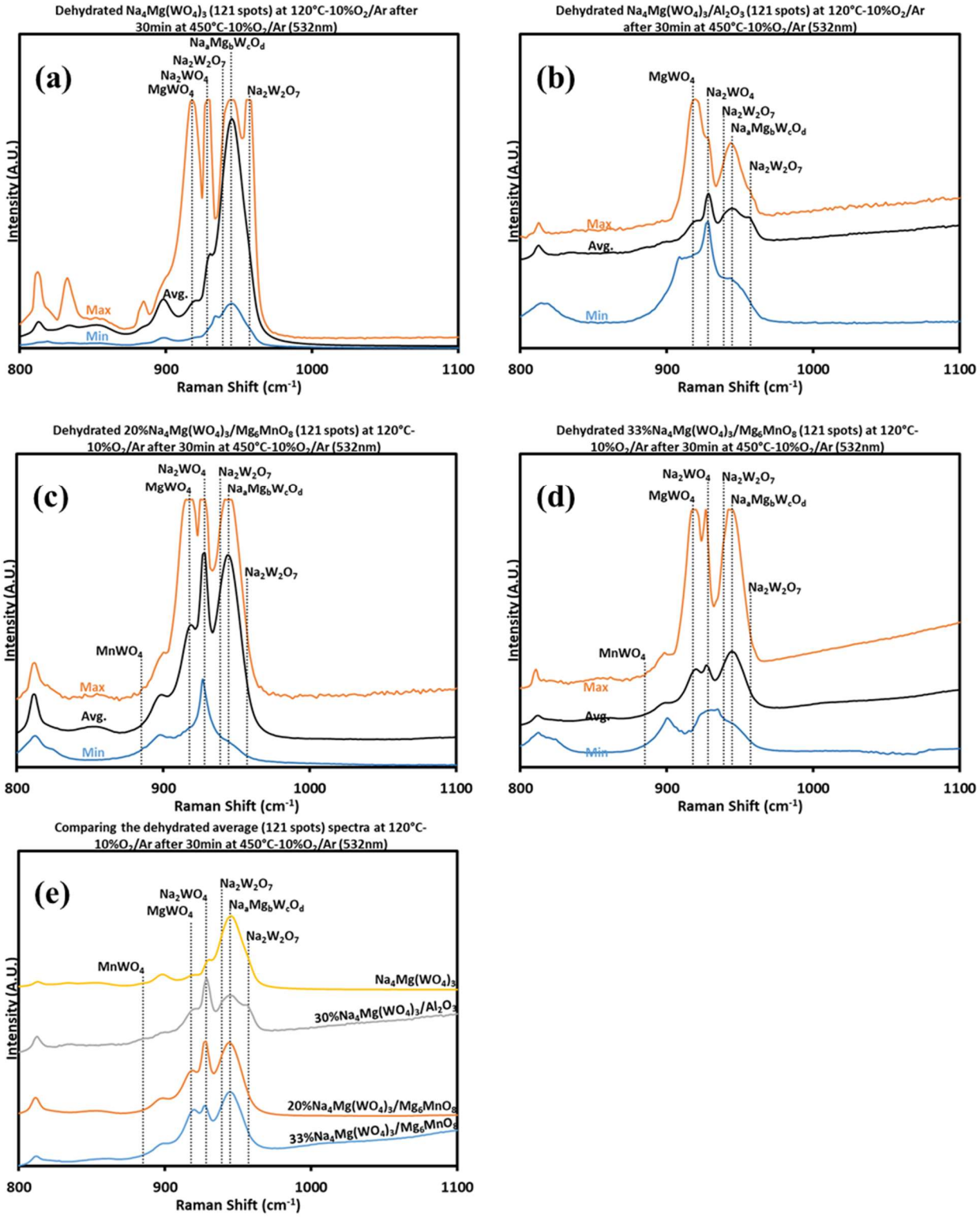

Figure 9. Average (black curves), maximal (orange curves) and minimal (blue curves) Raman intensities over 121 spatially distinct spectra acquired for: (a) bulk $Na_4Mg(WO_4)_3$, (b) $Na_4Mg(WO_4)_3/Al_2O_3$, (c) 20%$Na_4Mg(WO_4)_3/Mg_6MnO_8$ and (d) 33%$Na_4Mg(WO_4)_3/Mg_6MnO_8$. The average spectra for all four are further compared in subfigure (e).

***In situ* Raman characterization of the OCM catalyst (Lehigh)**

The dehydrated molecular structures of the OCM catalyst were characterized by *in situ* Raman spectroscopy. Oxide standards were measured under oxidizing and reducing conditions at various temperatures to help assign vibrations for the catalyst. As shown in Figure 10, after heating to 700°C under an oxidizing gas flow, the LaO_x sample exhibited a phase transition between a cubic La_2O_3 phase (112 and 302 cm^{-1}) and a hexagonal La_2O_3 phase (99, 178 and 391 cm^{-1}). This behavior was also detected under reducing (10%H_2/Ar) and inert (Ar) gas flows when the catalyst was subjected to heating, suggesting the phase transformation is temperature related.

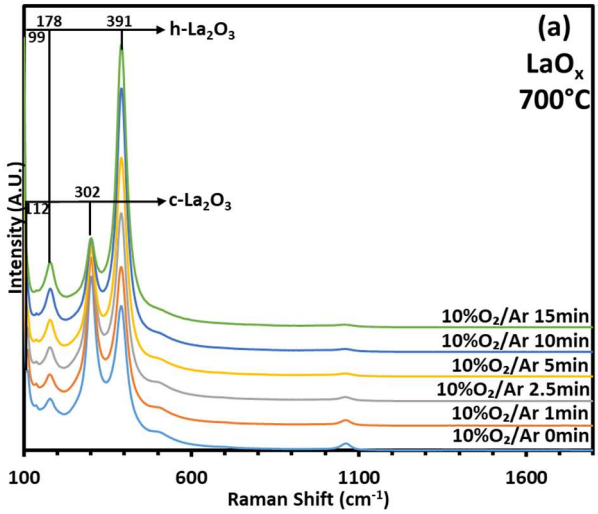

Figure 10. *In situ* Raman spectra acquired at (a) 700°C under 30 cc min^{-1} 10%O_2/Ar flow for a LaO_x sample.

When the fully oxidized mixed oxide support was switched to a 30 cc min^{-1} 1.5%CH_4/He OCM reaction gas flow, the Raman band at 572 cm^{-1} which was associated with the oxidized catalyst was slowly consumed, and a cubic phase (112 and 304 cm^{-1}) began to form in turn 20 min after the initial exposure to the reaction mixture (Figure 11a). Conversely, when the promoted oxide catalyst was subjected to a similar treatment, it transformed to a cubic phase (112 and 302 cm^{-1}) during the first 10 minutes of exposure to the OCM reaction gas flow, and then further transformed to a hexagonal phase (99, 179 and 391 cm^{-1}), which was the dominant phase after 10 minutes, and the sole detectable phase after 20 minutes (Figure 11b). These results suggest that the impregnated promoter not only increases the reducibility of the mixed oxide under OCM reaction flow, but that it promotes the formation of hexagonal bulk phase that is not generated in the bare oxide under similar conditions. While the exhibited cubic and hexagonal vibrations were closer in value to

those of the La_2O_3 phases, possible from cubic and hexagonal mixed oxide phases cannot be ruled out.

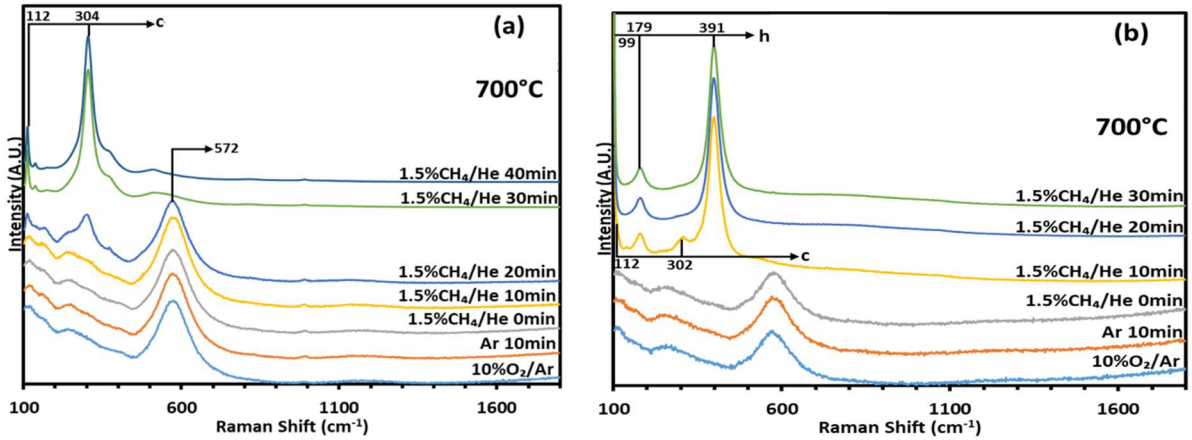

Figure 11. *In situ* Raman spectra acquired at 700°C while switching from a 10%O_2/Ar to a 1.5%CH_4/He 30 cc min^{-1} flow for (a) the bare oxide and (b) promoted oxide catalyst.

In situ Raman Mapping of the OCM catalyst (Lehigh)

The carbonate/$LaPrO_{3+x}$ based OCM catalyst was mapped to characterize the distribution of carbonate on its surface using *in situ* Raman spectroscopy. The catalyst was first oxidatively dehydrated at 700°C under a 3.33%O_2/3.33%CO_2/Ar gas flow before cooling to 120°C. The gas flow was then switched to 5%CO_2/Ar followed by heating to 700°C and cooling back to 120°C at which point the catalyst surface was mapped. The mapping was performed on a 50 μm by 50 μm area with Raman spectra taken 8.3 μm apart, resulting in 36 points of data. As shown in Figure 12a, the catalyst remains oxidized at these conditions as evidenced by the Raman band at 572 cm^{-1}. Zooming in on the Raman shift range of 1000-1200 cm^{-1} in Figure 12b, the carbonate Raman band at 1089 cm^{-1} is clearly visible on some spectra while weaker or even missing in other. A heat map plotting the area of the carbonate Raman band as a function of its spatial location on the sample shown in Figure 12c demonstrates the inhomogeneous dispersion of the carbonate on the surface after cooling, though the carbonate likely disperses on the surface during the reaction as the melting point of the carbonate is relatively low.

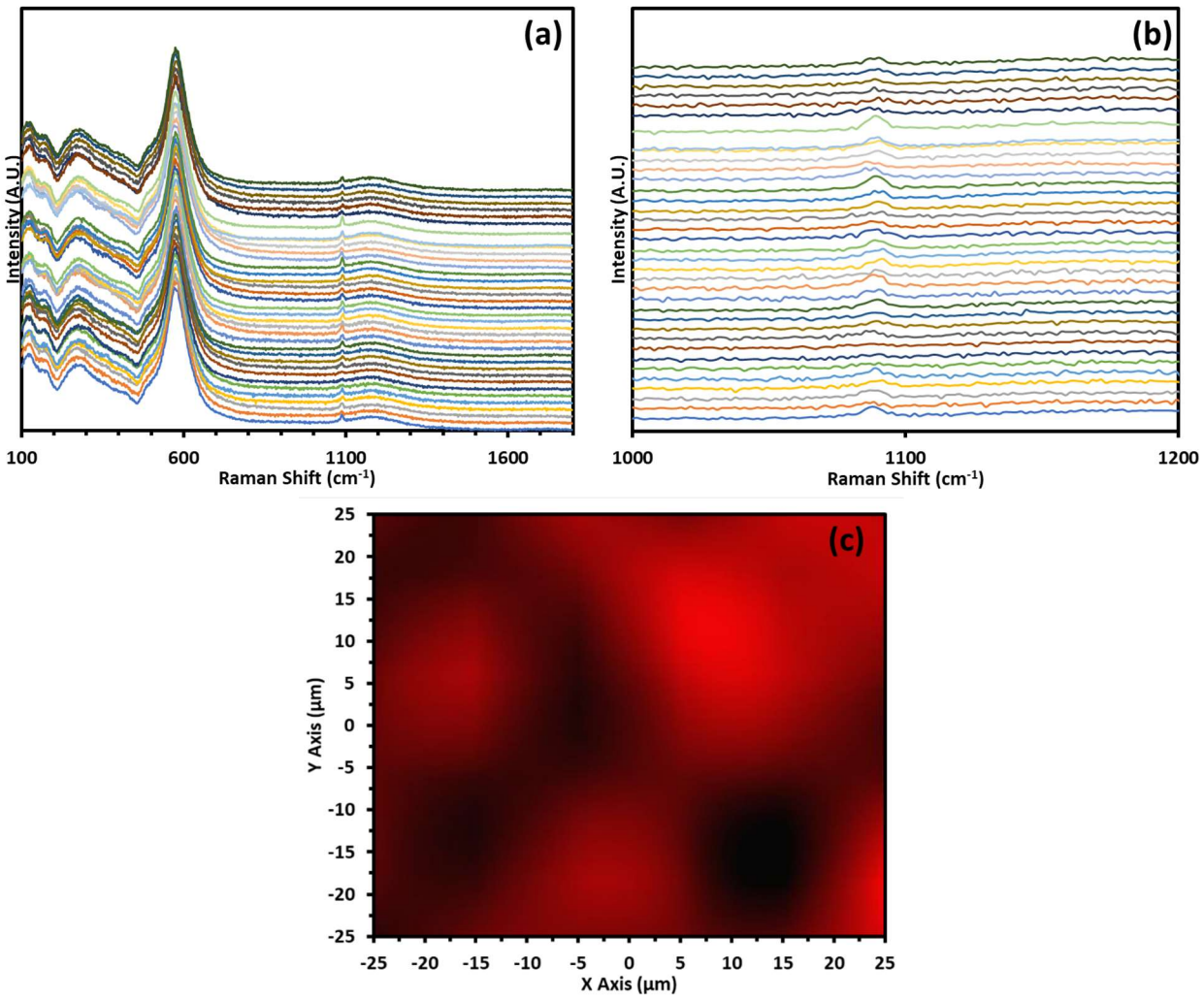

Figure 12. *In situ* Raman spectra taken at 36 different spots on the same oxidatively dehydrated and carbonated $LaPrO_{3+x}$ catalyst in the range of (a) 100-1800 cm^{-1} and (b) 1000-1200 cm^{-1}, and (c) the resulting heat map plotted using the area of the carbonate Raman band at 1089 cm^{-1}.

The carbonate/$LaPrO_{3+x}$ OCM catalyst was further characterized by quasi *in situ* high sensitivity low energy ion scattering (HS-LEIS) a technique capable of measuring the elemental composition on an atomic layer basis. The catalyst was first oxidatively dehydrated under 10%O_2/Ar at 600°C before being probed with He^+ ions and sputtered with Ar^+ ions in a cylic manner, thereby exposing progressively deeper atomic layer. While light elements cannot be directly detected by HS-LEIS due to the physical limitations of the technique, oxygen and La/Pr were detectable in the catalyst as shown in the resulting spectra in Figure 13a. The spectra clearly indicate that as more atomic layers are sputtered, the La+Pr signal at ~2615 eV increases while the background generated by the light elements at lower energies decreases. The lack of any La+Pr signal in the outermost

surface layer suggests that the catalyst is indeed covered by an atomic layer made up of light elements and oxygen. Subsequent HS-LEIS spectra acquired at a different spot after the catalyst was exposed to 10%CH_4/Ar at 600°C are shown in Figure 13b. The more intense background along with the quicker decrease with sputtering indicates that the catalyst is further covered in carbon when in contact with methane at such high temperatures.

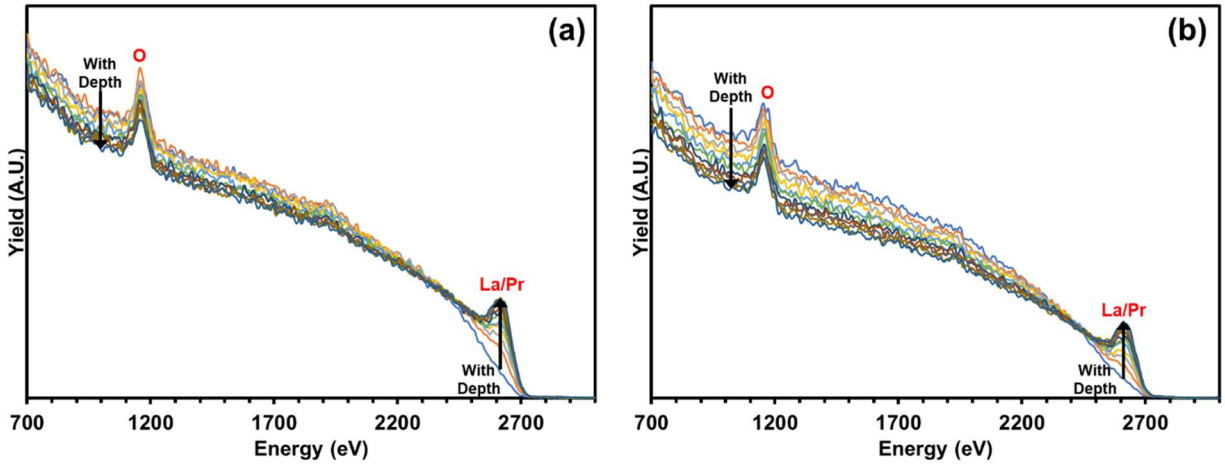

Figure 13. Quasi *in situ* HS-LEIS spectra of the carbonate/$LaPrO_{3+x}$ catalyst for increasingly deeper atomic layers acquired after annealing at 600°C under (a) 10%O_2/Ar and (b) 10%CH_4/Ar.

The carbonate/$LaPrO_{3+x}$ based OCM catalyst was characterized with Near Ambient Pressure X-ray Photoelectron Spectroscopy (NAP-XPS), a relatively recent development that enables the acquisition of XPS spectra at high temperature under reaction conditions. The catalyst was first oxidatively dehydrated at 600°C under a 10%O_2/Ar gas flow before switching to a reducing 10%CH_4/Ar gas flow at the same temperature. Finally, the catalyst was reoxidized under 10%O_2/Ar at 600°C. The NAP-XPS spectra allow not only to measure the changes in the oxidation states of the La and Pr counterion in the surface region (~top 3 nm) of mixed oxide through the La 3d and Pr 3d spectra, but also the changes in the atomic composition in the surface region as a function of the reaction conditions. As shown in Figures 14a and 14c, La was unreactive at 600°C and retains its La^{3+} oxidation state even under reducing conditions regardless of the impregnation of the Li_2CO_3. Conversely, Figures 14b and 14d demonstrate that the native oxidation state of the Pr in the surface region is affected by the impregnation of the Li_2CO_3, resulting in a mixture of Pr^{3+} and Pr^{4+} in the surface region under oxidizing conditions when Li_2CO_3 is impregnated compared to a pure Pr^{3+} oxidation state in the bare support. Once exposed to a flow of 10%CH_4/Ar

at 600°C, some of the Pr^{4+} was reduced to Pr^{3+}, although this reduction is not complete as evident when comparing the Pr 3d spectra of the Li_2CO_3 impregnated and Li_2CO_3-free $LaPrO_{3+x}$. The NAP-XPS spectra quantification (Figure 15) also demonstrate that the surface region of the catalyst is highly enriched in La, with ~70% La compared to the 50% expected based on the synthesis ratio. Furthermore, the surface region composition of the mixed oxide was also affected by the Li_2CO_3 impregnation as shown in Figure 15. While the counterion composition in the surface region of the $LaPrO_{3+x}$ was only weakly affected by the reaction conditions, the Li_2CO_3 impregnated $LaPrO_{3+x}$ catalyst decreased from a fraction of ~35% to ~25% at 600°C, demonstrating a more reactive surface region compared to the bare mixed oxide support. Combined, these results demonstrate the dynamic nature of the surface region of the catalyst after impregnation with Li_2CO_3.

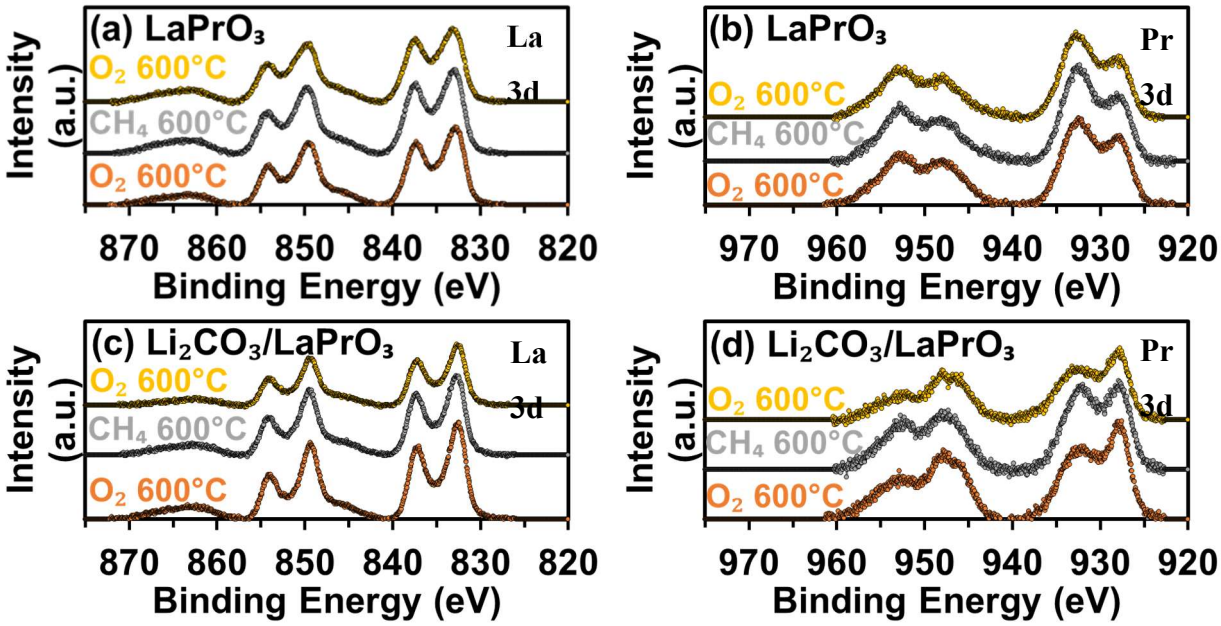

Figure 14. NAP-XPS (a and c) La 3d and (b and d) Pr 3d spectra of (a and b) the $LaPrO_{3+x}$ and (c and d) the $Li_2CO_3/LaPrO_{3+x}$ catalysts acquired under sequent flows of 10%O_2/Ar, 10%CH_4/Ar and again 10%O_2/Ar at 600°C.

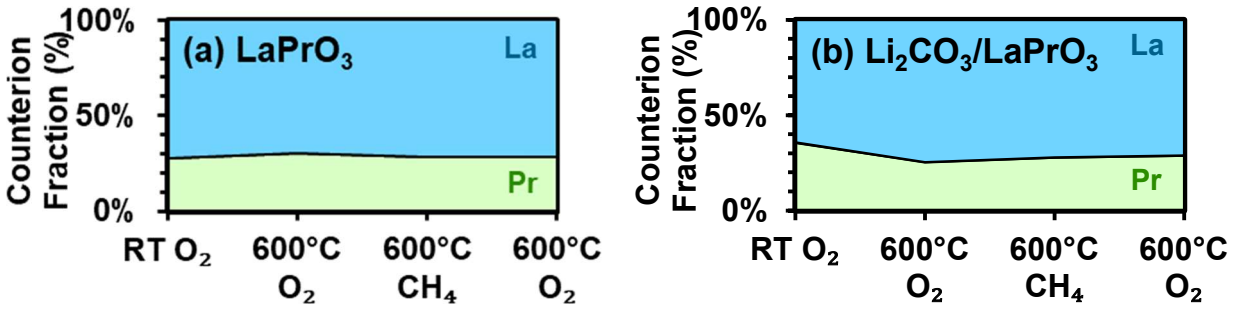

Figure 15. NAP-XPS derived counterion fraction as a function of conditions in the NAP cell for the (a) $LaPrO_{3+x}$ and (b) $Li_2CO_3/LaPrO_{3+x}$ catalysts.

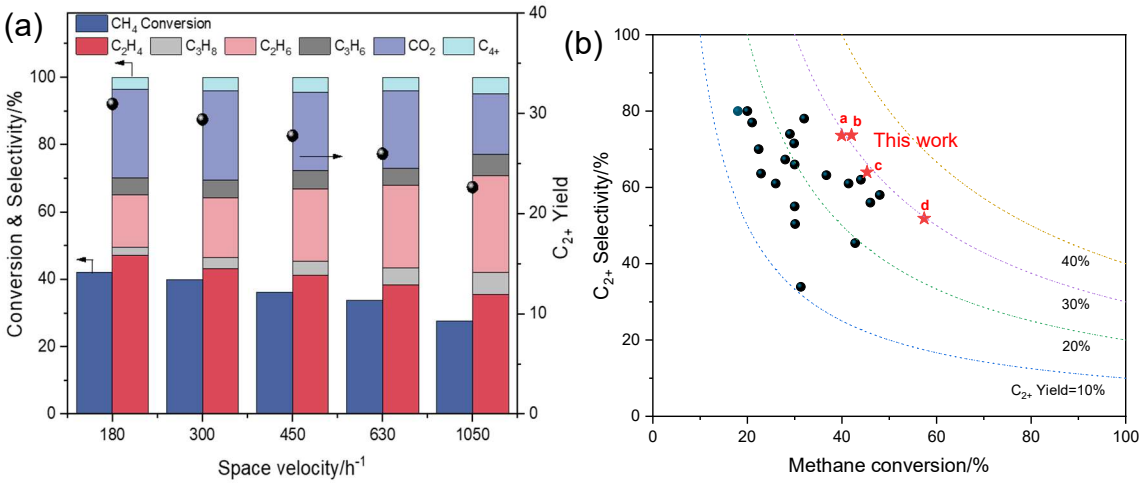

Figure 16. (a) CH_4 conversion, product selectivity and C_{2+} yield as function of space velocity using $5\%Li_2CO_3/MeMe'O_{3+x}$, reaction temperature T = 700°C, methane partial pressure P_{CH4} = 1.0. (b) Comparison of $5\%Li_2CO_3/MeMe'O_{3+x}$ with previously reported OCM catalysts.

The OCM reaction using $5\%Li_2CO_3/MeMe'O_{3+x}$ catalyst was optimized. Figure 16(a) demonstrates the effect of space velocity using undiluted methane as the feed (P_{CH4} = 1 atm) at 700 °C. As shown, methane conversion increases and C_{2+} selectivity decreases as space velocity decreases. At a space velocity of 180 h^{-1}, the total C_{2+} yield increased to 30.95%. Figure 16(b) compares the $Li_2CO_3/MeMe'O_{3+x}$ catalyst to other OCM catalysts previously reported. $Li_2CO_3/MeMe'O_{3+x}$ displayed the greatest OCM yield and is the only catalyst capable of exceeding a 30% C_{2+} yield. We also observe that the best working temperature of $Li_2CO_3/MeMe'O_{3+x}$ is 700°C, which is lower than most standard OCM catalysts, such as $Mn\text{-}Na_2WO_4/SiO_2$.

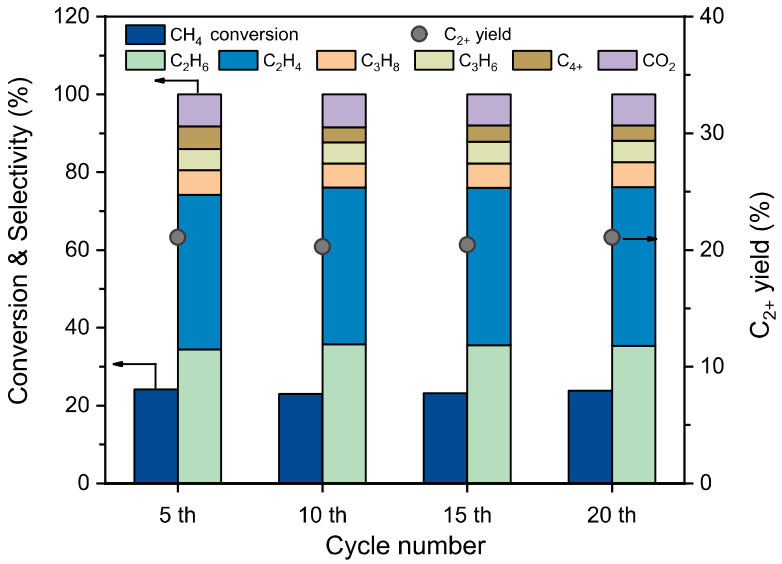

Figure 17. Effect of cycle number of CL-OCM on methane conversion, product selectivity, and C_{2+} yield using the salt doped metal oxide catalyst. (temperature= 700 °C, pressure= 1 bar, flow rate= 750 mL/(g_{cat} ·h), reduction: 80vol%CH_4/20vol%CH_4, oxidation 80vol%O_2/20vol%Ar).

To better understand the catalytic performance of the CL-ODH catalyst, OCM reactions under different conditions were conducted. As shown in Figure 17, 20 cycles of the OCM reactions, including reaction-regeneration cycles, were conducted. For each cycle, 2 g of catalyst was loaded in the OCM U-shaped quartz tube reactor. The reaction temperature was set at 700 °C. As the reduction step, 20 mL/min CH_4+5 mL/min Ar was fed into the reactor to react with the lattice oxygen of the catalysts and 25 mL/min Ar was fed to flush the reactor for 5 min to clear the reactor. As the oxidation step, 20 mL/min O_2 and 5 mL/min Ar were fed to regenerate the lattice oxygen of the catalysts. For the 5th cycle test, the methane conversion reached 24.1% and the C_{2+} yield reached 21.1%, with C_2H_6 selectivity at 34.5% and C_2H_4 selectivity at 39.7%. For the 20th cycle test, the methane conversion reached 23.9% and the C_{2+} yield reached 21.2%, with C_2H_6 selectivity at 35.3% and C_2H_4 selectivity at 40.8%. Therefore, the doped metal oxide catalyst underwent 20 cycles of reduction-oxidation with stable performance, which enables accurate catalyst test.

The effect of the methane partial pressure in the inlet gas was tested when keeping the gas hourly space velocity (GHSV) at 750 mL/(g_{cat} ·h). In Figure 18, 80% CH_4 concentration case and 40% CH_4 concentration case were tested for CL-OCM using a salt doped oxide catalyst. For the 80% CH_4 case, the CH_4 conversion reached 24.2% and the C_{2+} yield reached 21.2%, with C_2H_6 selectivity at 34.4% and C_2H_4 selectivity at 40.2%. For the 40% CH_4 case, the methane conversion

reached 27.6% and the C_{2+} yield reached 23.6%, with C_2H_6 selectivity at 35.3% and C_2H_4 selectivity at 41.2%. However, the CO_2 selectivity also increased from 8.1% for the 80% CH_4 case to 12.7% 8.1% for the 40% CH_4 case, indicating part of the hydrocarbon was further oxidized by the OCM catalyst. The lower CH_4 concentration in the inlet gas notably led to a higher CH_4 conversion and a higher C_{2+} yield, as the same amount of catalyst was contacted with less CH_4, achieving a higher extent in the reaction conversion.

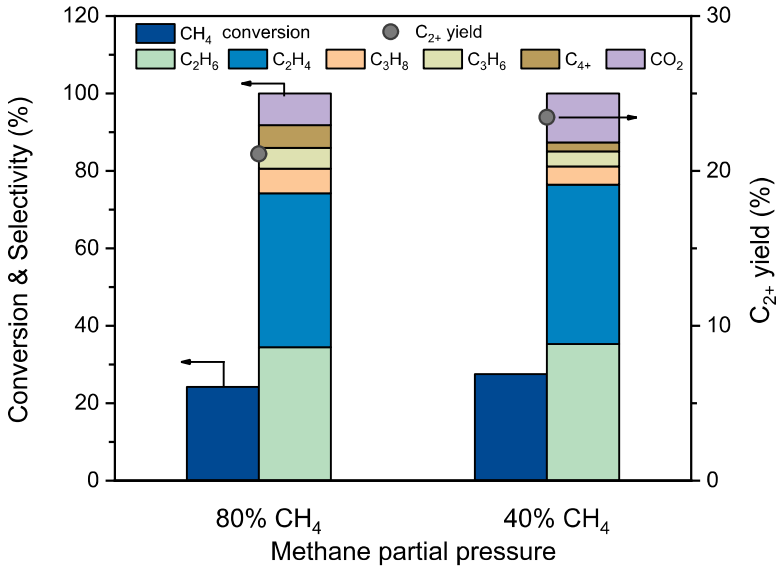

Figure 18. Effect of methane partial pressure of CL-OCM on methane conversion, product selectivity, and C_{2+} yield using a slat doped oxide catalyst. (temperature= 700 °C, pressure= 1 bar, GHSV= 750 mL/(g_{cat} ·h)).

The effect of the reactor system pressure was also investigated for the OCM catalyst. As shown in Figure 19, the increasing reactor pressure effectively promoted methane conversion. For reactor pressure at 1.0 bar, the methane conversion was about 23.1% and the C_{2+} yield was about 19.9%. For reactor pressure at 1.4 bar, the methane conversion was about 27.2% and the C_{2+} yield was about 23.7%. For reactor pressure at 1.8 bar, the methane conversion was about 29.3% and the C_{2+} yield was about 25.8%. Therefore, adjusting the OCM reactor system pressure can effectively utilize the catalyst and tune the catalytic performance.

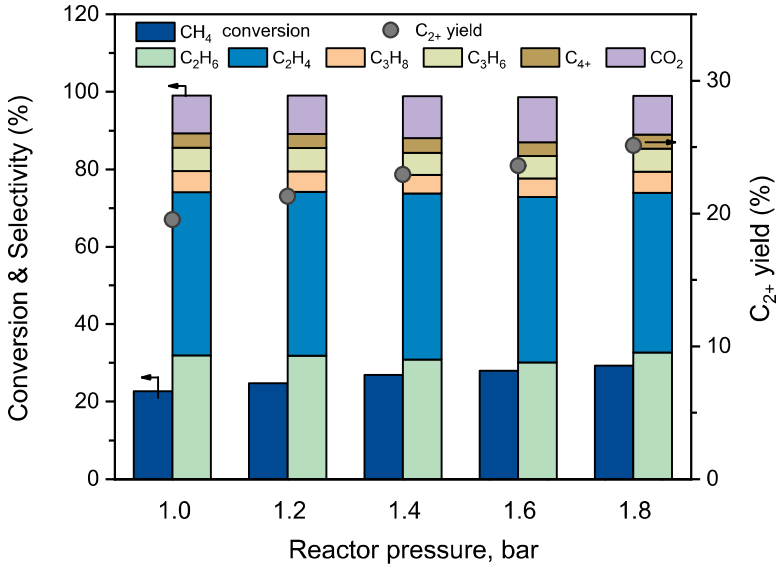

Figure 19. Effect of reactor pressure of CL-OCM on methane conversion, product selectivity, and C_{2+} yield over a salt doped metal oxide catalyst. (temperature= 700 °C, GHSV= 750 mL/(g_{cat} ·h), reduction: 80vol%CH_4/20vol%CH_4, oxidation 80vol%O_2/20vol%Ar).

Subtask 2.3: Methane DHA catalyst synthesis, characterization and testing

Two methods of synthesis for the DHA zeolite support, H-ZSM-5, were investigated. The two syntheses are referred to as the solid-state crystallization method (SSC) and conventional hydrothermal synthesis method (Con). The solid-state crystallization method is a two-stage process: stage 1 involves the synthesis of aluminosilicate nanogels (where water is present), and stage 2 is the solid-state crystallization to the hierarchical zeolites (in the absence of water). In contrast, the conventional hydrothermal synthesis method is traditionally performed within an autoclave under autogenous pressure (with water present). The optimal procedures and ratios of reactants were determined and are given in greater detail below. Solid-state crystallization synthesis begins by mixing tetrapropyl ammonium hydroxide (TPAOH, 1 M in H_2O), sodium aluminate ($NaAlO_2$), tetraethylorthosilicate (TEOS), and water with a particular molar ratio of 0.25 TPAOH: 0.03 Al_2O_3: 1 SiO_2: 80 H_2O. The water was added first to the Teflon insert of the autoclave and a stir bar was dropped in to begin stirring on a hot plate at room temperature. The TPAOH and the $NaAlO_2$ were dissolved in the water while stirring continuously. Lastly, TEOS was added slowly dropwise under the strong agitation of the stirring. The solution was kept stirring for 4 hours before being placed in an oven at 80°C for 12 hours. The clear solution obtained was dried and the

dry gel collected was ground into a powder. The dry powder aluminosilicate nanogels were then transferred into the Teflon-lined autoclave for crystallization in the oven at 160°C for 24 hours. After crystallization, the powder was washed using deionized water and then dried at 120°C for 12 hours. Finally, the powder was calcined in a muffle furnace and slowly heated to 550°C and held for 6 hours. The conventional hydrothermal synthesis begins with a similar solution being made using the same precursors as the solid-state crystallization method in a different molar ratio, 0.25 TPAOH: 0.03 Al_2O_3: 1 SiO_2: 40 H_2O. The solution was also stirred for 4 hours until being placed in the oven at 160°C for 4 days (96 hours). Once crystallization was complete, the precipitate was separated from the liquid using a centrifuge (5,000 rpm for 5 min) and washed with deionized water. The precipitate was then dried in an oven at 120°C for 12 hours. Finally, the powder was calcined in a muffle furnace and slowly heated to 550°C and held for 6 hours. Both methods considered here are preformed over the course of 5-7 days. During the optimization of the procedure, the synthesized zeolites were characterized using X-ray diffraction (XRD) to distinguish if the product had the characteristic peaks of ZSM-5. The first few attempts showed poor intensity of the unique peaks, so the crystallization step for each method was adjusted in both temperature and time. The final procedures were as stated above; each showed good intensity in the XRD spectrum and clearly showed the characteristic peaks of ZSM-5, seen below in Figure 20. After the synthesis methods showed satisfactory XRD patterns and intensity, a surface area analysis was completed on each zeolite produced. Each of the synthesis methods was designed to produce ZSM-5 zeolite with a silica/alumina ratio (SAR) of approximately 33. For a comparison, a commercially manufactured H-ZSM-5 with a SAR of 30 (CBV 3024E from Zeolyst International) was also tested. Results for all surface area analyses can be seen in Table 4. The two zeolites made in-house show comparable surface area with the CBV 3024E commercial zeolite.

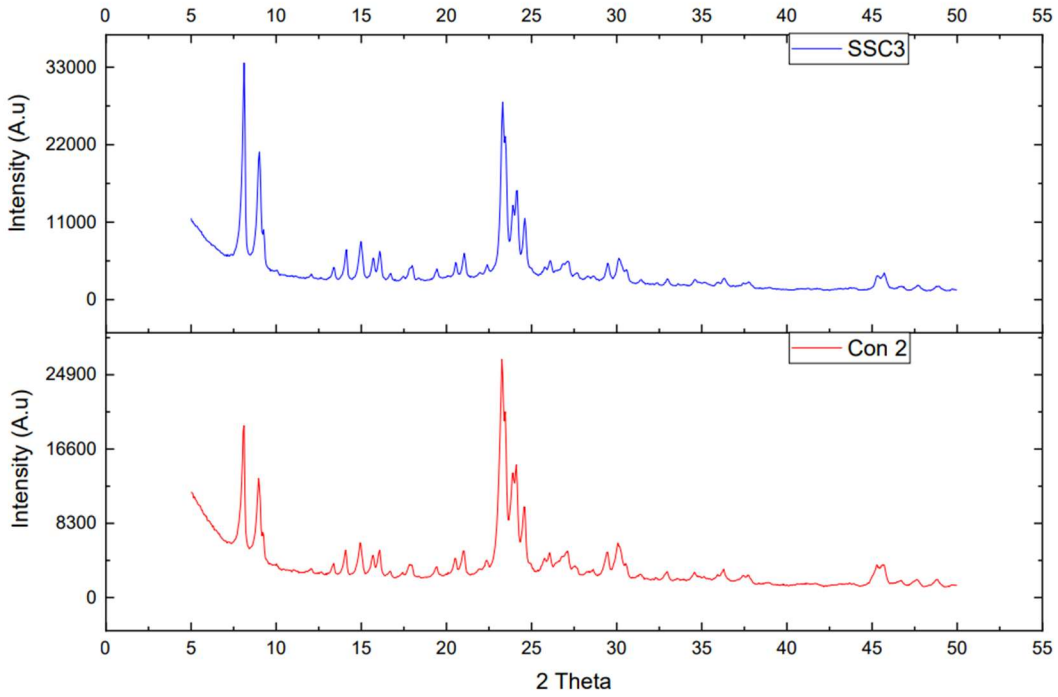

Figure 20. X-ray diffraction (XRD) patterns of solid-state crystallization method zeolite (SSC3) and the conventional hydrothermal synthesis method zeolite (Con2).

Table 4. BET Surface Area Analysis of Zeolite Synthesis Methods

Synthesis Method	BET Surface Area (m^2/g)	t-plot Micropore Area (m^2/g)	t-plot External Surface Area (m^2/g)
SSC	328.6454	229.0838	99.5616
Con.	339.6473	250.3177	89.3295
CBV 3024E	352.1867	223.8582	128.3285

In addition to the primary Mo promoter, secondary metal promoters such as Ga, Pt, or Fe, will also be impregnated onto the in-house synthesized zeolite support to determine the optimal metal combinations for the DHA reaction. Four catalysts were prepared using commercially manufactured zeolite, HZSM-5 CBV 2314, with a SAR of 23 (Zeolyst International). Each zeolite sample was loaded with 3 wt% molybdenum and some with an additional 0.5 wt% of a secondary promoter, such as Ga, Fe, or Pt. The four catalysts made were as follows: 3% Mo ZSM-5, 3% Mo + 0.5% Ga ZSM-5, 3% Mo + 0.5% Fe ZSM-5, 3% Mo + 0.5% Pt ZSM-5. This weight percent loading has been commonly used for DHA metal loaded catalysts. All four catalysts were prepared using a dry incipient impregnation method. First the commercial zeolite was calcined at 550°C for

4 hours in a muffle furnace in air to convert the zeolite from the ammonium form, NH4-ZSM-5, to the protonated form, H-ZSM-5. For the 3 wt.% Mo catalyst, the corresponding amount of the ammonium heptamolybdate tetrahydrate salt was dissolved in deionized water and added dropwise to H-ZSM-5. The catalyst was then dried in an oven at 100°C for 12 hours. Finally, the powder was calcined in air at 550°C for four hours. The three bimetallic catalysts were made by co-impregnation method, meaning both salt solutions were made and added dropwise consecutively to the zeolite powder. The precursors used were gallium nitrate hydrate, iron nitrate nonahydrate, and chloroplatinic acid hexahydrate for the secondary promoters. Once all four catalyst were prepared and calcined, each was tested under various DHA conditions. Five different sets of reaction conditions have been tested for all four catalysts, seen below in Table 5. The reactions were carried out in a Micromeritics Autochem 2950 analyzer connected to a micro gas chromatograph (micro-GC) for gas analysis. For each reaction, the amount of catalyst, seen in Table 5, was loaded into the quartz u-tube. The reaction was carried out under atmospheric pressure and continuous flow conditions. The catalyst was heated to the reaction temperature under 30 mL/min nitrogen flow at 10°C/min. Pure reactant gas, ethane or methane, was mixed with nitrogen to create a 30% reactant gas mixture. Each reaction was run for 30 minutes and then purged with nitrogen. The in-line product analysis was completed using a four column Agilent 3000 micro-GC. For each reaction, the reactant gas conversion, product selectivity, and product generation rate were plotted

Table 5. Descriptions of DHA reaction conditions 1 through 5

Reaction	1	2	3	4	5
Reactant Flow (Balance: N_2)	30% Ethane	30% Ethane	30% Ethane	30% Methane	30% Methane
Temperature	650 °C	600 °C	650 °C	700 °C	750 °C
Reaction Time	30 mins	30 mins	30 mins	30 mins	30 mins
Amount	0.2 g	0.3 g	0.3 g	0.3 g	0.3 g
GHSV	9000	6000	6000	6000	6000

For reactions 1-3 in Table 5, 30% ethane was flowed as the reactant gas. For reaction 1, the plots are shown below in Figure 21. In Figure 21a, the MoFe promoted catalyst showed slightly higher

ethane conversion throughout the 30 min reaction time. Due to the higher methane selectivity of the MoFe catalyst, the higher hydrogen production rate, in Figure 21b, is most likely due to the higher ethane conversion. This indicated the MoFe catalyst favors the hydrogenolysis of ethane to methane, also verified by the low ethylene production, in Figure 21c. The monometallic Mo and the bimetallic MoGa catalysts exhibited similar trends for the ethane dehydroaromatization reaction at 650°C. The MoPt showed a high ethylene production rate, which indicated that the MoPt catalyst is highly effective at the dehydrogenation of ethane to ethylene. However, the MoPt catalyst exhibited nearly identical aromatic production rates as the other catalysts.

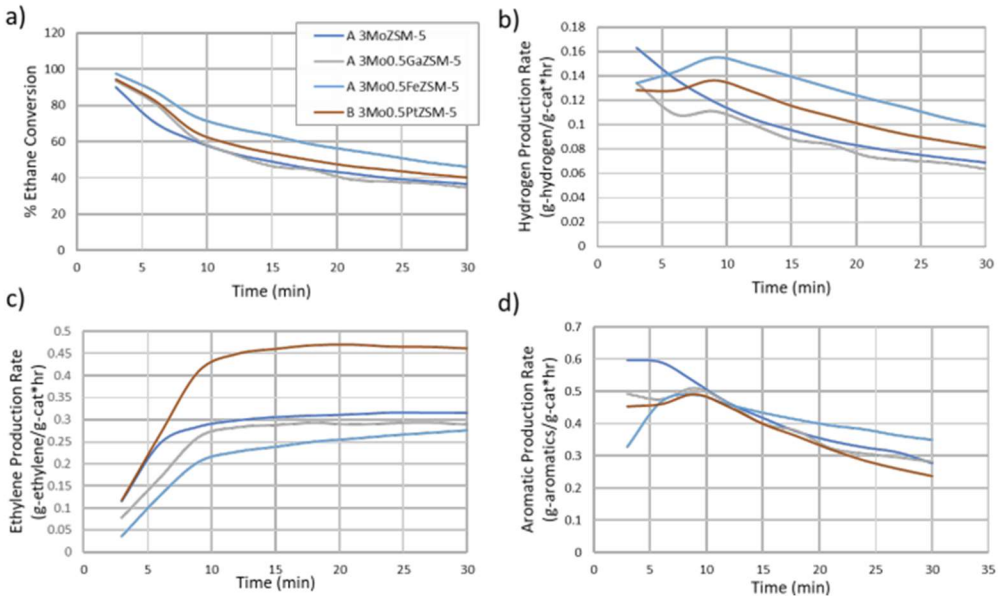

Figure 21. 30% Ethane DHA reaction data for all four catalysts at 650°C and 0.2 grams catalyst loading (Reaction condition 1); a) Ethane conversion, b) Hydrogen production rate, c) Ethylene production rate, and d) Aromatic production rate (includes benzene and toluene).

For reactions 4 and 5 in Table 5, 30% Methane was used as the reactant. The results for reaction 5 are shown below in Figure 22. As seen in Figure 22a, the MoFe promoted catalyst exhibited a higher methane conversion. However, the MoFe promoted catalyst suffered from a higher selectivity for the hydrogenolysis reaction, which is indicated by the low production rate of ethylene as seen in Figure 22c. The low selectivity to ethylene greatly impacted the aromatic production rate, as seen in Figure 22d. This indicates that the MoFe promoted catalyst would not be a good candidate for the methane DHA reaction at the high temperature of 750°C. However, our previous reaction data at a lower temperature of 700°C, not shown here, indicates that MoFe

becomes less selective to the undesired hydrogenolysis reaction. The presence of Ga or Pt promoters at 750°C gave little to no change in aromatic production rates compared to monometallic Mo. This is probably due to the strong endothermic nature of the methane DHA reaction. The three catalysts Mo, MoGa, and MoPt at 750°C show similar trends in Figure 22a-d.

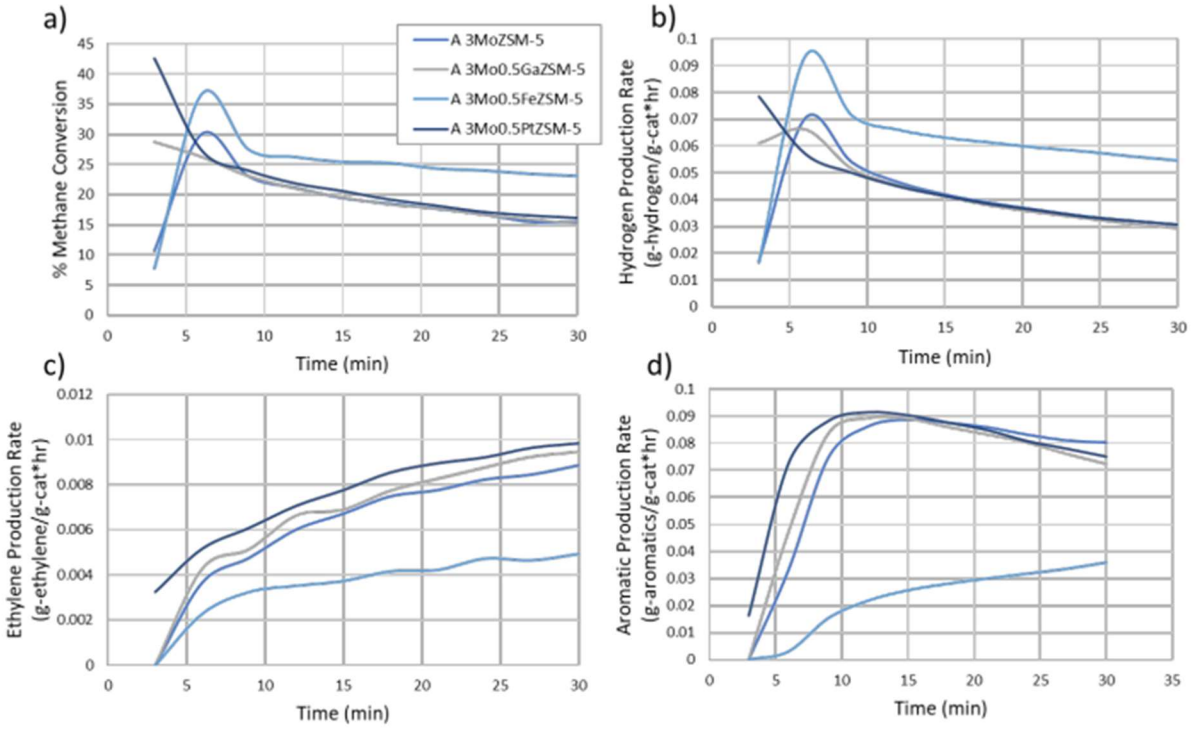

Figure 22. 30% Methane DHA reaction data for all four catalysts at 750°C and 0.3 grams catalyst loading; a) Ethane conversion, b) Hydrogen production rate, c) Ethylene production rate, and d) Aromatic production rate (includes benzene and toluene)

The four catalysts made were as followed: 3% Mo ZSM-5, 3% Mo 0.5% Ga ZSM5, 3% Mo 0.5% Fe ZSM-5, 3% Mo 0.5% Pt ZSM-5. The four catalysts performance were tested under various conditions for the DHA reaction. The coke formation of the spent catalysts from the 30-minute, 30% methane DHA reaction at 750°C, with 0.3g loading, was further investigated by a thermogravimetric analysis (TGA). The results of this study are shown in Figure 23. In comparison to the other promoted zeolites, the MoFe catalyst shows a significant increase in weight loss due to coke than the other three catalysts. The MoFe catalyst showed increased conversion in both the ethane and methane DHA reactions. However, in the ethane DHA reaction the catalyst favored the hydrogenolysis of ethane to methane, also verified by the low ethylene production. In the methane

DHA reaction the MoFe catalyst had the highest methane conversion, while exhibiting a high selectivity towards hydrogen, and a low selectivity towards ethylene and total aromatics. This indicates that the MoFe catalyst is very selective towards coke, which is confirmed by the 8 wt % loss due to coke in the TGA study. As seen in Figure 23, the MoFe catalyst exhibits a higher order of coke compared to the other promoted catalysts based on the weight loss due to coke at a higher temperature. Previously in our research group, the presence of Fe as a secondary promoter stimulates the growth of carbon nanotubes (CNTs), which corresponds to a higher burning order of coke.

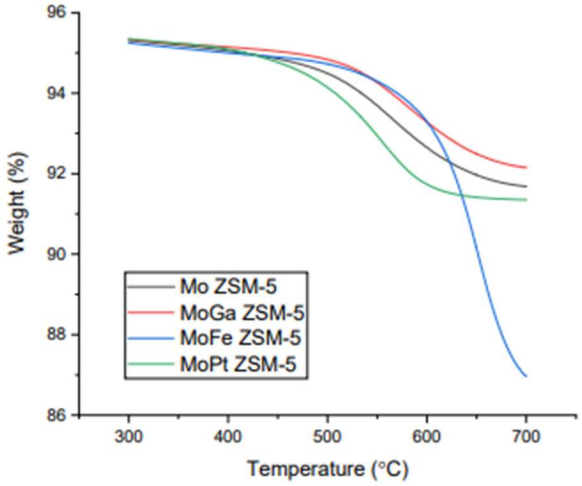

Catalyst	Weight Loss (%)
Mo	3.4%
MoGa	3.0%
MoFe	8.0%
MoPt	3.7%

Figure 23. Thermogravimetric analysis (TGA) of the coke formation during a 30-minute 30% Methane DHA reaction at 750°C, 0.3g loading, on the four metal-promoted commercial zeolite supported catalysts.

Two methods of synthesis were implemented and optimized to make the DHA support zeolite, HZSM-5, with a SAR of 33. These two methods used were solid-state crystallization method (SSC) and conventional hydrothermal synthesis method (CON). The activity of the two synthesized zeolites and a comparable commercial zeolite, CBV 3024E (SAR 30), was investigated for methane DHA. Each support was loaded with 3 wt % molybdenum for the performance studies via dry incipient impregnation method. The three catalysts prepared were: 3% Mo CBV 3024E, 3% Mo SSC, and 3%Mo Con. The three catalysts performance was tested and repeated for both 700°C and 750°C for 30-minute in 30% methane with 0.3g loaded. The reaction data, conversion, and production rate of products are plotted and shown in Figure 24 (700°C) and Figure 25 (750°C). As

seen in both figures, both the SSC and CON supported catalysts show similar activity with each other at both 700°C and 750°C. This indicates that both synthesis methods produce very comparable ZSM-5 supports. In comparison to the 3% Mo CBV 3024E, the 3%Mo SSC and 3%Mo Con show a lower performance at both temperatures.

The coke formation of the spent catalysts in Figure 25, were further investigated by a thermogravimetric analysis (TGA) shown in Figure 26. Interestingly, the SSC supported catalyst showed the highest weight loss due to coke, whereas the other synthesized support, CON, had the lowest weight loss due to coke. Indicating the metal promoted SSC catalyst is more selective to coke than the CON.

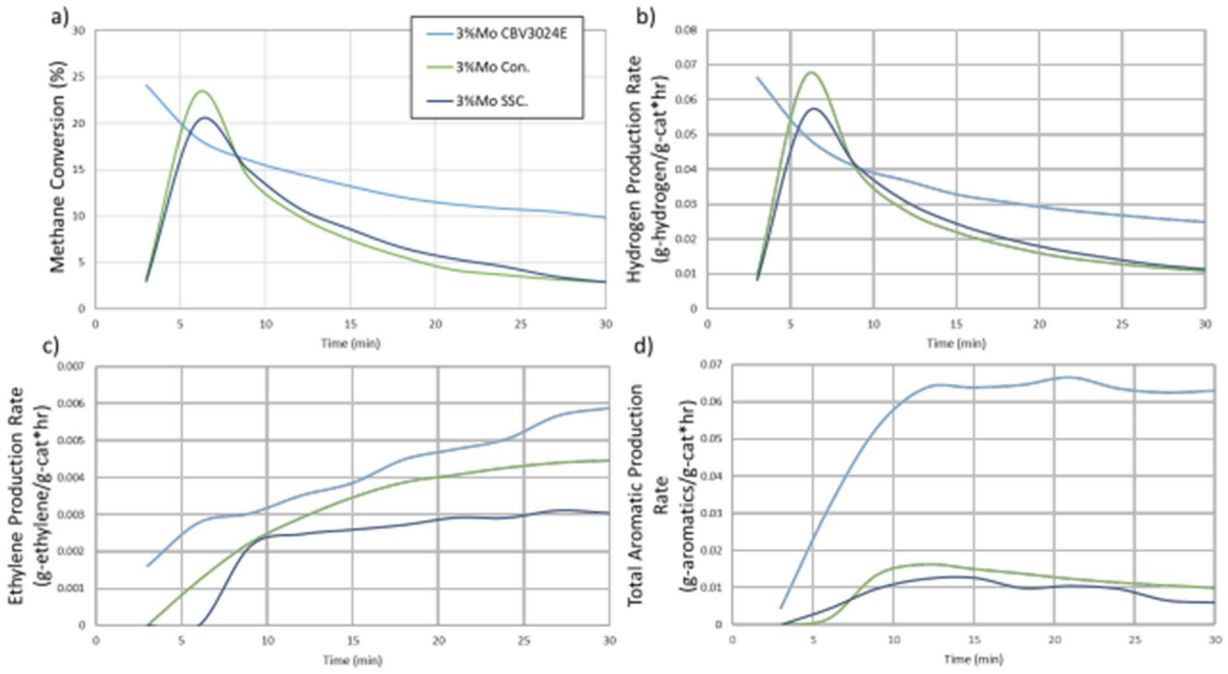

Figure 24. 30-minute 30% Methane DHA reaction data for the three catalysts: 3% Mo CBV 3024E, 3% Mo SSC, and 3%Mo Con. at 700°C and 0.3 grams catalyst loaded; a) Ethane conversion, b) Hydrogen Production Rate, c) Ethylene Production Rate, and d) Aromatic Production Rate (includes Benzene and Toluene).

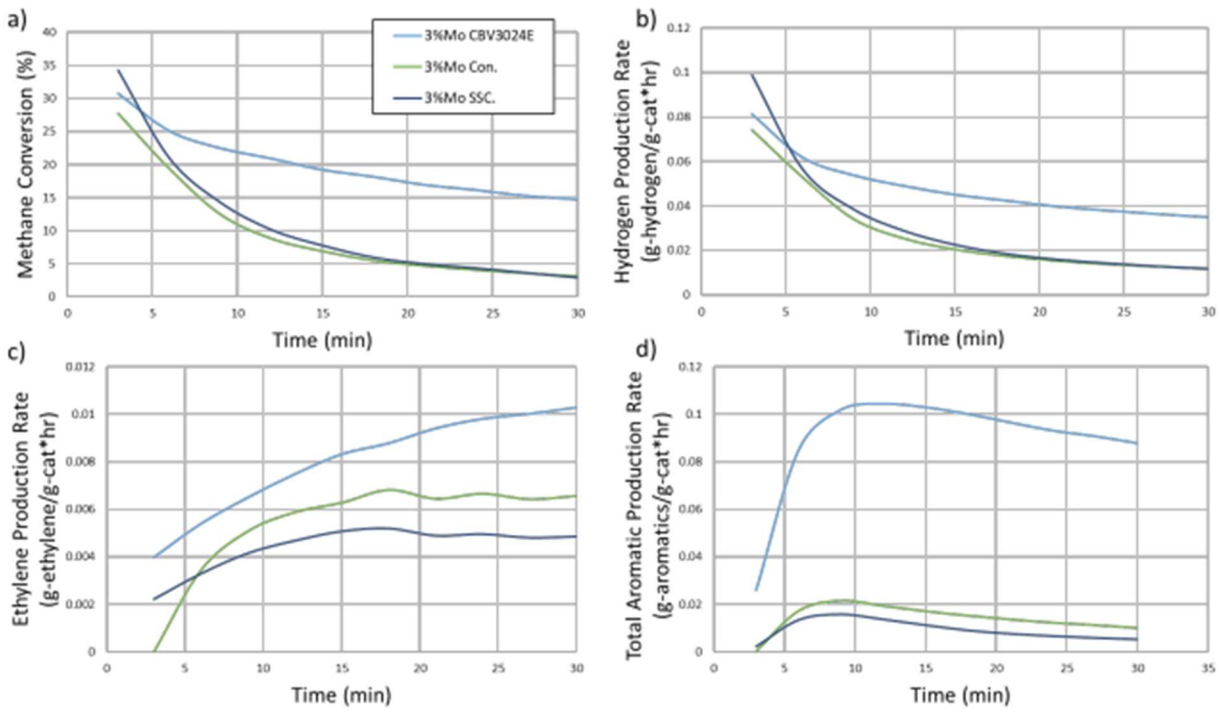

Figure 25. 30-minute 30% Methane DHA reaction data for the three catalysts: 3% Mo CBV 3024E, 3% Mo SSC, and 3%Mo Con. at 750°C and 0.3 grams catalyst loaded; a) Ethane conversion, b) Hydrogen Production Rate, c) Ethylene Production Rate, and d) Aromatic Production Rate (includes Benzene and Toluene).

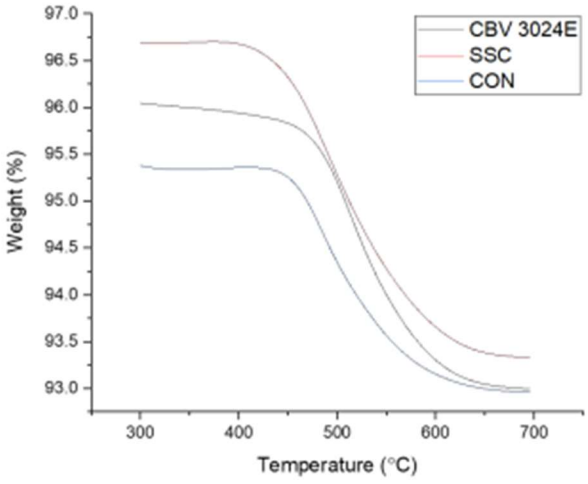

Catalyst	Weight Loss (%)
CBV 3024E	3.0%
SSC	3.3%
CON	2.4%

Figure 26. Thermogravimetric analysis (TGA) of the coke formation during a 30-minute 30% Methane DHA reaction at 750°C, 0.3g loading, on the three synthesized zeolite supported catalysts.

The elemental composition of the 3% Mo CBV 3024E, 3% Mo SSC, and 3%Mo Con catalyst were measured using Inductively Coupled Plasma-Optical Emission Spectrometer (ICP-OES) to further confirm the SAR value of the synthesized ZSM-5. The three catalysts all had a 2.7 wt.% loading of Mo which is consistent with the loaded amount, suggesting the incipient wetness impregnation method was successful at preparing the catalyst consistently. The expected SAR for the two synthesized zeolites, SSC and Con, was SAR 33 and the ICP-OES results showed a SAR of 36 which is close to the expected value. For the commercial zeolite, CBV 3024E, the expected SAR was 30 and the ICP-OES resulted in a SAR of 31. The ICP-OES results were similar to the expected results. We increased the partial pressure of methane in the reaction from our previous studies from 30% to 80% methane and performed additional tests to investigate the catalytic performance, selectivity to aromatics, and productivity of aromatics of the catalysts. The goal of this study was to identify three or more selective DHA catalyst which have an 80% selectivity to aromatics and >500 g/kgCat-hr aromatic productivity. Four different Mo-loaded catalysts were prepared via incipient wetness impregnation of SAR 23 commercial ZSM-5: 2.5%Mo, 4%Mo, 6%Mo, and 10%Mo. Each catalyst was synthesized, calcined, and pelletized using 40-60 mesh prior to reaction. Each of the four different metal-loaded catalysts were subjected to three different pretreatment processes prior to their reactions: no carburization, CH_4/H_2 carburization, and a CH_4 carburization. The catalysts subjected to no carburization, were heated to a reaction temperature of 700°C under inert flow at 10°C/min and held for 4 hours time-on-stream (TOS). The CH_4/H_2 carburized catalyst were carburized by heating the catalyst at 10°C/min to 700°C under a 20/80 mixture of CH_4/H_2 with a total flow of 50 mL/min. Once at 700°C each catalyst was held under the CH_4/H_2 mixture for 10 minutes. The CH_4 carburized catalyst were carburized under similar conditions to the CH_4/H_2 mix but the catalyst was subjected to 50 mL/min flow of pure methane. For each reaction, 0.3 grams of the catalyst was loaded into a quartz tube which was then loaded into the reactor. Within the reactor the catalyst was subjected to its carburization pretreatment and then purged with nitrogen for 20 minutes and held a 700°C for the 4-hour reaction. The methane conversion, aromatic selectivity, and aromatic production of each of the four catalysts following three different pretreatments can be seen in Table 6.

At 700°C, it can be seen in Table 6 that the catalyst approaches the production rate parameter but falls slightly below the 500 g/kgCat-hr value. The 10%Mo catalyst showed an increased methane conversion these catalysts suffer rapid deactivation over the reaction period. Therefore, moving

forward the 6%Mo was chosen for additional testing. The 6%Mo – no carb. showed an intense induction period of where the metal loading goes through a period of reduction upon exposure of the reactant gas. The 6%Mo – CH_4/H_2 carb. catalyst showed a higher TOS stability in conversion than the 6%Mo – no carb. and the 6%Mo – CH4 carb., so it was investigated further at different temperatures 700°C, 750°C, and 800°C, seen in Table 7.

Table 6. Mo-loading and carburization study at 700 °C.

Mo-Loaded ZSM-5 Catalysts (wt. %) and Carburization Method	Methane Conversion (%)	Selectivity to Aromatics (%)	Total Aromatic Production Rate (g/kgCat-hr)
2.5%Mo – no carb	12.8	84.3	333
2.5%Mo – CH_4/H_2	12.2	85.2	312
2.5%Mo – CH_4	10.0	84.1	245
4%Mo – no carb	15.4	86.2	427
4%Mo – CH_4/H_2	12.5	85.5	321
4%Mo – CH_4	7.3	85.5	269
6%Mo – no carb	15.5	84.7	380
6%Mo – CH_4/H_2	13.5	87.1	413
6%Mo – CH_4	13.0	86.2	340
10%Mo – no carb	25.6	80.6	305
10%Mo – CH_4/H_2	20.0	87.4	444
10%Mo – CH_4	11.3	85.7	292

In Table 7, we show the methane conversion, aromatic selectivity, and aromatic production for the 6%Mo – CH_4/H_2 carb. for the 4 hours TOS reactions at the various temperatures. We were successfully able to meet the goal as stated earlier of 80% selectivity to aromatics and >500 g/kgCat-hr aromatic productivity for the reactions at both 750°C and 800°C. Increasing the reaction temperature improved the production of aromatics by the 6%Mo catalysts. The reaction at 800°C shows the highest methane conversion and aromatic production however has a slight decrease in selectivity from the 750°C. At 800°C the 6%Mo – CH_4/H_2 carb. showed rapid deactivation in comparison to the catalyst at 750°C, therefore, in further reaction studies a temperature of 750°C was used.

Table 7. Temperature study of 6%Mo ZSM-5 -CH_4/H_2 Carb catalyst

6%Mo ZSM-5 - CH_4/H_2 Carb	Methane Conversion(%)	Selectivity to Aromatics (%)	Total Aromatic Production Rate (g/kgCat-hr)
700 °C	13.5	87.1	413
750 °C	15.5	87.1	523
800 °C	20.9	86.0	704

The 6%Mo – CH_4/H_2 carb. showed the best long-term stability towards aromatics at 750°C, so two additional catalysts were prepared and tested under the same conditions as previously described. Keeping the total metal-loading of 6% the same, 5.5%Mo 0.5%Fe/ZSM-5 and 5.5%Mo 0.5%/ZSM-5, were prepared via the co-incipient wetness impregnation method. These bimetallic catalysts were calcined and pelletized using 40-60 mesh prior to the pretreatment and reaction. In Table 8, the two additional promoted catalysts conversion, selectivity to aromatics, and aromatic productivity are shown following a CH_4/H_2 carburization pretreatment and a 4-hour reaction at 750°C with 80% methane feed. This table shows three catalysts that successfully achieved an 80% selectivity to aromatics and >500 g/kgCat-hr aromatic productivity.

Table 8. Promoter Study of the Mo ZSM5- CH_4/H_2 Carb Catalyst at 750 °C

Metal-Loaded ZSM-5 Catalysts with the Additional Secondary Promoters	Methane Conversion (%)	Selectivity to Aromatics (%)	Total Aromatic Production Rate (g/kgCat-hr)
6%Mo ZSM-5	15.5	87.1	523
5.5%Mo 0.5%Fe ZSM-5	17.3	84.3	625
5.5%Mo 0.5%Ga ZSM-5	14.5	86.5	512

A similar investigation was performed using 30% ethane, 4%Mo ZSM-5 at different reaction conditions such as temperature, GHSV, and grams loaded to determine the conversions, selectivity to aromatics, and production of aromatics, seen in Table 9. Increasing the GHSV of the 0.2 grams catalyst loaded increased the aromatic productivity but decreased the aromatic selectivity, indicating that the slower GHSV shows better conversion and selectivity. Increasing the 0.2 to 0.3 grams at 6000 GHSV, the conversion and selectivity towards aromatics. Changing the reaction

temperature was also tested for the catalytic activity, selectivity, and performance. Higher temperatures 650°C showed better overall results than the reactions at 625°C and 600°C. Additional testing of carburized catalysts CH_4 and CH_4/H_2 showed no improvement over the 0.3 grams reaction at 650°C. Although the reactions at 650°C, were successful at meeting the productivity parameter to aromatics of 500 g/kgCat-hr the selectivity towards aromatics was low. This is expected as ethane DHA is very selective to the formation of ethylene as well as aromatics.

Table 9. Ethane study of 4% Mo ZSM-5 under Different Reaction Conditions

Grams Loaded (grams)	GHSV (mL/hr/gram catalyst)	Temperature (°C)	Ethane Conversion (%)	Selectivity to Aromatics (%)	Production Rate to Aromatics (g/kgCat-hr)
0.2	9000	650	40.6	28.8	608.5
0.2	6000	650	55.2	30.4	501.2
0.3	6000	650	57.2	30.8	520.0
0.3	6000	625	45.5	30.0	451.3
0.3	6000	625	34.4	28.3	336.9

At 650°C and 80% methane the 6%Mo ZSM-5, 5.5%Mo 0.5%Fe/ZSM-5, and 5.5%Mo 0.5%/ZSM-5 catalysts pretreated by a CH_4/H_2 carburization successfully achieved an 80% selectivity to aromatics and >500 g/kgCat-hr aromatic productivity.

Both methane and ethane DHA reaction studies were performed to find catalysts which could successfully meet the goal of 80% selectivity to aromatics and >500 g/kgCat-hr aromatic productivity. The 2.5, 4, 6, and 10% Mo-loaded ZSM-5 catalysts were carburized three different ways (no carburization, CH_4 carb., and CH_4/H_2 carb.) and were tested at 700°C for the methane DHA reaction. The 6% Mo – CH_4/H_2 carburized catalyst showed the best performance so further temperature studies were performed to investigate if this catalyst would be able to meet the goal stated above. Finally, after the additional testing the 6% Mo – CH_4/H_2 catalyst at both 750 and 800°C was able to achieve the desired selectivity and productivity. Additional secondary promotors were added, such as Fe and Ga, and were also found to achieve the desired performance parameters. An ethane DHA reaction study was also performed by varying the reaction conditions,

such as amount loaded, gas space velocity, and finally temperature. At 650°C, the 4% Mo ZSM-5 catalyst was shown to meet the productivity parameter to aromatics of 500 g/kgCat-hr but the selectivity towards aromatics was low due to the larger product distribution of ethane DHA.

Continued improvement of the zeolite synthesis was conducted. The zeolite synthesis was performed in a CEM MARS 6 Synthesis unit which is a parallel microwave synthesizer. It has a turntable which holds 12 Teflon lined vessels which can hold up to about 75 mL of volume each. The instrument controls the reaction via two temperature sensors, one fiber optic probe and one IR sensor. The pressure and power input were also tracked by the instrument software. The microwave synthesizer was used, rather than the conventional hydrothermal autoclaves, to speed up the synthesis process and increase yield per run. The conventional hydrothermal autoclaves method could take anywhere from a week and a half to two weeks using the autoclaves we currently have, whereas the MARS 6 synthesis can take 2-3 days. Depending on the number of vessels used the instrument has a maximum power available for it to reach the reaction conditions. Similar to the previous conventional hydrothermal synthesis a solution using the precursors, tetrapropyl ammonium hydroxide (TPAOH, 1 M in H_2O), sodium aluminate ($NaAlO_2$), tetraethylorthosilicate (TEOS), and water, were used. The precursor ratio of 0.25 TPAOH: 0.03 Al_2O_3: 1 SiO_2: 40 H_2O was used for the synthesis of these zeolites with a SAR of 33. The solutions were also stirred for 4 hours prior to being loaded into the reaction vessels.

A temperature/time matrix was developed to find the optimal conditions for synthesis in the new CEM MW unit, seen in Table 10. The temperatures 160, 180, and 200°C were chosen as they are consistent with conventional hydrothermal methods. For each of the reaction temperatures three reaction times of 30, 60, and 90 mins were used. For each of these methods two solutions were stirred for 4 hours and placed into two vessels with small stir bars which stir the solution while in the CEM unit. The CEM was set to ramp for 30 mins to the reaction temperature while followed by a hold step for either 30, 60, or 90 mins. Following the hold step the reactions were allowed to cool and depressurize within the CEM until the next day. Once the vessels were cooled enough the precipitate and the solution were collected, separated, washed, and dried. A centrifuge was used to separate the precipitate out of the solution. The samples were centrifuged three times for 10 minutes and 8000 rpm, pouring off the liquid each time and washing with deionized water between each centrifuge. Following the separation and washing the precipitate was dries in an oven at

100°C overnight. Finally, the powder was calcined in a muffle furnace and slowly heated to 550°C and held for 6 hours.

Table 10. CEM MARS 6 Zeolite Synthesis Matrix

Sample ID	Temperature (°C)	Time (mins)	Zeolite Yield (g) for two vessels
1	160	30	0.8994
2	180	30	5.3761
3	200	30	6.8826
4	160	60	4.8251
5	180	60	6.2703
6	200	60	7.3201
7	160	90	4.9866
8	180	90	6.2958
9	200	90	7.1440

During the optimization of the procedure the zeolites synthesized in the CEM were characterized using X-ray diffraction (XRD) to distinguish if the product had the characteristic peaks of ZSM-5. Each of the 9 samples showed good intensity in the XRD spectrum and clearly had the characteristic peaks of ZSM-5, seen below in Figure 27.

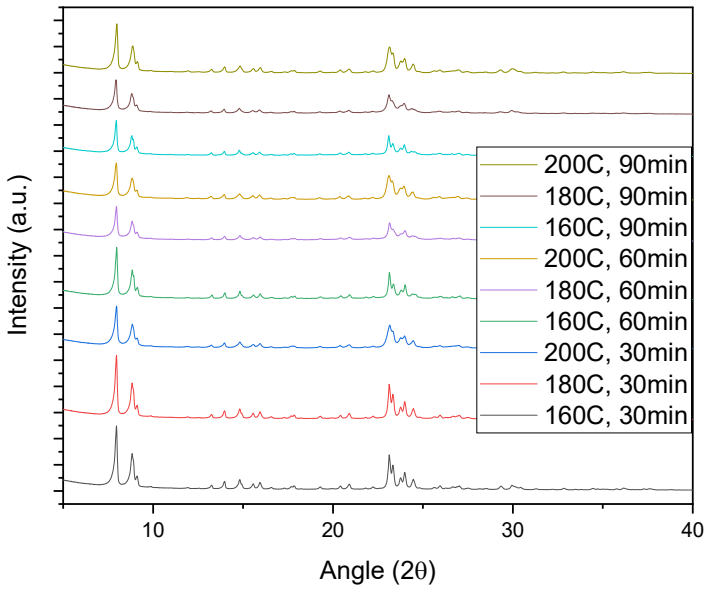

Figure 27. X-ray diffraction (XRD) patterns of CEM synthesis three different temperatures and times.

TEM was performed on each of the zeolites to characterize the uniformity among the zeolite crystalline particles for each of the reaction conditions. The size and shape of the zeolite crystals for sample 4 (160°C, 60 mins) are shown in Figure 28. Shown in figure 28a are sample 4's (160°C,

60 mins) TEM images showing a small cylindrical zeolite crystal with a diameter of about 600 nm in diameter. In figure 28b, the zeolite crystals can be seen stacking up on top of each other and are about 300 nm in width. In Figure 29 the SEM image of sample 4 shows uniform zeolite crystals. As the synthesis temperature was increased the zeolite showed more bunching of the crystalline particles in the TEM images, not shown here.

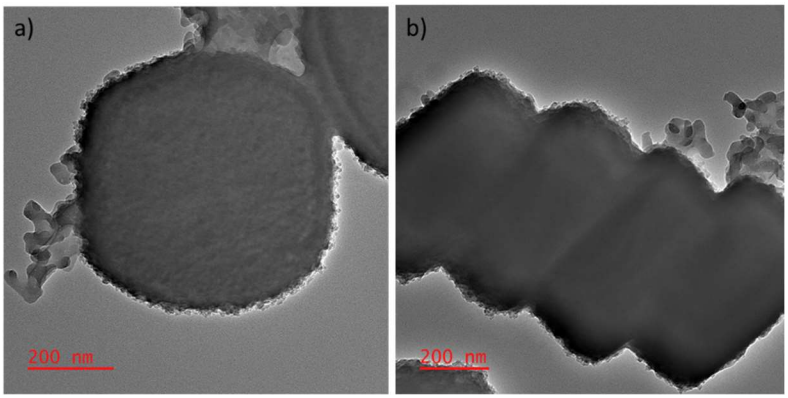

Figure 28. TEM images of Sample 4 – 160°C, 60mins synthesized in the CEM MW unit.

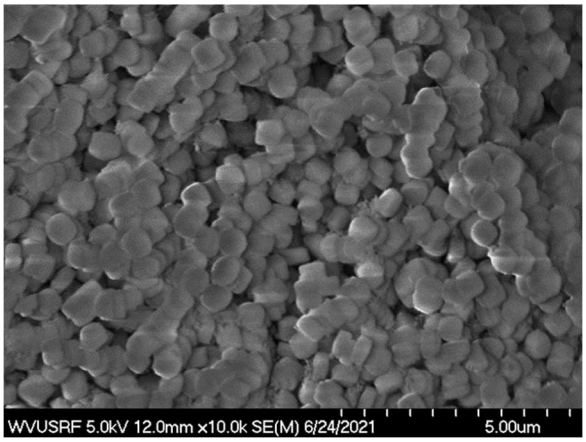

Figure 29. SEM image of Sample 4 – 160, 60 mins synthesized in the CEM MW unit.

Improvement of Synthesis Method for Zeolites and DHA catalysts (WVU)

The synthesized zeolites were characterized using SEM to investigate surface morphologies, size, and shape of the zeolite crystals. All the samples each showed the formation of the crystalline zeolite particles which were shaped like small cylindrical crystals. This was also represented by the BET surface area analysis among some of the zeolites in the matrix. It was seen that at higher

reaction temperatures and synthesis times there is an increase in agglomerations of the zeolite crystals. Shown in Figure 30 are some of the samples SEM images showing the agglomerations of the zeolite particles. This causes a decrease in surface area.

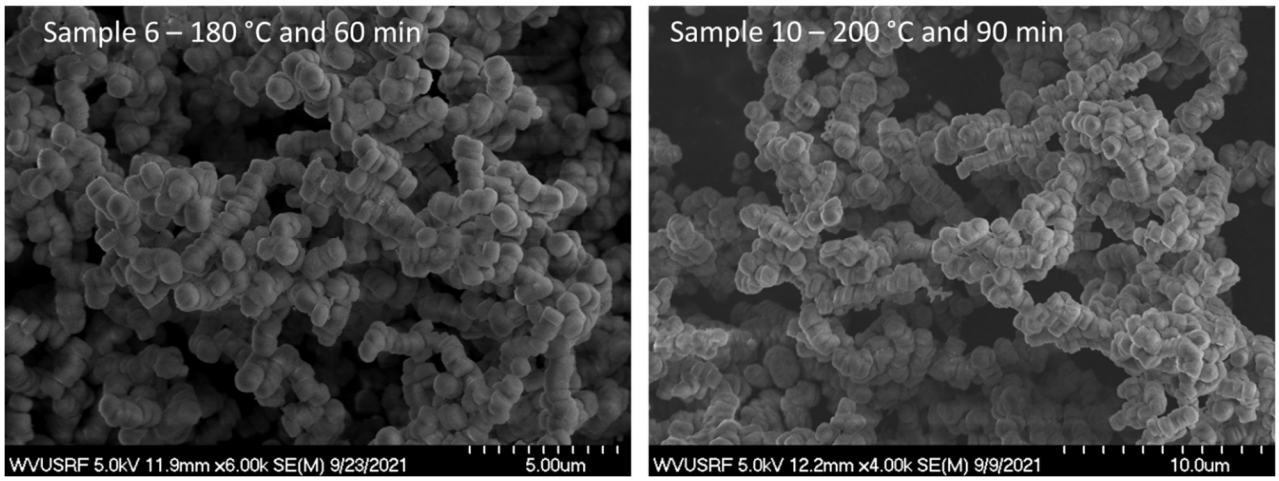

Figure 30. SEM image of Sample 6 - 180°C and 60 mins and Sample 10 - 200°C and 90 mins, showing some agglomerations of zeolite crystals.

The repeatability of the of the CEM MW Synthesizer was also tested by repeating the synthesis of the zeolites at specific temperatures and synthesis time. In Figure 31, the X-ray diffraction (XRD) patterns for the three samples 2, 2-1, and 2-2 can be seen. These three samples were all run at 160°C for 30 mins synthesis time. As seen by the XRD patterns each sample shows the characteristic peaks of ZSM-5 with good intensity. The similarity among the three can help confirm the reproducibility of the instrument for the synthesis of these zeolite supports.

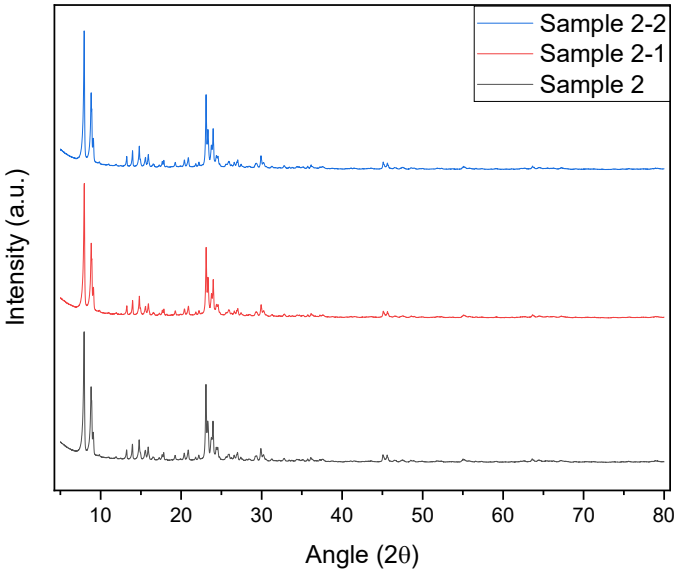

Figure 31. X-ray Diffraction (XRD) patterns of the three CEM synthesized zeolites samples ran at 160°C - 30mins.

These three zeolite samples were further characterized with the use of SEM and TEM. As seen in Figure 32, the SEM images of Sample 2, 2-1, and 2-2 are shown. They all show uniformly sized zeolite crystals with little to no agglomeration of the crystals. All three have crystals of similar size which shows the reproducibility of the CEM MW synthesizer. This was also seen in the TEM images not shown here.

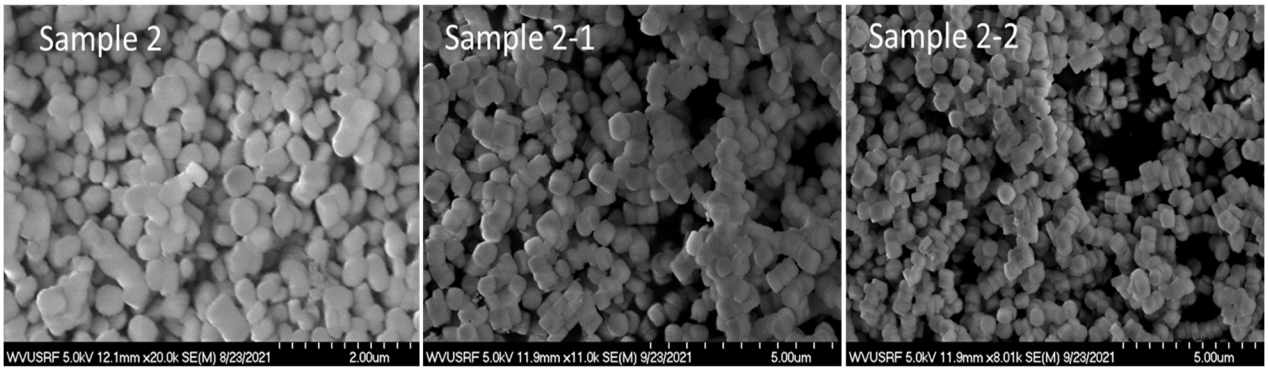

Figure 32: SEM images of Sample 2, 2-1, and 2-2, which were all at 160°C - 30mins.

We adjusted the Al_2O_3 content in the preparation of the solutions for the synthesis of the zeolites which allowed us to change the SAR. Currently, the matrix discussed above was performed using a SAR 33 solution, as it has been reliable and proven optimal for synthesizing zeolites in the autoclaves and the CEM so far. For the catalytic activity in a DHA we wanted to investigate the synthesis of zeolites with SAR 23 and 30, because lower SARs favor the production of aromatics.

So seen in Figure 33, the XRD patterns show that we were successful in forming ZSM-5 crystals for SAR 30 but not SAR 23. These were compared to SAR 33 and Sample 6 which were run at the same conditions of 180°C and 60 mins as SAR 30 and 23. These conditions were chosen because they had a high sample yield of precipitate in the previous matrix. SAR 23 may need the solution adjusted or the conditions of synthesis investigated. Also seen in Figure 34 are the SEM images of the SAR 23 and 30 compared to the SAR 33. It is also seen from these that the SAR 30 was successful in synthesizing a similar crystal structure and shape as the SAR 33.

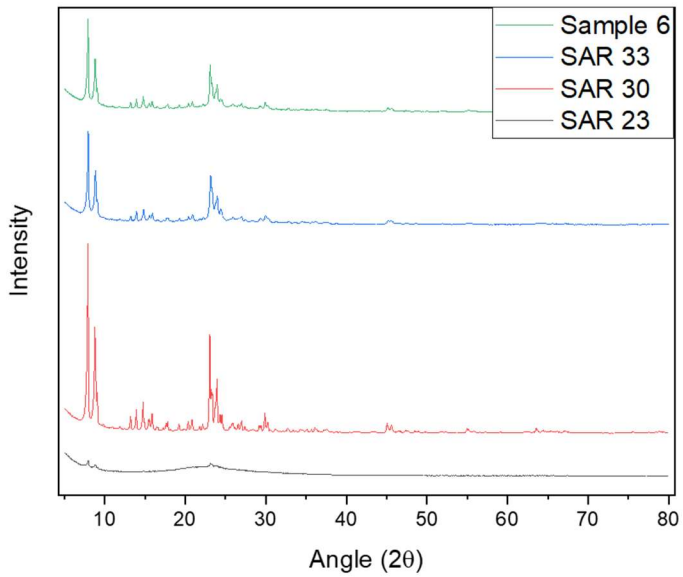

Figure 33. X-ray Diffraction (XRD) patterns of the different SAR CEM synthesized zeolites samples ran at 160°C – 30 mins.

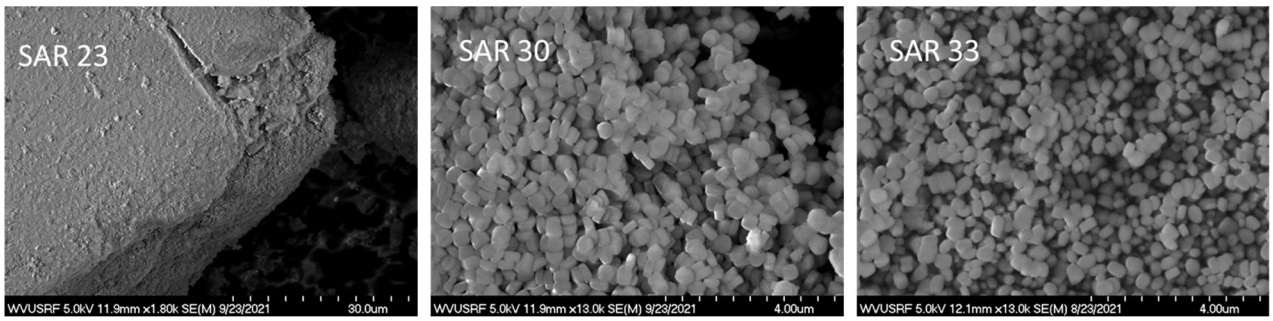

Figure 34. SEM images of the different SARs.

Recently, the CEM zeolites were loaded with 3% Mo and the activity testing was started. The zeolite showed little activity (not shown here), so we concluded further treatment post-synthesis is necessary to convert the CEM zeolites into the active form. Each raw zeolite (un-loaded) is

currently being treated with an ion exchange process which allows for Na-ZSM-5 to become NH_4-ZSM-5 form. A 1:10 ratio of zeolite to 1M NH_4NO_3 solution was made and heated to 90°C for 90 mins and this was repeated three times. Between each wash the solution was filtered out via vacuum a filtration set-up and dried prior to re-washing. Following the three repeated washed the zeolite was dried and then calcined in a muffle furnace 550°C for four hours to become the H-ZSM-5 form.

Subtask 2.4: C2-DHA catalyst synthesis, characterization and testing

Then dehydroaromatization occurs when ethane/ethylene goes through the DHA bed. The production of water in the OCM causes the issue in the following C2-DHA bed, as it would favor the steam reforming of C2 hydrocarbons and restrain the dehydroaromation. Although we added a water-removal bed in the earlier design and got an 8.2% benzene yield, the regeneration of the water-removal bed makes the process complicated, and the limited lifetime of the water-removal bed determine the overall lifetime of the entire sequential packed bed. Therefore, we focused on developing a steam resistant C2-DHA catalysts to replace the previously reported GaPt/HZSM5.

According to literature review and basic knowledge in zeolite, we hypothesize that Ga-in-framework HZSM-5 (denoted as HGaAlMFI) and P/Ga/modified HZSM-5 have the good ethane DHA performance and water-resistant property. HGaAlMFI was synthesized following the procedure in a published paper [13]. P/Ga/HZSM-5 was prepared by loading 0/4% P and 2% Ga using incipient wetness impregnation method onto the commercial HZSM-5.

Figure 35 shows that both catalysts achieved the ethane conversion of ~45%. HGaAlMFI produces 0.3 ml/min benzene while P/Ga/HZMS-5 produces 0.4 ml/min, equivalent to benzene yield of 4.5% and 6%. Compared to HGaAlMFI, P/Ga/HZMS-5 produces more methane and less hydrogen. However, when these two catalysts were applied in the OCM + C2-DHA route, the yield of benzene over P/Ga/HZSM-5 is less than HGaAlMFI, as shown in Figure 35. The water produced in OCM step has little effect on the following DHA. However, water from OCM induced steam reforming of methane and ethane over P/Ga/HZSM-5, reducing the production of benzene in DHA. It can be verified by the fact that methane conversion remains a plateau from 122 to 128 min over

OCM + P/Ga/HZSM-5, different from OCM + HGaAlMFI, over which methane conversion drops consistently from 15 to 20 min due to the consumption of oxygen in OCM catalyst. The increase in CO_2 amount in also indicates P/Ga/HZSM-5 favors the steam reforming and water-gas shift reaction. Therefore, we report HGaAlMFI as a promising catalyst to be used in the OCM + C2-DHA route because of its relatively high benzene yield and water-resistance.

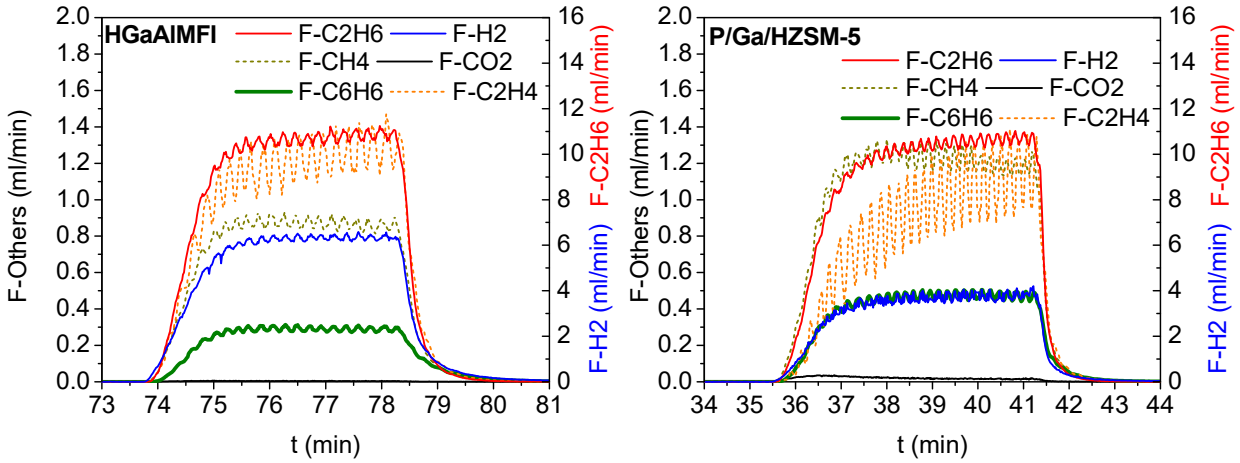

Figure 35. Ethane dehydroaromatization tests over HGaAlMFI and P/Ga/HZSM-5. 0.8 g catalysts at 700 °C, feeds are 20 ml/min ethane and 5 ml/min Ar.

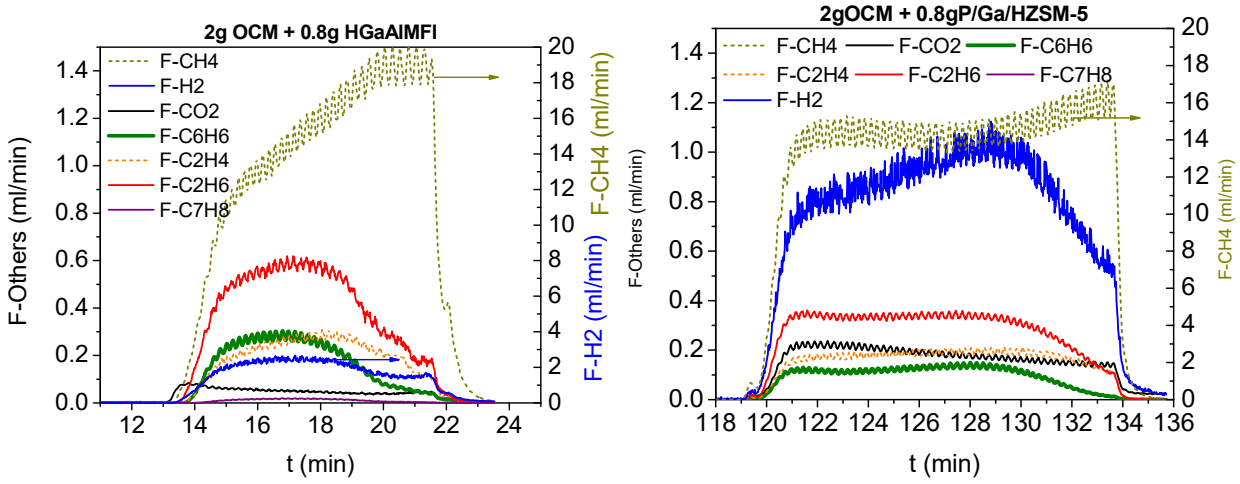

Figure 36. Methane dehydroaromatization tests in OCM + C2-DHA strategy. 2g OCM + 0.8g C2-DHA at 700 °C, feeds are 20 ml/min methane and 5 ml/min Ar.

Investigation of SHC effect on C2-DHA in the sequential bed

We evaluated the effect of SHC catalyst on the DHA of ethane by studying four cases using different packed bed configures: (1) single DHA bed; (2) DHA + SHC sequential bed; (3)

DHA/SHC mixture single bed and (4) DHA/SHC + DHA sequential bed. In these cases, 0.8g HGaAlMFI was used for DHA and 0.4g $Na_2WO_4/CaMnO_3$ was used for SHC. Compared to the case with single DHA bed in Figure 37a, SHC in the following bed combusted ~75% H_2 produced from DHA before the oxygen in the SCH was consumed, as shown in Figure 37b. The combustion of H_2 coincided with the formation of CO_2, indicating SHC, although selectively combust H_2, could also combust a small portion of hydrocarbons. When mixing DHA and SHC (Figure 37c), only 50% H_2 was combusted, and more CO_2 was formed. In consideration the formation of water by hydrogen combustion in case 3, the relatively stable benzene yield in the cases of with and without SHC verifies that HGaAlMFI is a water-resistant catalyst for C2-DHA. In Case 4, when an additional 0.8 g DHA bed was applied after the DHA/SHC mixture bed, the benzene flow rate increased from 0.3 ml/min to 0.35 ml/min.

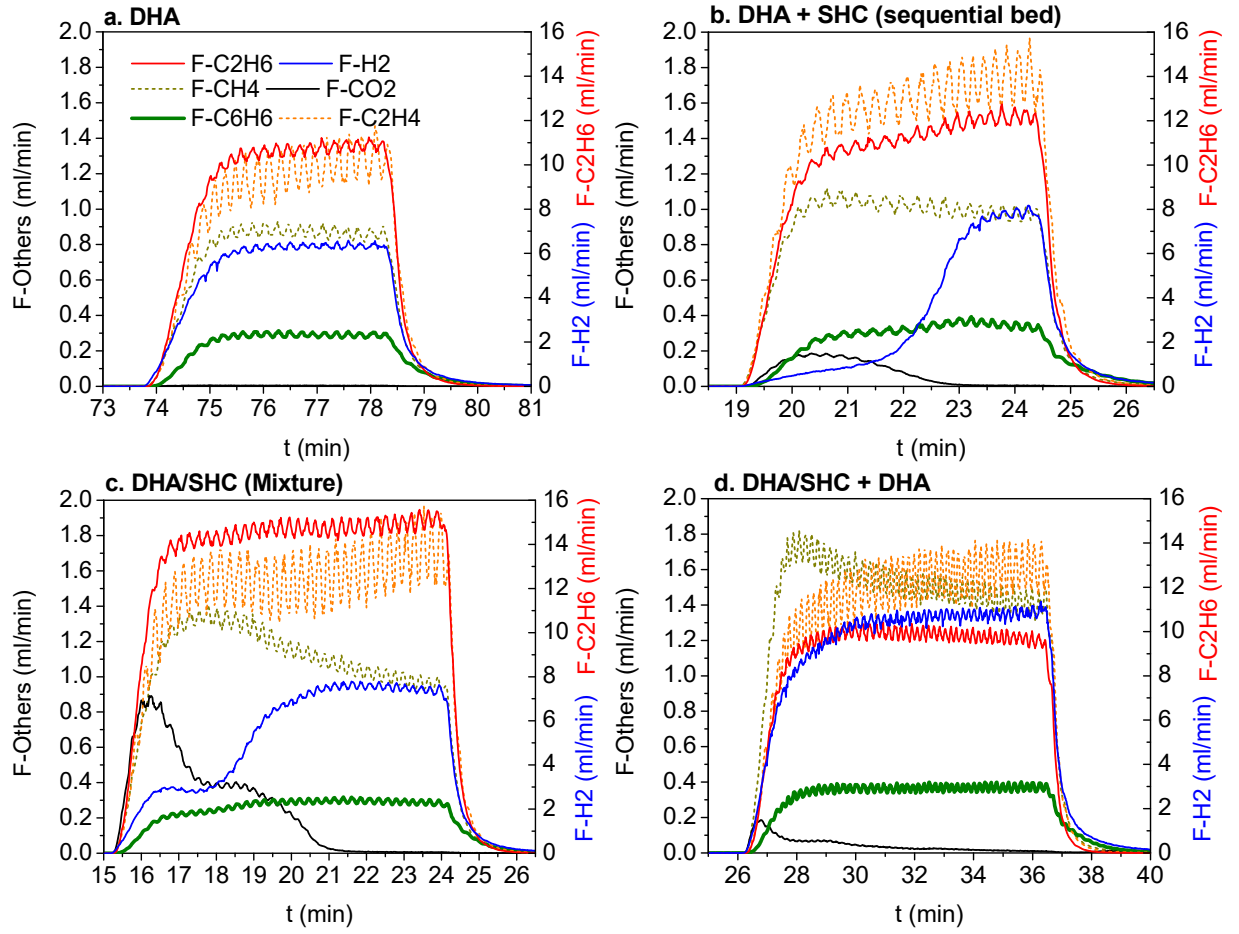

Figure 37. Investigation of SHC effect on ethane dehydroaromatization. In each case, 0.8g HGaAlMFI was used for DHA and 0.4g Na2WO4/CaMnO3 was used for SHC at 700 °C, the feeds are 20 ml/min ethane and 5 ml/min Ar.

The test of methane DHA using OCM + DHA route was also carried out in two cases, in which DHA bed is compose of: (1) DHA catalyst only, or (2) DHA/SHC mixture. In Figure 38a of Case 1 (the same result adopted from Figure 38a), 2 mL/min H_2 was produced, while in Figure 38b of Case 2, the H_2 flowrate drop to less than 0.2 ml/min. SHC in this route could combust more than 90% H_2. In Figure 38a, it shows that even without SHC, a maximum benzene flow rate of 0.3 ml/min can be obtained, comparable to Case 2 with SHC, which is equivalent to a benzene yield of 9%. It further proves that HGaAlMFI as a C2-DHA catalyst is water resistant. It is noteworthy that, without SHC, there is about ~0.7% toluene (C_7H_8) in the product, whereas in the case of with SHC, only trace amount toluene can be detected. It could be because SHC catalyst is selective to H_2 over benzene but not toluene, which need further verification. It is possible that the toluene produced in DHA was combusted by SHC, which could explain the high amount of CO_2 observed in Case 2. Considering that toluene is also an important aromatic product we expect, it would be beneficial to configurate the OCM + DHA sequential bed without SHC component in this strategy.

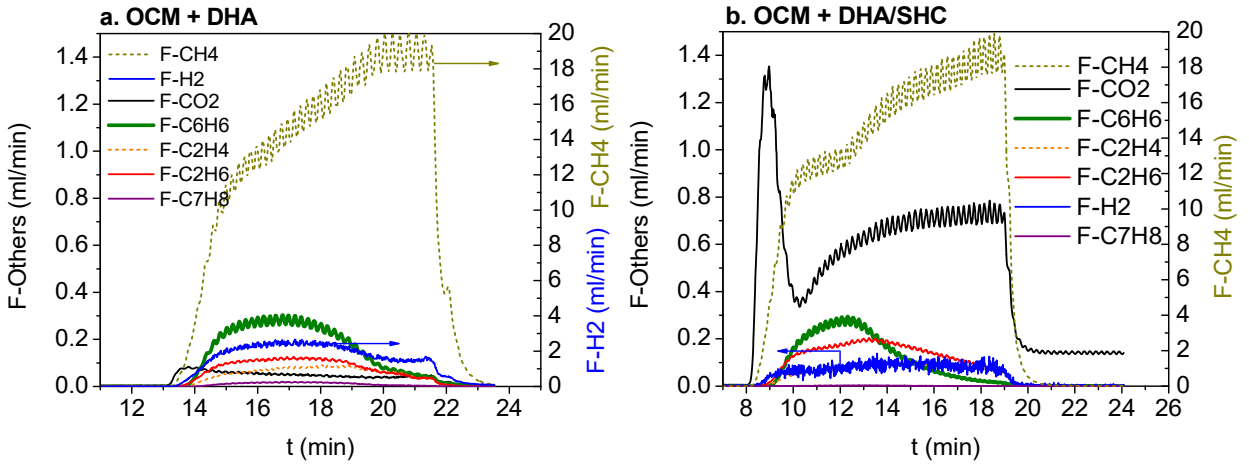

Figure 38. Investigation of SHC effect on ethane dehydroaromatization in OCM + DHA route. 0.8g HGaAlMFI was used for DHA and 0.4g $Na_2WO_4/CaMnO_3$ was used for SHC at 700 °C, feeds are 20 ml/min methane and 5 ml/min Ar.

Improvement of Synthesis Method for Zeolites and DHA catalysts (WVU)

For the catalytic activity in a DHA, we wanted to investigate the synthesis of zeolites SAR 23 and 30, because the lower the SAR the better it has been in the production of aromatics. In the early testing of this, we were able to successfully synthesize zeolite with a SAR of 30 but the SAR 23 samples are still being changed.

Prior to the catalytic testing, the samples' acidity was investigated using NH_3 temperature-programmed desorption experiments. The temperature-programmed desorption of ammonia (NH_3-TPD) was conducted using a Micromeritics ASAP-2020 unit equipped with a thermal conductivity detector (TCD). The powdered synthesized zeolite was measured out and 0.1g loaded into a quartz u-tube. Once loaded into the instrument, the catalyst was heated 10°C/min to 300°C under helium and held for 2 hrs to dry the powder. The temperature was then cooled to 100°C, where the catalyst was then exposed to 15% ammonia at 30 mL/min balanced in helium for 30 mins. Following the dosing, the system was then purged out under helium. The catalyst was heated 20°C/min to 800°C to obtain the ammonia desorption profiles seen below in Figure 39. As seen in Figure 39 and Table 11, the 200°C samples all showed the highest strong to weak acid site ratio (S/W), this indicated the strong acid sites produced by the synthesis at 200°C.

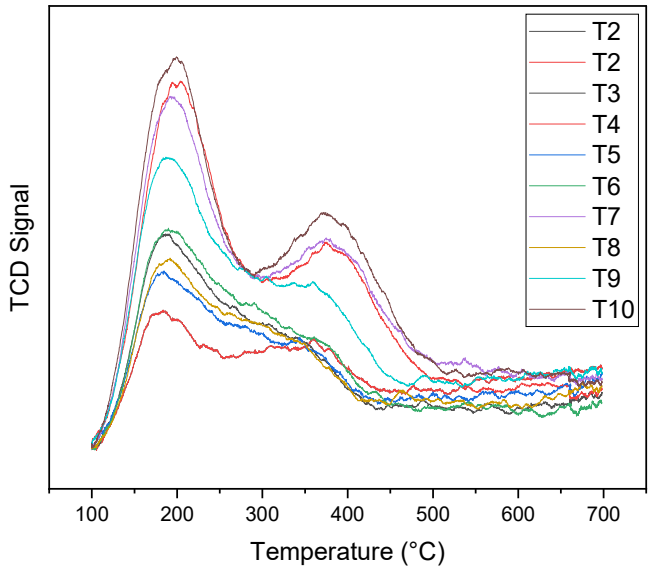

Figure 39. Ammonia temperature programmed desorption profiles of the 9 treated MW synthesized zeolite samples.

Table 11. MW Synthesized Zeolite Ammonia TPD

Sample ID	Temp. (°C)/ Time (mins)	Strong/Weak	SAR from ICP
2	160, 30	0.43	66
3	180, 30	0.31	31
4	200, 30	0.45	32
5	160, 60	0.34	35
6	180, 60	0.37	31
7	200, 60	0.48	33
8	160, 90	0.34	33
9	180, 90	0.44	31
10	200, 90	0.64	34

Each of the 9 different samples from the temperature and synthesis time matrix, seen in Table 12, were loaded with 3%Mo via incipient wetness impregnation method. The reaction performance of each 3%Mo loaded synthesized zeolite was tested in an automated micro-reactor fixed bed (MRFB). For each experiment, 0.3g of the fresh metal-loaded catalysts was loaded into the quartz u-tube of the MRFB. The catalyst was then heated to 625°C under 30 mL/min of nitrogen flow. Once the temperature equilibrated, the gas was switched to a mixture of 30% ethane in nitrogen and held for 2 hours. The ethane conversion of the catalysts at 30 mins TOS can be seen in Table 12. As indicated by a star (*), the conventionally synthesized zeolite catalyst (Con) and the three 200°C microwave synthesized zeolite catalysts, which showed the highest conversion and total aromatic selectivity at 30 min TOS. The three microwave 200°C synthesized catalysts, i.e. Sam 4, 7, and 10, showed a significant improvement in conversion in comparison to the 160 and 180°C synthesized samples. This is a possible indication that the synthesis of well-structured, crystalline zeolites is more complete at the 200°C synthesis temperature rather than the other temperatures. Also, the 200°C synthesis temperature samples are more comparable with that of the conventional hydrothermally synthesized zeolite-supported catalyst with the same SAR.

Table 12. Synthesized Zeolite Ethane Conversion and Aromatic Selectivity.

Sample ID	Synthesis Temperature (°C)	Synthesis Time (mins)	Ethane Conversion at 30 mins TOS (%)	Total Aromatic Selectivity at 30 mins TOS (%)
Con.	160	5760	36.1*	23.4*
2	160	30	19.6	9.11

3	180	30	13.4	3.74
4	200	30	33.1*	23.2*
5	160	60	16.0	4.24
6	180	60	12.4	4.97
7	200	60	29.3*	21.5*
8	160	90	11.0	3.48
9	180	90	21.4	15.1
10	200	90	31.0*	22.6*

As stated previously, the 200°C synthesis temperature has the highest conversion compared to the other synthesis temperatures (160 and 180°C), as seen in Table 12. The 30 mins TOS conversion was chosen to avoid the induction period seen in the first 20 mins of the reaction in Figure 40. The Con sample had the highest ethane conversion over the course of the 2-hour and the 200°C, 30 mins sample had the second highest conversion. Further investigation of the product stream can be seen in the Figure 41 selectivity plot.

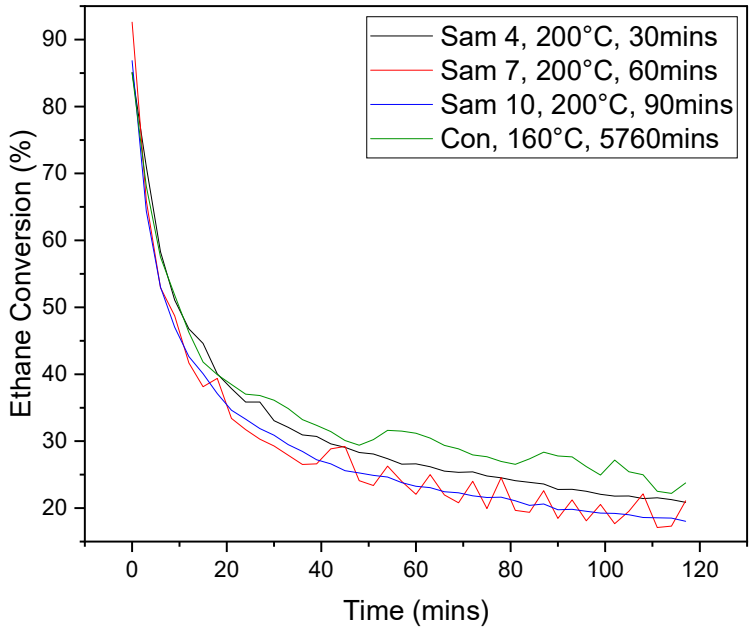

Figure 40. Ethane conversion (%) for conventionally synthesized zeolite supported catalyst, Con, and the three microwave synthesized zeolite supported catalysts, Sam 4, 7, and 10, over the 2-hrs reaction period at 625°C.

The methane, ethylene, benzene, and toluene selectivity of each of the four samples is shown in Figure 41. The two catalysts which had the highest conversion, Con and Sam 4, both are the most

selective to aromatics when compared to the other two samples. The Sam 4 - 200°C, 30min exhibited the best overall total aromatic selectivity, not shown here. When Sam 4 is compared to the other two microwave synthesized zeolites, Sam 7 and 10, Sam 4 has higher conversion and aromatic selectivity. This can be partially explained by the increase in surface area Sam 4 exhibited in the SEM images in Figure 42d compared to the agglomerated Sam 7 and 10, Figure 42 e and f, respectively. BET surface area analysis is being performed currently.

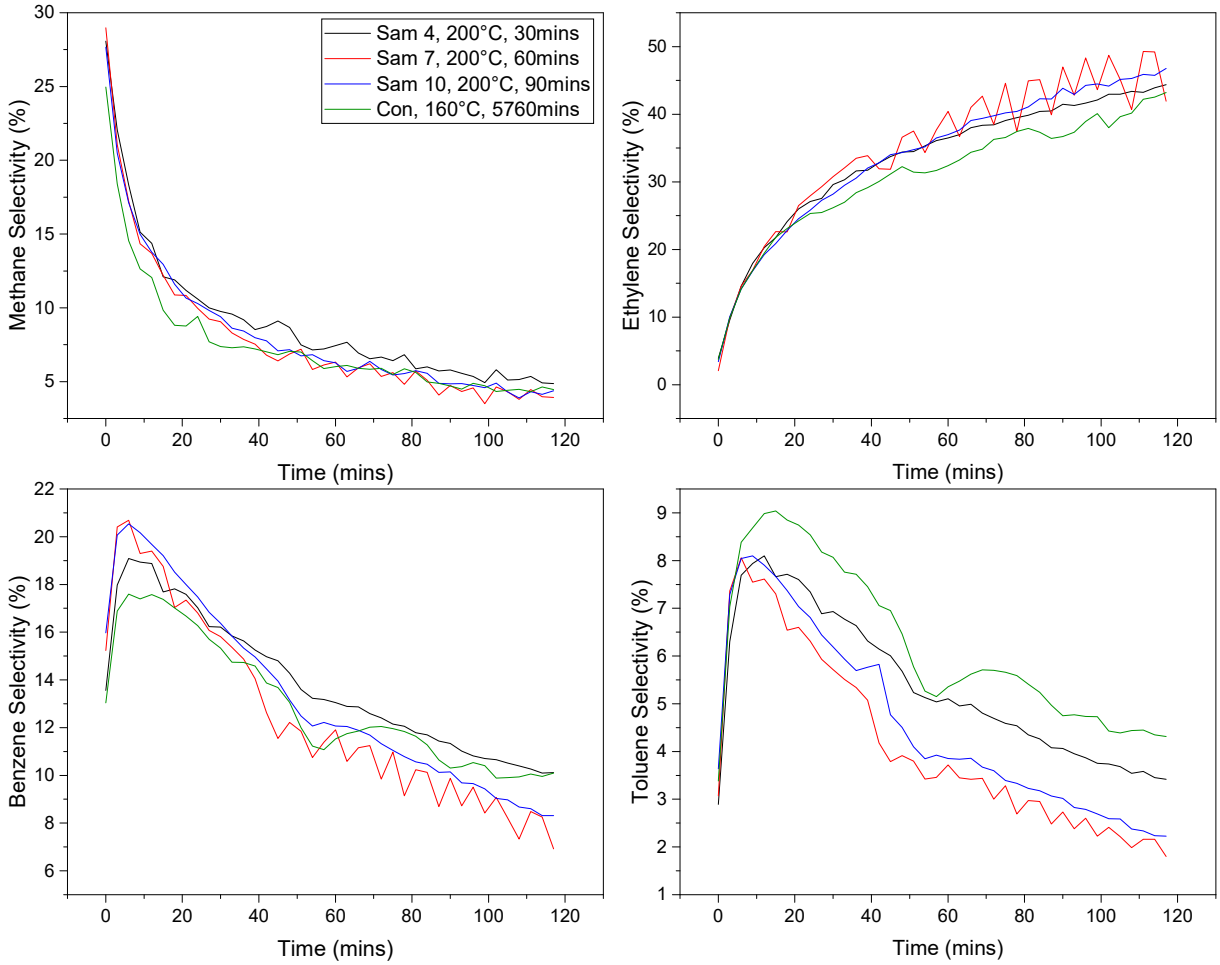

Figure 41. Comparison of the product selectivity for the Con, Sam 4, 7, and 10, catalysts in a conventional fixed bed at 625°C for 2-hrs; (a) methane selectivity, (b) ethylene selectivity, (c) benzene hydrocarbon selectivity, and (d) toluene selectivity.

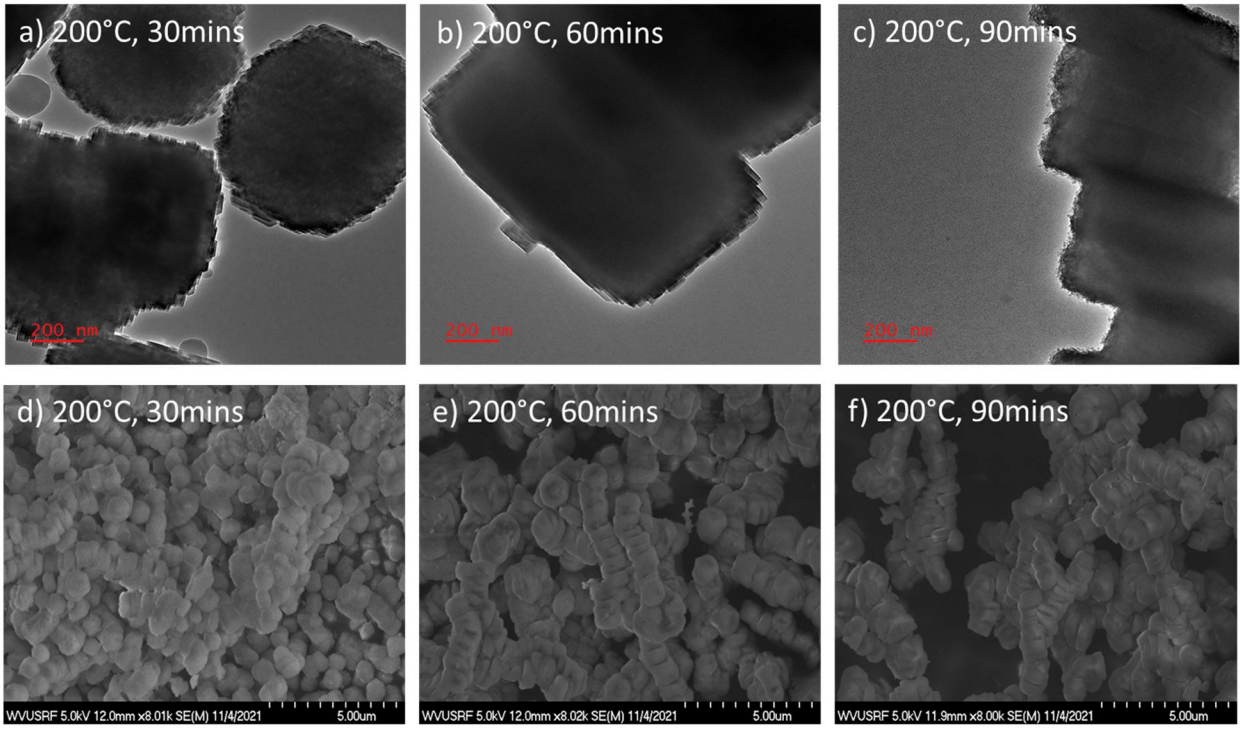

Figure 42. TEM images of Samples 4, 7, and 10, all 200°C synthesis temperature and 30-, 60-, and 90-mins synthesis time. TEM Images: (a) 200°C, 30mins (b) 200°C, 60mins (c) 200°C, 90mins and SEM Images: (d) 200°C, 30mins (e) 200°C, 60mins (f) 200°C, 90mins.

Thermogravimetric analysis of the coke formation after the 2-hour ethane dehydroaromatization reaction was performed. The weight loss due to coke for the Sam 4, 7, and 10 was 7.49, 7.56, and 7.75%, respectively, shown in Figure 43. For the microwave synthesized samples, the increasing synthesis time showed to have a slight increase in coke formation across the 2-hours. Also, the 60- and 90-min synthesis time exhibited a shift in the DTA curve towards higher burning coke. This higher burning coke is considered to be poly-aromatic rather than amorphous.

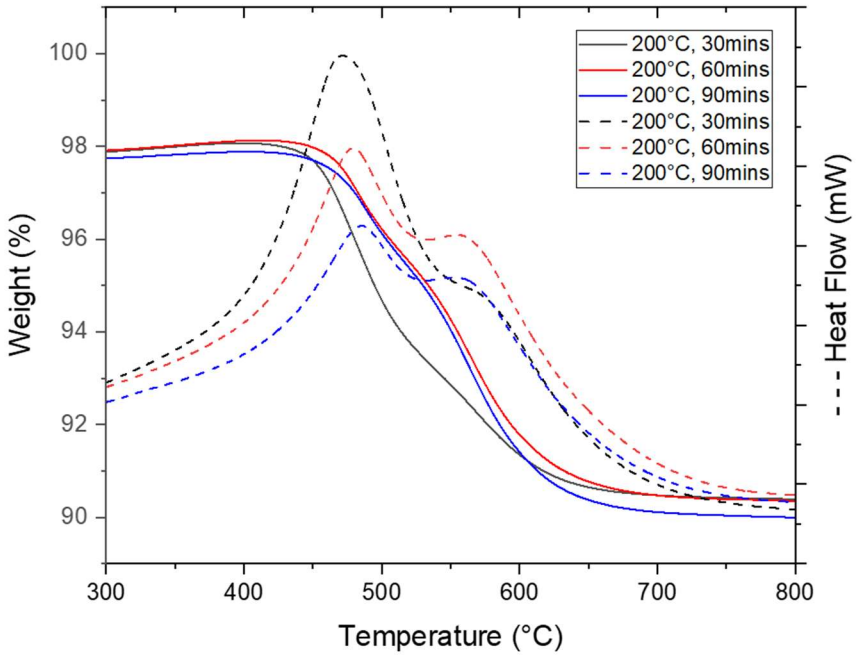

Figure 43. Thermogravimetric analysis (TGA) and differential thermal analysis (DTA) of the Con, Sam 4, 7, and 10, after the 2-hour reaction.

Further investigation into the explanation of the catalytic performance tests of the conventionally and microwaved synthesized zeolites is currently being conducted, such as TEM imaging of spent samples, acidity testing of fresh catalysts, and surface area analysis of the fresh samples. But from what can be seen here, the synthesis temperature and time of the zeolite synthesis in the microwaves has an effect on the catalytic activity of the zeolite support. Also, this study confirms that the two synthesis methods can make comparable zeolite support, which performs similarly for the ethane dehydroaromatization reaction.

Following the reaction testing, further investigation into shorter synthesis time of 15 mins, higher temperature of 220°C, and different stir times was performed. The additional samples were characterized using SEM, TEM, XRD, all not shown here. They showed similar uniformly shaped zeolite crystals. Two of the samples were synthesized at 200°C and 30 mins but stirred for 4 and 24 hours. The 24-hour stirred sample showed some slightly smaller crystal size compared to the 4 hour stirred sample. Also, another two of the samples were synthesized at 220°C with 4 hours stirring and different synthesis time, 15 and 30 mins. The less time led to slightly smaller crystals.

Adaption of conventional synthesis to microwave-assisted method (WVU)

We adapted the conventional hydrothermal synthesis that NCSU used to synthesize the HGaAlMFI catalysts to be applicable to the microwave synthesizer unit. The current conventional synthesis procedure called for the synthesis of the catalyst in the oven in autoclaves at 170°C for 72 hours. In order to adapt this method into the microwave synthesizer, the same solution preparation was used but the synthesis temperature was increased to 220°C and only 30 mins of synthesis time. This decrease in synthesis time increases the product efficacy of the synthesis because from 2 vessels, same solution prep, the microwave synthesized ~8 grams of the HGaAlMFI catalyst in less time than conventionally. This sample was then dried, calcined, and treated with a very similar process to the conventional method. Followed by the final drying and calcination, giving the final HGaAlMFI catalyst. The conventional HGaAlMFI has been characterized using ICP-OES and has 1.59 wt.% Ga, 42.6 wt.% Si, 1.35 wt.% Al (SAR 60.7). The microwave HGaAlMFI is currently being tested in ICP.

Seen in Figure 44, the XRD pattern of the microwave synthesized showed the characteristic peaks of ZSM-5 with no distinct peaks from the gallium species in the catalyst. This indicates the gallium is well incorporated into the structure and well dispersed. In Figure 45, the SEM images of the conventionally synthesized HGaAlMFI in (a) & (b) and the microwave synthesized HGaAlMFI in (c) and (d). The SEM images show that shape and uniformity of the zeolite crystals from the conventional synthesis and the microwave synthesis are very similar. However, the conventional synthesis did result in slightly smaller sized crystals compared to the microwave synthesis. DHA reaction testing is currently being performed on the microwave synthesized catalysts too.

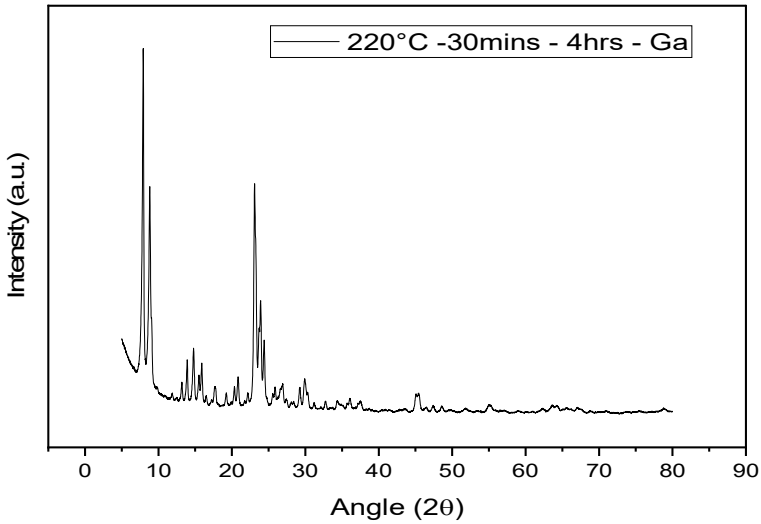

Figure 44. XRD pattern of Microwave-HGaAlMFI catalyst.

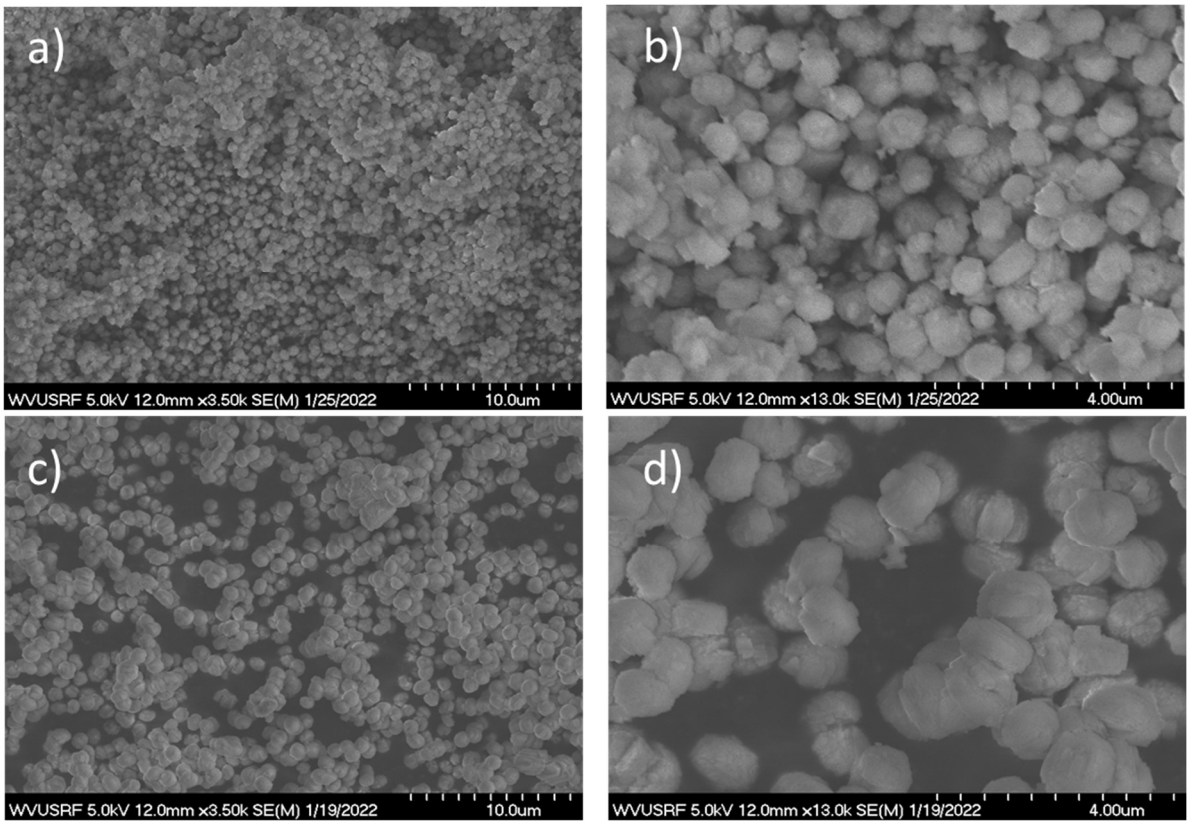

Figure 45. SEM images of the HGaAlMFI synthesized zeolite catalysts (a) & (b) Conventional HGaAlMFI and (c) & (d) Microwave HGaAlMFI.

From the synthesis method reported in literature of the HGaAlMFI catalyst an adapted synthesis method for the microwave synthesizer was created. Like the matrix of synthesis conditions for the

microwave synthesized H-ZSM-5, the optimal conditions from that study of 200°C and 30 mins were the main area of focus when the synthesis of HGaAlMFI begun. The different synthesis temperatures of 200 and 220°C and the different synthesis time 15 and 30 mins of the microwave-HGaAlMFI samples are seen in Table 13. The two additional samples Si/Ga=30 and Si/Ga=50 are samples which NCSU synthesized following the procedure from the literature reference but with the Si/Ga ratio altered to be 30 and 50, respectively. Each sample was tested using Inductively Coupled Plasma-Optical Emission Spectrometer (ICP-OES) to confirm the elemental composition of the as-prepared fresh catalyst. The samples were prepared by a sodium peroxide fusion followed by acid digestion. Following the calcination of the fresh powder catalysts, 0.1g of each sample was fused with sodium peroxide. The fuse was then dissolved in a dilute nitric acid/hydrochloric acid solution. The sample elemental analysis was performed in an Agilent 720 ICP-OES. The microwave samples showed similar ICP results across the different synthesis conditions with come slight differences. These differences between microwave samples can be explained by the potential affect the synthesis conditions have on the samples. The sample 1 and 1a are from the same batch and so even from sample-to-sample ICP results can be slightly different. However, the Si/Ga 30 and 50 samples do show some significant differences in the expected Si/Ga ratio and the actual ICP Si/Ga. This could be something from the synthesis or post-synthesis treatment. This is still being investigated now. Also we are currently attempting to confirm the elemental composition of the Ga, Al, and Si potentially by solid-state NMR.

Table 13. Microwave Synthesis Conditions of the HGaAlMFI Samples and ICP results

Sample ID	Synthesis Temp. (°C)	Synthesis Time (mins)	Ga%	Si%	Al%	Si/Al	Si/Ga	Si/(Al+Ga)
1 - HGaAlMFI	220	30	2.1	26.6	1.7	29.8	31.6	20.3
1a - HGaAlMFI	220	30	2.1	30.2	1.7	34.0	35.6	23.0
2 - HGaAlMFI	220	15	1.9	37.9	1.7	43.8	49.5	30.4
3 - HGaAlMFI	200	30	2.0	35.2	1.8	37.8	43.3	26.3
Si/Ga = 50	170	72 hours	1.1	41.6	1.6	49.2	92.5	38.9
Si/Ga = 30	170	72 hours	1.8	41.1	1.7	47.3	54.9	33.4

In addition to ICP testing, a temperature-programmed desorption of ammonia (NH_3-TPD) was conducted using a Micromeritics ASAP-2020 unit equipped with a thermal conductivity detector (TCD). The powdered catalyst was measured out and 0.1g loaded into a quartz u-tube. Once loaded into the instrument, the catalyst was heated 20°C/min to 700°C under helium and held for 2 hrs to

dry the powder. The temperature was then cooled to 100°C, where the catalyst was then exposed to 15% ammonia at 30 mL/min balanced in helium for 30 mins. Following the dosing, the system was then purged out under helium. The catalyst was heated 20°C/min to 700°C to obtain the ammonia desorption profile. In Figure 46, the ammonia temperature desorption profiles for the different HGaAlMFI samples are shown. The MW HGaAlMFI samples have a higher overall acidity compared to the Si/Ga 30 and 50 samples, which is consistent with the expectation based on the precursor ratio of the synthesis.

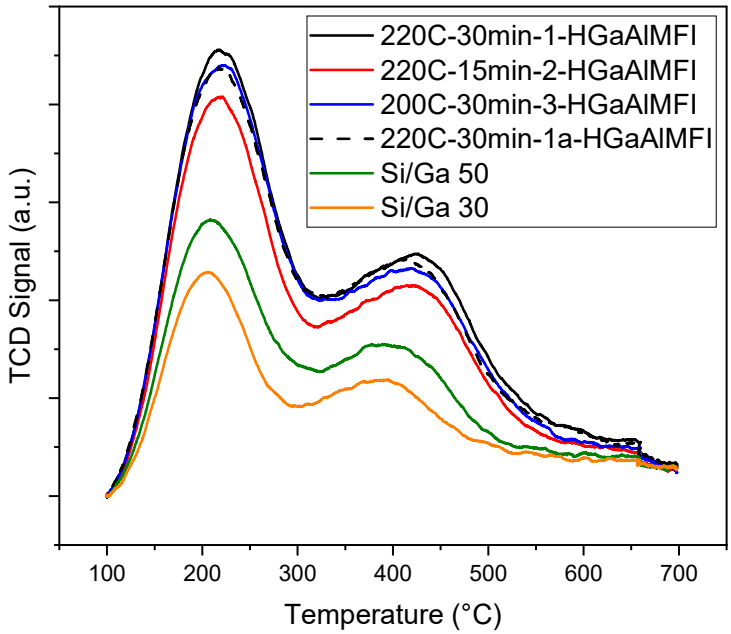

Figure 46. Ammonia temperature programmed desorption (NH_3-TPD) profiles of the different HGaAlMFI samples.

The catalytic performance testing of the microwave synthesized HGaAlMFI samples was performed. Three reaction feeds were chosen to determine the catalytic activity of the microwave HGaAlMFI samples: (1) 10% Ethane in N_2, (2) 10% Ethylene in N_2, and finally (3) 10% of each (10%Ethane and 10%Ethylene) in N_2. These reactions were performed at 700°C for 60 mins each with 0.5g loaded into the u-tube reactor setup. A total gas flow of 30 mL/min was used and the gas hourly space velocity was 3600 mL/h/gcat. Each of the outlet component flowrate plots for each of the reactions are seen in Figure 47. For the 10% Ethane in N_2 reaction, the product distribution is consistent with the expected performance of a metal-loaded zeolite for ethane DHA. For the 10% Ethylene in N_2 reaction, there is a delay in the production of benzene until about the 15 min mark.

This could be because for the first 15 mins the ethylene is being heavily converted straight to and as the reaction proceeds the catalysts starts to deactivate. The reaction with ethylene only also did have about an 11% weight loss due to coke. This reaction is being repeated to determine if this is a consistent trend and not just an issue with the reactor setup. For the 10% of each (10%Ethane and 10%Ethylene) in N_2 reaction, the addition of ethylene to the ethane feed lowered the H_2 production over the course of the reaction. Also, the addition of ethylene to the ethane also shifted the ethane reaction to produce more coke.

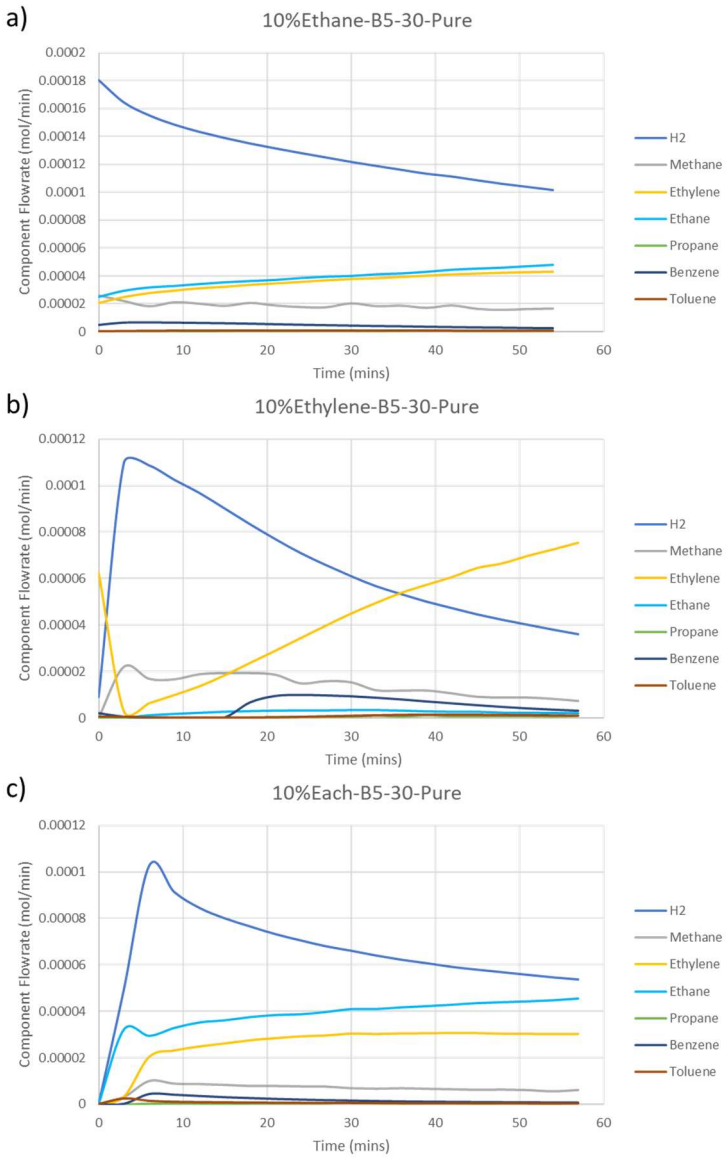

Figure 47. Catalytic performance testing of the microwave HGaAlMFI samples under three different reaction feeds: (1, a) 10% Ethane in N_2, (2, b) 10% Ethylene in N_2, and finally (3, c) 10% of each (10%Ethane and 10%Ethylene) in N_2.

To better understand the second bed in this sequential bed strategy. i.e. C2-DHA, we studied the conversion of ethylene and ethane over C2-DHA, as they are the main products from the first catalyst bed (OCM). In the earlier tests, OCM catalyst achieved an approximate 20% methane conversion with 7.5% ethane yield and 7.5% ethylene yield. In addition, we verified that methane did not get involved in the reaction on C2-DHA. Therefore, we blended the gases with following flow rates to simulate the reactive gas mixture which are produced from the OCM catalysts: 4 ml/min C_2H_6 + 4 ml/min C_2H_4 + 42 ml/min Ar. In separate scenarios, 4 ml/min C_2H_6 + 46 ml/min Ar and 4 ml/min C_2H_4 + 46 ml/min Ar were also tested to study the cases with ethane and ethylene alone. To study the effect of Ga loading on the performance of C2-DHA, HGaAlMFI zeolites with two Ga loadings, i.e. Si/Ga = 30 and 50, were prepared and tested at 700 °C under 1 atm pressure.

Figure 48b shows a gradual increase in ethylene, benzene and toluene flow rates, in accordance with the observation in Figure 47b. This is probably because ethylene was activated on (or activating) the catalyst first, and then produce aromatics. When the flow rate of ethylene feed was low, the small dose of ethylene would correspond to a delay in the observation of ethylene and aromatics signals. This surface species could be either coke or other intermediates which are retained on the catalyst. For instance, Wang et al proposed a hydrocarbon pool mechanism for the propane aromatization on Ga/ZSM-5 catalyst [14]. It is possible that, in this case, ethylene was also converted to hydrocarbon pool and then aromatics are produced.

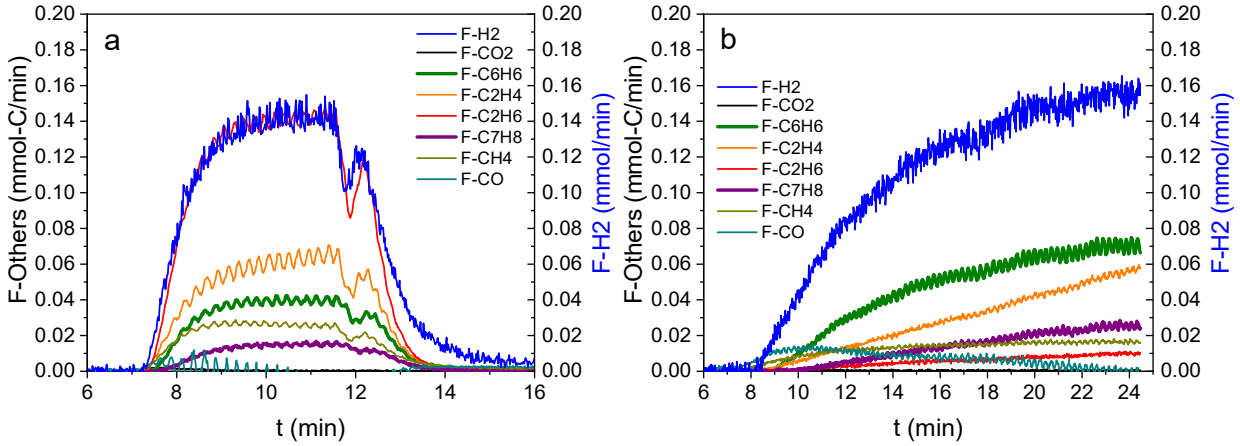

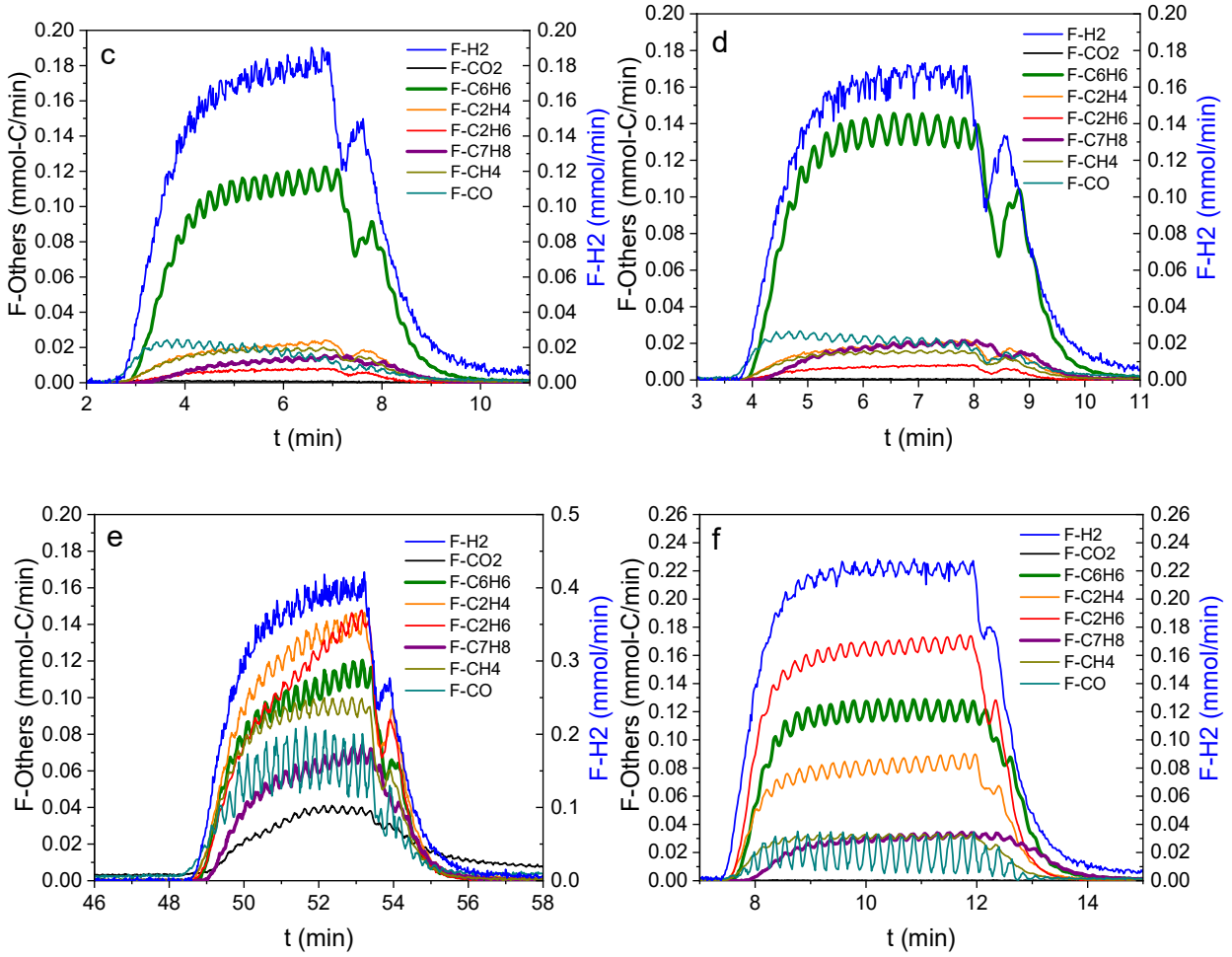

Figure 48. (a) C_2H_6 and (b) C_2H_4 conversion on HGaAlMFI zeolite with Si/Ga = 30; (a) C_2H_6 and (b) C_2H_4 conversion on HGaAlMFI zeolite with Si/Ga = 50; C_2H_6/C_2H_4 mixture conversion on HGaAlMFI zeolite with (e) Si/Ga = 30 and (f) Si/Ga = 50. Reaction condition: 700 ºC, 1 atm.

The catalyst test results are summarized in Table 14. For both catalysts, C_2H_4 is easier to aromatize than C_2H_6, as the yield of C_6H_6+C_7H_8 are higher when the feed is C_2H_4. The zeolite with lower Ga loading (Si/Ga = 50) is beneficial for the production of aromatics, possibly due to two reasons: (1) For C_2H_6 conversion, higher Ga would results in higher amount of surface Ga, which was not successfully incorporated in the zeolite framework. This type of Ga favors the dehydrogenation of ethane to form ethylene, as can be compared in Table 14 that 16.8 % of C_2H_4 were produced on HGaAlMFI (Si/Ga = 30) while only 5.9 % of C_2H_4 on HGaAlMFI (Si/Ga = 50). (2) Higher Ga loading gives rise to higher Brønsted acid site density, hence causes the formation of more polyaromatics [15]. The amount of polyaromatics could not been quantified yet by currently employed analytical methods, but the undetected carbons could be attributed to these species. In the case of co-feeding C_2H_4 and C_2H_6, although the yield of C_6H_6+C_7H_8 lies between the yields

obtained from two separate single feed, the aromatics production on HGaAlMFI (Si/Ga = 50) is less than on HGaAlMFI (Si/Ga = 30). It is apparent that the conversion of ethane and ethylene are not independent in the co-feeding reaction. The interaction of two reactants could only be better understood when the other undetected compounds are quantified.

Table 14. Catalytic tests of HGaAlMFI with different Si/Ga ratio

Feed	4 ml/min C_2H_6 + 46 ml/min Ar		4 ml/min C_2H_4 + 46 ml/min Ar		4 ml/min C_2H_6 + 4 ml/min C_2H_4 + 42 ml/min Ar	
Si/Ga ratio	30	50	30	50	30	50
C2 Conv.	60.8 % (C_2H_6)	97.8 % (C_2H_6)	86 % (C_2H_4)	95 % (C_2H_4)	61.6 % (C_2H_6) 59.1 % (C_2H_4)	52.1 % (C_2H_6) 78.4 % (C_2H_4)
CH_4 Yield	7.6 %	5.2 %	4.2 %	4.5 %	12.6 %	1.5 %
C2 Yield	16.8 % (C_2H_4)	5.9 % (C_2H_4)	2.5 % (C_2H_6)	2.2 % (C_2H_6)	-	-
C_6H_6 Yield	11.5 %	30.3 %	11.5 %	38.1 %	15.8 %	16.4 %
C_7H_8 Yield	4.2 %	3.4 %	6.2 %	5.6 %	9.4 %	4.2 %
C_6H_6+C_7H_8	15.7 %	33.7 %	17.7 %	43.7 %	25.2 %	20.6 %

The effects of temperature and C_2H_6 partial pressure on DHA were studied using the catalyst prepared by WVU via the microwave-assisted hydrothermal method. The catalyst were synthesized at 220 ºC for 30 min and the condition was optimized. In a typical test, a total flow rate of 50 ml/min C_2H_6 + Ar mixture was injected for 5 min into the U-tube shape reactor loaded with 0.8 g catalyst. Temperature varied from 600 to 700 ºC with 8% C_2H_6 in the feed. At 650 ºC, a higher C_2H_6 partial pressure was used as comparison. The catalytic test results are summarized in Table 15.

Table 15. Temperature effect on C_2H_6 DHA

	Temperature/ºC (C_2H_6 partial pressure)			
	700 (8%)	650 (8%)	600 (8%)	650 (32%)
C_2H_6 Conversion	92.5 %	60.45 %	22.7 %	62.7 %
C_2H_4 Yield	5.7 %	6 %	4.1 %	4.3 %
C_6H_6 Yield	10.7 %	8.1 %	4.8 %	5.7 %
C_7H_8 Yield	0.9 %	1.5 %	1.4 %	2.6 %
Coke Yield	16.1 %	7.2 %	7.4 %	2.1 %
C Balance	58.4 %	71.6 %	98.6 %	80.7 %

Higher C_2H_6 conversion were achieved with increasing temperature. The total C_6H_6+C_7H_8 yield at 600, 650 and 700 ºC were 8.8%, 9.6% and 11.5% respectively. It is comparable to its counterpart prepared via conventional synthesis method with HGaAlMFI (Si/Ga = 30). In addition, it produced

less C_2H_4 at 700 ºC, indicating the microwave method probably promoted the formation of in-framework Ga hence reduced the surface Ga. This hypothesis needs to be testified by ^{71}Ga NMR characterization in future work. Higher temperature enhanced the coke formation on the zeolite as evidence by the coke yield, analyzed by tracing the CO_x amount from the post-reaction combustion. The lower temperature, the higher carbon balance can be obtained. This is because higher temperature leads to higher yield of aromatics and, furthermore, high temperature favors the polycondesation of the aromatics to produce polyaromatics, which is not yet able to be detected by currently used analytical methods. At 650 ºC, when C_2H_6 was increased from 8% to 32%, the conversion and the total C_6H_6+C_7H_8 yield are in the same level. More toluene and less benzene was produced in higher C_2H_6 partial pressure. There were only 2.1% of coke formation on the zeolite in the 32% C_2H_6 feed, less than 8% C_2H_6 feed.

Multiple batches of catalyst were prepared, synthesized, treated, and screened to confirm the reliability of the 220°C and 30mins synthesis method and post-synthesis treatment. The previously adapted microwave synthesis mainly focused on synthesizing HGaAlMFI with a Si/Ga ratio of 30, the same synthesis method was used to prepare catalysts with a Si/Ga ratio of 50 by changing the precursor ratio of the prepared solution prior to synthesis. Each of the catalysts prepared was screened using XRD, SEM, TEM, ICP, and tested catalytically. In Figure 49, the XRD patterns show that we were successful in forming ZSM-5 crystals with a uniform crystallinity. Also, the Si/Ga ratio 30 and 50 show similar spectra indicating that adjusting the solution preparation did not negatively affect the synthesis and crystal growth of the HGaAlMFI catalysts.

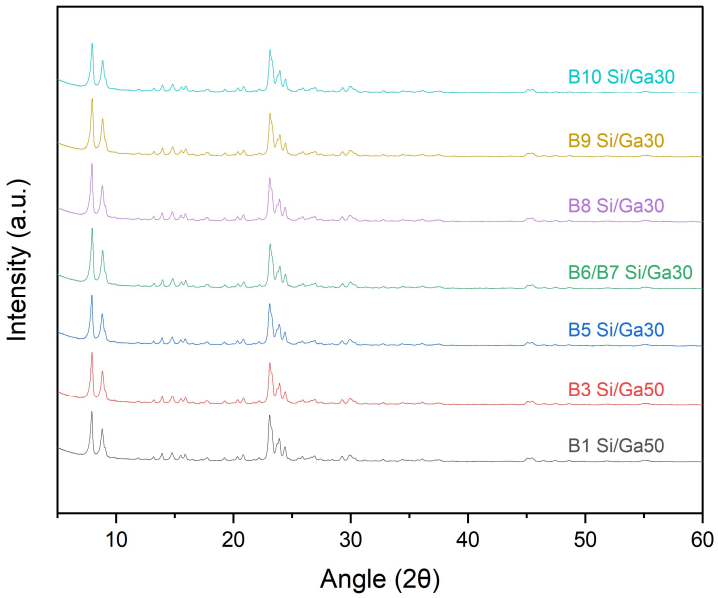

Figure 49. X-ray Diffraction (XRD) patterns of the CEM synthesized zeolites samples, both Si/Ga 30 and Si/Ga 50, all ran at 220°C - 30mins.

Some of these zeolite samples were further characterized with the use of SEM. As seen in Figure 50, the SEM images of B1 of the Si/Ga 50, B5 and B6/B7 of the Si/Ga 30 HGaAlMFI catalysts are shown. They all show uniformly sized zeolite crystals with little to no agglomeration of the crystals. All three have crystals of similar size which shows the reproducibility of the CEM MW synthesizer. This was also seen in the TEM images not shown here.

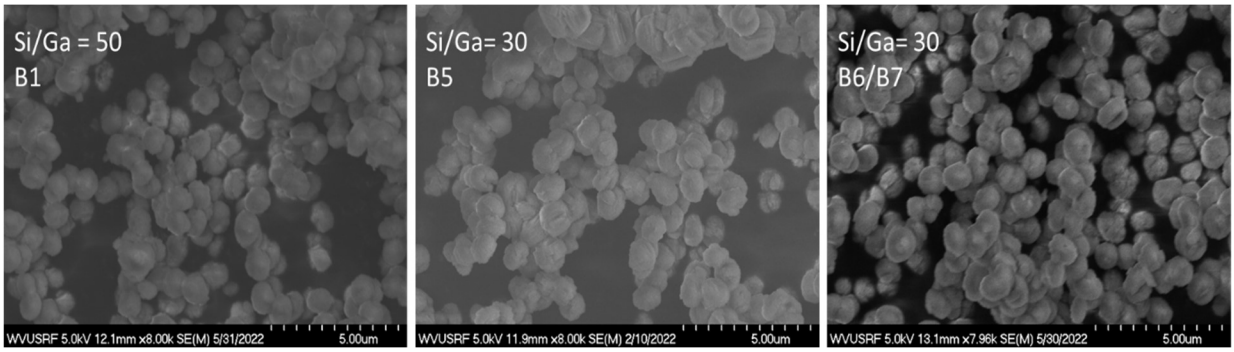

Figure 50. SEM images of B1 Si/Ga 50, B5 and B6/B7 of the Si/Ga 30 HGaAlMFI catalyst zeolite crystals.

The catalytic performance testing of the microwave synthesized HGaAlMFI samples was performed. Three reaction feeds were chosen to determine the catalytic activity of the microwave

HGaAlMFI samples: (1) 10% Ethane in N2, (2) 10% Ethylene in N2, and finally (3) 10% of each (10%Ethane and 10%Ethylene) in N2. These reactions were performed at 700°C for 60 mins each with 0.5g loaded into the u-tube reactor setup. A total gas flow of 30 mL/min was used and the gas hourly space velocity was 3600 mL/h/gcat. For one batch, B5 of the Si/Ga ratio of 30, was tested for all the different reactions. Some of the catalytic performance data collected from these runs is shown below in Table 16. It shows that across batches B5, B8, and B9 of the Si/Ga 30 all perform very similarly for the same reaction 10% Ethane. Then across the same batch, B5, for different reactions. This showed that for the reaction where it's a pure ethylene field there is more carbon unaccounted for seen by the higher percent of carbon missing following the reaction (~52%) and the amount still left in the reactor line or not analyzed (~47%). As stated above the stream CB is the percent of missing carbon following the reaction and the aromatic CB is the amount of carbon still lost following the TGA analysis. The Si/Ga 50 batches show some slight differences in performance, so another set of samples was made to test now.

Table 16. Reaction Data for the Different Batches and Si/Ga ratios [Temp] (Syn. Batch)

	10%Ethane [700C] (SiGa30-B5)	**10%Ethane [700C] (SiGa30-B8)**	**10%Ethane [700C] (SiGa30-B9)**	**10%Ethylene [700C] (SiGa30-B5)**	**10%Each [700C] (SiGa30-B5)**	**10%Ethane [700C] (SiGa50-B1)**	**10%Ethane [700C] (SiGa50-B3)**
C2H6 Conv.	72 %	73 %	75 %	-	65 %	65 %	75 %
C2H4 Conv.	-	-	-	87 %	57 %	-	-
C2H4 Sel.	38 %	35 %	32 %	-	-	40 %	30 %
C2H6 Sel.	-	-	-	3 %	-	-	-
CH4 Sel.	12 %	12 %	12 %	8 %	11 %	11 %	11 %
C3H8 Sel.	1 %	0.7 %	1 %	.4 %	1 %	2 %	0.8 %
C6H6 Sel.	26 %	25 %	25 %	29%	28 %	32 %	29 %
C7H8 Sel.	2 %	2 %	2 %	2 %	5 %	4 %	3 %
Stream CB/Missing	30 %	38 %	38 %	52 %	35 %	45 %	50 %
Aromatic CB	25 %	32 %	32 %	47 %	31 %	32 %	40 %

Following each reaction, a thermogravimetric analysis was performed to determine the amount of carbon that was formed on the catalyst surface during the reaction. The TGA weight loss curved are shown in Figure 51 along with the differential thermal analysis (DTA) curves. The other reactions not shown in this curve are still currently being tested and plotted. The two Si/Ga 30

samples, B5 and B8, show a very close weight loss due to coke as each other, 5.1 and 5.4 wt.% respectively. The Si/Ga 50 samples were not as close, B1 with 4 wt.% and B3 with 5 wt.% loss due to coke, due to the difference in the reaction performance.

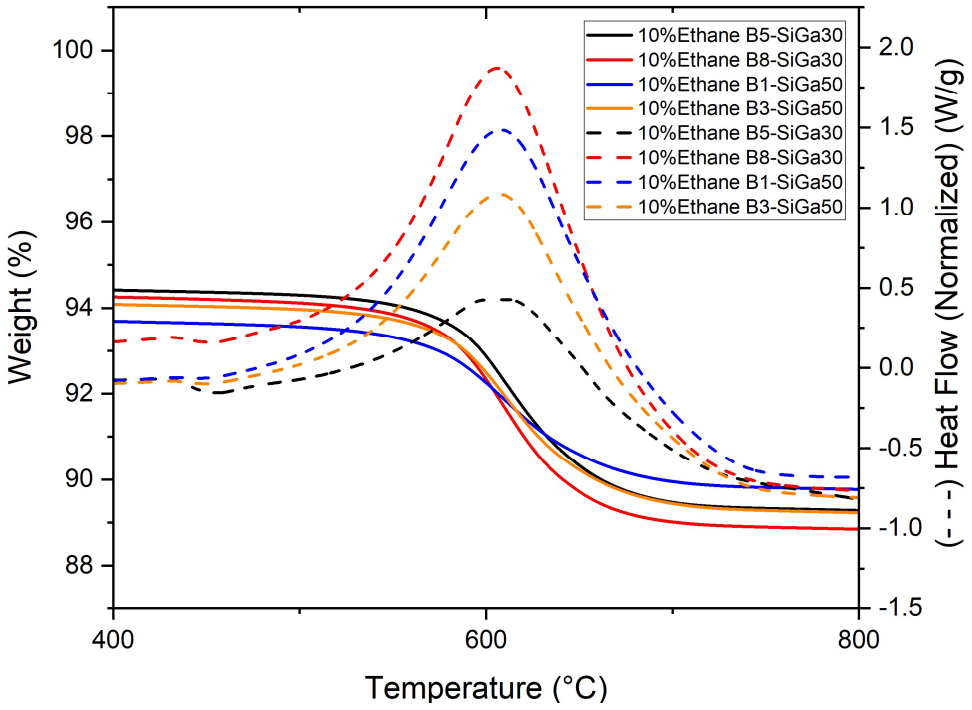

Figure 51. Thermogravimetric analysis curves of % weight loss and heat flow of each of the four different reactions run.

We developed a measuring method and obtained an improved carbon balance calculation. In this measuring method, the product in different phases were all collected and analyzed by different instrumentation. Figure 52 exhibits the schematic of the setup and shows how the product was collected. DHA process was performed in the U-shape quartz tube loaded with catalyst. The outlet of the reactor was connected to an impinger tube. The temperature of the stainless-steel line between the U-tube and the impinger tube was kept at 220 °C in order to vaporize the potential polyaromatic components in the product, preventing the tube clog. It was found that, even it was kept at 220 °C, there were still a considerable amount of aromatics retained in the line. Therefore, collecting the residue in this line and quantifying it plays an important role to achieve a good carbon balance. In a typical measurement, after reaction, dodecane ($C_{12}H_{26}$) was used to rinse the line and collected for quantification.

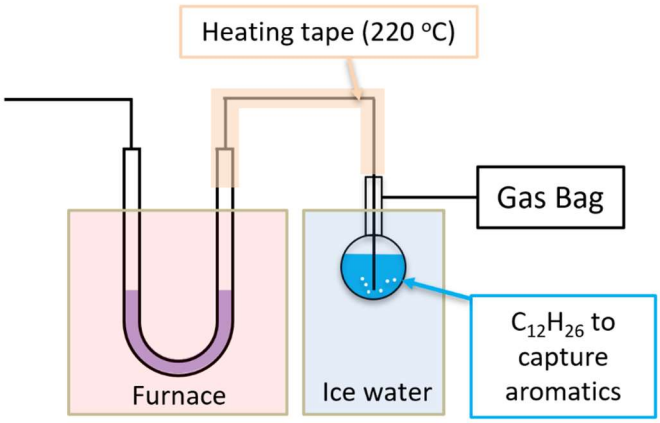

Figure 52. Schematic of the experimental setup.

The impinger tube was filled with 2 mL dodecane, as the solvent, to capture the non-gas phase product (mainly liquid or solid aromatics depending on ring numbers + water). The impinger tube was immersed in the ice water to increase its capture capacity. Gas flow went through the impinger tube and was collected by a gas bag. The product in the gas bag was analyzed by the GC for gas sample, while the solution in the impinger tube as well as the rinse were separately quantified by the GC for liquid sample. The amount of coke formed on the catalyst was determined by oxidizing the spent catalyst online and measuring CO_x with the MS. Since the oxidizing gas flow brought out some of the captured product from the impinger tube (mainly benzene and toluene), C_6H_6 and C_7H_8 were also measured by MS, in addition to CO_x, and added on the total in the calculation of carbon balance. Table 17 lists the sources of the carbon-containing components in the product and the approaches to quantify them by various instrumentation.

Table 17. Components of the products collected from different sources and analytical tools used for measurement.

Source	C-containing Component	Analytical Tool
Gas Bag	1. C1-C3 hydrocarbons, 2. Minimal aromatics which were not captured by impinger tube.	GC for gas
Impinger Tube	1. Aromatics (e.g. benzene, toluene) 2. Polyaromatics (e.g. naphthalene)	GC for liquid
Heated Line Rinse	Polyaromatics (e.g. naphthalene)	GC for liquid
CO_x from oxidation of spent catalyst	Coke	MS

Aromatics from oxidation gas flow	Benzene and toluene	MS

In the development of the measurement method, ethane DHA was performed over fresh HGaAlMFI catalyst prepared by WVU using the microwave approach. In a typical run, 0.8 g catalyst was used. 20 mL/min C_2H_6 + 5 mL/min Ar was continuously flown through the catalyst at 700 ºC for 5 min. In order to push all the product into the impinger tube and gas bag, an additional 10 min purge with 25 mL/min Ar was carried out. Afterwards, the spent catalyst was oxidized by 10% O_2/Ar mixture for coke analysis using MS while benzene and toluene were also monitored at the same time. Then, the heated line and the impinger tube were disassembled from the system. The line was rinsed by 2mL dodecane and the rinse solution was analyzed by GC.

Table 18 summarizes the ethane conversion and the yield of each component. The carbon balance based on this measurement reached up to 87%, which was greatly improved when compared to the results we reported before. The improvement is due to the modified setup which enables the maximum collection of the product as well as the rinse of the heated line. Since some of the components were just rough estimates, it is possible that the actual carbon balance could attain nearly 100% once these components are determined and calibrated. For example, several components categorized in "others" in the table are unknown. But they are very likely to be polyaromatics as they were present with naphthalene together in the heated line. The estimation of these components was performed by using the same calibration factor as Naphthalene (C10). Replicate experiments have been run several times. Both the conversion and yield results repeated very well. The carbon balance range from 82% to 110%.

Table 18. Ethane DHA measurement and carbon balance calculation.

C_2H_6 conversion	63.7%		
Aromatic yield[a]	Benzene	6.6% (imp[b]) + 1.9% (MS)	30.6%
	Toluene	3.0% (imp) + 0.4% (MS)	
	Naphthalene	11.0% (imp 2.8%, rinse[c] 7.8%)	
	Others (~C8-C11)[d]	~8.5% (imp 3.2%, rinse 5.2%)	
	C6+[e] in gas bag	0.7%	
CH_4 yield	7.4%		
C_2H_4 yield	4.5%		

C3+ yield	0.43%
CO yield	1.1%
Coke yield	5.5%
Carbon Balance	**87%**

[a] all the yield listed in this table is on carbon basis
[b] imp stands for the yield portion calculated from the impinger tube
[c] rinse stands for the yield portion calculated from the rinse solution
[d] others are the unknown components mainly collected from the rinse solution. They were estimated by using the naphthalene calibration factor.
[e] C6+ are the vapors not captured by impinger tube and ended up in the gas bag.

The new HGaAlMFI samples were screened via a procedural characterization and catalytic performance testing process. During the screening of the HGaAlMFI synthesized samples, each was characterized using X-ray diffraction (XRD) to distinguish if the product had the characteristic peaks of ZSM-5. Each of the new batches, B3-50, B9-30, B10-30, B11-30 (Batch#-Si/Ga Ratio) showed good intensity in the XRD spectrum and clearly exibiteded the characteristic peaks of ZSM-5, seen Figure 53 below. TEM was performed on each of the zeolites to characterize the uniformity of the zeolite crystalline particles for each sample. The shape and close up crystal structure of the zeolite crystals of B10-30 is shown in Figure 54. TEM imaging of B11 & B12 is planed. SEM images of each of the HGaAlMFI samples are shown in Figure 55 a-c. All three samples show uniformity in size.

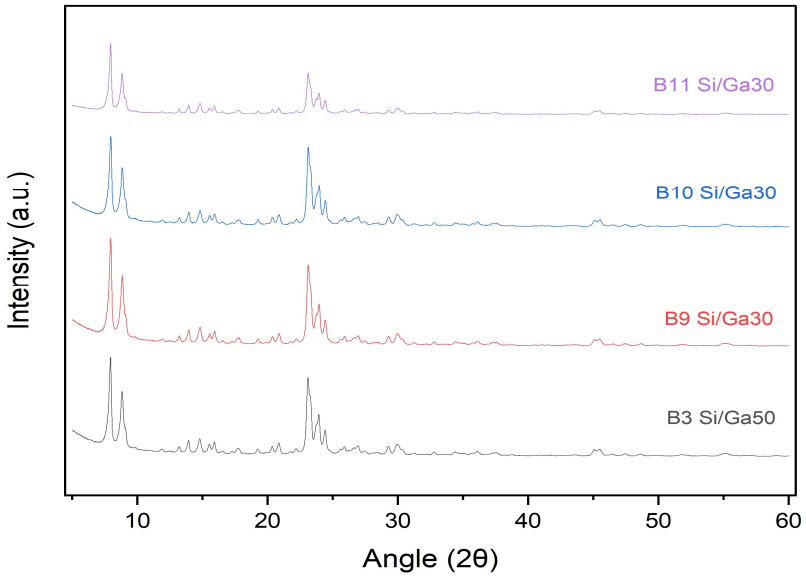

Figure 53. Powder X-ray Diffraction (XRD) of different batches of both Si/Ga 30 and 50 HGaAlMFI samples. B3-50, B9-30, B10-30, and B11-30 are all shown here.

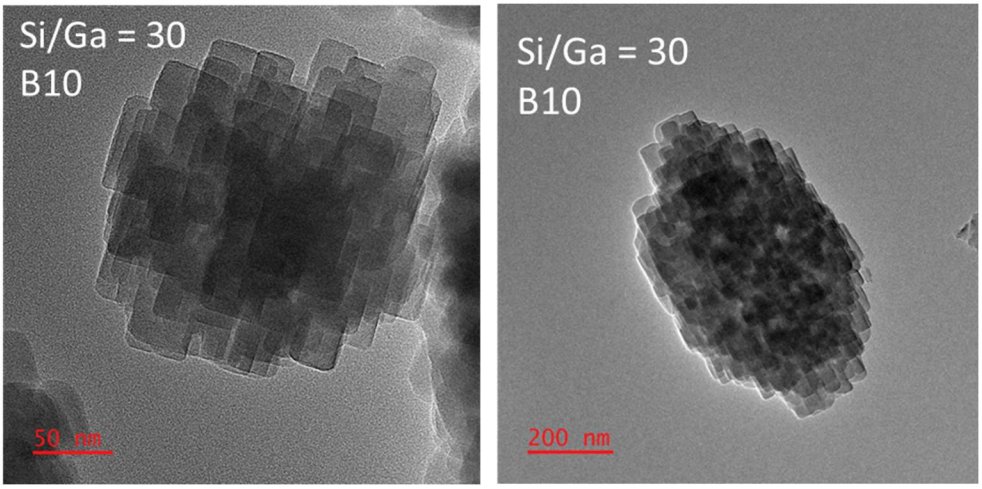

Figure 54. TEM Image HGaAlMFI sample, B10-30.

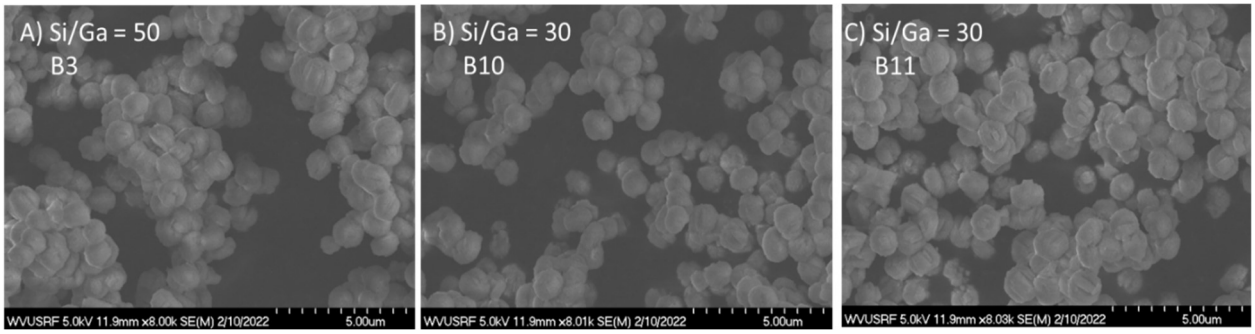

Figure 55. SEM images of different batches of both Si/Ga 30 and 50 HGaAlMFI samples. A) B3-50, B) B10-30, and C) B11-30.

Also, the catalytic performance tests of the newly synthesized batches of the Si/Ga 30 and the Si/Ga 50 HGaAlMFI samples were characterized before further OCM-DHA reaction testing by the NCSU team. These reactions were performed at 700°C for 60 mins each with 0.5g loaded into the u-tube reactor setup. A total gas flow of 30 mL/min was used and the gas hourly space velocity was 3600 mL/h/g-cat. Some of the catalytic performance data collected from these runs is shown below in Table 19. It shows that batches B10, B11, and B12 of the Si/Ga 30 all perform very similarly in 10% ethane. The total ethane conversion for each of the Si/Ga=30 samples was ~77 % and the product selectivity remained very close across the three batches, indicating the catalytic activity was reproducible between each synthesis batch.

Thermogravimetric analysis of the coke formation after the 1-hour of ethane dehydroaromatization was conducted. The weight loss due to coke for each sample was determined by temperature

programmed oxidation in a TGA. The weight loss is shown in Figure 56. For B3-50, B10-30, B11-30, and B12-30, the corresponding weight loss due to coke was 5.4, 5.0, 5.1, and 5.0 wt. % respectively. B3-50 exhibited a small shift in the DTA curve toward higher coke oxidation temperature. This higher temperature burning coke is consistent with more structured coke.

Accounting for the coke deposited on the surface the carbon balance was about ~70-73% for the three Si/Ga=30 batches. To further investigate the additional products being made, a cold trap was incorporated to collect and condense out heavier products. The cold trap was connected at the outlet of the reactor right after the t-connecter for the micro-GC collection. Following each run the cold trap is allowed to come to room temperature and washed thoroughly with chloroform before being injected in 1uL injections into our GC-MS. In Figure 57, the qualitative data for each of the four runs from Table 19 can be seen with the most probable chemical compounds listed in the top spectrum for each peak. This method may not catch heavier compounds that can condense in the heated for line to the cold trap.

Table 19. 10%Ethane [700°C] for each Syn. Batch

TOS: ~9.5 mins	SiGa50-B3	SiGa30-B10	SiGa30-B11	SiGa30-B12
C2H6 Conv.	80.1 %	79.0 %	77.3 %	76.9 %
C2H4 Sel.	29.0 %	31.0 %	33.1 %	32.4%
CH4 Sel.	11.0 %	11.2 %	11.1 %	11.0 %
C3H8 Sel.	0.98 %	1.0 %	0.9 %	0.9 %
C6H6 Sel.	31.9 %	31.0 %	28.0 %	28.3 %
C7H8 Sel.	5.7 %	7.15 %	6.68 %	6.20 %
Stream CB (Missing/ Unaccounted)	57.9% (42.1 %)	70.0 % (30.0 %)	68.2 % (31.8 %)	68.7 % (31.3 %)
Aromatic CB (C8+) (Missing/ Unaccounted after TGA)	68.0 % (32.0 %)	73.0 % (27.0 %)	70.2 % (29.8 %)	71.4 % (28.6 %)

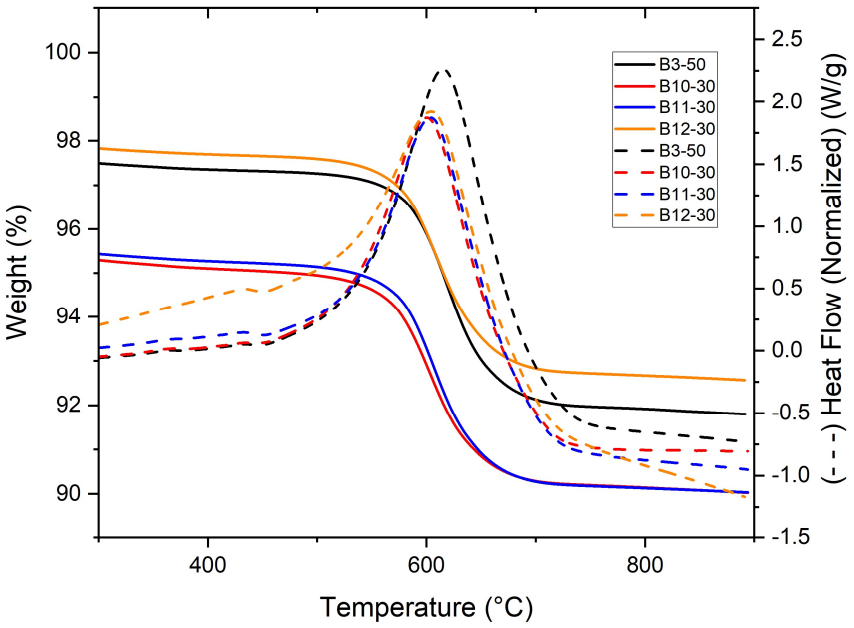

Figure 56. Thermogravimetric Analysis (TGA) of HGaAlMFI samples percent (%) weight loss and heat flow of each of the four different reaction runs.

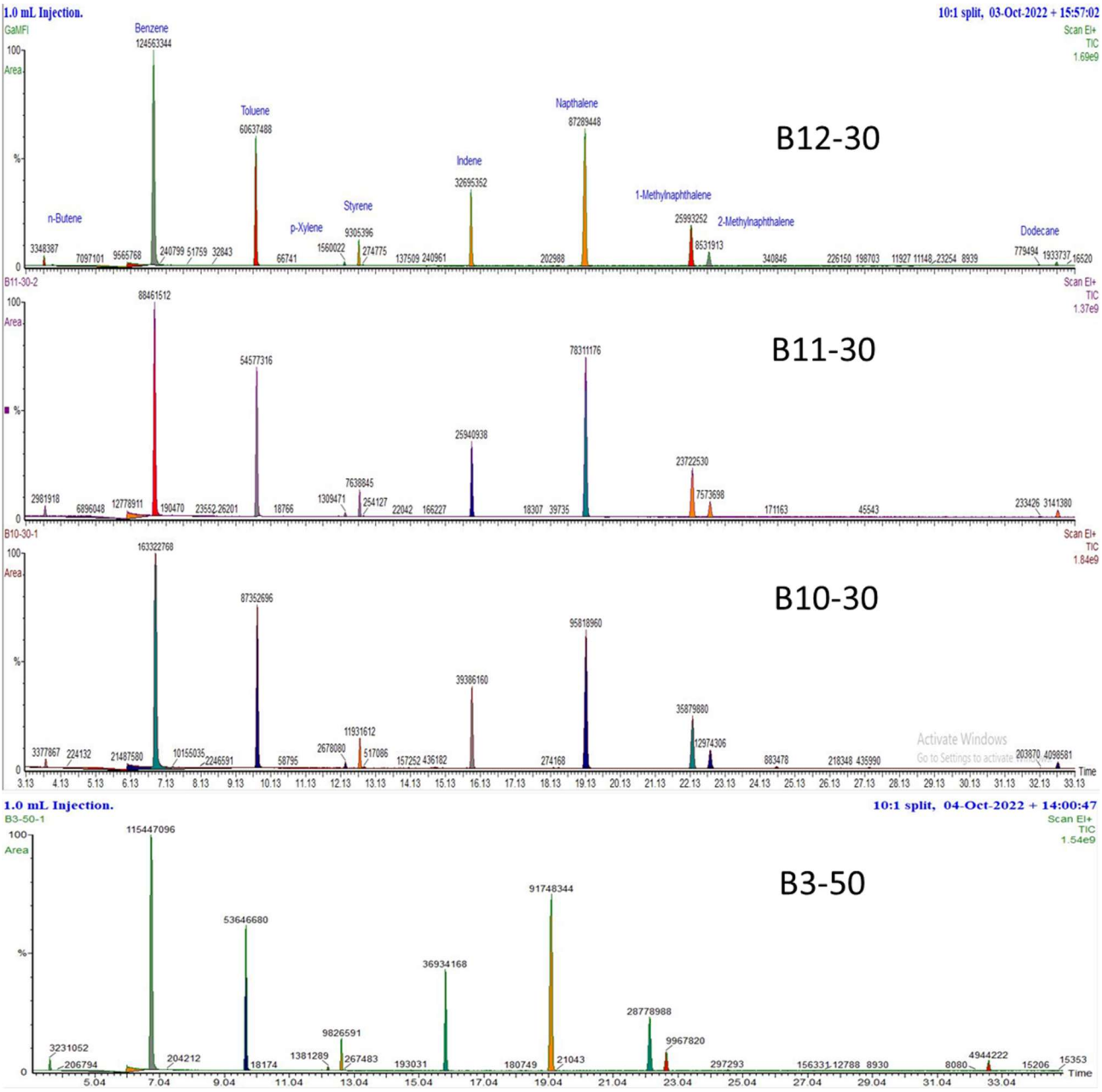

Figure 57. Qualitative analysis of the condensable from each a ethane DHA reaction for B3-50, B10-30, B11-30, and B12-30.

The C2-DHA reaction was investigated using the improved product analysis configuration, and the Ga-ZSM-5 catalysts synthesized by WVU were evaluated. For the product analysis, the gas product and the liquid product were collected and analyzed by GC and the coke deposition was analyzed by analysis of oxidation products using MS. The average carbon balance of the improved product analysis system reached 100.4 ± 6.5%, which was better than the previous 82%- 110%. The carbon balance results of the C2-DHA reactions have been found to be reproducible. The same

analysis method can also be applied to the OCM+DHA system. Based on our initial OCM+DHA test, most of the liquid products of the OCM+DHA were the same as the liquid products of the DHA reaction using ethane as the reactant.

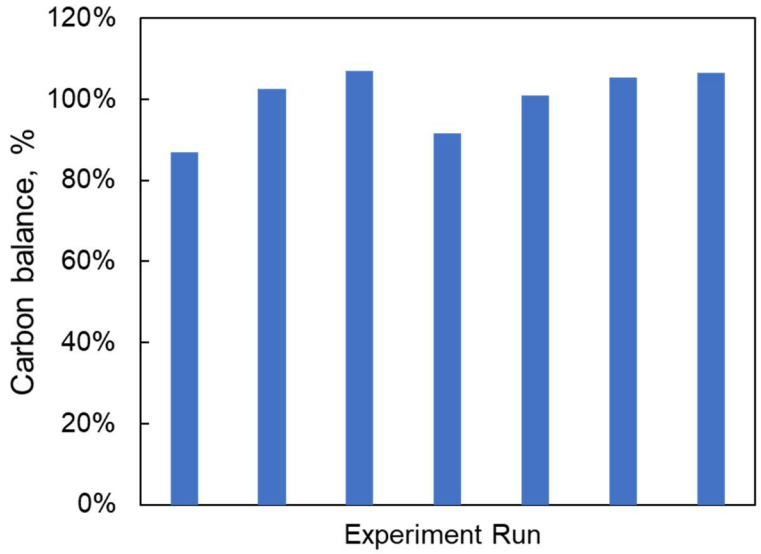

Figure 58. Carbon balance results of the different experiments based on the newly-developed analysis system for C2-DHA reaction.

Table 20. Conversion, carbon balance, and product distribution (based on carbon yield, mol%) of C2-DHA reaction using Ga-ZSM-5 catalysts.

Approach	Ga-ZSM-5 (Si/Ga=30)	Ga-ZSM-5 (Si/Ga=50)
C_2H_6 conversion	59.4%	62.5%
Carbon balance	100.8%	92.4%
C-yield		
yield_gas		
CH_4	8.19%	7.29%
C_2H_4	5.08%	2.57%
C3+	0.62%	0.80%
CO	0.98%	0.45%
yield_liquid		

benzene	15.23%	16.68%
toluene	5.16%	4.55%
xylene	0.35%	0.31%
A9+	1.87%	1.50%
naphthalene	6.84%	5.16%
A11+	9.75%	7.34%
yield_solid		
coke	5.50%	5.86%

As for the catalytic performance, similar results were obtained using Ga-ZSM catalysts with Si/Ga=30 or Si/Ga=50 from WVU. For instance, the C_2H_6 conversion of the Ga-ZSM-5 catalyst with Si/Ga=30 was 59.4%, and the C_2H_6 conversion of the Ga-ZSM-5 catalyst with Si/Ga=50 was 62.5%. The main liquid products of the C2-DHA are the benzene, toluene, naphthalene, and A11+ (C12+ aromatics, mainly methyl-naphthalene). Higher benzene yield at 16.68% can be achieved for Ga-ZSM-5 with Si/Ga=50 catalyst as compared to that at 15.23% for Ga-ZSM-5 with Si/Ga=30 catalyst, while higher toluene yield at 5.16 % can be achieved for Ga-ZSM-5 with Si/Ga=30 catalyst. For both catalysts, the coke formation was about 5-6 %. Although the coke formation might lead to deactivation, the oxidation stage of our OCM+DHA chemical looping technique can remove the coke and regenerate the catalyst.

Each of the new batches, B4-50, B13-30, B14-30, and B15-30 showed good intensity in the XRD spectrum and had the characteristic peaks of ZSM-5 (Figure 59 B15-30 not shown). The TEM and SEM images of B4-50, B13-30, and B14-30 catalyst zeolite crystals are seen in Figure 59 (a-c). Across the TEM images of all the batches the crystal structure appeared consistent across batches. SEM imaging indicates uniformity in size of the zeolite crystals between the two batches of Si/Ga 30 samples, B13 & B14, and the B4-50 with the previously synthesized B3-50.

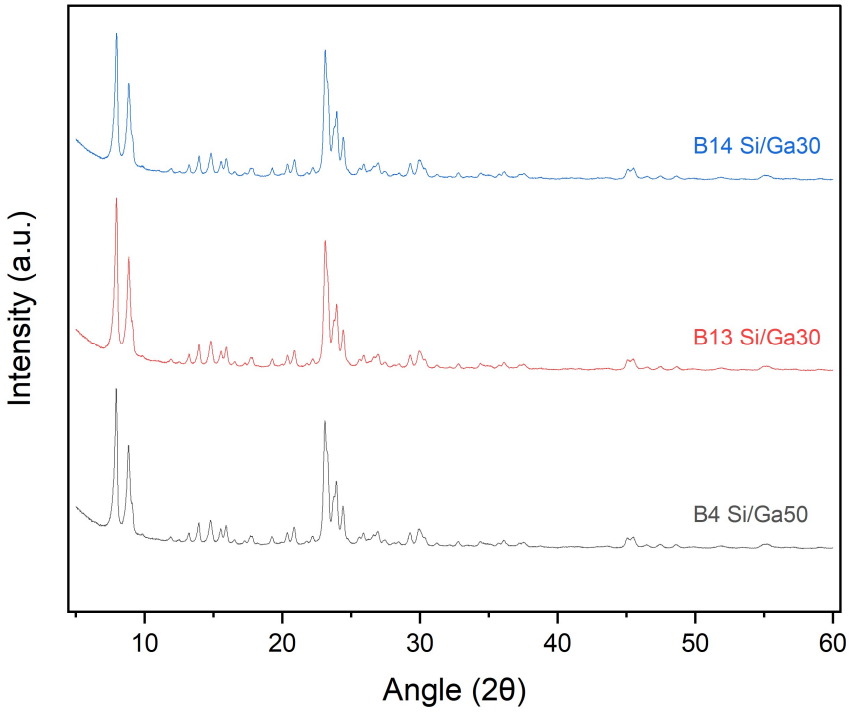

Figure 59. Powder X-ray Diffraction (XRD) of different batches of both Si/Ga 30 and 50 samples. B4-50, B13-30, and B14-30 are all shown here.

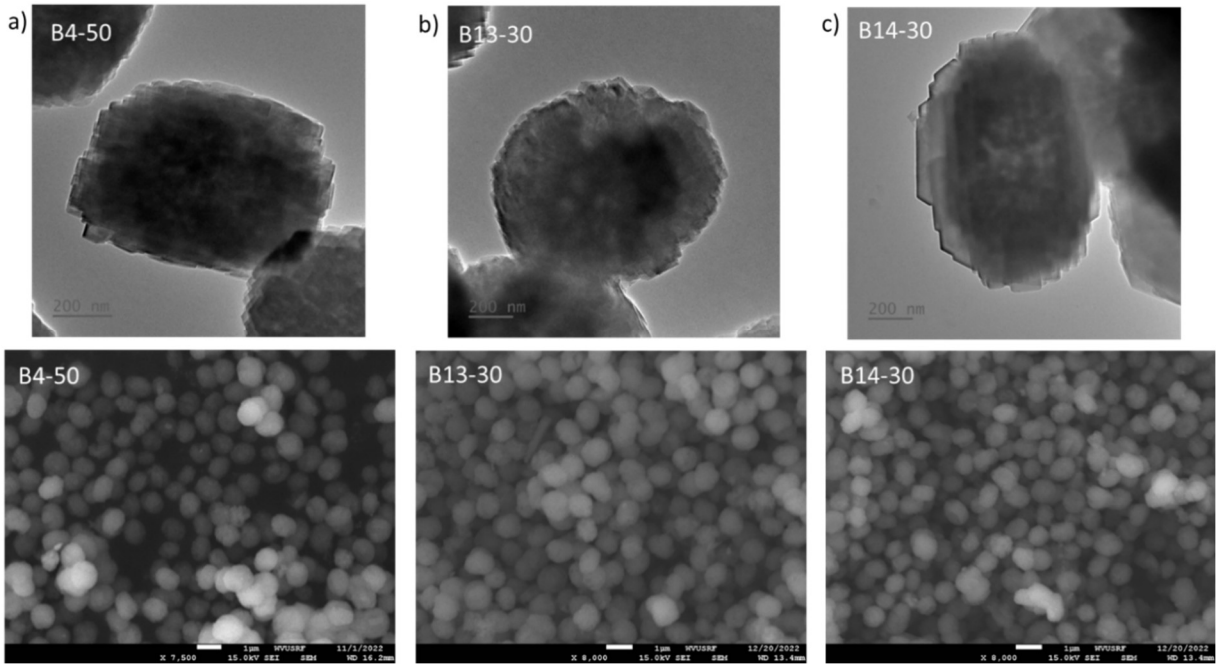

Figure 60: TEM and SEM images of a) B4-50, b) B13-30, and c) B14-30 zeolite catalyst crystals.

Also, the catalytic performance tests of the newly synthesized batches of the Si/Ga 30 and the Si/Ga 50 samples were characterized before further OCM-DHA reaction tests by the NCSU team. These reactions were performed at 700°C for 60 mins and 120 mins each with 0.5g loaded into the u-tube reactor setup. A total gas flow of 30 mL/min was used, giving a gas hourly space velocity of 3600 mL/h/g-cat. Select catalytic performance data collected from these runs is shown below in Table 21. It indicates that across batches B4-50 performed similarly to the previously tested B3-50 for the same 1 hour, 10% Ethane reaction. B13, and B14 of the Si/Ga 30 performed very similarly for the same reaction 10% Ethane over a 2-hour reaction time. The total ethane conversion for each of the Si/Ga=30 samples is ~78.5 % and the product selectivity also remains very close across the two new batches, indicating the catalytic activity is reproducible between each synthesis batch.

Temperature programed oxidation with thermogravimetric analysis was used to quantify coke formation after 1-hour & 2-hour 10% ethane dehydroaromatization (Figure 61). The B4-50 was a 1-hour reaction which had about 5.5 % weight loss due to the coke formed on the catalyst surface. The B13-30 and B14-30 where run for two hours and showed an increase in coke formation (8.3% and 9.5%, respectively) consistent with longer reaction time. This is similar the results of the B12 which was re-run for 2 hours (not shown).

Accounting for the coke deposited on the surface the carbon balance was about ~71-72% for the three Si/Ga=30 batches, B12, B13, and B14. To further investigate the additional products being made a cold trap was incorporated to collect the large condensable products. The cold trap was connected at the outlet of the reactor right after the t-connecter for the micro-GC collection. Following each run the cold trap is allowed to come to room temperature and washed thoroughly with chloroform before being injected in into our GC-MS. In Figure 62, the qualitative data for each of the three new runs from Table 21 can be seen with the assigned chemical compounds listed next to each peak. This analysis likely excludes larger carbon species such as polyaromatics.

Table 21. 10%Ethane at 700 °C for Each Syn. Bath

TOS: ~9.5 mins	SiGa50 - B4 (1 hour)	SiGa30 - B12 (1 hour)	SiGa30 - B13 (2 hour)	SiGa30 - B14 (2 hour)
C2H6 Conv.	78.4 %	76.9 %	77.0 %	80 %
C2H4 Sel.	33.4 %	32.4 %	35.0 %	32.0 %
CH4 Sel.	11.6 %	11.0 %	12.4 %	13.0 %
C3H8 Sel.	1.1 %	0.9 %	0.8 %	0.9 %
C6H6 Sel.	32.0 %	28.3 %	28.3 %	28.9 %
C7H8 Sel.	6.4 %	6.2 %	5.9 %	5.2 %
Stream CB (Missing/ Unaccounted)	68.2% (31.8 %)	68.7 % (31.3 %)	69.6 % (30.4 %)	70.0 % (30.0 %)
Aromatic CB (C8+) Missing/ Unaccounted after TGA	71.9 % (28.1 %)	71.4 % (28.6 %)	71.5 % (28.5 %)	71.0 % (29.0%)

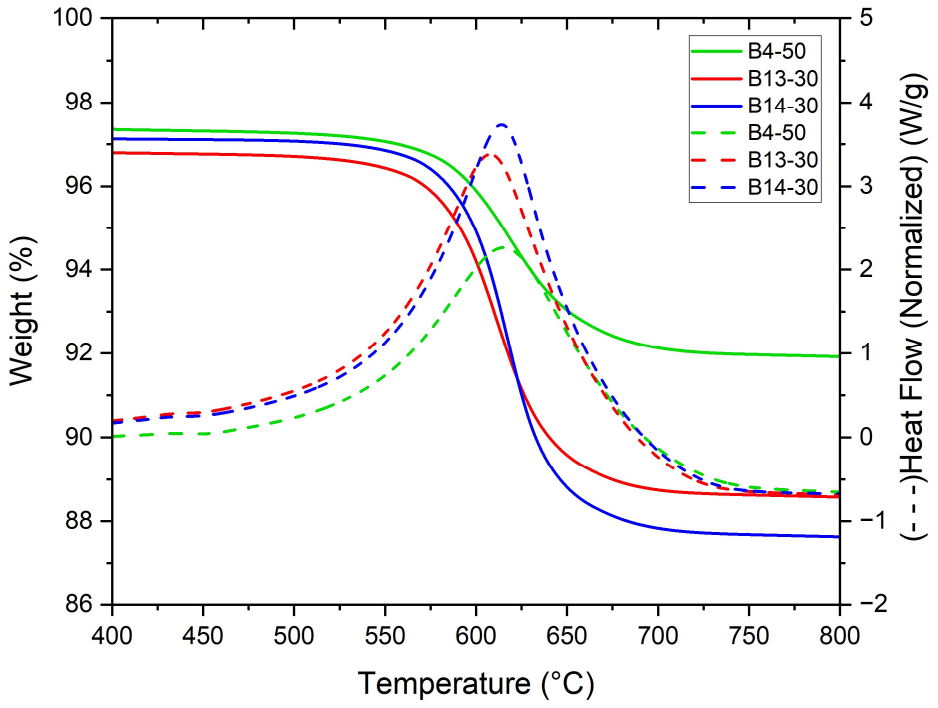

Figure 61. Thermogravimetric Analysis (TGA) of zeolite samples percent (%) weight loss and heat flow of each of the three different reaction runs.

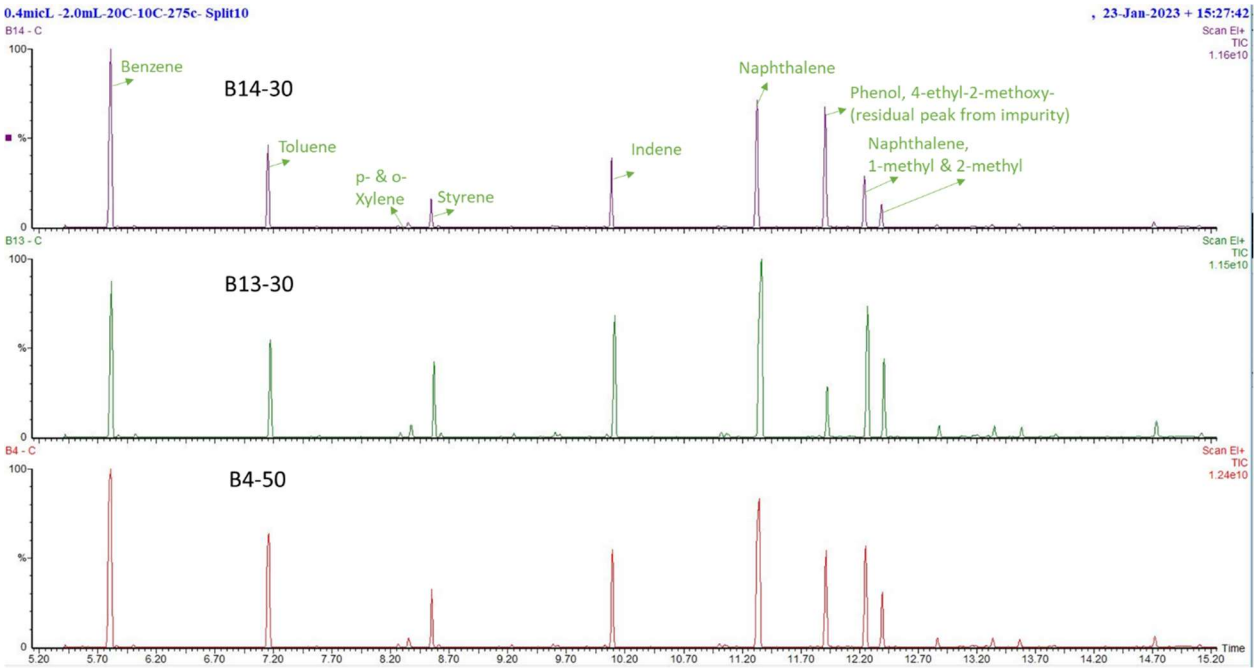

Figure 62. Qualitative analysis of the condensable from each an ethane DHA reaction for B4-50, B13-30, and B14-30.

During the screening of the HGaAlMFI synthesized samples, each of the samples was characterized using X-ray diffraction (XRD) to distinguish if the product had the characteristic peaks of ZSM-5, as shown in Figure 63. All the batches are consistent with the MFI framework, H-ZSM-5, which contains distinct peaks at 2θ equal to 8-9° and 22-25°. The TEM and SEM images of B15-B20 Si/Ga-30 HGaAlMFI zeolite crystals are seen in Figure 64 & 65. Across the TEM images, the crystal structure looked consistent across batches, which shows repeatability within the synthesis method. More visible in the SEM images is the uniformity in size of the zeolite crystals between the few batches of Si/Ga 30 samples, B15-B20. B21-B24 of Si/Ga 30 and B5-B6 Si/Ga 50 are still being tested now.

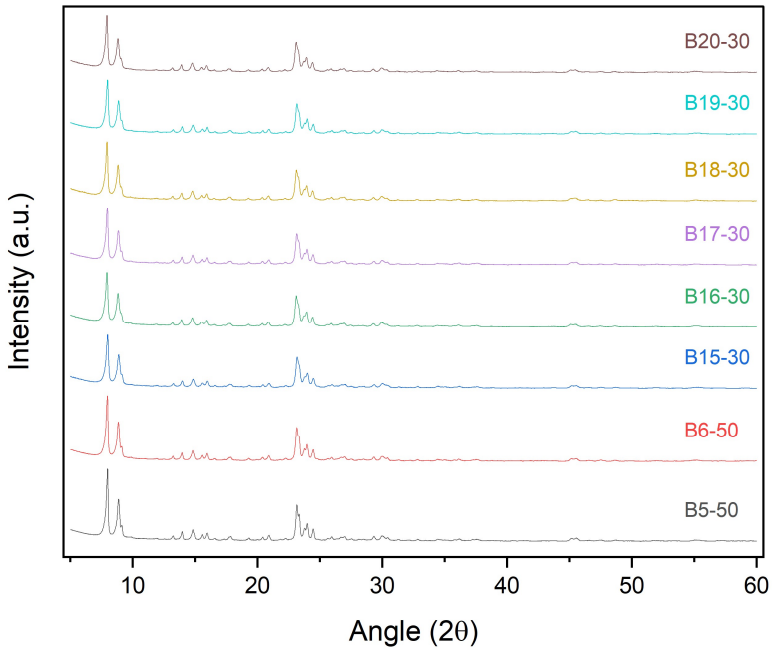

Figure 63. Powder X-ray Diffraction (XRD) of different batches of both Si/Ga 30 and 50 HGaAlMFI samples. B5 &B6 for Si/Ga 50, B15-B20 for Si/Ga 30 are all shown here.

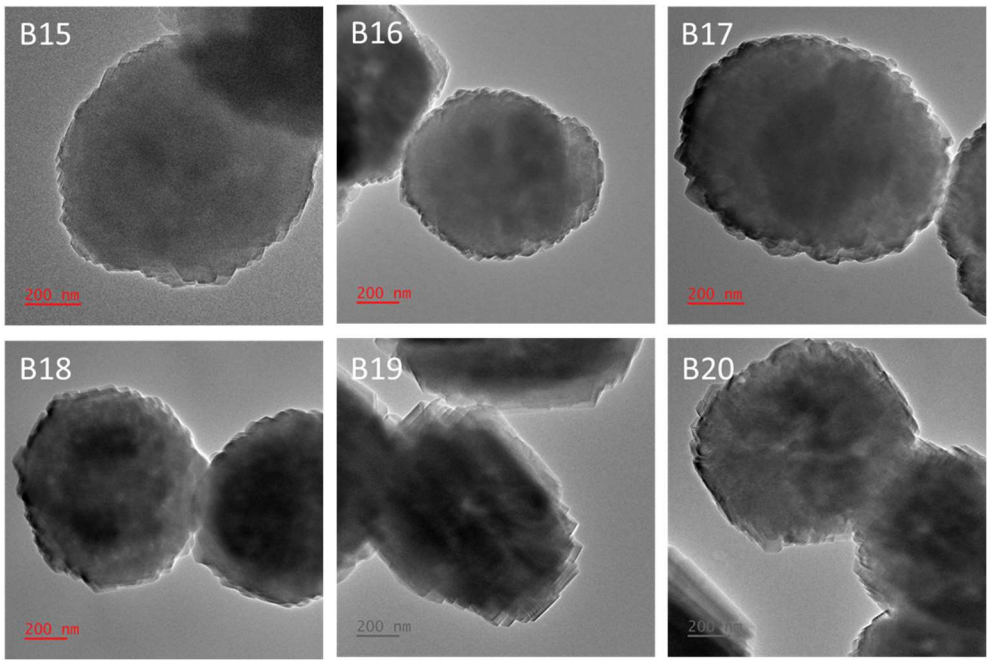

Figure 64: TEM images of B15- B20 of the Si/Ga 30 HGaAlMFI catalyst zeolite crystals.

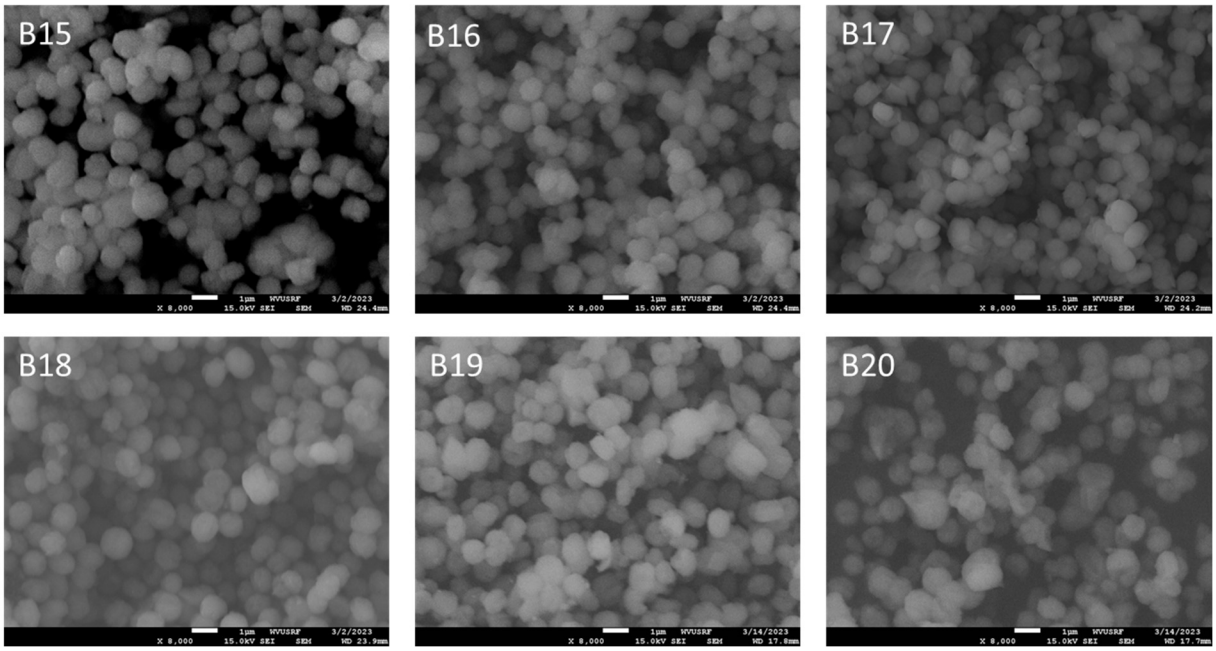

Figure 65: SEM images of B15- B20 of the Si/Ga 30 HGaAlMFI catalyst zeolite crystals.

Also, the catalytic performance tests of the newly synthesized batches of the Si/Ga 30 and the Si/Ga 50 HGaAlMFI samples were screened before further OCM-DHA reaction tests by the NCSU team. These reactions were performed at 700°C for 60 mins and 120 mins each with 0.5g loaded into the u-tube reactor setup. A total gas flow of 30 mL/min was used and the gas hourly space velocity was 3600 mL/h/g-cat. Some of the catalytic performance data collected from these runs are shown below in Table 22. Across the five Si/Ga 30 batches, the product selectivity between samples shows repeatability in performance. An analysis of the coke deposited onto the surface of the catalyst following the reaction using thermogravimetric analysis. The weight loss due to coke and the heat flow for TGA of each sample is shown in Figure 66. All the batches, B15-20, experience about a 7-8 wt.% weight loss due to coke over the course of the 1-hour reaction. B21-B24 of Si/Ga 30 and B5-B6 Si/Ga 50 are still being tested now.

Table 22. 10%Ethane at 700 °C for Each Syn. Bath

TOS: ~9.5 mins	SiGa30 – B15 (1 hour)	SiGa30 - B16 (1 hour)	SiGa30 - B17 (1 hour)	SiGa30 - B18 (1 hour)	SiGa30 - B19 (1 hour)	SiGa30 – B20 (1 hour)
C2H6 Conv.	72.0 %	74 %	71 %	72.5 %	68.9 %	74.0 %
C2H4 Sel.	28.7 %	31.0 %	32.0 %	32.1 %	33.0 %	32.0 %
CH4 Sel.	12.6 %	12.5 %	12.5 %	12.4 %	12.3 %	12.5 %
C3H8 Sel.	1.8 %	0.9 %	0.9 %	1.0 %	0.9 %	0.9 %
C6H6 Sel.	23.7 %	23.4 %	23.1 %	23.8 %	23.2 %	23.4 %
C7H8 Sel.	5.3 %	5.4 %	5.4 %	5.7 %	5.5 %	5.5 %
Stream CB (Missing/ Unaccounted)	70.3% (29.7 %)	69.5 % (30.5 %)	70.0 % (30.0 %)	70.1 % (29.9 %)	68.4 % (31.6 %)	69.5 % (30.5 %)
Aromatic CB (C8+) Missing/ Unaccounted after TGA	71.3 % (28.7 %)	70.6 % (29.4 %)	72.2 % (27.8 %)	71.5 % (28.5 %)	70.0 % (30.0 %)	71.0 % (29.0 %)

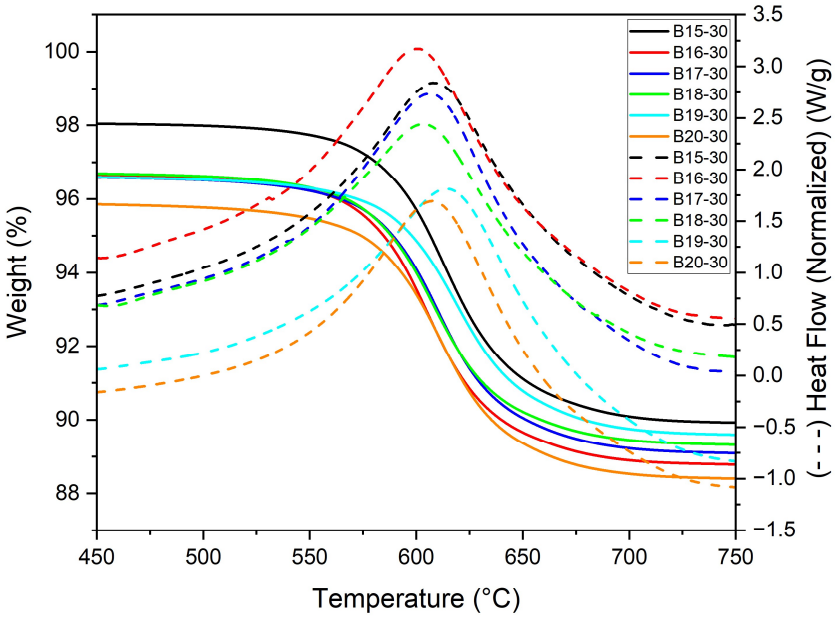

Figure 66. Thermogravimetric Analysis (TGA) of HGaAlMFI samples percent (%) weight loss and heat flow of each of the three different reaction runs.

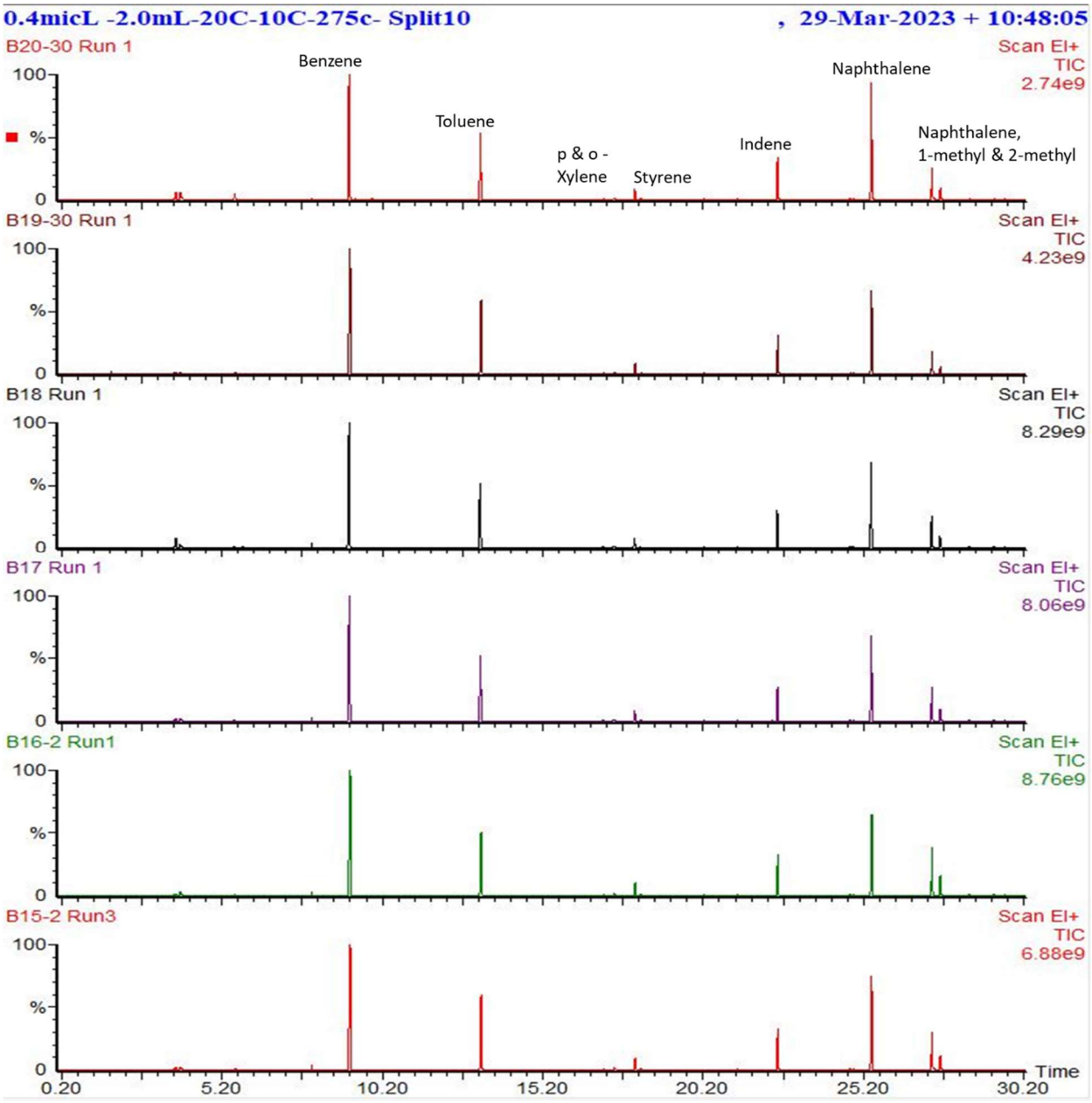

Figure 67. Qualitative analysis of the condensable from each ethane DHA reaction for B15 - B20 of Si/Ga 30 samples.

Accounting for the coke deposited on the surface, the carbon balance was about ~70-72.2% for the Si/Ga=30 batches, B15-B20. To further investigate the additional products being made, a cold trap was incorporated to collect and condense out these larger products. The cold trap was connected at the outlet of the reactor right after the T-connecter for the micro-GC collection. Following each run the cold trap is allowed to come to room temperature and washed thoroughly with chloroform before being injected in 0.4-uL injections into our GC-MS. In Figure 67, the qualitative data for

each of the new runs from Table 23 can be seen with the most probable chemical compounds listed in the top spectrum for each peak. Of course, we have larger carbon species, either chains or aromatics.

In addition to the screening tests of B15-B20 Si/Ga 30, an ICP-OES analysis was done on the HGaAlMFI samples prior to calcination and the ion exchange treatment to investigate the volatility of gallium within the HGaAlMFI catalysts. B21 and B22 were used in this study to determine if the HGaAlMFI samples were experiencing a loss in gallium from synthesis treatments. B21 was synthesized, centrifuged, and allowed to dry where a sample before calcination (B4-Cal) was collected. An additional sample was collected following calcination but before the ion-exchange treatment (Cal-UnT). As seen below the calcination at 550°C did not make a difference in the percent gallium in B21. Also, in the test with B22, the sample B4-Cal and after calcination and the ion exchange treatment (Cal-T) didn't experience a loss of gallium either. This is a good indication that the calcination and ion exchange does not affect the composition of Si, Al, and Ga in the HGaAlMFI.

Table 23. 10%Ethane at 700 °C for Each Syn. Bath

Table 2: ICP – OES Results of Batches Before and After Calcination and Treatment									
	Al	**Si**	**Ga**	**SAR**	**Ga %**	**Si%**	**Al%**	**Si/(Al+Ga)**	**Si/Ga**
B21-30 B4-Cal	704.4	12403.9	340.2	35.2	2.4	34.7	1.9	23.7	36.5
B21-30 Cal-UnT	697.3	12183.1	338.4	34.9	2.4	34.1	1.9	23.5	36.0
B22-30 B4-Cal	624.1	12307.7	311.3	39.4	2.2	34.5	1.7	26.3	39.5
B22-30 Cal-T	686.0	13234.2	349.1	38.6	2.4	37.1	1.9	25.6	37.9

We applied the developed microwave synthesis method to three different zeolite compositions. Zeolites were characterized by SiO_2/Al_2O_3 ratios (SAR) and in the case of HGaAlMFI the Si/Ga ratio. The catalyst HGaAlMFI-30 and HGaAlMFI-50 both have a SAR of 20 and Si/Ga ratios of 30 and 50, respectively. In addition to the two that were made in the past three new samples, 1, 2, and 3 seen below, were synthesized with different Si/Al ratios and, one as synthesized with a different Si/Ga ratio.

Table 24. Sample Names and Expected Si/Ga and Si/Al

Sample #	Sample ID	Expected Si/Ga	Expected Si/Al
1	HGaAlMFI-30-30	30	30
2	HGaAlMFI-30-10	30	10
3	HGaAlMFI-20-20	20	20
4	HGaAlMFI-30-20	30	20
5	HGaAlMFI-50-20	50	20

During the screening of the HGaAlMFI synthesized samples, each of the samples was analyzed using X-ray diffraction (XRD) to distinguish if the product had the characteristic peaks of MFI type zeolites. All the samples are consistent with the MFI framework except the 2-HGaAlMFI-30-10 sample. The other samples all contain the unique peaks at 2θ of 8-9° and 22-25° typical for MFI type zeolites, as seen in Figure 68. The TEM and SEM images of five different compositions of the HGaAlMFI zeolite crystals are displayed in Figure 69. Across the TEM images of all the batches, the crystal structures appear consistent across samples in shape, except for the 2-HGaAlMFI-30-10. The 2-HGaAlMFI-30-10 does not seem to have been completely crystalized, which is attributable to the decreased Si/Al ratio which can inhibit crystallization. Similar results are visible in the SEM images. The 3-HGaAlMFI-20-20 sample does seem to have larger diameter crystals than samples 1, 4, and 5. ICP-OES testing is being conducted on these new batches to determine if the Si/Al and Si/Ga ratio were as expected.

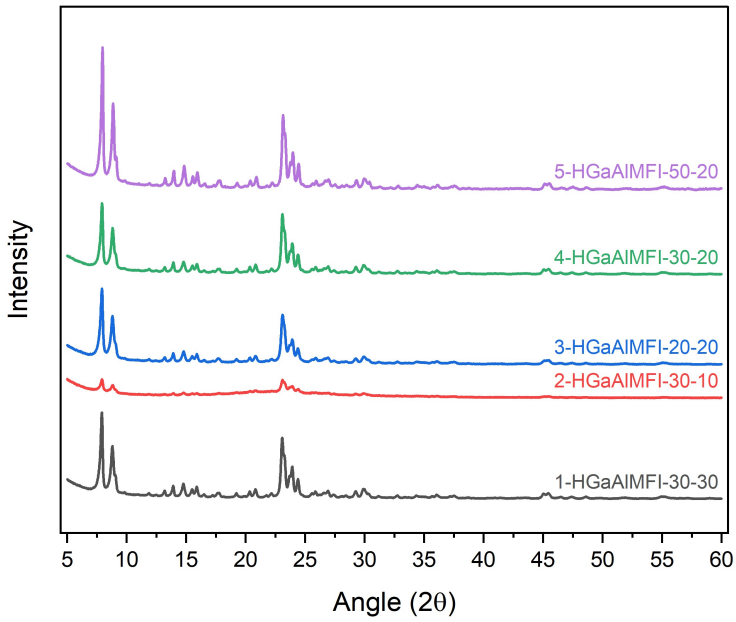

Figure 68. Powder X-ray Diffraction (XRD) of the new compositions of HGaAlMFI.

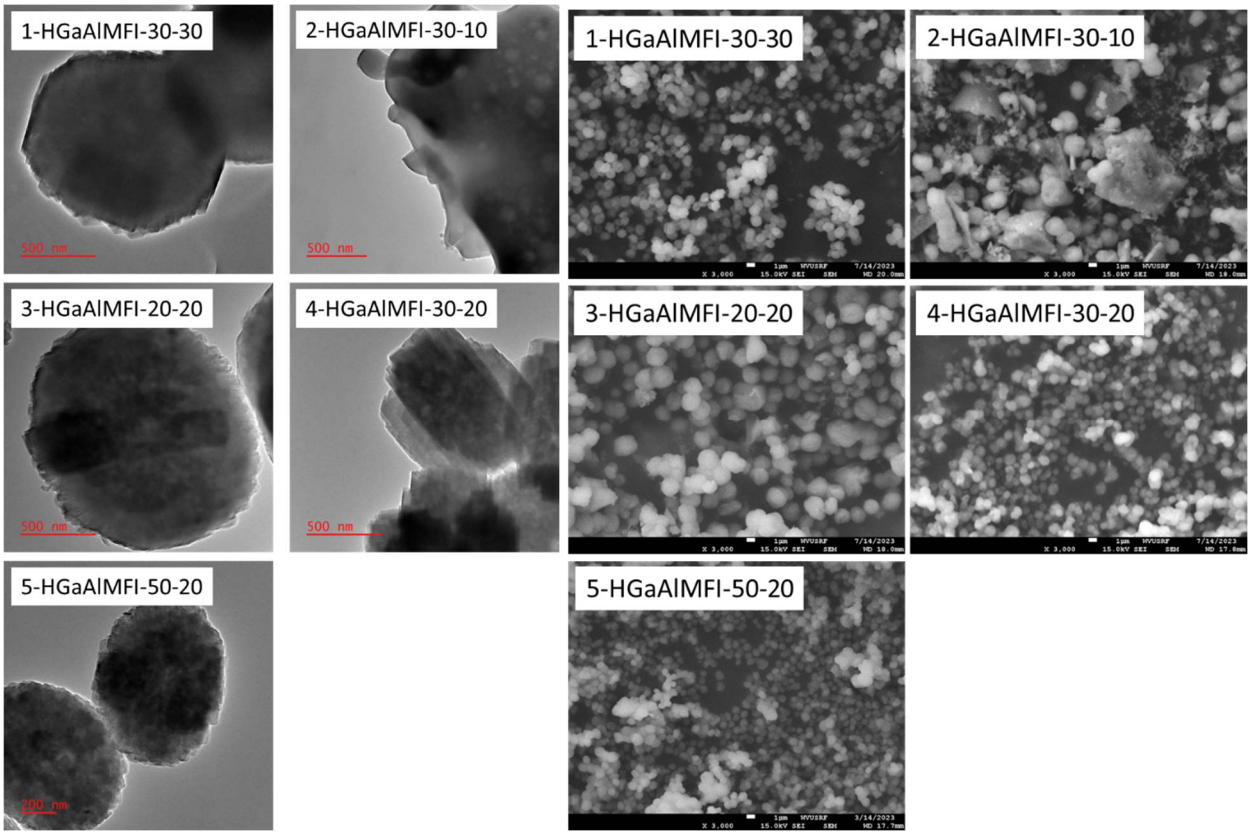

Figure 69: TEM images (left) and SEM images (right) of the new compositions of HGaAlMFI.

Also, the catalytic performance tests of the different composition samples were screened and characterized prior to OCM-DHA reaction testing by the NCSU team. These reactions were performed at 700°C for 60 mins each with 0.5g loaded into the u-tube reactor. A total gas flow of 30 mL/min was used, and the gas hourly space velocity was 3600 mL/h/g-cat. Select catalytic performance data from these runs is shown below in Table 25. As seen in the table below the sample 2-HGaAlMFI-30-10 had poor performance compared to the other samples, as is consistent with its poor crystallinity. Sample 3 had a higher ethylene selectivity compared to 1, 4, and 5 which are all more consistent with each other. An analysis of the coke deposited onto the surface of the catalyst following the reaction using thermogravimetric analysis is still ongoing.

Table 25. 10% Ethane at 700 °C for Each Syn. Batch

Table 2: 10%Ethane [700°C] for each Syn. Batch					
TOS: ~9.5 mins	**1-HGaAlMFI-30-30**	**2-HGaAlMFI-30-10**	**3-HGaAlMFI-20-20**	**4-HGaAlMFI-30-20**	**5-HGaAlMFI-50-20**
C2H6 Conv.	78.9 %	36.7 %	80.0 %	82.1 %	83.4 %
C2H4 Sel.	39.0 %	11.0 %	62.6 %	38.4 %	27.3 %
CH4 Sel.	13.5 %	--	12.1 %	12.6 %	13.6 %
C3H8 Sel.	1.0 %	--	1.4 %	0.8 %	0.9 %
C6H6 Sel.	29.1 %	2.0 %	28.4 %	31.3 %	29.4 %
C7H8 Sel.	6.7 %	--	10.5 %	7.5 %	5.3 %

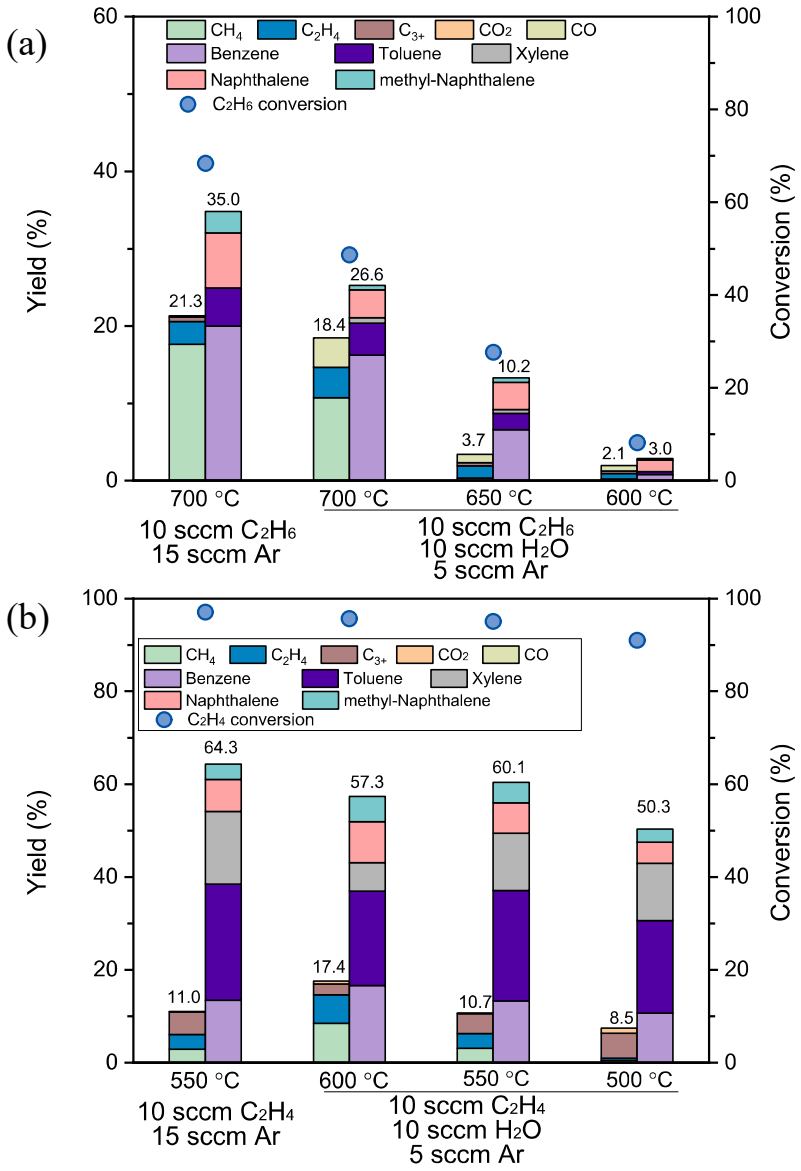

Figure 70. (a) Effect of temperature on the yield and conversion of C_2H_6+H_2O co-feeding DHA reaction. (catalyst loading: 0.8 g HGaAlMFI catalyst, feed: 10 mL/min C_2H_6 +15 mL/min Ar or 10 mL/min C_2H_6 + 10 mL/min H_2O + 5 mL/min Ar); (b) Effect of temperature on the yield and conversion of for C_2H_4+H_2O co-feeding DHA reaction (catalyst loading: 0.2 g HGaAlMFI catalyst, feed: 10 mL/min C_2H_4 +15 mL/min Ar or 10 mL/min C_2H_4 + 10 mL/min H_2O + 5 mL/min Ar).

The effect of temperature on the yield and conversion of the "wet" C_2H_6 +H_2O co-feed DHA reaction or C_2H_4+H_2O co-feeding DHA reaction was investigated in detail. In Figure 70a, the DHA tests with C_2H_6+H_2O co-feed at 600, 650, and 700 °C were conducted. A dry C_2H_6 DHA reaction at 700 °C was performed for comparison. For the dry C_2H_6 condition, the C_2H_6 a conversion of 69.1% and aromatic yield of 35.0% were achieved at 700 °C, whereas a C_2H_6 conversion of 48.2%

and aromatic yield of 26.6% were achieved for C_2H_6+H_2O condition at 700 ℃. This indicates that steam is not inert but rather leads to a decrease in the C_2H_6 conversion. Additionally, the decrease in temperature led to the lower performance of the C2-DHA reaction. For example, a C_2H_6 conversion of 27.7% and an aromatic yield of 10.2% were observed at 650 ℃, and a C_2H_6 conversion of 8.2% and an aromatic yield of 3.0% were observed at 600 ℃. This is attributable to the C_2H_6 DHA reaction being favored at high temperature due to more facile dissociation of the C-H bonds.

As for the C_2H_4+H_2O reaction, the DHA tests with C_2H_4+H_2O co-feed at 500, 550, and 600 °C and a dry C_2H_4 DHA reaction at 550 °C were performed. As seen in Figure 70b, a C_2H_4 conversion of 97.1% and an aromatic yield of 64.3% were achieved at 550 ℃ for dry C_2H_4 conditions. For the C_2H_4+H_2O reaction, a C_2H_4 conversion of 95.1% and an aromatic yield of 60.1% were achieved at 550 ℃. A C_2H_4 conversion of 95.7% and an aromatic yield of 57.3% were achieved at 600 ℃ and the a C_2H_4 conversion of 91.1% and an aromatic yield of 50.3% were achieved at 500 ℃. Notably, the aromatic yield of 60.1% at 550 ℃ was somewhat higher than the aromatic yield of 57.3% at 600 ℃, which is attributable to less gas yield from cracking reactions and/or less carbon deposition at a lower the temperature. Based on the results shown in Figure 70, the higher conversion and higher aromatic yield are more promising for the wet C_2H_4+H_2O compared to the C_2H_6+H_2O reaction, which indicated the C_2H_4-DHA reaction was more effective than the C_2H_6-DHA reaction and the effect of H_2O was less significant for C_2H_4.

Based on OCM+DHA cycling test, the stability and regeneration issue of the DHA HGaAlMFI catalyst has been the focus of further study. Therefore, the stability test of the C_2-DHA reaction using C_2H_4 and H_2O co-feed was conducted as shown in Figure 71. For the 5 min, the yield of the gas product reached 19.3% and the aromatic yield reached 46.3%, with the ethylene conversion of 86.3%. After a time on stream (TOS) of 10 min, the gas product yield reached 20.1% and the aromatic yield reached 21.5%, with the ethylene conversion of 62.8%. The conversion further decreased to 10.2% gas product yield and 3.5% aromatic yield for the 25 min. The deactivation of DHA catalyst in the C_2H_4+H_2O co-feeding indicated that the DHA catalyst deactivation is the main reason for the deactivation of the OCM+DHA reaction setup. To further determine the root cause and clarify the deactivation of the DHA catalyst, oxidation was conducted to remove the carbon species. For the following 25-35 min, the catalyst was still not active, with the gas product yield

of 10.1% and aromatic yield of 3.2%, which indicated the carbon deposition was not the main cause of deactivation. Then the reduction was conducted for the catalysts, which underwent 1-h 50 mL/min 2vol%H_2/98vol%Ar treatment. After the H_2-reduction treatment, the catalyst could be mostly recovered. For instance, the aromatic yield reached 45.8% and recovered 99% of the fresh catalyst's activity. Therefore, the deactivation may result from the possible loss of Ga-H on the HGaAlMFI catalyst. The H_2O as a side product from OCM may affect the Ga-H species at reaction conditions. Since H_2O was not a common feed for the C2-DHA reaction, the effect of H_2O on DHA deactivation was further investigated.

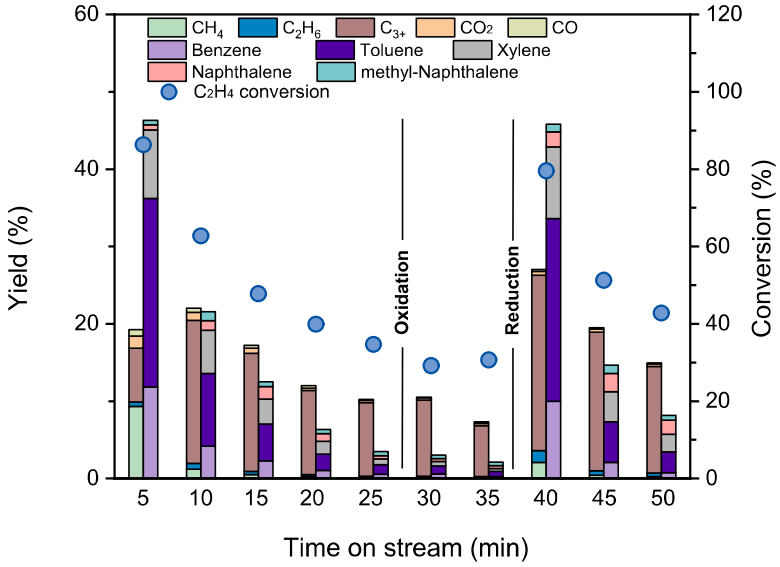

Figure 71. Stability test of the DHA reaction: DHA catalyst: 0.1 g HGaAlMFI catalyst at 550 °C, pressure= 1 bar, reaction: 25 mL/min 40vol%C_2H_4/40vol%H_2O(g)/20vol%Ar; oxidation: 1-h 50 mL/min 2vol%O_2/98vol%Ar; reduction: 1-h 50 mL/min 2vol%H_2/98vol%Ar).

The effect of H_2O concentration on the DHA catalyst stability is shown in Figure 72. In this experiment, we conducted 25-min C2-DHA experiments with 40% C_2H_4 + 0-40% H_2O (Ar as balance) to illustrate the effect of H_2O. For the 40% C_2H_4 + 0% H_2O experiment, a relatively stable catalytic performance can be obtained, with 67% aromatic yield at the 5 min and 64.2% aromatic yield at the 25 min. Similar results can also be found for 40% C_2H_4 + 2% H_2O experiment. For the 40% C_2H_4 + 2% H_2O, 59.6% aromatic yield at 5 min and 58.1% aromatic yield at 25 min, whereas the aromatic yield decreased from 57.0% at 5 min to 45.7% at 25 min for 40% C_2H_4 + 4% H_2O experiment. When the concentration of H_2O further increased to 20% and 40%, severe deactivation was observed. For instance, the aromatic yield decreased from 48.2% to 6.5% for the 20% H_2O

experiment and decreased from 46.3% to 3.5% for the 40% H_2O experiment. Therefore, the existence of H_2O is detrimental to the HGaAlMFI DHA catalyst, in terms of both the initial activity and the stability. Based on the 0-40% H_2O experiment, the concentration in the C2-DHA reactor should be no higher than 2% to ensure the stability of the HGaAlMFI, whereas our OCM results indicate, ~15-20 vol% H_2O will be generated as the side product of the OCM result and fed into the DHA reactor. Therefore, strategies to mitigate steam can be necessary to ensure longer catalyst life between regenerations through either limiting the H_2O concentration for the DHA catalyst and/or enhancing the water-resistance of the DHA catalyst. Potential strategies include adding a water-sorbent between the DHA and OCM bed, diluting methane feed, recycling H_2 to the DHA step to preserve Ga-H species, implementing the reduction step, among others.

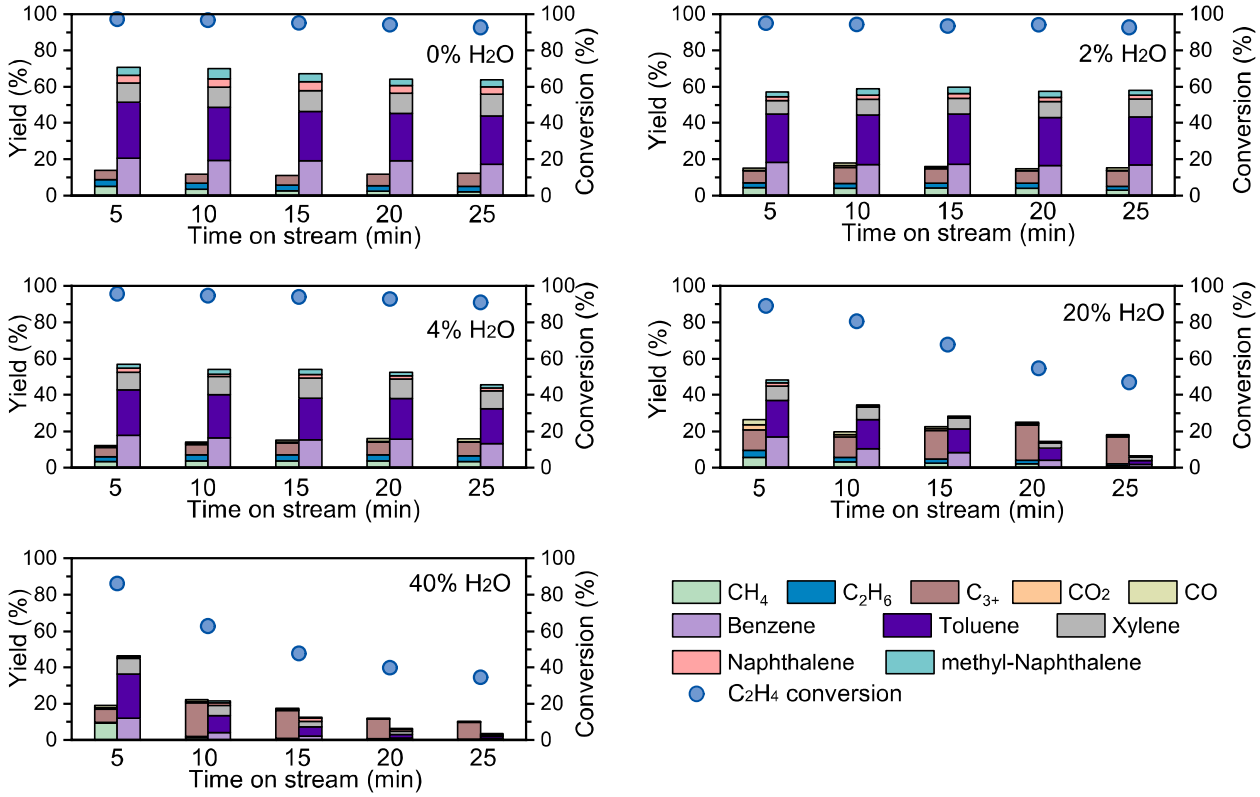

Figure 72. Stability test of the DHA reaction: DHA catalyst: 0.1 g HGaAlMFI catalyst at 550 °C, pressure= 1 bar, reaction: 25 mL/min 40vol%C_2H_4, 0-40vol%H_2O(g) and Ar as the balance).

We further investigated the effect of H_2O on DHA catalyst stability by inert dilution of the water feed. As shown in Figure 73, we conducted 25-min C_2-DHA experiments where we decreased the water concentration by inert dilution with Ar. The flow rates used were 10 mL/min C_2H_4 and 2.5 mL/min H_2O(g) as the main co-fed gas, and the inert Ar as the balance where total flow rates of25

mL/min, 50 mL/min, and 100 mL/min were applied corresponding to a H_2O concentration of 10, 5, and 2.5 vol%, respectively. For the condition with H_2O concentration at 10%, there was a gradual decrease witnessed in both the ethylene conversion and the aromatic yield. After 5 minutes, the ethylene conversion reached 92.4% and the overall aromatic yield reached 57.7%, with the benzene, toluene, and xylene yield at 18.1, 23.5, and 9.8%, respectively. At the 15-minute mark, The ethylene conversion declined to 69.6%, leading to a reduction in the overall aromatic yield to 29.2%, comprising benzene at 8.0%, toluene at 11.6%, and xylene at 8.4% with the balance naphthalene and methyl-naphthalene. This significant deactivation likely results from the effect of water. When the H_2O concentration was diluted from 10% to 5% the resulting deactivation behavior was similar. For the first 5 minutes, the ethylene conversion reached 86.8% and the overall aromatic yield reached 57.9%, with benzene yield at 18.5%, toluene yield at 23.3%, and xylene yield at 11.5%. At 15 minutes, the ethylene conversion decreased to 71.7% and the overall aromatic yield decreased to 29.2%, with benzene yield at 8.0%, toluene yield at 11.6%, and xylene yield at 8.4%. When the H_2O concentration was further diluted to 2.5%, the ethylene conversion reached 71.7% and the overall aromatic yield reached 55.2%, with benzene yield at 19.4%, toluene yield at 14.4%, and xylene yield at 16.5% within the first 5 minutes. At the end of 25 minutes, the ethylene conversion reached 76.3% and the overall aromatic yield reached 34.1%, with benzene yield at 10.9%, toluene yield at 11.0%, and xylene yield at 6.4%. While deactivation was still evident, it was not as severe as for the higher H_2O concentration conditions.

While deactivation was still evident even after incorporating the dilution strategy, the observed relative yield loss decreased from ~49% for the 10% and 5% cases to ~38% for the highest dilution of 2.5%. By comparison, the aromatic yield loss was ~20% when the total flow rate was 25 mL/min with H_2O concentration at 4%. This indicates the actual flow rate of H_2O is also important for the deactivation behavior of the DHA catalyst.

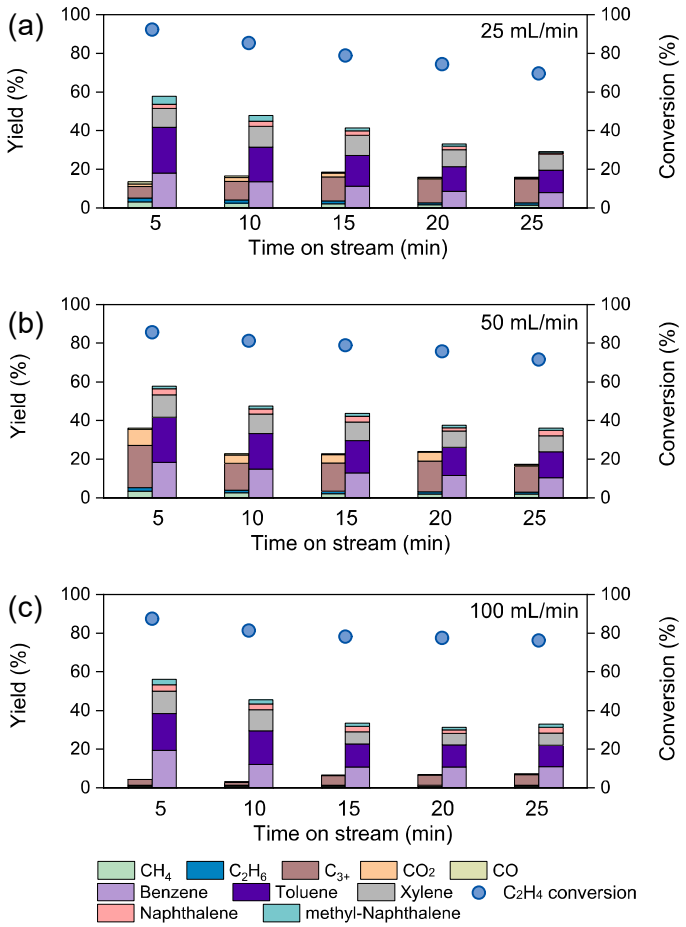

Figure 73. Stability test of the DHA reaction: DHA catalyst: 0.1 g HGaAlMFI catalyst, temperature 550 °C, pressure= 1 bar, reaction feeding: 10 mL/min C_2H_4, 2.5 mL/min H_2O(g) and Ar as the balance. (a) total reaction feeding rate =25 mL/min, H_2O concentration = 10% (b) total reaction feeding rate =50 mL/min, H_2O concentration = 5% (c) total reaction feeding rate =100 mL/min, H_2O concentration = 2.5%.

We also explored the Ag-based catalyst. Ag-ZSM-5 catalyst was prepared by ion-exchanged method with HZSM-5 catalyst soaked in $AgNO_3$ solution for 8h and calcination at 400 °C for 3 h in a muffle furnace. The catalyst was then tested for C_2H_4-DHA reaction. As shown in Figure 74, the Ag-ZSM-5 catalyst exhibited good performance in converting C_2H_4 into aromatics products. At 5 minutes, the ethylene conversion reached 90.4% and the overall aromatic yield reached 38.3%, with benzene yield at 3.1%, toluene yield at 17.0%, and xylene yield at 16.4%. In particular, CO yield at ~7.6%, which may result from the reduction of Ag_2O into metallic Ag by C_2H_4 or intermediates. At 10 minutes, the conversion reached 91.8% and the overall aromatic yield reached 46.0%, at which point the catalyst exhibited stable performance with similar results. At 25 minutes, the ethylene conversion reached 90.8% and the overall aromatic yield reached 45.7%, with benzene yield at 3.8%, toluene yield at 18.0%, and xylene yield at 19.7%. Notably, the Ag-ZSM-

5 catalyst has a higher selectivity for the xylene production as compared to the Ga-MFI catalysts, which may result from the nature of the active sites during the aromatization reaction.

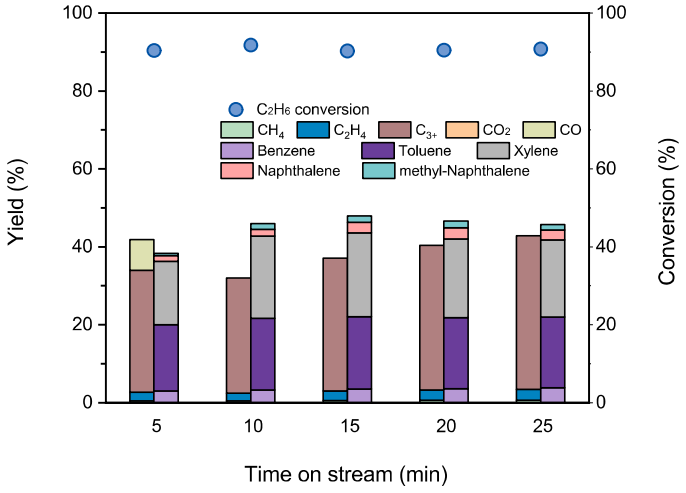

Figure 74. Stability test of the DHA reaction: DHA catalyst: 0.1 g Ag-ZSM-5 catalyst at 450 °C, pressure= 1 bar, reaction: 25 mL/min 40vol%C_2H_4/60vol%Ar.

The Ag-ZSM-5 was tested for C_2-DHA with C_2H_4 and H_2O co-feeding, as shown in Figure 75. Deactivation of the Ag-ZSM-5 catalyst was still witnessed during the C_2-DHA reaction as evidenced by a 50% decrease in aromatics yield over 25 minutes. At the 5 minutes, the conversion reached 83.3% and the overall aromatic yield reached 42.9%, with benzene yield at 1.9%, toluene yield at 12.8%, and xylene yield at 24.4%. At 15 minutes, the conversion reached 65.4% and the overall aromatic yield reached 28.7%, with benzene yield at 1.8%, toluene yield at 10.6%, and xylene yield at 16.3%. At 25 minutes, the conversion reached 56.2% and the overall aromatic yield reached 21.1%, with benzene yield at 2.0 %, toluene yield at 7.8%, and xylene yield at 9.3%. Generally, the effect of H_2O is not a concern in the C_2-DHA reaction as it is not a common reactant/product. However, our experiment results indicate the presence of H_2O can strongly affect the catalyst performance for both activity and stability, leading to deactivation of the catalysts for Mo, Zn, Ga, Ag-based catalysts. Concerning the role of H_2O, it might interact with active metal sites and even possibly affect the fundamental reaction mechanism of C_2-DHA. Further investigation may be needed to develop water-resistant DHA catalysts.

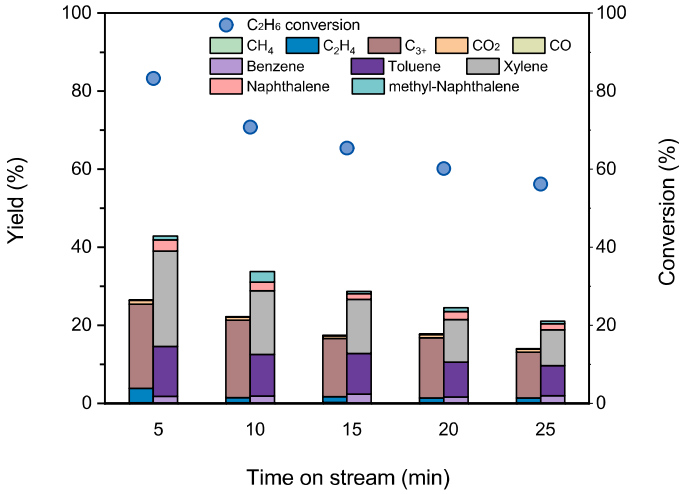

Figure 75. Stability test of the DHA reaction: DHA catalyst: 0.1 g Ag-ZSM-5 catalyst at 450 °C, pressure= 1 bar, reaction: 25 mL/min 40vol%C_2H_4/50vol%Ar with 10vol%H_2O(g) added.

Task 3: SHC-DHA Catalyst Combination

Several risks for the technology were identified, particularly relating to the compatibility of DHA and SHC catalysts when comingled in a physical mixture (at the particle scale), potentially resulting in a shift towards a sequential bed-style process (not unlike the industrial Houdry process) if the mixed SHC-DHA catalysts are not compatible after further refinement and optimization. Here we provide an overview of the findings for the combined DHA+SHC experiments at 700°C. In the following experiments, the DHA catalyst was 3 wt.% Mo/HZSM-5 (zeolite CBV-3024E from Zeolyst International; silica-to-alumina ratio or SAR = 30), synthesized and provided by the WVU team. Mo/HZSM-5 was carburized at 700°C under 80% CH_4 flow; unless otherwise specified, the carburization reaction was carried out immediately prior to the main DHA reaction. All experiments were conducted at a total flowrate of 25 ml/min during the DHA step (80% CH_4, bal. Ar). In each experiment, the loading of Mo/HZSM-5 was 700 mg, while that of the SHC redox catalyst varied. The SHC catalyst in all cases was 20 wt.% $Na_2WO_4/CaMnO_3$, which demonstrated ~75% selectivity towards H_2 combustion at 700°C. We anticipate to continuously evaluate additional redox catalysts as the project goes on. We begin by showing the baseline performance of the Mo/HZSM-5 catalyst in methane DHA (Figure 76). The catalyst performs as expected, meeting the typical figures for methane conversion (~10%) and benzene selectivity (70-80%) after about 30 min of time-on-stream. The initial 30 min consists of the well-documented carburization

step, in which the MoO_3 contained within the zeolite pores of the fresh DHA catalyst is reduced in CH_4 to form the active MoC_xH_y sites (molybdenum carbide, hereafter referred to by MoC_x). The byproducts of this carburization step are H_2, CO, and CO_2, and the most intense period is the first ~5 min induction period, after which benzene production begins and steadily rises until reaching a pseudo-steady state at 30 min. This is the base case DHA performance against which future experimental runs using both DHA and SHC are compared.

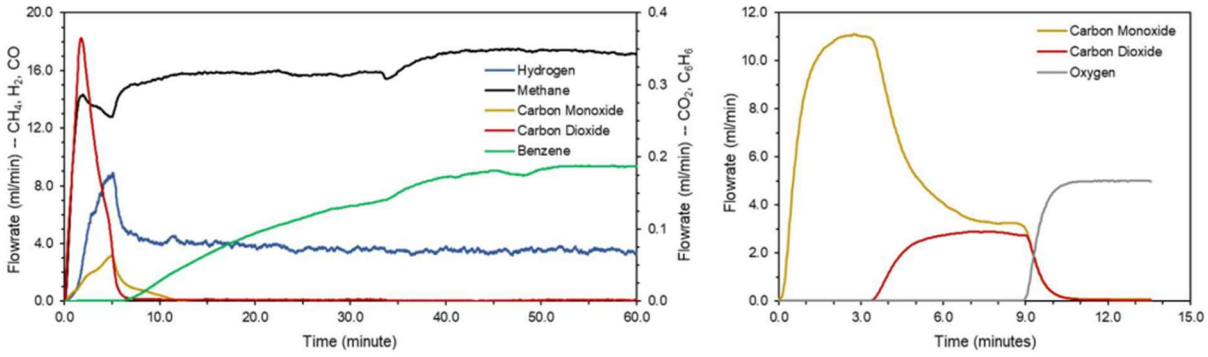

Figure 76. Base case performance for 0.7 g 3 wt.% Mo/HZSM-5 catalyst in methane DHA. Left: DHA reaction step using 80% CH4 and balance Ar, T = 700°C. CO2 and C6H6 flowrates use secondary axis for clarity. Right: Regeneration step using 16.7% O2 and balance Ar.

The right-hand side of Figure 76 shows the regeneration step for the DHA catalyst. The relative lack of stability for Mo/HZSM-5 is also well-documented in the literature, with most forms of the catalyst deactivating due to heavy coke and polyaromatic formation within 12-36 hours. Typical approaches for regenerating the DHA catalyst use an oxidative approach to remove coke and C_xH_y as CO and CO_2; however, the selective combustion of coke without re-oxidizing the MoC_x active sites remains a significant challenge in the community, and successful methods can include pulsing of O_2. In this report, we accept for now the complete removal of MoC_x sites following regeneration, and a key future challenge will be to discover a methodology not only for combusting coke, but also restoring the lattice oxygen of depleted SHC catalysts, without extensively oxidizing zeolitic MoC_x. This is conceptually similar to the composite core-shell OAS catalyst that will ultimately be developed and optimized. Figure 77 shows three sets of experimental results for three different physical mixtures, representing different mass ratios of DHA catalyst to SHC catalyst: 7-to-1, 7-to-4, and 7-to-7. The 0.7 g Mo/HZSM-5 is constant in all cases.

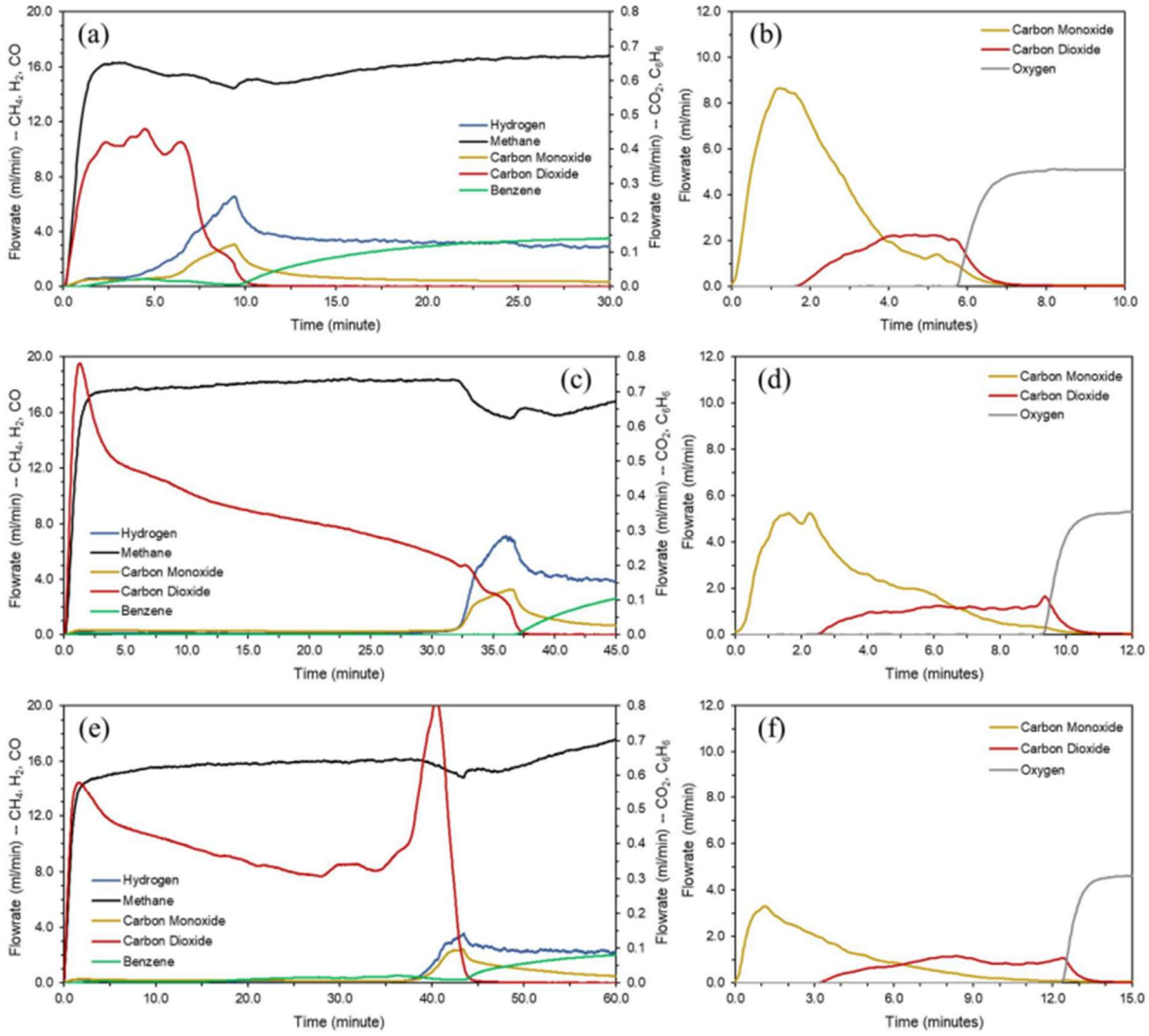

Figure 77. Three sets of DHA+SHC experiments in a physical mixture mode at 700°C. (a-b) 0.1 g SHC mixed with 0.7 g DHA catalyst. (c-d) 0.4 g SHC mixed with 0.7 g DHA catalyst. (e-f) 0.7 g SHC mixed with 0.7 g DHA catalyst. CO_2 and C_6H_6 flowrates use secondary axis for clarity. The x-axis is at different scale across the three sets of plots, the result of the reaction steps lasting longer with larger SHC mass loading.

The most significant finding from the physical mixture experiments depicted in Figure 78 is that the production of benzene is absent for as long as the redox catalyst is donating lattice oxygen (until t = 10 min in Figure 77a; t = 35 min in Figure 77c; t = 45 min in Figure 77e). Up until this point in each experiment, CO_2 is detected in substantial quantity, indicating either that the benzene is produced and directly combusted in entirety, or that the redox catalyst is reacting with the feed methane, a key intermediate such as ethylene, or potentially the MoC_x itself. The duration of the

CO_2 production (and the delay of benzene onset) is roughly proportional to the mass loading of the SHC redox catalyst, further supporting the conclusion that the redox catalyst is involved. In a practical sense, the loading of the SHC catalyst should be as large as possible so as to remove as much co-product H_2 as possible, and therefore we continue on with the largest mass ratio of 7-to7 to continue exploring the interactions between the two catalysts. Moving forward from the experiments of Figure 77, our prevailing theory was that the redox catalyst was interfering with or preventing the carburization step for the DHA catalyst, which is necessary for the MoC_x active sites to form. As a consequence, we attempted to spatially separate the two catalysts as a next step to verify that the two can perform their functions independently but in situ within the same reaction condition. Figure 78 shows the result of a sequential bed experiment using 0.7 g of each catalyst. In this case, the DHA catalyst has been previously carburized, such that there is no induction period for the production of benzene.

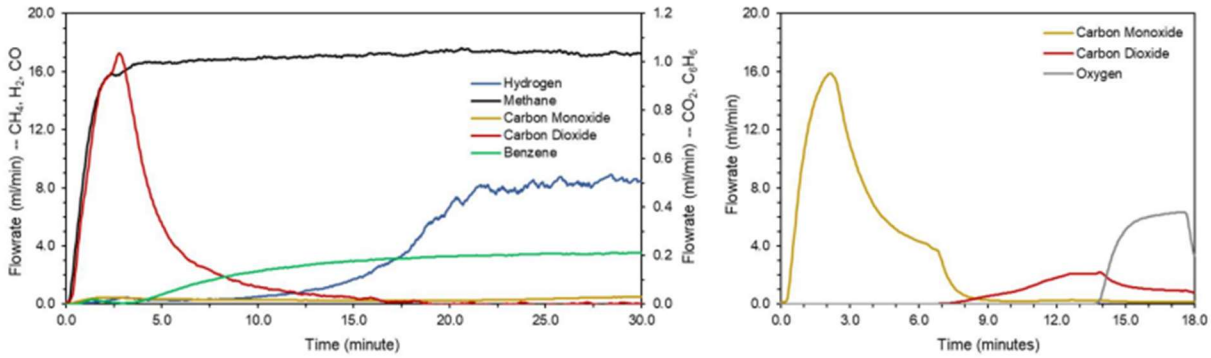

Figure 78. DHA+SHC experiment in a sequential bed mode, with 0.7 g Mo/HZSM-5 upstream of 0.7 g $Na_2WO_4/CaMnO_3$. The DHA catalyst has been pre-carburized prior to the depicted experiment.

Figure 78 shows that the sequential bed mode works in principle, allowing the selective combustion of H_2 (blue line) while minimizing the combustion of benzene and generation of CO_2 (red line). However, this selective performance exists only in an intermediate range of solid conversion, lasting from approximately t = 5 to 15 min, before which the non-selective surface oxygen of the SHC material leads to the combustion of benzene into CO_2, and after which the SHC redox catalyst is depleted of oxygen. This finding, to some extent, agrees with the H_2/C_6H_6 co-feed screening experiments and suggests that there may be an optimal regeneration condition which only partially reoxidizes the SHC redox catalyst to give the most H_2 combustion while losing the least benzene product. Importantly, this shows that the absence of benzene in Figure 77

is likely not due to poor benzene selectivity in the presence of the SHC catalyst, and is more likely to do with interference between the redox catalyst and the DHA active sites. However, it is also possible that certain radical DHA intermediates with short-length scales are being combusted in the physical mixture setting due to the intimate mixing of the DHA catalysts and the SHC oxygen source, but not in the sequential bed setting due to the spatial separation (~0.5") of the two catalyst beds. Switching from a sequential bed to a physically mixed mode, but utilizing a pre-carburized DHA catalyst, shed additional light on the material compatibility challenges between the DHA and SHC catalysts. If the lack of benzene or the appearance of CO_2 in the physical mixture setting was due to an initial interference of the redox catalyst with the carburization step, i.e. not allowing carburization to proceed, then the use of a pre-carburized catalyst in the mixture with the SHC catalyst should have resembled the results of Figure 78. In contrast, the results of the physical mixture shown in Figure 79 illustrate that this method more closely resembles the earlier results of Figure 77, in which a non-carburized DHA catalyst was mixed with the SHC redox catalyst.

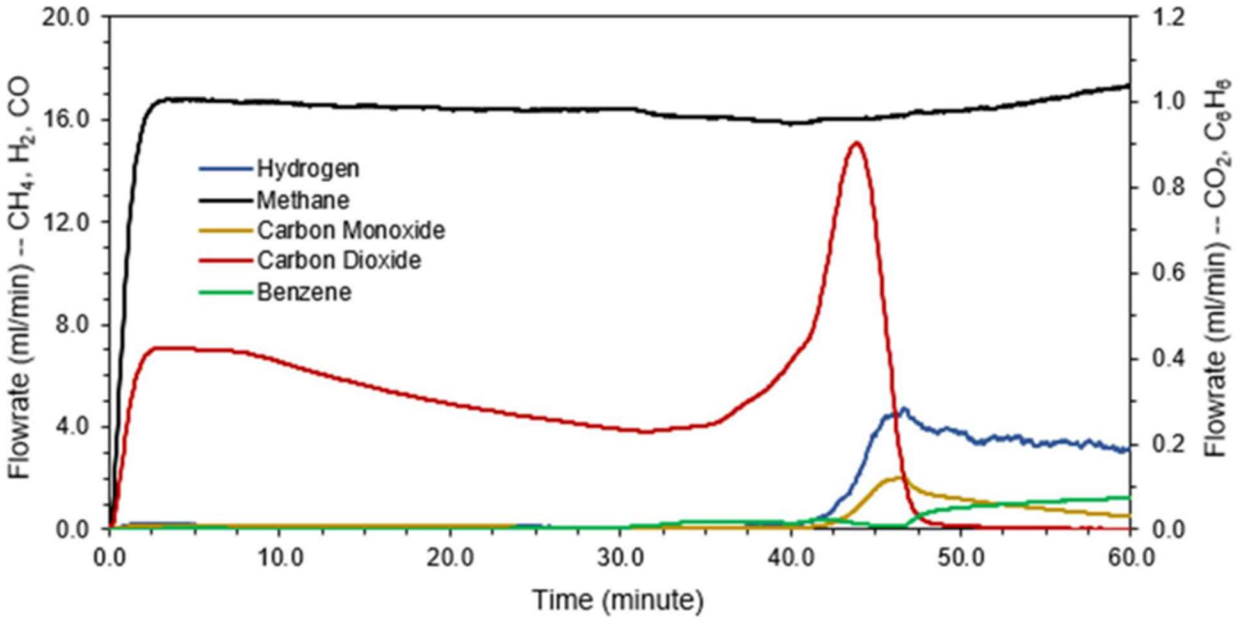

Figure 79. DHA+SHC experiment in a physical mixture mode, 0.7 g Mo/HZSM-5 mixed with 0.7 g Na2WO4/CaMnO3. The DHA catalyst has been pre-carburized prior to the depicted experiment.

As with Figure 77, the onset of benzene formation – and in fact, the appearance of H_2 and CO as telltale byproducts of MoO_3 carburization and MoC_x formation – are significantly delayed until

the redox catalyst is depleted. However, in the case of Figure 79, the catalyst had already been precarburized, and the results clearly indicate that the Mo/HZSM-5 underwent a second carburization around t = 45 min. The results show that the CO_2 formation is most likely due to an interaction, whether direct or indirect, between the lattice oxygen of $Na_2WO_4/CaMnO_3$ and the MoC_x active sites. This inhibits benzene from forming until the sites can be reformed in the presence of methane and the absence of available oxygen, as occurs at t = 45 min.

DHA+SHC composite bed investigation

The production of benzene is absent as long as the redox catalyst is donating lattice oxygen. Up to this point, only CO_2 and CO have been produced. Our hypothesis is that the redox catalyst can partially react with hydrocarbons and produce H_2O and CO_2 and the H_2O/CO_2 formed will inhibit the pre-carburization process to form MoC_x active species for benzene formation. Discussion with Lehigh, who has extensive experience characterizing the Mo/HZSM-5 catalyst, confirms the likelihood of this undesirable effect. To address this challenge and to further verify this hypothesis, we separately pre-carburized Mo/HZSM-5 and mixed it with fully oxidized $Na_2WO_4/CaMnO_3$. However, this still leads to significant amount of CO_2 formation and no benzene was formed, until all active lattice oxygen in the redox catalyst has been consumed.

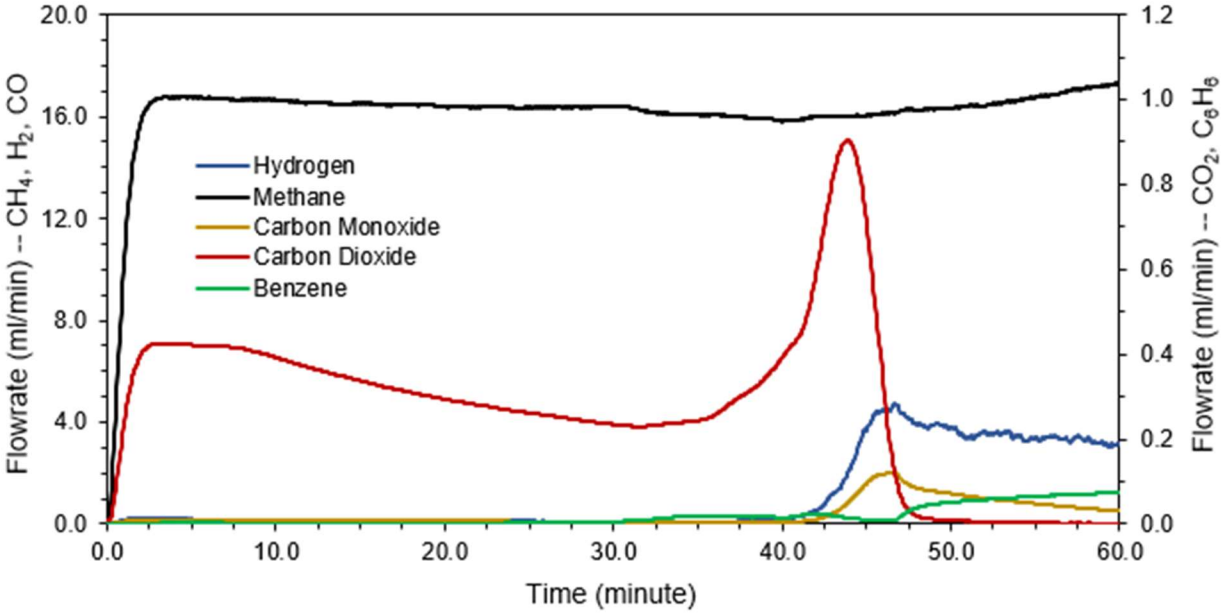

Figure 80. DHA+SHC experiment in a physical mixture mode, 0.7 g Mo/HZSM-5 mixed with 0.7 g $Na_2WO_4/CaMnO_3$. The DHA catalyst has been pre-carburized prior to the depicted experiment.

Our previous assumption for the cause of this issue is that the CO_2 formation is due to an interaction, either directly or indirectly, between the lattice oxygen of $Na_2WO_4/CaMnO_3$ and the MoC_x active sites. This may be caused by either physical contact between the over-active oxygen sites on $Na_2WO_4/CaMnO_3$ and MoC_x, or contact between the gaseous O_2 uncoupled from $Na_2WO_4/CaMnO_3$ and MoC_x. This inhibits benzene from forming until the sites can be reformed in the presence of methane and the absence of available oxygen. To counter this potential issue, we have prepared a partially oxidized $Na_2WO_4/CaMnO_3$ and we have taken measures to ensure minimal amounts of gaseous O_2 can be released from the partially oxidized $Na_2WO_4/CaMnO_3$. The partially oxidized $Na_2WO_4/CaMnO_3$ was prepared as such: first, a fully oxidized $Na_2WO_4/CaMnO_3$ was fully reduced under H_2 at 800°C; then, it was partially oxidized with air under lower temperature (450°C); then, the gas was switched to inert gas and the partially oxidized $Na_2WO_4/CaMnO_3$ was heated under inert gas to 800°C to uncouple any gaseous O_2. After these procedures, the partially oxidized $Na_2WO_4/CaMnO_3$ was physically mixed with a separately pre-carburized Mo/HZSM-5. The results were shown in Figure 81(a): at the beginning of methane injection (Time = 72 min to Time = 76.5 min), there was small amount of H_2 formation and no CO_2 and benzene formation were observed. After Time = 76.5 min, there was a sharp increase of both H_2 and benzene formation. Although there was no CO_2 formation throughout this process, after Time = 76.5 min, there was also no active lattice oxygen available for SHC. This can be more clearly shown when we track the Mass 18 signal from the mass spec as a characteristic peak for H_2O. As can be seen in Figure 81(b), from Time = 72 min to Time = 77 min, there was an increase in Mass 18 signal, indicating that some of the H_2 formed was combusted into H_2O. After Time = 77 min, there was a decrease of Mass 18 signal, indicating that the active lattice oxygen in the partially oxidized $Na_2WO_4/CaMnO_3$ has been consumed and there was no continued H_2O formation. We notice that this increase and then decrease of H_2O signal almost coincides with the time scale for benzene formation in Figure 81(a), especially when we take note that H_2O signal in a mass spec usually has around one or two mins signal delay. Figure 81 seems to indicate that the presence of water is inhibiting benzene formation on Mo/HZSM-5, even for a pre-carburized Mo/HZSM-5. These results further confirm that the active MoC_x species are highly sensitive to the presence of high concentration steam (and CO_2), i.e. the presence of soft oxidants such as steam at high concentrations would convert MoC_x into inactive/nonselective sites, preventing the formation of benzene. This finding indicates that our originally proposed composite or core-shell

concept, which intimately integrates Mo/HZSM-5 catalyst and SHC material, will not likely to work under practical conditions. We note that the enhancement for Mo/HZMS-5 with SHC material has been reported previously. However, the benzene yield in those cases were relatively low (4 Carbon% without SHC and 6 Carbon% with SHC). This, coupled with the less than ideal SHC activity in the previous reports, resulted in relatively low steam concentration in the system (e.g. 1.5 Vol.%).[16] The highly effective SHC material in the current study has resulted in much higher steam concentrations, negatively affecting the MoC_x stability.

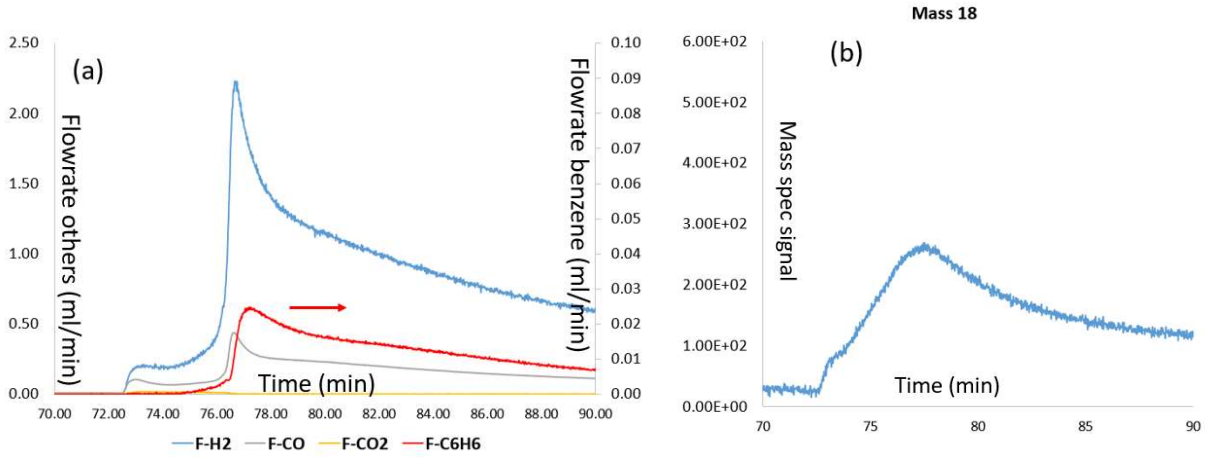

Figure 81. (a) DHA+SHC experiment in a physical mixture mode, 50 mg pre-carburized Mo/HZSM-5 mixed with 200 mg partially oxidized $Na_2WO_4/CaMnO_3$. Smaller amounts of samples were used for multiple screening experiments. (b) Mass 18 signal evolution using a mass spec. Mass 18 signal is characteristic of H_2O.

DHA+SHC and DHA+SHC+DHA sequential bed investigation

To better understand to effect of SHC product especially H_2O effect on the Mo/HZSM-5, we have compared three cases using different reactor bed configurations: (1) a single DHA bed; (2) a "DHA+SHC" 2-layer sequential bed and (3) a "DHA+SHC+DHA" 3-layer sequential bed. In these experiments, smaller amounts of Mo/HZSM-5 (50 mg) and $Na_2WO_4/CaMnO_3$ (100 mg) were used for proof-of-concept purposes and to save materials. The Mo/HZSM-5 used was fresh catalyst and the $Na_2WO_4/CaMnO_3$ was under fully oxidized state. For the single DHA bed, the products profile was consistent with previous reports, where a small amount of CO was formed at the beginning following the formation of benzene and large amount of H_2 (Figure 82a). For the "DHA+SHC" 2-layer sequential bed (Figure 82b), it was observed 93.2% of the H_2 formed in the single DHA bed

has been combusted before the H_2 "breakthrough" at Time = 285 min. From Figure 83(a) to 83(d), the benzene formation rate are also barely affected. Further extending the methane flow leads to fully consumption of the lattice oxygen from the redox catalyst and a "breakthrough" of H_2 flow rate. It was also noted that the CO formed in the single DHA bed has been mostly converting to CO_2 after the SHC bed. This is actually beneficial as CO_2 is much easier to separate than CO. These results indicate that a "DHA+SHC" 2-layer sequential bed is feasible in terms of selectively combusting H_2 and maintaining the benzene yield.

With established "DHA+SHC" 2-layer sequential bed concept, the "DHA+SHC+DHA" 3-layer sequential bed was further attempted as in Figure 82(c). From Time = 210 min to Time = 222 min, it was noticed that similar profiles of products (benzene, H_2, CO and CO_2) with "DHA+SHC" 2-layer sequential bed were formed following the injection of methane and there was effective H_2 combustion. However, there was not any effective further increase of benzene yield as would be anticipated if the equilibrium has been shifted in the 2nd DHA bed. It was observed that there was a sharp decrease of benzene flow rate and a quickly increased benzene flow rate at Time = 222 min, and the ever-increased benzene flow rate was higher than that of before. Moreover, it was noticed that also at Time = 222 min, there was a sharp increase of both CO and H_2 signal, a characteristic profile for the carburization of the DHA catalyst. As there is a large amount of H_2 formation after Time = 222 min, it is safe to assume that the SHC redox catalyst has been deprived of active lattice oxygen after Time = 222 min. To understand this figure, steam was negatively affecting the 2nd DHA bed from Time = 210 min to 220 min, during which time the 2nd DHA bed is not carburized or functioning. After T= 220 min, the 2nd DHA bed starts to carburize and for benzene. The slightly higher benzene yield after T=220 min is because of the higher amount of overall DHA catalyst loading (100 mg). This observation is entirely consistent with the previous observations in DHA+SHC physical mixtures in this and previous reports, where the presence of H_2O would affect both the formation and the stability of the MoC_x active sites and benzene formation.

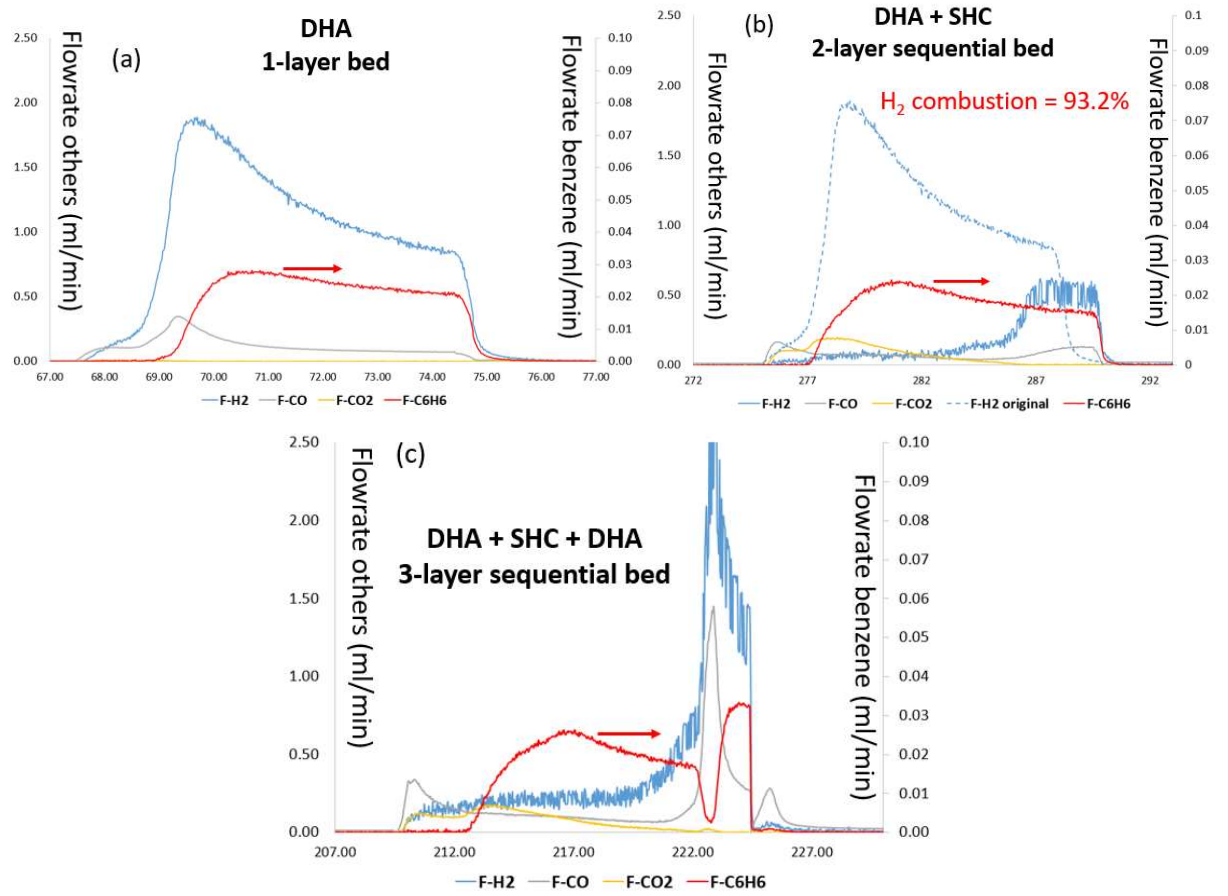

Figure 82. (a) a single DHA bed reactor; (b) a "DHA+SHC" 2-layer sequential bed reactor; (c) a "DHA+SHC+DHA" 3-layer sequential bed reactor. Each DHA bed has 50 mg of fresh Mo/HZSM-5 and each SHC bed has 100 mg of fully oxidized $Na_2WO_4/CaMnO_3$.

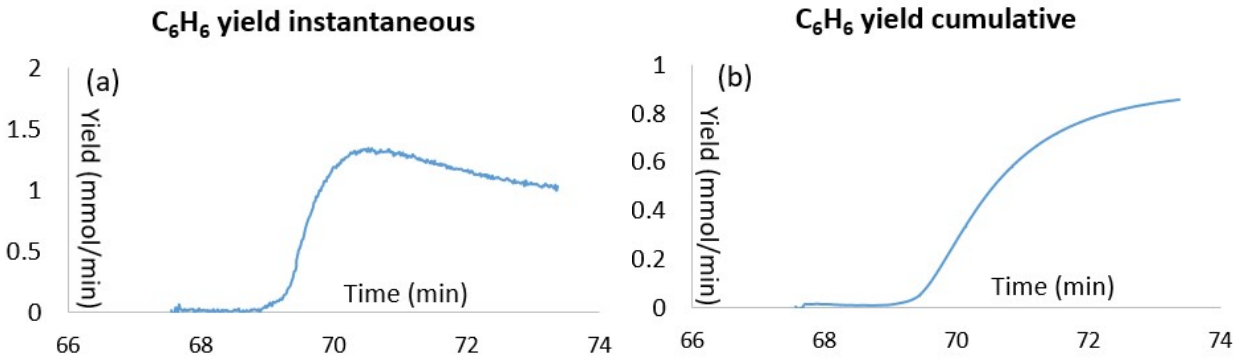

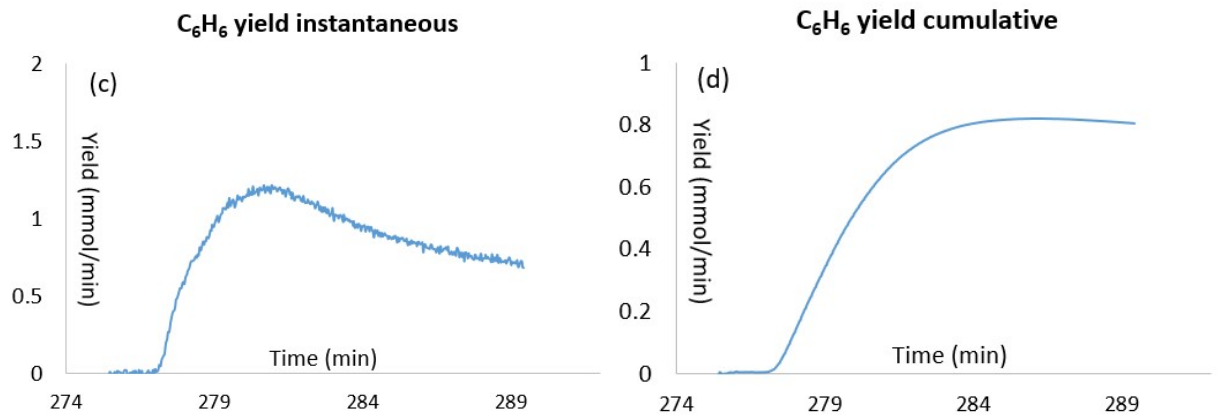

Figure 83. (a) and (b): instantaneous and accumulated benzene yield for a single DHA bed reactor; (c) and (d): instantaneous and accumulated benzene yield for a "DHA+SHC" 2-layer sequential bed reactor

Task 4: Aspen Models

As described in the revised initial TEA, the basis of the simulation is 50 bbl./day of liquid aromatics. The process models are being built using the AspenPlus™ simulation software. Using V11 of the software, a sequential modular scheme with modified Peng-Robinson equation of state (EOS) is being is being employed. For the base case, experimental values of DHA (non-oxidative) process are used from the literature since no commercial plant data is available. The major process parameters to be analyzed are: • Carbon efficiency (%) • Methane-to-liquid aromatic yield (%) • Modular process feasibility (process simplicity) • Total process energy demand (GJ/ton liquid product) The OAS process will also be compared with the GTL technology, which is industrially used to obtain liquid fuels from natural gas. There is detailed process analysis available in literature for the GTL process. In AspenPlus™, the OAS process is built using the scheme shown below, which involves three broad sections: reactor, power generation and product separation. Experimental redox results from NCSU, are being used to model the OAS reactor.

Base Case (Conventional Methane DHA)

The base case process model (Figure 82) assumes steady-state catalytic performance based on the best available results from literature (11% methane conversion; 8% benzene yield; 2% naphthalene yield; 1% coke yield)1 . The DHA catalyst (3 wt% Mo/HZSM-5) is represented by SiO_2 and is added in an amount corresponding to WHSV = 1 kg SiO_2/kg CH_4 feed per hour (or 1 h-1), matching

optimal conditions from experimental findings. For a production rate of ~50 bbl/day benzene, approximately 4800 kg SiO2 is required in total, with CH4 entering the reactor at 4800 kg/hr (~40% fresh feed, 60% recycled). Solid C is formed during the reaction and separated from the gas stream along with SiO_2, representing coke deposition and catalyst deactivation. An air regenerator is modeled to combust C (forming a CO_x-containing flue gas) and restore the catalyst to its initial state. Counter-current heat exchangers are included after the DHA reactor and the regenerator to pre-heat the methane and air flows, respectively, using the reactor effluent. The separation section includes a 4-stage compressor to increase the gas stream pressure to 20 bar followed by a cooler where the temperature is dropped to –50°C. This enables total removal of aromatics in a flash vessel. The vapor primarily contains CH_4 (~85 mol%) and H_2 (~15 mol%), from which methane needs to be separated for recycle. This can be achieved by commercial membranes like SEPURAN® (from Evonik2), which can do efficient CO_2/CH_4 separation. In this case, H_2/CH_4 mixture can be assumed to behave like CO_2/CH_4 mixture, since the desired product is pure methane with no hydrogen, for recycle. This separation is modeled as a Sep block, with 75% separation efficiency of methane, with close to 100% purity. This stream is mixed with the fresh methane stream as the reactor feed. The retentate is low pressure crude hydrogen containing methane. This can be used as a low carbon fuel for in-plant utilization. Oxidative Aromatization System (Methane DHA + SHC) For the oxidative aromatization system (OAS), the most substantial upstream changes are the inclusion of: (a) the redox catalyst for selective hydrogen combustion (SHC), (b) the addition of a reactor for SHC, (c) a second regenerator for the redox catalyst, and (d) adjustments to the DHA catalyst performance based on anticipated synergy between DHA and SHC catalysts. The OAS system (Figure 83) assumes steady-state DHA catalytic performance of 25% methane conversion, 16% single-pass benzene yield, 4% naphthalene yield, and 5% coke yield. The substantial increase in coke is based on literature observations that the removal of product H_2 favors heavy hydrocarbon and coke formation in methane DHA. The WHSV for the DHA catalyst remains the same at 1 h-1, though the DHA catalyst loading decreases by ~40% due to the higher methane conversion and commensurate decrease in methane flowrate needed to achieve 50 bbl/day benzene production. The SHC catalyst is modeled as an equimolar mixture of CaO and MnO_2 solids, representing the $CaMnO_3$ redox catalyst. The reduction of the redox catalyst is included as the reaction: $H_2 + 2\ MnO_2 \rightarrow H_2O + Mn_2O_3$. We include sufficient redox catalyst to combust 90% of the H2 present and assume that 60% of the redox catalyst's available oxygen

capacity is utilized, equating to approximately 4 wt.% oxygen donation at steady-state, which is comparable to recent experiment results. The amounts of DHA and SHC catalyst are 3100 kg/hr and 28600 kg/hr, respectively. Similar to the base case, all solids are separated from the gas stream and sent to the regenerator section; in the OAS case, a second regenerator uses O_2 from air to completely re-oxidize Mn_2O_3 to MnO_2, and both regenerated catalysts are recycled to the reactor. In the separation section, the primary consequences of SHC are: (a) lower methane input for the same aromatics yield as a result of higher methane conversion, and (b) 90% removal of H_2 as H_2O. To take the steam out of the products stream, a knockout vessel is included prior to the compressor. The interstage liquid streams from the multi-compressor remove most of the remaining water, while the flash unit (again operating at 20 bar and –50°C) removes the liquid aromatics at ~50 bbl/day (most of it being benzene). A similar membrane step (as described above) is simulated to purify the recycle methane stream, with the permeate containing all H_2 (at a significantly lower amount than the base case due to the SHC reaction) and remaining aromatics. The mixed feed stream for the DHA reactor is approximately 50% fresh feed and 50% recycled methane.

This is an initial process model for the two processes.

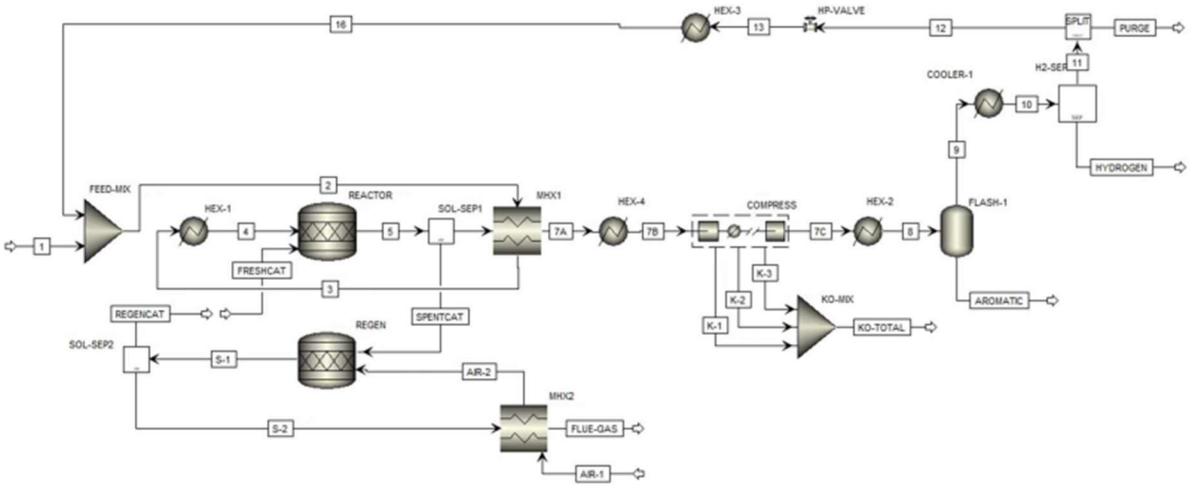

Figure 84. AspenPlus (V11) model for the base case of methane DHA.

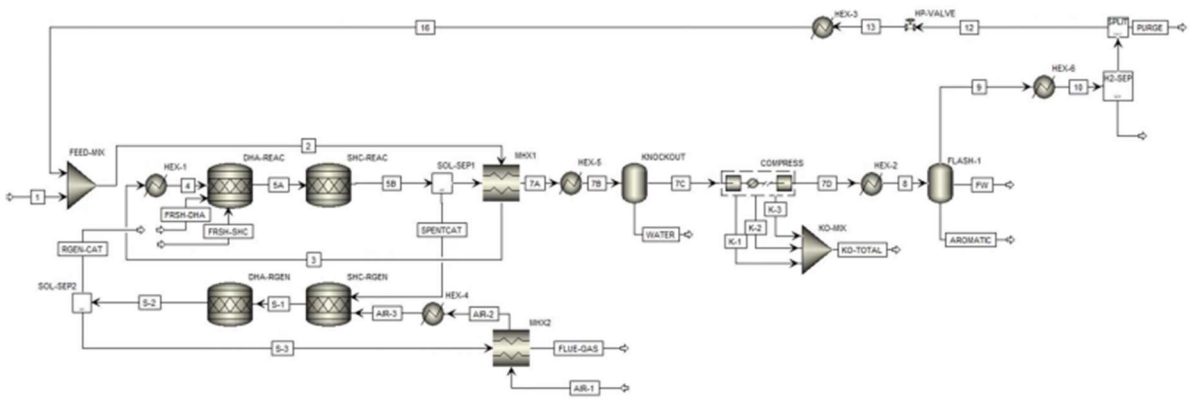

Figure 85. OAS process scheme for production of liquid aromatics

The analysis performed by Susteon involved four cases

Table 26. Four different case classes

Case	Description
Base Case	Non-oxidative methane dehydroaromatization (DHA), using typical literature aromatic yield of 10% over a 3% Mo/HZSM-5 catalyst for the reactor performance specifications.
OAS 10%Y	The oxidative aromatization system (OAS) proposed by NCSU, assuming 90% of all co-produced H_2 is combusted to water by the redox catalyst, but assuming that the aromatics yield remains at 10% per pass (no yield improvement over Base Case).
OAS 20%Y	A variant of the oxidative aromatization system (OAS) proposed by NCSU, assuming 90% of all co-produced H_2 is combusted to water by the redox catalyst, and assuming that aromatics yield is doubled to 20% per pass in response to lifting of equilibrium limitations.
OAS 40%Y	A variant of the oxidative aromatization system (OAS) proposed by NCSU, assuming 90% of all co-produced H_2 is combusted to water by the redox catalyst, and assuming that aromatics yield reaches 40% per pass in response to lifting of equilibrium limitations (equal to the target outlined in the proposal).

The basis for the four cases is an aromatics production rate of approximately *19 kg/s* (including benzene, toluene, and naphthalene), which derives from a natural gas process feed flowrate of 5 MMSCF/h in the Base Case. These values are selected to match a detailed non-oxidative DHA scenario published by Huang *et al*. (2019)[17], upon which the Base Case of this analysis is modeled. The Base Case and the OAS 10%Y case use this same 5 MMSCF/h feed flowrate, while the feed flowrates of the two higher-yield cases are slightly lower. All cases lead to the same aromatics production rate of approximately 19 kg/s.

In determining the process energy consumption for each of the cases, the **following major streams and unit operations** are considered:

- Energy content of feed and product streams
- Reactor feed pre-heating
- Reactor heating requirements
- Heat recovery and steam generation from exiting hot streams
- Compression work
- Refrigeration (including distillation column condensers)
- *For OAS cases*: Heat released from the selective hydrogen combustion (SHC) reaction.
- *For OAS cases*: Heat released from the redox catalyst regeneration.

In developing the AspenPlus™ process models and performing the energy analysis, the **following assumptions** are made:

- The feed natural gas contains 95.3% CH_4 and balance of natural gas liquids (C_2H_6, C_3H_8, *n*-C_4H_{10}). It is assumed that N_2 and CO_2 are removed prior to entering the process.
- In the Base Case and in the OAS 10%Y case, the reactor gives standard methane DHA performance of ~11% CH_4 conversion and an approximate product distribution of 5.5% C_6H_6, 4% $C_{10}H_8$, 0.5% C_7H_8, 1% coke, all on a molar basis.
- In the OAS 20%Y and 40%Y cases, the yields are scaled by a factor of two and four, respectively, with no difference in the relative product ratios.
- The redox catalysts in the OAS technology are taken as an equimolar mixture of CaO and MnO_2, representing the $CaMnO_3$ redox catalyst. The reduction of the redox catalyst is the reaction: $H_2 + 2\ MnO_2 \rightarrow H_2O + Mn_2O_3$. We include sufficient redox catalyst to combust 90% of the H_2 present and assume that 60% of the redox catalyst's available oxygen capacity is utilized, equating to approximately an oxygen donation of 4 wt.% at a steady state.
- The redox catalysts in the OAS technology are capable of combusting 90% of all H_2 *in situ*, which releases heat. It is assumed that the heat resulting from selective hydrogen combustion (SHC) can be directly used to maintain reactor temperature and heat the feed gases at 60% efficiency.

- It is assumed that no non-selective combustion occurs (e.g., of benzene) that would result in product losses.
- The regeneration of the redox catalyst releases heat in a separate regenerator reactor. It is assumed that this heat can be recovered and used to superheat steam for electricity requirements with a total heat-to-electric efficiency of 40%.
- Heating and cooling duty requirements for major units are taken from AspenPlus™.
- Heat and electricity requirements are assumed to be supplied by natural gas firing. The amount of gas required is calculated by assuming 60% efficiency of steam heating and 40% efficiency of natural gas-to-electricity conversion. While not considered at this time, the "losses" due to inefficiency contain valuable energy for heating elsewhere in the process and can be used for minor lower-temperature duties, such as column reboilers.
- For the refrigeration sections (cryogenic coolers and the condenser of the cryogenic high-pressure demethanizer column), the compression work requirement is calculated using the cooling duty from AspenPlus™ and a set of empirical factors derived from Luyben *et al*. (2017)[2] for a three-stage refrigeration unit with methane or ethylene as the refrigerant.
- Energy content of feed and product streams are calculated using lower heating value (LHV) on a mass basis at 15°C.

During the model development, however, Susteon determined that the modular scale would not be suitable for *non-oxidative* DHA, and that a 50 bbl./day aromatic production rate would only be feasible for the proposed OAS technology; the principal reason for this is the difficulty of H_2/CH_4 separation at modular scale and the poor economic value of the resulting crude hydrogen stream. Accordingly, to obtain a fair comparison between non-oxidative DHA and OAS, new process models were developed at a larger scale, representing aromatics production in a centralized facility fed by natural gas delivered at pipeline conditions.

The base case was modeled after the work of Huang *et al*. (2019),[17] the most complete representation of industrial-scale non-oxidative DHA in the literature. There is currently no industrially practiced version of methane DHA, but Huang and coworkers provide a detailed framework and reasonable technoeconomic analysis for what non-oxidative DHA could look like at scale. Figure 86 depicts the scheme laid out in Huang et al[17]. Beginning at left, fresh natural

gas and a recycle stream are mixed and enter the catalytic DHA reactor (R-1). Feed pre-heating and reactor heating requirements are met by firing of natural gas with air. The exiting hot stream is used to superheat steam for power generation to offset electricity needs elsewhere in the process (E-1). The cooled product stream then goes through a series of compressors (C-n) and flash vessels (F-1 to F-5) to incrementally separate heavier aromatics (toluene, naphthalene) from the lighter gases, before entering cryogenic separation (E-n, F-6 to F-9), which removes the bulk of benzene and separates high-purity hydrogen from methane. H_2 leaves as a product stream and a CH_4-rich heavy stream is recycled to the reactor, containing residual H_2, C_6H_6, and other compounds. Several distillation columns (D-1 to D-3) handle the separation of (1) C_1 from C_2, (2) naphthalene from single-ring aromatics, and (3) toluene from benzene.

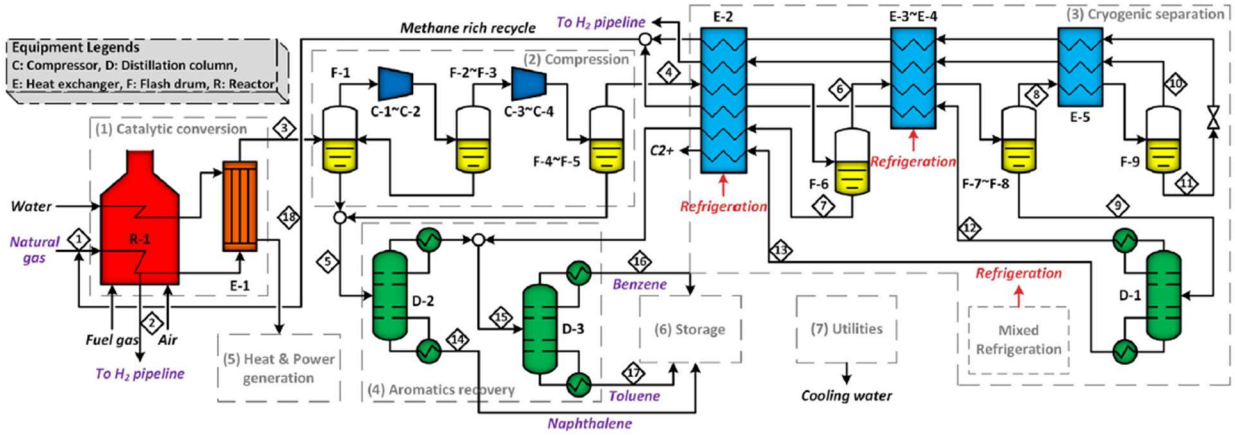

Figure 86. Process scheme for non-oxidative methane dehydroaromatization (DHA) at a scale of 5.0 MMSCF/h natural gas feed flowrate, from Huang *et al*. 2019.[17] The Huang model has been recreated by Susteon and used as the base case against which OAS is compared.

The base case, along the lines of the Huang model[17], was simulated by Susteon using AspenPlus™, as illustrated in Figure 87 (upstream) and Figure 88 (downstream). The model is laid out to achieve visual parity with the PFD from Huang *et al*. (Figure 88). Fresh natural gas at pipeline specifications (25°C, 31 bar), consisting of 95.3% CH_4 with small amounts of ethane, propane, and *n*-butane, is throttled and mixed with a recycle stream containing primarily methane. The feed is pre-heated and sent to the DHA reactor, which is modeled as two blocks, one which handles the gaseous reactions (REACTOR, an R-Gibbs block) and one which simulates coke deposition (COKING, an R-Stoic block). The coke is removed (SOLIDSEP) and the stream passes

through a heat recovery unit, which superheats steam at 30 bar and cools the process stream to 120°C. A final cooler brings the stream to 30°C.

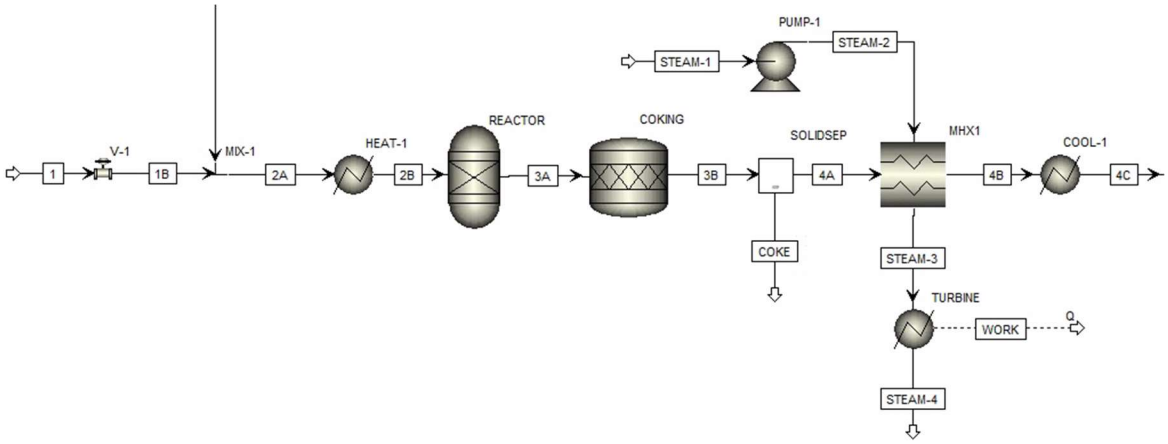

Figure 87. Recreation of the non-oxidative DHA process model from Huang et al.,[17] built in AspenPlus™. The upstream section is shown, including the feed mixing and pre-heating, catalytic reactor, and heat recovery steam generation systems.

The cooled product stream enters the compression and flash separation section (Figure 88, left side), where a series of flash vessels at 30°C remove most of the toluene and all of the naphthalene at increasing pressure. The pressurized stream (at 36 bar), still containing most of the benzene, then enters the cryogenic separation system, where the benzene is removed at -72°C. The remaining flash units and coolers are for the separation of H_2 and CH_4, which requires a final temperature of -167°C. The vapor H_2 exits as a pure product stream (>97% purity), while the liquid methane is heat exchanged with other streams to return to vapor phase and join the distillate of column D-1 to create the reactor recycle stream, which is roughly six times greater than the fresh feed rate due to the low conversion of the DHA reactor.

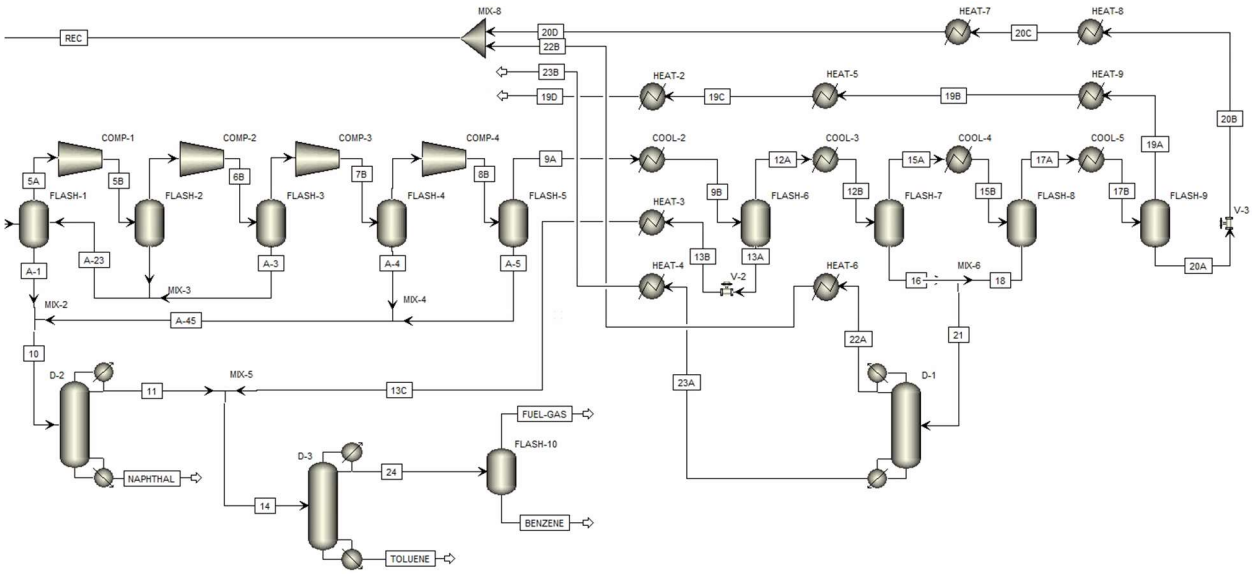

Figure 88. Recreation of the non-oxidative DHA process model from Huang et al.,[17] built in AspenPlus™. The downstream section is shown, including the compression, flash separation, cryogenic separation, and distillation sections.

Distillation column D-1 handles a CH_4-rich stream which contains some H_2 and all of the C_{2+} compounds (which includes any remaining natural gas liquids as well as ethylene, propylene, and butenes). These exit as bottoms from D-1 and leave the system (stream 23) in a mixture without further purification. Columns D-2 and D-3 handle aromatics purification, with D-2 separating naphthalene from the single-ring aromatics and D-3 separating toluene from benzene. A final flash vessel is added to the Huang model to remove CH_4 from the D-3 distillate, which contains the product benzene; this stream is treated as fuel gas and can be used as an offset later when the TEA is refined.

The upstream section of the OAS process model is shown in Figure 89. The feed mixing and pre-heating are similar to the base case. The reactor is split into two R-Stoic blocks. "DHA-REAC" uses an identical CH_4 conversion and product distribution to the reactor blocks in the base case ("REACTOR" and "COKING"), and in this case the DHA and coking reactions occur in the same reactor. Fresh DHA and SHC catalysts are added to the reactor. The DHA catalyst (3 wt% Mo/HZSM-5) is represented by SiO_2 and is added in an amount corresponding to a WHSV = 1 kg SiO_2 / kg CH_4 feed per hour (or 1 h^{-1}), matching optimal conditions from experimental findings. In the "SHC-REAC" block, the selective combustion of 90% of the H_2 proceeds to give water. Solid separation block removes the redox catalyst components (CaO, MnO_2, Mn_2O_3) and coke (C),

which go to the regenerator reactor. Air is fed in 20% excess to oxidize all Mn_2O_3 to MnO_2 and all C to an equimolar mix of CO and CO_2, which is contained in the "FLUE-GAS" stream. The main process stream, containing unreacted CH_4, NGLs, olefins, aromatics, and water, is cooled with a similar heat recovery steam generation system as in the base case ("MHX1"). A knockout vessel at 20°C removes most of the water.

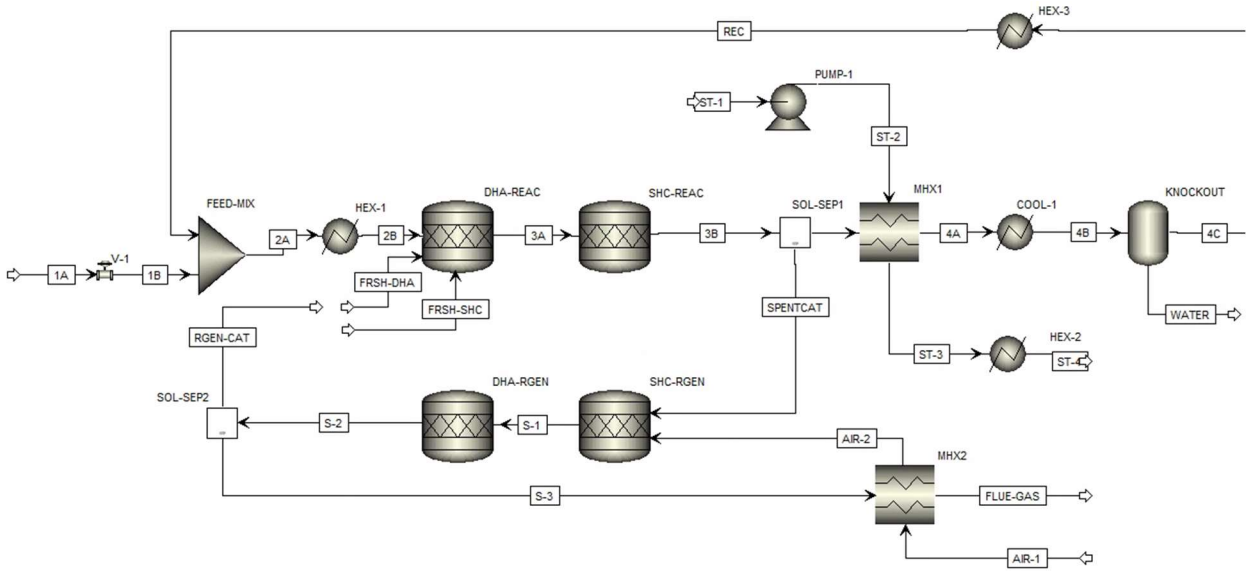

Figure 89. Upstream section of the OAS process model. Significant additions to the base case model include the SHC reactor (which models the combustion of H_2 and does not represent a second physical reactor), the regenerator (which re-oxidizes the redox catalyst and *does* represent separate equipment), the redox catalyst loop, air pre-heating, and water knockout.

The downstream section of the OAS process model is shown in Figure 90. Most of the separations are similar to the base case of Huang et al[17]., with a few significant simplifications which make OAS advantageous. The compression and flash section (left-hand side of Figure 90) are mostly identical to the base case (Figure 88), as are distillation towers D-2 and D-3, as the OAS process does not simply aromatics separation. By contrast, the later cryogenic separation section (right-hand side of Figure 90) is significantly less complicated in terms of both energy and equipment requirements, a consequence of the removal of H_2 via reactive separation (SHC) in the DHA reactor, rather than at cryogenic conditions. "FLASH-6" operates at the same conditions as in the base case (36 bar, -72°C) to remove benzene from the light gases, and the exiting vapor is sent directly to column D-1 to remove C2+ compounds. D-1 still requires cryogenic conditions and operates in an identical manner to the base case as the feed composition underwent little change.

The distillate, comprising primarily CH_4 and most of the 10% of H_2 which was not combusted via SHC, is recycled to the DHA reactor. This fraction of H_2 returning to the DHA reactor is similar to the amount which returns to the reactor in the Huang reference case. In summary, the OAS allows for three of the ten flash vessels from the base case to be removed, while the lowest temperature requirement for cryogenic flash separation is -72°C, rather than -167°C, enabling significant energy savings in refrigeration.

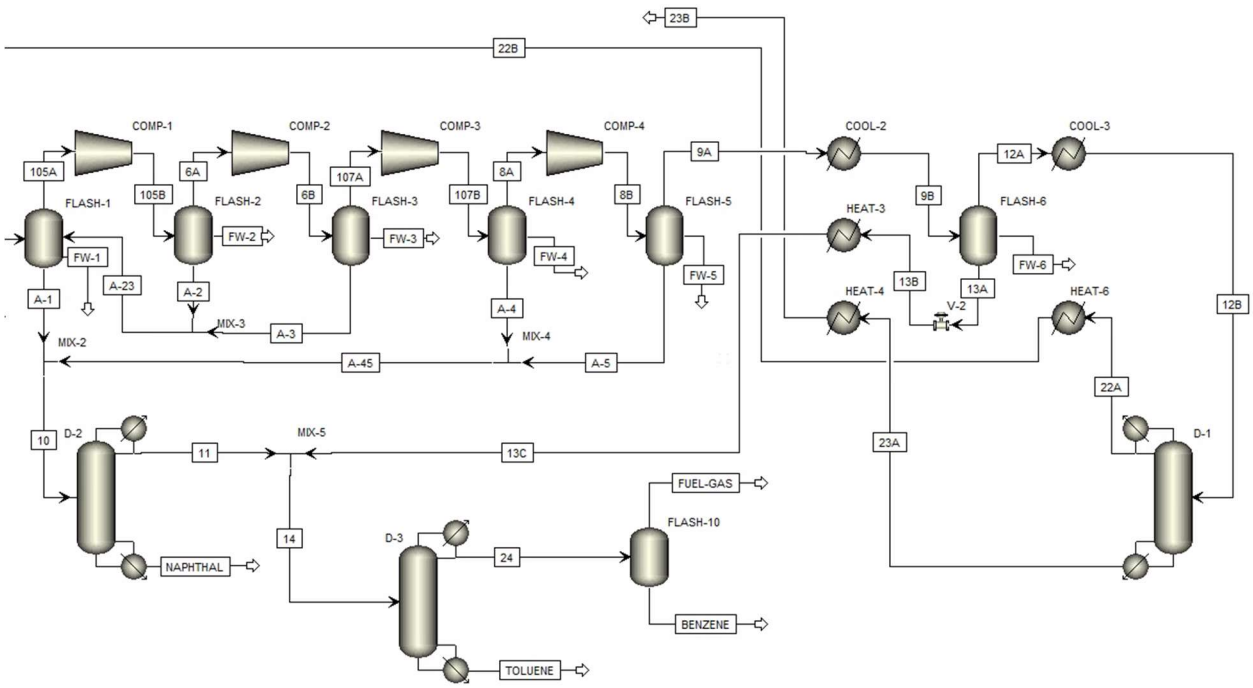

Figure 90. Downstream section of the OAS process model. This section is mostly identical to the base case (Huang et al.[17]). Some equipment is removed, most notably the later cryogenic flash vessels (F-7 to F-9) and accompanying coolers. The distillate of column D-1 now contains the recycle methane and hydrogen and returns to the front of the process as stream "22B".

Process Energy Balances

The process models illustrated in Figure 87-90 are used as the basis to directly compare the OAS technology with the base case, non-oxidative methane DHA, on an identical scale. Three versions of the OAS process model were prepared to simulate the 10%, 20%, and 40% aromatics yield cases.

Table 27 summarizes the process energy balances for the Base Case, OAS 10%Y, OAS 20%Y, and OAS 40%Y cases. In the **Base Case**, which is based upon the non-oxidative methane DHA process described by Huang *et al*.[17], a net energy input of **1659.2 MW** is required to produce aromatics at a rate of 18.8 kg/s, which equates to an energy demand of **88.3 MJ/kg** aromatics. This calculation assumes that all H_2 produced during the process is directly used as a fuel gas to meet process heat requirements, which is not assumed in the reference. Approximately 60% of the energy input comes from the energy content of the natural gas feed stream, with the balance coming from the natural gas fuel stream. Nearly 67% of the energy is lost to heat and work requirements across the process, with 33% exiting in the products.

Table 27. Process energy balances for non-oxidative methane DHA (Base Case) and three scenarios for OAS.

Values in MW (unless otherwise noted)	**Base Case**	**OAS 10%Y**	**OAS 20%Y**	**OAS 40%Y**
Inlet Flows				
Natural Gas (Feed Stream)	1400.0	1400.0	1355.0	1330.5
Outlet Flows				
Benzene	334.5	345.1	339.0	337.7
Toluene	15.5	15.6	14.8	14.7
Naphthalene	456.4	471.6	460.0	454.6
C2+	14.4	24.7	23.6	22.7
Hydrogen	681.5	0.0	0.0	0.0
Coke	121.0	138.3	135.0	133.0
Fuel Gas	25.7	32.4	18.1	7.9
Heat				
Input (Reactor, Pre-heating, etc.)	679.1	694.0	424.1	293.8
Output (H_2 combustion) [a]	0.0	-265.8	-259.3	-256.0
Net Heat Required	**679.1**	**428.2**	**164.8**	**37.8**
Electricity				
Compression	168.3	141.5	62.8	24.7
Refrigeration	285.5	262.8	96.7	15.6
Generation (HRSG, Regen, etc.) [b]	-191.6	-266.4	-159.5	-121.9
Net Work Required	**262.2**	**137.9**	**0.0**	**-81.5**
Fuel Credits				
Hydrogen	681.5	0.0	0.0	0.0
Fuel Gas	25.7	32.4	18.1	7.9
Excess Heat (i.e., Exotherms) [c]	0.0	0.0	23.6	0.0

Totals				
NG for Heat (60% eff.)	1131.8	713.7	274.7	63.0
NG for Electricity (40% eff.)	655.5	344.9	0.0	-203.9
Fuel Requirement before Credits	1787.3	1058.5	274.7	63.0
Fuel NG Requirement after Credits	**1080.1**	**1026.1**	**233.1**	**-148.8**
Energy in Valuable Products	820.9	857.0	837.3	829.8
Net Energy Demand (Energy Lost) [d]	**1659.2**	**1569.1**	**750.8**	**352.0**
Aromatics Production Rate (kg/s)	18.8	19.4	19.0	18.8
Specific Net Energy Demand (MJ/kg)	88.3	80.9	39.6	18.7
% Reduction in Energy Demand	**--**	**8.4%**	**55.2%**	**78.8%**

a) 60% efficiency penalty applied to *in situ* heat generation from selective H_2 combustion reaction.
b) 40% efficiency penalty applied to electricity from heat recovery steam generator / steam heated by regeneration.
c) For the OAS 20%Y case, a small amount of excess energy was available from HRSG and regeneration after all process work requirements were met. The difference was treated as fuel gas and applied to stream heating. For the OAS 40%Y case, a large enough excess of work was available to treat the process as a net generator of electricity.
d) "Net Energy Demand (Energy Lost)" is defined as all input energy (Natural Gas Feed and Natural Gas for Fuel) minus that energy which exits the system as valuable products (Benzene, Toluene, Naphthalene, and C2+; the latter is primarily ethylene, ethane, and propylene). Losses go to process heat/work requirements and undesired products.

The **OAS 20%Y case** assumes that H_2 removal by the redox catalysts will enable aromatics yield of 20% from methane. As a result, the gas flowrate through the reactor is halved (as is the necessary DHA catalyst loading), and the methane-rich recycle flowrate decreases by over 50% (approx. 3-to-1 ratio with the fresh feed, compared with ~7-to-1 in the Base Case). The decrease in overall system flowrate has significant impacts across the process, with the feed pre-heating requirement and the compression and refrigeration work requirements all decreasing by more than half. The reactor heat input stays roughly the same, as the ΔH of the reactions do not change; similarly, the exotherms from H_2 combustion and redox catalyst regeneration stay the same, as the amount of H_2 combustion (and the loading of SHC redox catalyst) do not change. Overall, the OAS 20%Y case requires a net energy input of **750.8 MW**, equating to a specific energy demand of **39.6 MJ/kg** aromatics, and an **energy reduction of 55.2%**.

For the **OAS 10%Y case** (which is a lower end OAS case), the same reactor performance is assumed as in the Base Case, with the selective H_2 combustion (SHC) reaction and the presence of the regeneration step being the only differences. Taken together, the SHC reaction and the regeneration reaction roughly equal the *ex situ* burning of hydrogen gas in the Base Case. As a result of this, and because the feed basis and feed-to-recycle ratio remain the same, the two cases closely resemble one another in terms of energy demand: the OAS 10%Y case requires input of **1569.1 MW**, leading to a specific energy demand of **80.9 MJ/kg**, and **a reduction of 8.4%**. The thermal efficiency of the process improves slightly (35.3% energy in products). The slight improvement in energy demand comes primarily from the reduction in compression and refrigeration work. The absence of gaseous hydrogen in the products stream in the OAS process reduces the load on the compressors. Additionally, the *in situ* reactive separation of H_2 from the other gases allows for simplified downstream separation and the removal of several cryogenic flash vessels, which separated hydrogen from methane in the Base Case.

The case of 40% single-pass aromatics yield, identified in the proposal as the target performance at the end of the project period, is described in the **OAS 40%Y scenario**. The recycle-to-feed ratio decreases to ~1.2, which further reduces the pre-heating, compression, and refrigeration energy requirements from the 20%Y case. Due to the exothermicity of the SHC reaction and redox catalyst regeneration, both of which are held constant, the OAS 40%Y process is capable of generating more work than it requires for compression and refrigeration, allowing this process to become a net generator of electricity. A small amount of natural gas is required for stream and reactor heating. Overall, the OAS 40%Y case requires a net energy input of **352 MW**, most of which comes from the energy content of the natural gas feed stream by way of H_2 production and combustion, and **-82 MW of useful work** can be exported. The input equates to a specific energy demand of 18.7 MJ/kg aromatics, representing a **process energy demand reduction of 78.8%**.

The system-wide energy balances for the Base Case and the OAS 10%Y case are illustrated as block flow diagrams in Figure 91 and Figure 92, respectively.

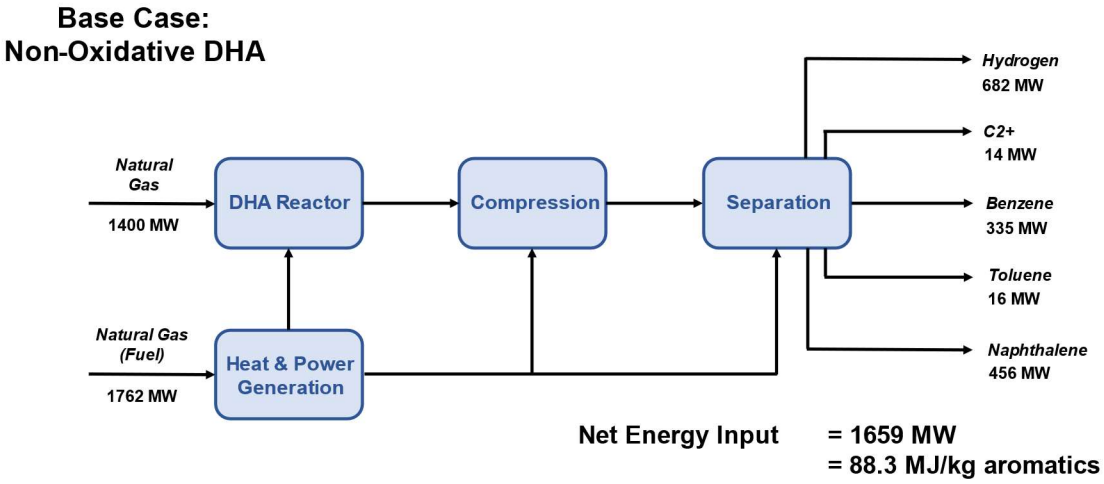

Figure 91. Block flow diagram depicting the system-wide energy balance for the Base Case, including major unit operations and major material streams with energy content.

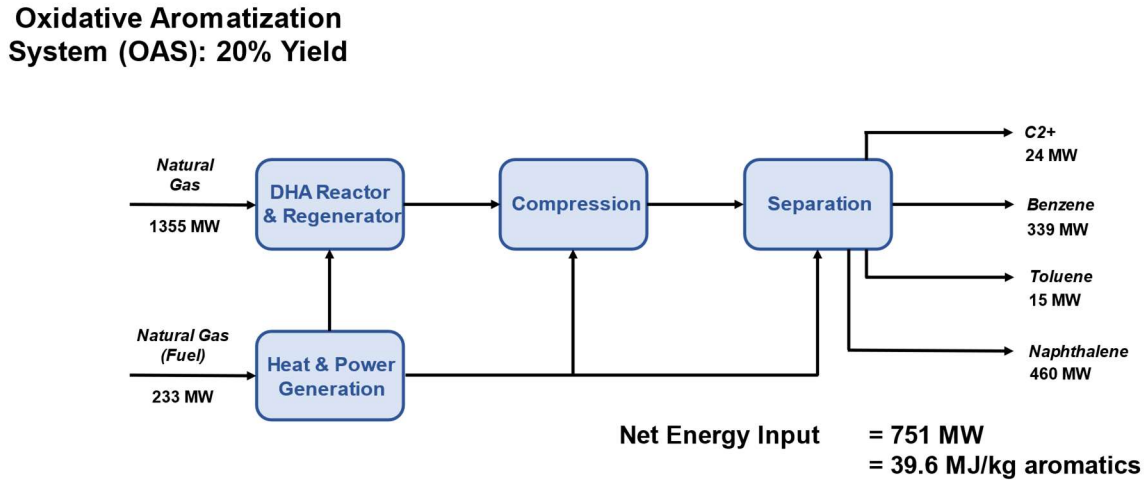

Figure 92. Block flow diagram depicting the system-wide energy balance for the OAS 20% Yield case, including major unit operations and major material streams with energy content.

Using oxidative coupling of methane (OCM) followed by DHA+SHC. The first step produces ethane and ethylene, which is then aromatized with selective hydrogen combustion. At 20% aromatics yield, which is twice the base-case non-oxidative DHA yield, a *55% reduction in net energy demand* is estimated. A higher reduction of 78% can be achieved at *40% aromatics yield*. The model was extended to the approach of utilizing OCM+DHA+SHC, which shows a *61% reduction in net energy demand*.

Table 28. Reactions and corresponding high yields used for the process model

Step	Reaction	Yield per pass (C basis, except SHC)	
OCM	$2CH_4 \rightarrow C_2H_4 + 2H_2$	15% of CH_4	30% to C_2
	$2CH_4 \rightarrow C_2H_6 + H_2$	15% of CH_4	
DHA	$3C_2H_4 \rightarrow C_6H_6 + 3H_2$	20% of C_2H_4	80% to aromatics
	$5C_2H_4 \rightarrow C_{10}H_8 + 6H_2$	20% of C_2H_4	
	$3C_2H_6 \rightarrow C_6H_6 + 6H_2$	20% of C_2H_6	
	$5C_2H_6 \rightarrow C_{10}H_8 + 11H_2$	20% of C_2H_6	
SHC	$H_2 + 2MnO \rightarrow H_2O + Mn_2O_3$	90% of H_2	

An initial process model was developed to analyze the advantages of integrating an OCM step. For simplicity, the above reactions and corresponding high yields were considered in the model. Pure methane was assumed with no selectivity to solid carbon. The Mn-based oxide, as used in the other OAS cases, was incorporated in the model with 90% hydrogen combustion. Table 29 and 30 summarize the key process results from the simulation for the Base Case, OAS 40%Y and OCM+OAS case.

Table 29. Mass flows obtained from the simulation (for OCM+OAS, all products clubbed as fuel gas)

Energy Flows (MJ/kg aromatic product)	Base Case	OAS 40%Y	OCM+OAS
Benzene	17.8	18.0	16.6
Toluene	0.8	0.8	-
Naphthalene	24.3	24.2	18.4
C_{2+}	0.8	1.2	
Hydrogen	36.3	0.0	
Coke	6.4	7.1	-
Fuel Gas	1.4	0.4	27.0

For the OCM+OAS, for 100 t/hr. of pure methane, roughly, 28.5 t/hr. of benzene, 28 t/hr. of naphthalene, 27 t/hr. of fuel gases (unreacted $CH_4 + C_2H_4 + C_2H_6$) and 16.5 t/hr. of hydrogen (fixed as water after SHC) was obtained. This shows an overall benzene and naphthalene yield of 35% each (on a carbon basis) with remaining getting converted to C_2H_4 and C_2H_6 in the OCM step. On

an energy basis, as shown in Table 30, this case shows slightly less reduction in energy demand as compared to the OAS 40% Y, since the benzene yields are slightly higher in the OAS case.

Table 30. Process energy balances for non-oxidative methane DHA (Base Case) and three scenarios for OAS.

Parameter*	**Base Case**	**OAS 40%Y**	**OCM+OAS**
Aromatics Production Rate (kg/s)	18.8	18.8	**17.0**
NG for Heat (MJ/kg) (60% eff.)[1]	60.2	2.1	**18.0**
Net Work Required (MJ/kg)[2]	35.0	-10.8	**4.4**
Fuel Credits (MJ/kg)	-37.6	-0.3	**-27.0**
Feed Natural Gas/Methane (MJ/kg)	74.5	71.8	**74.0**
Fuel NG Requirement (MJ/kg)	57.6	-9.0	**-4.6**
Energy in Valuable Products (MJ/kg)	-43.6	-44.1	**-35.0**
Specific Net Energy Demand (MJ/kg)	**88.5**	**18.7**	**34.4**
% Reduction in Energy Demand	**--**	**78.8%**	**61.1%**

*Normalized to aromatic production (per kg, wherever shown)

[1] 60% efficiency penalty applied to *in situ* heat generation from selective H_2 combustion reaction

[2] 40% efficiency penalty applied to electricity from heat recovery steam generator / steam heated by regeneration.

[3] "Net Energy Demand (Energy Lost)" is defined as all input energy (Natural Gas Feed and Natural Gas for Fuel) minus that energy which exits the system as valuable products (Benzene, Toluene, Naphthalene, and C2+; the latter is primarily ethylene, ethane, and propylene). Losses go to process heat/work requirements and undesired products.

When using oxidative coupling of methane (OCM) followed by DHA+SHC, the first step produces ethane and ethylene, which is then aromatized with selective hydrogen combustion. Overall, 20% CH_4-to-aromatics yield has been assumed, out of which 9.5% is benzene, 9.5% is naphthalene and 1% is toluene. Herein, experimental product distributions obtained at NCSU with an overall 20% yield to aromatics has been used to show roughly *43% reduction in net energy demand*. The model utilizes the approach of using OCM+DHA+SHC.

Table 31. Reactions and corresponding high yields used for the process model

Step	**Reaction**	**Yield per pass (C basis, except SHC)**	
OCM	$2CH_4 \rightarrow C_2H_4 + 2H_2$	12.5% of CH_4	25% to C_2
	$2CH_4 \rightarrow C_2H_6 + H_2$	12.5% of CH_4	
DHA	$3C_2H_4 \rightarrow C_6H_6 + 3H_2$	19% of C_2H_4	

	$5C_2H_4 \rightarrow C_{10}H_8 + 6H_2$	19% of C_2H_4	80% to aromatics
	$3.5C_2H_4 \rightarrow C_7H_8 + 7H_2$	2% of C_2H_4	
	$3C_2H_6 \rightarrow C_6H_6 + 6H_2$	19% of C_2H_6	
	$5C_2H_6 \rightarrow C_{10}H_8 + 11H_2$	19% of C_2H_6	
	$3.5C_2H_6 \rightarrow C_7H_8 + 10.5H_2$	2% of C_2H_4	
SHC	$H_2 + 2MnO \rightarrow H_2O + Mn_2O_3$	90% of H_2	

For simplicity, the above reactions and corresponding high yields were considered in the model. Pure methane was assumed with no selectivity to solid carbon. The Mn-based oxide, as used in the other OAS cases, was incorporated in the model with 90% hydrogen combustion. Table 32 summarizes the key process results from the simulation for the Base Case and OCM+OAS 20 case.

Table 32. Process energy balances for non-oxidative methane DHA (Base Case) and OCM+OAS 20.

Parameter*	**Base Case**	**OCM+OAS 20**
Aromatics Production Rate (kg/s)	18.8	**15.6**
NG for Heat (MJ/kg) (60% eff.)[1]	60.2	**19.2**
Net Work Required (MJ/kg)[2]	35.0	**0.6**
Fuel Credits (MJ/kg)	-37.6	**1.9**
Feed Natural Gas/Methane (MJ/kg)	74.5	**74.0**
Fuel NG Requirement (MJ/kg)	57.6	**17.9**
Energy in Valuable Products (MJ/kg)	-43.6	**-42.0**
Specific Net Energy Demand (MJ/kg)	**88.5**	**50.3**
% Reduction in Energy Demand	**--**	**43.2%**

*Normalized to aromatic production (per kg, wherever shown)

[1] 60% efficiency penalty applied to *in situ* heat generation from selective H_2 combustion reaction

[2] 40% efficiency penalty applied to electricity from heat recovery steam generator / steam heated by regeneration.

[3] "Net Energy Demand (Energy Lost)" is defined as all input energy (Natural Gas Feed and Natural Gas for Fuel) minus that energy which exits the system as valuable products (Benzene, Toluene, Naphthalene, and C2+; the latter is primarily ethylene, ethane, and propylene). Losses go to process heat/work requirements and undesired products.

Susteon developed a set of AspenPlus™ process models which demonstrate significant energy savings for OAS as compared to the base case non-oxidative DHA.

- At 20% aromatics yield, which is twice the base-case non-oxidative DHA yield, a *55% reduction in net energy demand* is estimated.
- A higher reduction of 78% can be achieved at *40% aromatics yield*.
- With the approach of utilizing OCM+OAS (30% C1 to C2, followed by 80% of C2 to aromatics), a *61% reduction in net energy demand* is estimated
- Experimental product distribution obtained at NCSU with overall 20% yield to aromatics (OCM+OAS) was used to show roughly *43% reduction in net energy demand.* The following table shows summarizes the key process results from these simulations.

With better resolution of the aromatic compounds the following product distribution has been obtained for the liquid products: Benzene (C_6H_6): 38% of liquid products on C basis, Toluene (C_7H_8): 13%; Xylene (C_8H_{10}): 1%; Naphthalene ($C_{10}H_8$): 23% and Cyclododecahexaene ([12] annulene, $C_{12}H_{12}$): 25%.

Table 33. The reactions and corresponding high yields to be used for the process model:

Step	**Reaction**	**Yield per pass (C basis, except SHC)**	
OCM	$2CH_4 \rightarrow C_2H_4 + 2H_2$	15% of CH_4	30% to C_2
	$2CH_4 \rightarrow C_2H_6 + H_2$	15% of CH_4	
DHA	$3C_2H_4 \rightarrow C_6H_6 + 3H_2$	15.2% of C_2H_4	80% to aromatics
	$3.5C_2H_4 \rightarrow C_7H_8 + 3H_2$	5.2% of C_2H_4	
	$4C_2H_4 \rightarrow C_8H_{10} + 3H_2$	0.4% of C_2H_4	
	$5C_2H_4 \rightarrow C_{10}H_8 + 6H_2$	9.2% of C_2H_4	
	$6C_2H_4 \rightarrow C_{12}H_{12} + 6H_2$	10% of C_2H_4	
	$3C_2H_6 \rightarrow C_6H_6 + 6H_2$	15.2% of C_2H_6	
	$3.5C_2H_6 \rightarrow C_7H_8 + 6.5H_2$	5.2% of C_2H_6	
	$4C_2H_6 \rightarrow C_8H_{10} + 7H_2$	0.4% of C_2H_6	
	$5C_2H_6 \rightarrow C_{10}H_8 + 11H_2$	9.2% of C_2H_6	
	$6C_2H_6 \rightarrow C_{12}H_{12} + 12H_2$	10% of C_2H_6	
SHC	$H_2 + 2MnO \rightarrow H_2O + Mn_2O_3$	90% of H_2	

The OCM + DHA + SHC approach was used in the model. Three reactors in series were setup respectively. For the OCM, section, 25% CH_4 conversion was used, with 40% selectivity each to C_2H_6 (ethane) and C_2H_4 (ethylene). The DHA section involved the conversion of both ethane and ethylene to the following products (Table 34). A conversion of 60% was used both for ethane and ethylene. In the SHC reactor, a H_2-to-H_2O conversion of 75% was used. The process model, comprising of the three broad sections: upstream, separation and purification, is shown in **Figure 93** below.

Table 34: Product Distribution used for the DHA step (C_2H_6 and C_2H_4 conversion to other hydrocarbons)

Product		**Yield (%) for ethane feed**	**Yield (%) for ethylene feed**
CH_4	Methane	10.9	11.9
C_2H_4	Ethane	4.9	
C_3H_6	Ethylene	0.6	0.6
C_6H_6	**Benzene**	**15.6**	**16.9**
C_7H_8	**Toluene**	**4.1**	**4.5**
C_8H_{10}	**Xylene**	**0.2**	**0.3**
C_9H_{12}	**Isopropyl Benzene**	**1.2**	**1.3**
$C_{10}H_{18}$	**Naphthalene**	**6.5**	**7.1**
$C_{12}H_{12}$	**Dimethyl Naphthalene**	**9.0**	**9.8**
C	Coke	4.9	5.3
CO	Carbon Monoxide	2.0	2.2

Table 35: Stoichiometric reactions used for the OCM, DHA and SHC step.

Step	**Reaction**	**Yield per pass (C basis, except SHC)**	
OCM	$2CH_4 \rightarrow C_2H_4 + 2H_2$	10% of CH_4	20% to C_2
	$2CH_4 \rightarrow C_2H_6 + H_2$	10% of CH_4	
	$CH_4 \rightarrow CO + 2H_2$	1.25% of CH_4	
	$CH_4 + 8PrO_2 \rightarrow CO_2 + 4Pr_2O_3 + 2H_2O$	3.75% of CH_4	
DHA	$C_2H_4 + H_2 \rightarrow 2CH_4$	12% of C_2H_4	76% to aromatics
	$3C_2H_4 \rightarrow 2C_3H_6$	1% of C_2H_4	
	$3C_2H_4 \rightarrow C_6H_6 + 3H_2$	17% of C_2H_4	
	$3.5C_2H_4 \rightarrow C_7H_8 + 3H_2$	4% of C_2H_4	
	$4C_2H_4 \rightarrow C_8H_{10} + 3H_2$	0% of C_2H_4	
	$9C_2H_4 \rightarrow 2C_9H_{12} + 6H_2$	1% of C_2H_4	
	$5C_2H_4 \rightarrow C_{10}H_8 + 6H_2$	7% of C_2H_4	

	$6C_2H_4 \rightarrow C_{12}H_{12} + 6H_2$	10% of C_2H_4	
	$C_2H_4 + 8MnO_2 \rightarrow 2CO_2 + 4Mn_2O_3 + 2H_2O$	2% of C_2H_4	
	$C_2H_4 \rightarrow 2C_{(s)} + 2H_2$	5% of C_2H_4	
	$C_2H_6 \rightarrow C_2H_4 + H_2$	4.9% of C_2H_6	
	$C_2H_6 + H_2 \rightarrow 2CH_4$	12% of C_2H_6	
	$3C_2H_6 \rightarrow 2C_3H_6 + 3H_2$	0.6% of C_2H_6	
	$3C_2H_6 \rightarrow C_6H_6 + 6H_2$	15.6% of C_2H_6	
	$7C_2H_6 \rightarrow 2C_7H_8 + 13H_2$	4.1% of C_2H_6	
	$4C_2H_6 \rightarrow C_8H_{10} + 7H_2$	0.2% of C_2H_6	
	$9C_2H_6 \rightarrow 2C_9H_{12} + 15H_2$	1.2% of C_2H_6	
	$5C_2H_6 \rightarrow C_{10}H_8 + 11H_2$	6.5% of C_2H_6	
	$6C_2H_6 \rightarrow C_{12}H_{12} + 12H_2$	9% of C_2H_6	
	$C_2H_6 + 10MnO_2 \rightarrow 2CO_2 + 5Mn_2O_3 + 3H_2O$	2% of C_2H_6	
	$C_2H_6 \rightarrow 2C_{(s)} + 3H_2$	4.9% of C_2H_6	
SHC	$H_2 + 2MnO_2 \rightarrow H_2O + Mn_2O_3$	75% of H_2	

Stoichiometric reactions for the OCM, DHA, and SHC steps are listed in detail in Table 35 (used for the RStoic reactor shown in **Figure 94**). PrO_2 to Pr_2O_3 transition was used for the OCM step whereas MnO_2 to Mn_2O_3 for the SHC and DHA. Solid C was denoted as coke in the model, which was burned in air during regeneration. Both Mn_2O_3 and Pr_2O_3 were regenerated to their respective starting oxidized states in air. The mass flows for the key streams are listed in Table 36 and Table 37 below.

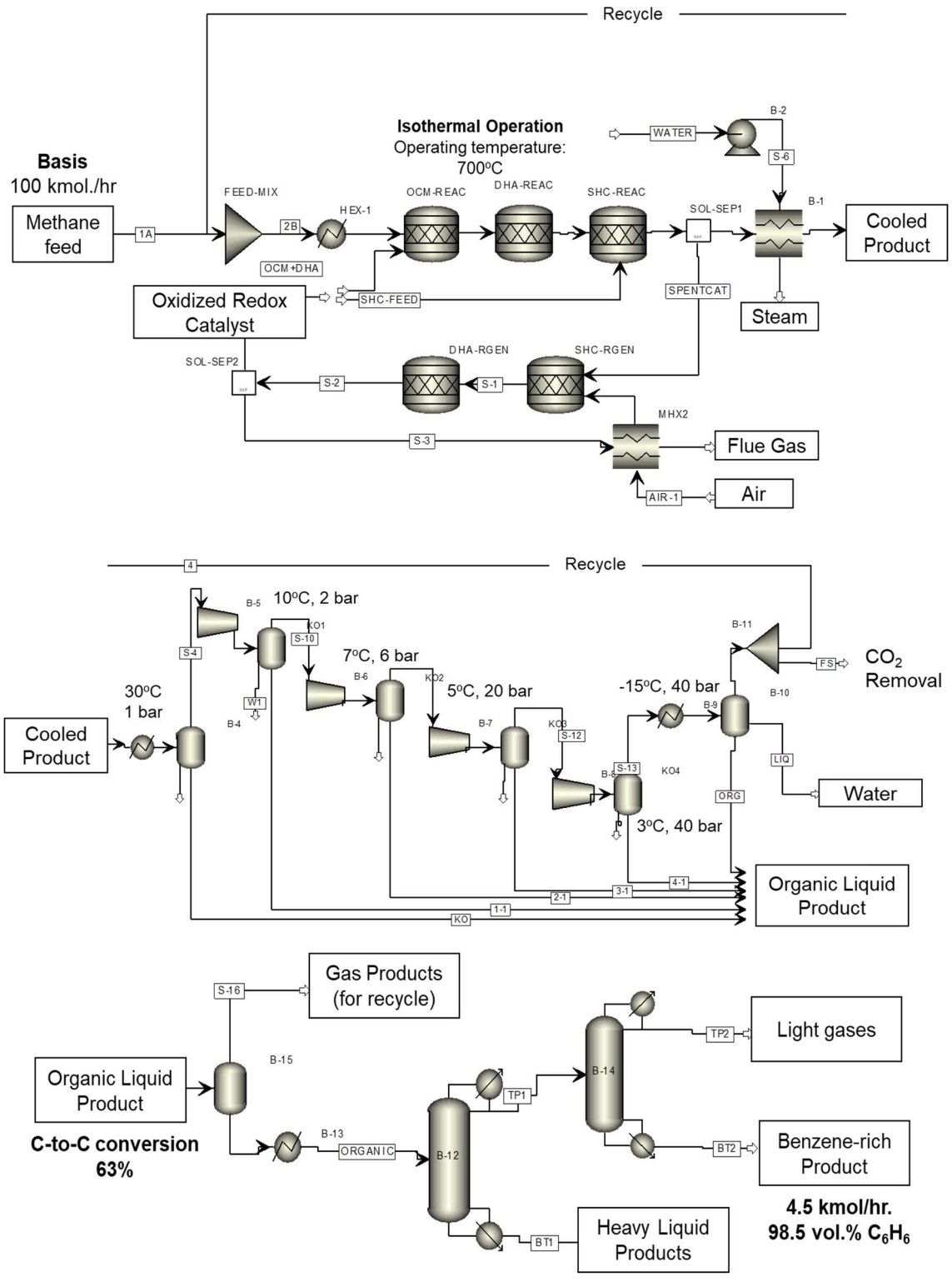
Recycle
Isothermal Operation
Operating temperature:
700ºC
Basis
100 kmol./hr
Methane feed
1A
FEED-MIX
2B
HEX-1
OCM-REAC
DHA-REAC
SHC-REAC
SOL-SEP1
B-1
Cooled Product
WATER
B-2
S-6
OCM+DHA
Oxidized Redox Catalyst
SHC-FEED
SPENTCAT
Steam
SOL-SEP2
DHA-RGEN
SHC-RGEN
S-2
S-1
MHX2
S-3
Flue Gas
AIR-1
Air
4
Recycle
B-5
10ºC, 2 bar
KO1
S-10
S-4
7ºC, 6 bar
B-6
KO2
5ºC, 20 bar
30ºC
1 bar
W1
B-4
B-7
KO3
S-12
-15ºC, 40 bar
B-11
FS
CO2 Removal
B-9
B-10
Cooled Product
S-13
KO4
LIQ
Water
B-8
ORG
3ºC, 40 bar
Organic Liquid Product
4-1
3-1
2-1
1-1
KO
S-16
Gas Products (for recycle)
B-15
Organic Liquid Product
C-to-C conversion
63%
B-13
ORGANIC
B-12
TP1
B-14
TP2
Light gases
BT2
Benzene-rich Product
4.5 kmol/hr.
98.5 vol.% C6H6
BT1
Heavy Liquid Products

Figure 93. Three sections of the overall CH_4 OCM + DHA + SHC process: First the upstream reactors with redox catalyst regeneration using air, followed by liquid product separation using a train of compressors and intermediate cooling, followed by liquid product purification using distillation to eventually concentrate benzene as the desired product. The other liquid products have been lumped in one stream.

Overall, with the recycling of unreacted methane, an overall yield of 63% was obtained for CH_4-to-Liquid Product conversion. The final concentrated benzene product (98 vol.%) was obtained containing 4.5 kmol/hr. of benzene. **This implies an overall CH_4-to-Benzene yield of 27%.**

The liquid product stream primarily contains $C_{12}H_{12}$ (or dimethyl naphthalene), followed by naphthalene and toluene. Roughly 78 kmol/hr. of steam (120 bar, 320^oC) is generated during the cooling of the hot product gas from the catalyst reduction steps. Before recycling, CO_2 needs to be separated from the product gas stream. A CO_2 separation of 99% has been assumed, using an amine-based liquid solvent or a membrane-based system since the recycle stream is at high pressure.-

Table 36: Molar flows of the key process streams

	Units	Methane feed	Steam	Air	Organic Product	CO_2	Benzene	Heavy Liquids
Temperature	C	25	325	25	11	25	10	297
Pressure	bar	31	120	1	10	20	6	10
Molar Vapor Fraction		1.0	1.0	1.0	0.0	1.0	0.0	0.0
Mass Density	kg/m^3	21.1	64.1	1.2	754.9	50.1	875.6	716.1
Average MW		16.0	18.0	28.9	94.7	44.0	75.6	128.3
Mole Flows	**kmol/hr**	**100**	**78**	**589.0**	**8.91**	**17.8**	**4.59**	**3.63**
CH_4	kmol/hr	100	0	0	0.09	0	0	0
H_2	kmol/hr	0	0	0	0.00	0	0	0
CO	kmol/hr	0	0	0	0.10	0	0	0
CO_2	kmol/hr	0	0	0	0.03	17.8	0	0
H_2O	kmol/hr	0	78	0	0.12	0	0.07	0
C_2H_6	kmol/hr	0	0	0	0.03	0	0	0
C_2H_4	kmol/hr	0	0	0	0.03	0	0	0
C_3H_6	kmol/hr	0	0	0	0.37	0	0	0
C_6H_6	**kmol/hr**	**0**	**0**	**0**	**4.52**	**0**	**4.52**	**0**
C_7H_8	**kmol/hr**	**0**	**0**	**0**	**0.96**	**0**	**0**	**0.96**
$C_{10}H_8$	**kmol/hr**	**0**	**0**	**0**	**1.12**	**0**	**0**	**1.12**
C_8H_{10}	**kmol/hr**	**0**	**0**	**0**	**0.20**	**0**	**0**	**0.20**
C_9H_{12}	**kmol/hr**	**0**	**0**	**0**	**0.02**	**0**	**0**	**0.02**
$C_{12}H_{12}$	**kmol/hr**	**0**	**0**	**0**	**1.32**	**0**	**0**	**1.32**
N_2	kmol/hr	0	0	465.3	0	0	0	0
O_2	kmol/hr	0	0	123.7	0	0	0	0

Table 37.: Mole fractions of the key process streams

	Units	Methane feed	Steam	Air	Organic Product	CO_2	Benzene	Heavy Liquids
Temperature	C	25	325	25	11	25	10	297
Pressure	bar	31	120	1	10	20	6	10
Molar Vapor Fraction		1.0	1.0	1.0	0.0	1.0	0.0	0.0
Mass Density	kg/m^3	21.1	64.1	1.2	754.9	50.1	875.6	716.1
Average MW		16.0	18.0	28.9	94.7	44.0	75.6	128.3
Concentration	**%**							
CH_4	%	100%	0	0	1.0%	0	0	0
H_2		0	0	0	0	0	0	0
CO		0	0	0	1.2%	0	0	0
CO_2		0	0	0	0	100%	0	0
H_2O		0	100%	0	1.4%	0	1.5%	0
C_2H_6		0	0	0	0	0	0	0
C_2H_4		0	0	0	0	0	0	0
C_3H_6		0	0	0	4.3%	0	0	0
C_6H_6		**0**	**0**	**0**	**50.9%**	**0**	**98.5%**	**0**
C_7H_8		**0**	**0**	**0**	**11.1%**	**0**	**0**	**27%**
$C_{10}H_8$		**0**	**0**	**0**	**12.6%**	**0**	**0**	**31%**
C_8H_{10}		**0**	**0**	**0**	**2.6%**	**0**	**0**	**6%**
C_9H_{12}		**0**	**0**	**0**	**0**	**0**	**0**	**1%**
$C_{12}H_{12}$		**0**	**0**	**0**	**14.9%**	**0**	**0**	**36%**
N_2		0	0	79%	0	0	0	0
O_2		0	0	21%	0	0	0	0

Task 5: OCM-SHA Catalyst Combination

Subtask 5.1: OCM-SHA Catalyst Screening

Alternative schemes for yield enhancement

Incompatibility of SHC and DHA catalyst is observed. The results obtained from Task 3 indicates that the active sites for methane DHA on the ZSM-5 catalyst were not stable in the presence steam generated by the SHC redox catalyst. Besides the "methane DHA (Mo/HZSM-5) + SHC ($Na_2WO_4/CaMnO_3$) strategy" for H_2 combustion and increased benzene yield, we have also adopted an alternative strategy. To achieve the originally proposed targets for OAS, the project team has proposed an innovative approach of combining oxidative coupling of methane (OCM) with ethane DHA. In this route, the 1st-layer bed contains a chemical-looping oxidative methane coupling (OCM) redox catalyst operated at 700°C. The OCM bed will partially convert methane into C_2H_6 and C_2H_4 with nearly 20% yield. The OCM bed partially convert methane into C_2H_6 and C_2H_4 (C2) with a high yield. The 2rd-layer bed contains a C2-DHA catalyst, which has the composition of Ga-containing zeolite, and converts C2 hydrocarbons to aromatics.

We have conducted reactivty tests for "OCM+Ehane DHA" 2-layer bed and "OCM+Water removal+Ethane DHA" 3-layer bed. The last $Na_2WO_4/CaMnO_3$ SHC bed has yet to be added but our previous experiments have proved the effectiveness of this material. As shown in Figure 94 below, the "OCM+Ehane DHA" 2-layer bed reactor exhibits a large CO yield (~7%), and benzene yield is limited to less than 5%. The large CO yield is due to the presence of H_2O formed from the 1st-layer OCM bed. The as-formed H_2O will participate in steam reforming reaction over GaPt/HZSM5 and reform benzene and other hydrocarbons into CO and H_2. A water removal bed was added to reduce the degree of reforming reactions with a "OCM+Water removal+Ethane DHA" 3-layer bed configuration. As can be seen in Figure 94, the CO yield was decreased to only ~2% and benzene yield up to 8.2% has been obtained. This benzene yield is comparable with the best results obtained over a single methane DHA catalyst at 700°C and can be further improved with improvement on the OCM catalyst and the ethane DHA catalyst (GaPt/HZSM5).

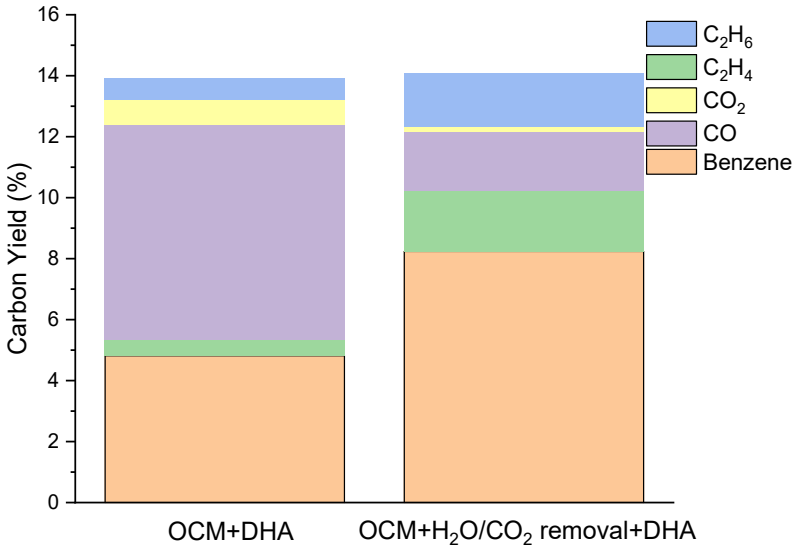

Figure 94. Catalytic performance of the "OCM+Ehane DHA" 2-layer bed and "OCM+Water removal+Ethane DHA" 3-layer bed configurations. Ethane DHA catalyst is GaPt/HZSM5, with 0.5 g loading.

Improvement of the OCM+DHA catalyst (NCSU)

We changed the C2-DHA bed weight so that the gases exiting the OCM bed might have various space velocities through DHA bed. 20 ml/min methane and 3 ml/min argon were flown as the feed through the OCM + DHA sequential bed. 2g OCM catalyst were used constantly while the DHA catalyst were 0.2 g, 0.6 g and 0.8 g in three independent tests. The product was analyzed by the mass spectrometry and results are shown in Figure 95. The comparison of Figure 95a and 95c indicates that there were lower ethane conversion and less benzene yield over 0.2 g DHA catalyst than 0.6 g. The smaller produced H_2 amount also confirmed that there was less conversion of ethane to benzene. It is interesting to find that methane flow rate was reduced by adding more DHA catalyst, indicating the HGaAlMFI catalyst may have the ability to catalyze methane conversion. The difference of benzene yield shown in Figure 95b and 95c are not observable. However, the H_2 flow rate increased by more than ~30%. This could be a result of the formation of more polyaromatics, e.g. naphthalene. The polyaromatics product is prone to condense in the reactor existing line and can hardly be detected and quantified by MS. The method of quantifying the polyaromatics needs to be developed to have a better understanding of the OCM + DHA route.

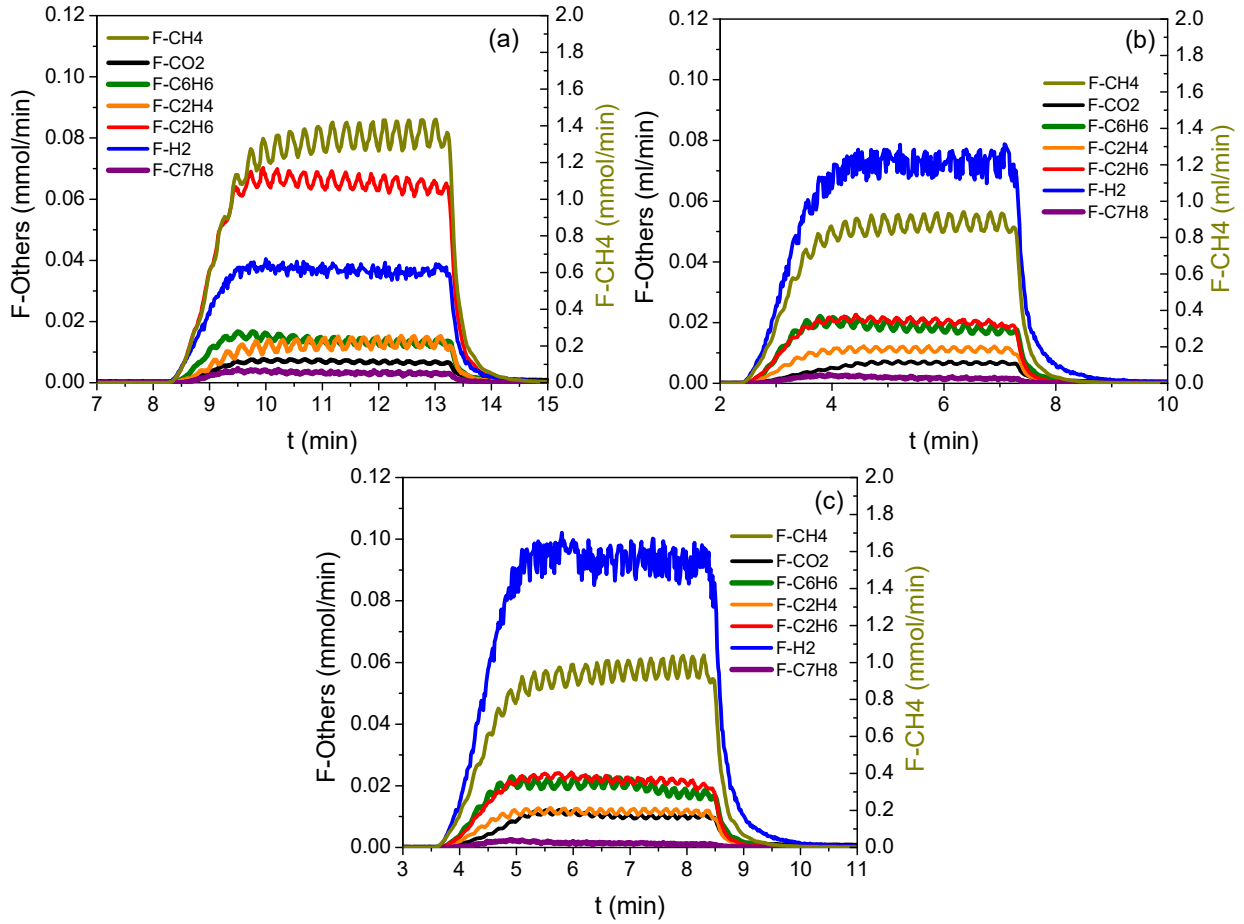

Figure 95. Methane DHA in OCM+C2-DHA route with various C2-DHA catalyst weight: 2g OCM + (a) 0.2g C2-DHA, (b) 0.6g C2-DHA, (c) 0.8g C2-DHA.

It is reported that the production of aromatics can be enhanced by pretreating the Ga-based ZSM-5 catalysts with hydrogen. [1] It is believed that when Ga is loaded in the framework of the zeolite, $[Ga(OH)_2]^+$ is generated as the active sites. After H_2-pretreament, the sites turn into $[GaH_2]^+$ which is preferable for the formation of aromatics. To verify this finding and employ it in this project, we reduced the C2-DHA catalyst with 5% H_2 in Ar at 700 ºC for 2 h. Then, methane DHA tests were carried out at 700 ºC and 720 ºC.

At 700 ºC, as exhibited by the comparison of Figure 96a and 96b, the benzene yield was increased by 50%. It is noteworthy that, even though the benzene yield is higher over the H_2-pretreated catalysts, the overall methane conversion is lower. If the earlier assumption that the C_2-DHA catalyst can also catalyze methane conversion is true, then the ability of $[GaH_2]^+$ sites, which were formed after pretreatment, to activate methane is weaker. The comparison of Figure 96c and 96d

shows the same trend in the changes of product distribution. The benzene yield over H_2-pretreated C2-DHA catalyst is 90% higher than the unpretreated.

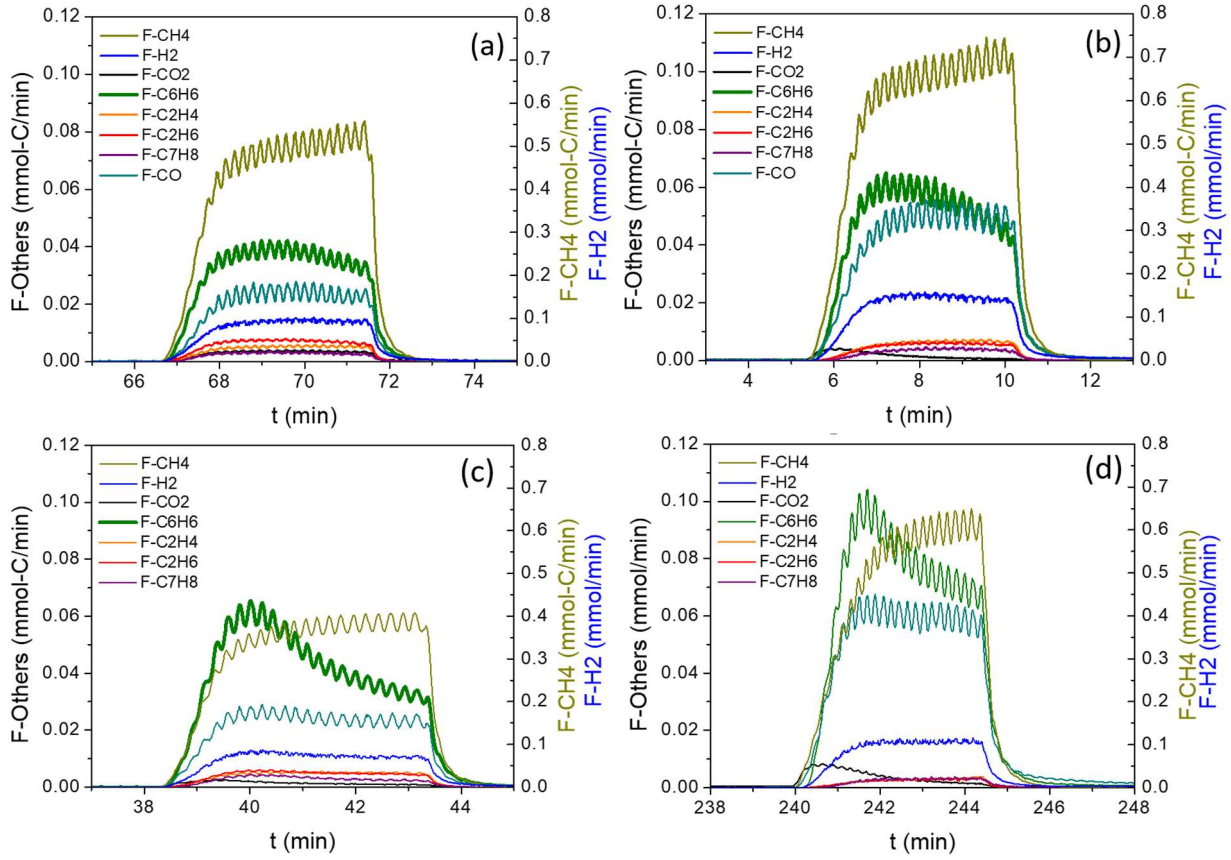

Figure 96. Methane DHA tests in OCM+DHA route at 700°C (a) without H_2-pretreatment, (b) with H_2-pretreatment and 720°C (c) without H_2-pretreatment (d) with H_2-pretreatment.

The results shown in Figure 96 brought up two challenges: (1) the activity of C2-DHA catalysts synthesized in various batches are not consistent. It is presumed that Ga was not properly loaded in the framework of the zeolite, rather, a higher portion of Ga is present in the extra framework, resulting a different type of active sites. The difference in batches will be confirmed by characterization of the catalysts using NH_3-TPD, BET, and TPR methods. (2) the carbon balance in the tests needs significant improvement. For example, less than 20% carbon balance were attained in the testing over the catalyst without pretreatment, and less than 50% were attained over the pretreated catalyst. The low carbon balance makes it difficult to quantify the advantages of the OCM+DHA route.

To qualitatively analyze the species in the aromatic product, the reaction setup was modified so that the aromactics can be collected for GC analysis. As shown in Figure 97a, the exiting line from the second reactor was wrapped with a heating tape to prevent the condensation of the polyaromatics. It was connected to a container filled with dodecane as the solvant to capture the aromatics. The container was immersed in the ice water and the outlet is connected to MS for the analysis of gas phase. At first, 2g OCM + 0.8g DHA were used for methane DHA at 720°C. The reaction time was 4 min. The GC spectrum of the liquid product captured in the cold trap exhibited a dominant dodecane peak and a tiny peak signed to benzene. Since the benzene peak takes only 0.3% of the total peak area, the concentration in the product is too low for GC analysis. There could be other aromatics produced, e.g. toluene, naphthalene, but not adequte to be deteced by GC.

In order to accumulate more aromatic product so that GC can show a recognizable signial, cyclic DHA experiments were carried out via the OCM + DHA route. After the DHA reaction, the sequetial beds were oxidized and purged for the generation of the catalysts. The DHA reaction time was 8 min, and a total of 5 cycles were carried out. Figure 97b exhibite the MS signals for the cyclic DHA process. The catalyst were stable with in the studied 5 cycles. Although benzene were expected to be captured in the cold trap, there is a portion of benzene detected by MS, indicating a fraction of aromatics exited from the cold trap.

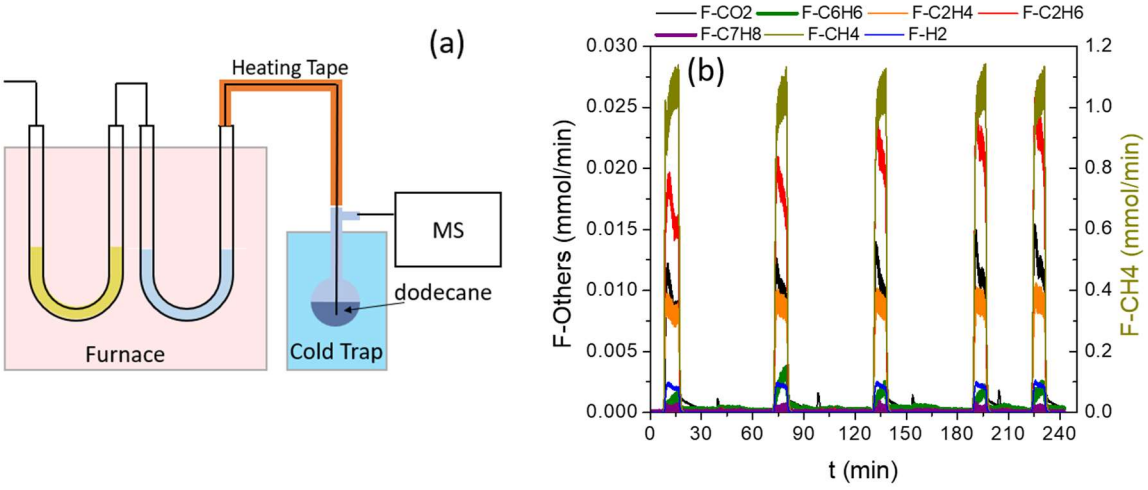

Figure 97. (a) Reaction setup for capturing the aromatics product in cold trap. (b) MS signals for the cyclic Methane DHA, 5 cycles.

The dodecane blank run indicates the multiple peaks including the dominant one at 16.73 min can be assigned to dodecane solvent and the contaminants in it (Figure 98). Aside from these, the peaks in the lower spectra of Figure 98 appeared at 3.63 min and 5.06 min were attributed to benzene and toluene respectively. The peaks at 16.12 min, 19.1 min and 19.5 min are possibly the contribution from the polyaromatics. The calibration of the polyaromatics, e.g. naphthalene is in process. Since the peak area of these polyaromatics is very close to that of benzene, so it is reasonable to estimate that the yield of polyaromatics is at least 9%, comparable to benzene yield. This estimation leads to a total of approximately 20% aromatics yield, which is used in the modeling developed by Susteon.

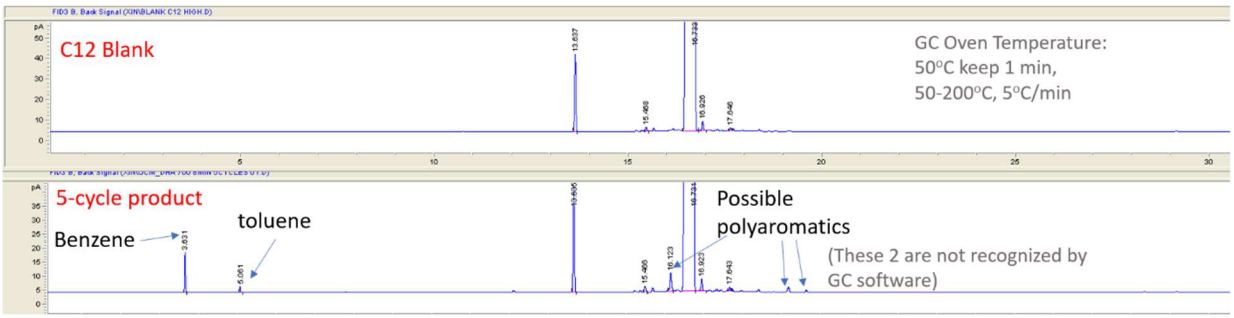

Figure 98. Comparison of GC spectra between the dodecane blank and the liquid product collected captured by dodecane solvent.

The OCM+DHA reactor system was built. Two U-shaped quartz tube reactors loaded with the OCM catalyst and DHA catalyst were placed sequentially in the furnace. . An impinger trap containing dodecane and submersed in ice water was used to capture condensable products. A heating tape was applied to vaporize the heavy aromatic/polyaromatic product and limit product condensation before the impinger trap and avoid blocking of the tube. A gas bag was used to collect the non-condensable gaseous products. GC and MS were used to analyze the product distribution. For a typical OCM+DHA test, 2.0 g Li_2CO_3/MeMe'O_{3+x} catalyst was loaded in OCM reactor U-tube and 0.8 g Ga-ZSM-5 catalyst was loaded for in DHA reactor U-tube. The catalyst was first pretreated at 700 ºC in 5 mL/min O_2 + 25 mL/min Ar to remove possible impurities. In the typical chemical looping run, 20 mL/min CH_4+5 mL/min Ar was continuously fed into the reactor for 5 min as the reduction step. Then, the feed gas was switched to 25 mL/min Ar to purege the reactor for 5 min. The oxidation step of the chemical looping reaction used 20 mL/min O_2 and

5 mL/min Ar to regenerate the catalyst, which regenerates the oxygen sites of the Li_2CO_3/MeMe'O_{3+x} catalyst and removes the deposited coke.

Table 38. Conversion, carbon balance, and product distribution (based on carbon yield, mol%) of OCM+DHA reaction using Li_2CO_3/MeMe'O_{3+x} and Ga-ZSM-5 catalysts.

Approach	5%Li_2CO_3/MeMe'O_{3+x} +Ga-ZSM-5 (Si/Ga=30)	5%Li_2CO_3/MeMe'O_{3+x} +Ga-ZSM-5 (Si/Ga=50)
CH_4 conversion	26.3%	29.4%
Carbon balance	94.2%	86.9%
C-yield		
yield_gas		
C_2H_6	0.82%	0.38%
C_2H_4	0.53%	0.35%
CO_2	3.59%	1.67%
CO	6.51%	5.21%
C_{3+}	0.01%	0.00%
yield_liquid		
benzene	5.48%	4.78%
toluene	0.17%	0.50%
xylene	0.00%	0.08%
A_{9+}	0.00%	0.00%
naphthalene	2.97%	1.86%
A_{11+}	1.58%	1.71%

Initial tests of OCM+DHA were carried out using the 5%Li_2CO_3/MeMe'O_{3+x} catalyst and the Ga-ZSM-5 from WVU, as shown in Table 38. Notably, the gaseous hydrocarbons (C_2H_6, C_2H_4, and C_{3+}) exhibited a very low yield, indicating most of the C_{2+} components underwent the dehydroaromatization reaction. The combination of OCM and DHA can successfully convert CH_4 into liquid aromatics. For the Li_2CO_3/MeMe'O_{3+x} catalyst and the Ga-ZSM-5 with Si/Ga= 30, the methane conversion was 26.3%, with a carbon balance of 94.2%. For this catalyst, the benzene yield reached 5.48% and the naphthalene yield reached 2.97%, with a total of 10.2% aromatic yield. For the Li_2CO_3/MeMe'O_{3+x} catalyst and the Ga-ZSM-5 with Si/Ga= 50 catalyst, the benzene

yield reached 4.78% and the naphthalene yield reached 1.86%, with a total of 8.9% aromatic yield. These results indicate that the combination of OCM and DHA is promising in converting methane to valuable aromatics.

The yield of the OCM+DHA can be projected based on our experimental results, as shown in Figure 99. For the practical OCM reaction, the C_2H_6 yield can reach 20.5% and the C_{2+} yield can reach 30.9%. Assuming the 60% conversion of C_2H_6 and the complete conversion of other C_{2+} components, the projected yield can be estimated. For the projected results of OCM+DHA, the benzene yield can reach 8.1%, and the total liquid aromatics can reach 17.4%. This catalysts still have more potential optimizations to explore, and better performance can likely be achieved for a suitably designed and optimized the system. For further experiments, the catalyst can be improved to get a higher performance, including activity, selectivity, and stability. Besides, the reaction setup, parameters such as the catalyst loading amount, the catalyst loading configuration, reactor temperature, and the gas hourly space velocity, can be further explored.

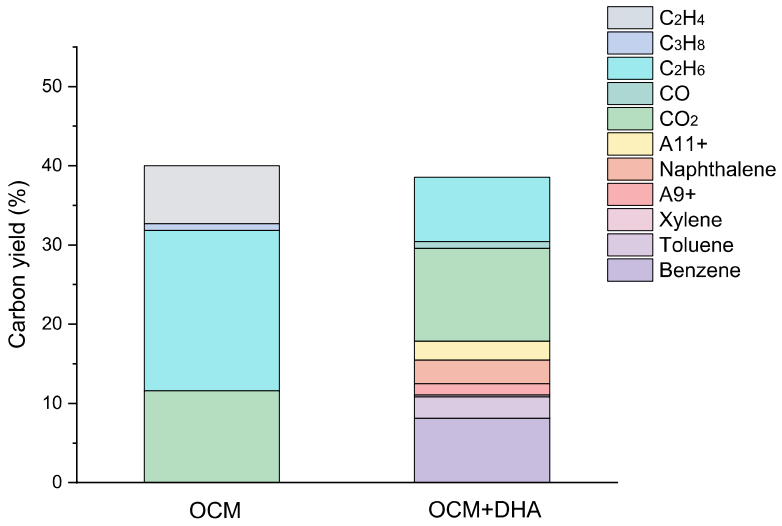

Figure 99. Production distribution for the OCM reaction with the improved OCM catalyst, and the corresponding (projected) product distribution for the OCM+DHA catalyst based on the carbon yield.

The catalyst performance test for the CL-OCM+DHA reaction was conducted in two U-shaped quartz tube reactors, one loaded with the OCM catalyst for the OCM reaction and the other loaded with the zeolite catalyst for the C2-DHA reaction. In this configuration, CH_4 first enters the first reactor for OCM reaction and reacts with the lattice oxygen of the salt doped metal oxide catalyst catalyst. Then, the generated light olefins from the OCM reaction enter the second reactor for the

C2-DHA reaction, react on the zeolite catalyst, and generates the aromatic products. The effect of the inlet gas flow rate was also investigated with 80%CH_4/20%Ar (Figure 100). When the inlet gas flow was at 25 mL/min, the methane conversion was 26.3% and the aromatics yield was 10.2%; When the total flow rate of the inlet gas decreased to 10 mL/min, the methane conversion was 32.6% and the aromatics yield was 10.8%. The gas product is mainly CO and CO_2, with a total yield of 6.7%. In the liquid phase products, the benzene yield was 4.4% and the naphthalene yield was 5.1%. The lower inlet flow rate led to s deeper extent of reaction.

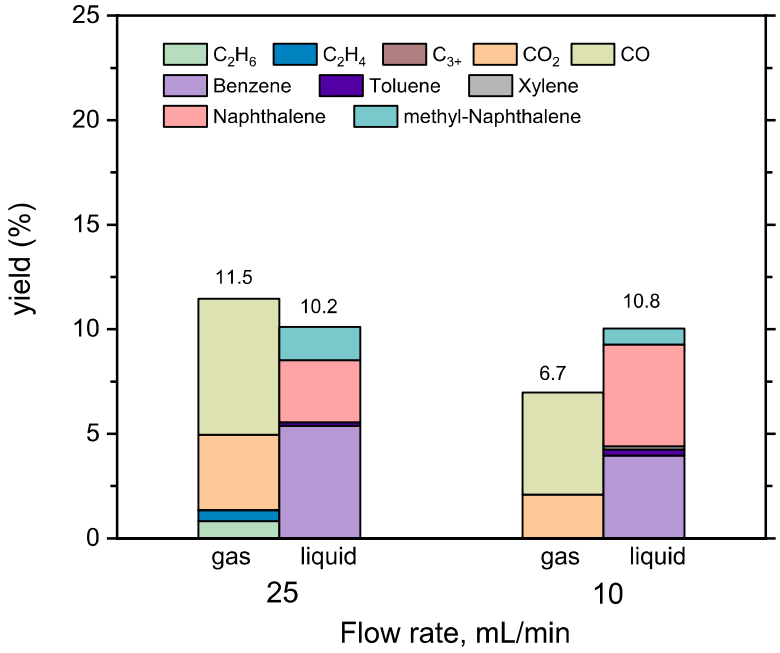

Figure 100. Effect of the inlet flow rate of CL-OCM+DHA on methane conversion, product selectivity, and C_{2+} yield using the salt doped metal oxide catalyst. (temperature= 700 °C, OCM catalyst: 2g, DHA catalyst: 0.8 g, reduction: 80vol%CH_4/20vol%CH_4, oxidation 80vol%O_2/20vol%Ar).

The effect of the methane partial pressure on CL-OCM+DHA was investigated using the 80% CH_4 concentration case and the 40% CH_4 concentration case (Figure 101). For the 80% CH_4 concentration case, the methane conversion reached 26.3% and the carbon balance reached 94.2%, with a total of 10.2% aromatic yield. For the 40% CH_4 concentration case, the methane conversion reached 31.1% and the carbon balance reached 97.4%, with a total of 12.3% aromatic yield. Almost no C_2H_6 and C_2H_4 in the gas phase product, and increased CO_2 (CO_2 yield of 11.8%) was found for the 40% CH_4 concentration case than that (CO_2 yield of 3.8%) of the 80% CH_4 concentration case. The higher CO_2 yield for the 40% CH_4 concentration is indicative of over-oxidation due to

the low CH_4 concentration. Notably, the benzene yield reached 4.7% and the naphthalene yield reached 5.4%, which indicated that further DHA reaction took place on the zeolite catalyst. The results generally indicate that enhanced CH_4 conversion and yield can be achieved when using lower CH_4 concentration while the suitable methane concentration is important to avoid over-oxidation and side reactions. The 12.3% aromatics yield demonstrates the promising potential of the CL-OCM+DHA reaction combination in converting shale gas into valuable products.

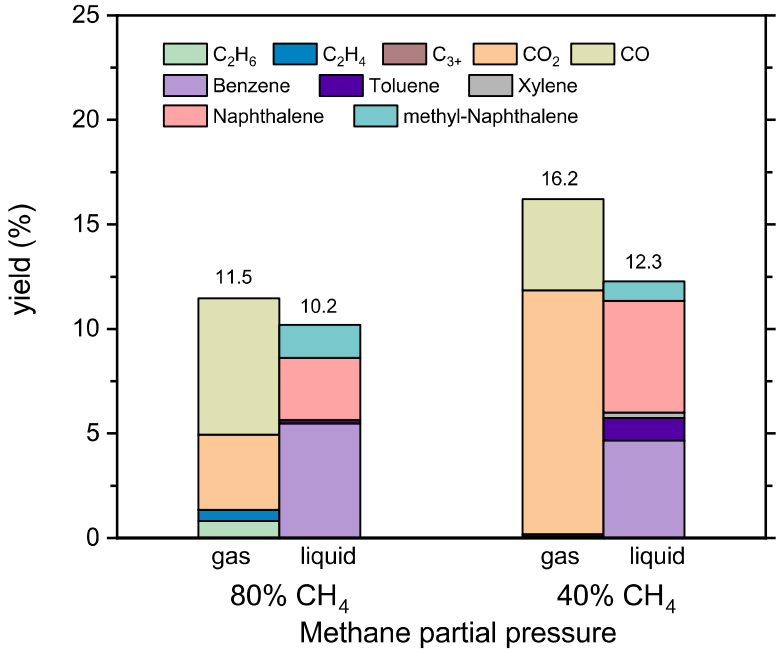

Figure 101. Effect of the methane partial pressure of CL-OCM+DHA on methane conversion, product selectivity, and C_{2+} yield using salt doped metal oxide catalyst. (temperature= 700 °C, OCM catalyst: 2g, DHA catalyst: 0.8 g, total flow rate 25 mL/min).

To enhance the OCM+DHA reaction, the layering catalyst loading configuration methods were tested. As shown in Figure 102a, the OCM+DHA loading method and OCM+DHA+OCM+DHA loading method were compared. In this test, 2.0 g 5%Li_2CO_3/$LaPrO_{3+x}$ catalyst for the OCM reaction and 0.8 g HGaAlMFI catalyst for the DHA reaction were used for the OCM+DHA loading method. As for the OCM+DHA+OCM+DHA loading method, the 1.0 g 5%Li_2CO_3/$LaPrO_{3+x}$ catalyst, the 0.4 g HGaAlMFI catalyst, the 1.0 g 5%Li_2CO_3/$LaPrO_{3+x}$ catalyst, and the 0.4 g HGaAlMFI catalyst were used for the OCM+DHA+OCM+DHA loading method. For the OCM+DHA loading method, the gas yield reached 13.4% and the aromatic yield reached 9.2%, with the methane conversion at about 29.2%. For the OCM+DHA loading method, the methane

conversion was about 35.1% and the aromatic yield reached 11.9%. Besides the better conversion and yield, the gas product selectivity was different. For instance, the CO_2 selectivity was 5.9% and CO selectivity was 6.1% for the OCM+DHA loading method, and the CO_2 selectivity was 15.2% and CO selectivity was 0.9% for the OCM+DHA+OCM+DHA loading method, which indicated that the further oxidation on the $5\%Li_2CO_3/LaPrO_{3+x}$ catalyst took place due to the additional OCM catalyst layer for the OCM+DHA+OCM+DHA loading method.

Cycling performance was also investigated using the OCM+DHA+OCM+DHA loading method. However, the catalysts didn't exhibit a good cycling performance. As shown in Figure 102b, the 2nd cycle had a significantly lower performance with the gas yield at 17.2% and the aromatic yield at 9.8%, which was still better than the OCM+DHA combination loading method. Besides, the methane conversion also decreased from 35.1% for the 1st cycle to 31.3% for the 2nd cycle. For the following cycles, the catalyst performance further decreased and was not recovered, even during the oxidation step in O_2/Ar. Therefore, the decrease in the activity indicated that the catalyst stability was not ideal, limiting the potential application in converting methane to aromatics.

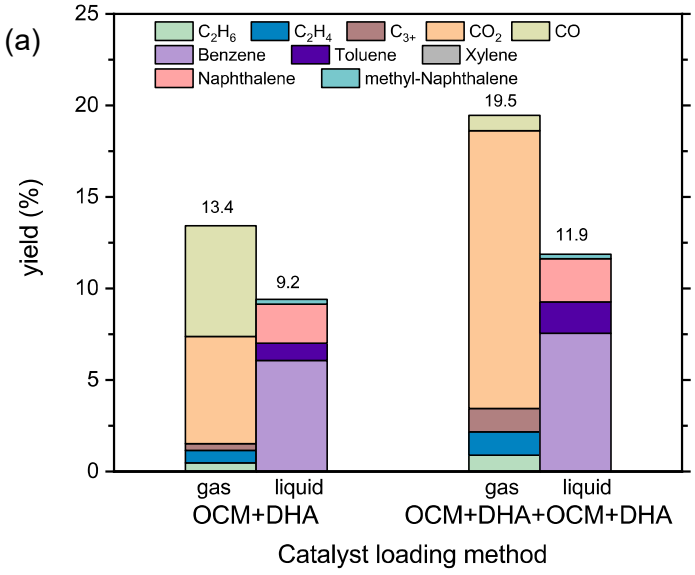

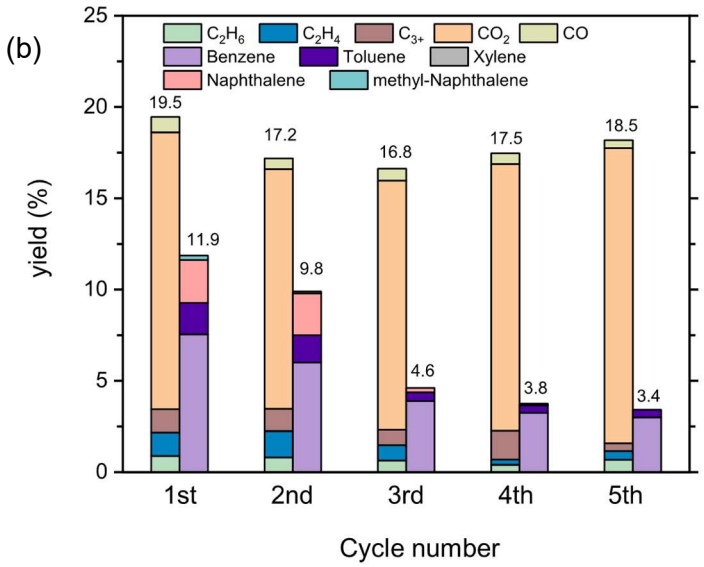

Figure 102. (a) Effect of the different catalyst loading methods: OCM + DHA loading method and OCM+DHA+OCM+ DHA loading method. (b). Effect of cycle number for the OCM+DHA+OCM+ DHA loading method (OCM catalyst: 5%Li_2CO_3/$LaPrO_{3+x}$ catalyst, DHA catalyst: HGaAlMFI catalyst, temperature= 700 °C, pressure= 1 bar, flow rate= 25 mL/min, reduction: 80vol%CH_4/20vol%Ar, oxidation 10vol%O_2/90vol%Ar).

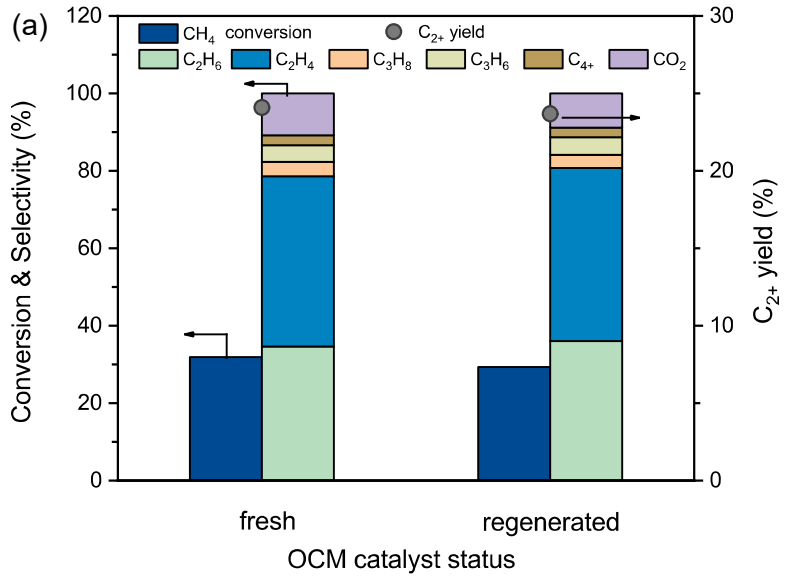

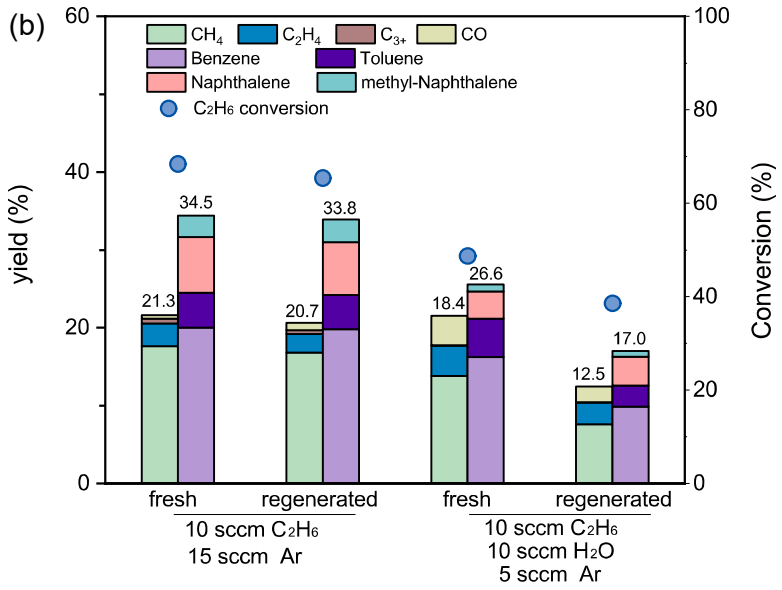

Figure 103. (a) Effect of OCM catalyst status on methane conversion, product selectivity, and C_{2+} yield using 5%Li_2CO_3/$LaPrO_{3+x}$ catalyst. (temperature= 700 °C, GHSV= 750 mL/(g_{cat} ·h) , reduction: 80vol%CH_4/20vol%CH_4, oxidation 80vol%O_2/20vol%Ar). (b) Effect of DHA catalyst status and the inlet feed on ethane conversion, product yield using HGaAlMFI catalyst. (temperature= 700 °C, GHSV= 1875 mL/(g_{cat} ·h) , reduction: 80vol%C_2H_6/20vol%Ar or 40vol%C_2H_6/40vol%H_2O/20vol%Ar, oxidation 10vol%O_2/90vol%Ar).

To further investigate the deactivation, fresh and regenerated catalysts were tested for both OCM and DHA reactions. As shown in Figure 103a, both the fresh catalyst and the regenerated catalyst after the OCM+DHA reaction were tested for the OCM reaction using the same 2.0 g 5%Li_2CO_3/$LaPrO_{3+x}$ catalyst. From both the methane conversion and product selectivity, the fresh catalysts and regenerated catalysts had similar results. For the fresh catalyst, the methane conversion reached 31.4% and the C_{2+} yield reached 24.1%, with the C_2H_6 selectivity at 34.6% and the C_2H_4 selectivity at 44.0%. As for the regenerated catalyst, the methane conversion reached 29.9% and the C_{2+} yield reached 23.8%, with the C_2H_6 selectivity at 35.9% and the C_2H_4 selectivity at 44.3%. Besides, the 5%Li_2CO_3/$LaPrO_{3+x}$ catalyst exhibited great stability in our previous cycling test with almost no deactivation in 20 cycles. In the OCM+DHA reaction, the reactant inlet feed and the reaction condition for 5%Li_2CO_3/$LaPrO_{3+x}$ catalyst are almost the same as the OCM reaction only. Therefore, it would be reasonable that the OCM catalyst had good stability during the OCM+DHA reaction or OCM reaction only.

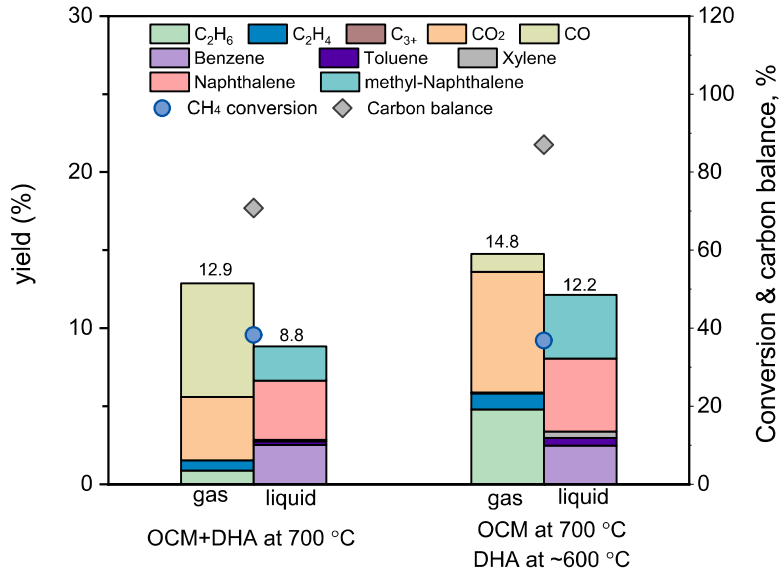

Figure 104. Effect of reaction temperature for OCM+DHA (OCM catalyst: 5%Li_2CO_3/$LaPrO_{3+x}$ catalyst, DHA catalyst: HGaAlMFI catalyst, pressure= 1 bar, flow rate= 25 mL/min, reduction: 80vol%CH_4/20vol%Ar, oxidation 10vol%O_2/90vol%Ar).

As for the HGaAlMFI catalyst for the DHA reaction, the different reactant inlet feed and the catalyst status both exhibited significant effects. The regeneration was conducted in 5%O_2/95%Ar at 600 °C for 30 min. In the OCM+DHA reaction case, the gas flow had both hydrocarbons and significant amounts of steam. For instance, producing one C_2H_6 molecule stoichiometrically produces one H_2O molecule and producing one C_2H_4 molecule stoichiometrically produces two H_2O molecule during the OCM reaction, and therefore there can be steam entering the DHA reactor. Under this circumstance, the effect of reactant inlet feed should be taken into consideration. As shown in Figure 103b, the regenerated HGaAlMFI catalyst exhibited a similar result to the fresh HGaAlMFI catalyst in the C_2H_6+Ar inlet feed condition. For the fresh catalyst, the total gas yield reached 21.3% and the aromatic yield reached 34.5%, with the C_2H_6 conversion at 68.1%. For the regenerated catalyst, the total gas yield reached 20.7% and the aromatic yield reached 33.8%, with the C_2H_6 conversion at 66.5%. However, there appears to be a negative effect of H_2O on the performance of the HGaAlMFI catalyst. Under a C_2H6+H_2O+Ar inlet feed condition, the fresh catalyst only had the gas yield at 18.4% and the aromatic yield at 26.6%, with the C_2H_6 conversion at 48.7%, which indicated the H_2O was not inert during the C2-DHA reaction. Moreover, the regenerated catalyst had a lower performance, with the gas yield at 12.5%, the aromatic yield at 17.0%, and the C_2H_6 conversion at 38.6%. The lower performance indicates the detrimental effect

of water on t the HGaAlMFI catalyst. Therefore, further work needs to be done to enhance the DHA catalyst in terms of water-resistance properties.

To have a better understanding of HGaAlMFI catalyst behavior in the OCM+DHA reaction, the OCM+DHA reaction was further conducted with a lower reactor temperature for the DHA reactor in Figure 104. The OCM reactor was heated at 700 °C and the DHA reactor was heated at 600 °C. Under this circumstance, a better result could be seen in terms of the aromatic yield. When the OCM+DHA were both at 700 °C, the gas yield reached 12.9% and the aromatic yield reached 8.8%, with the methane conversion at 36.9%. For OCM at 700 °C and DHA at 600 °C, the gas yield reached 14.8% and the aromatic yield reached 12.2%, with the methane yield at 37.4%. Notably, the two conditions exhibited a similar CH_4 conversion. Besides, the higher gas yield and aromatic yield indicated there might be some heavier species than the detected aromatics, such as coke. We further investigated the carbon balance and found the carbon balance for the OCM+DHA at 700 °C was about 72% and the carbon balance for the OCM at 700 °C and DHA at 600 °C was about 87%. It should be noted that there were C_2H_4 and C_2H_6 that entered the DHA reactor. Generally speaking, the C_2H_4 should have a better capacity in dehydroaromatization reaction and thus requires a lower reaction temperature. Therefore, adjusting the DHA reactor temperature would be good to keep the balance of C_2H_4 and C_2H_6 dehydroaromatization and thus result in a better aromatic yield.

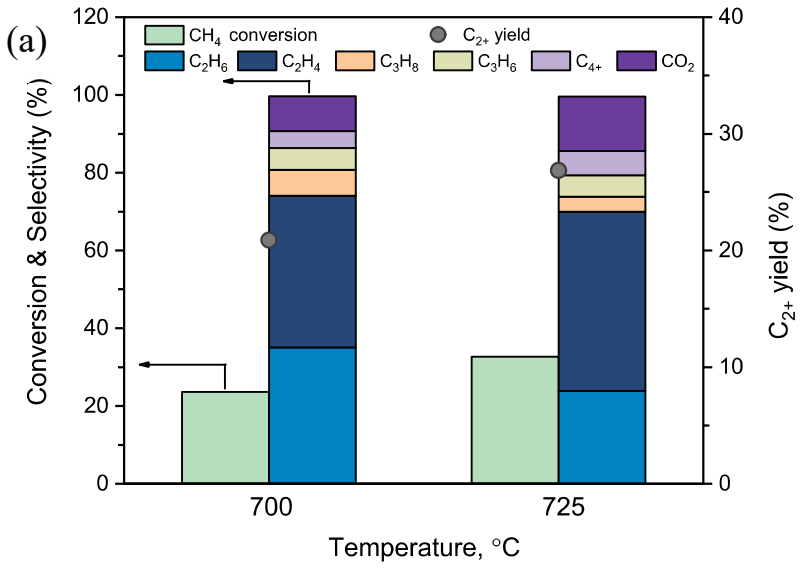

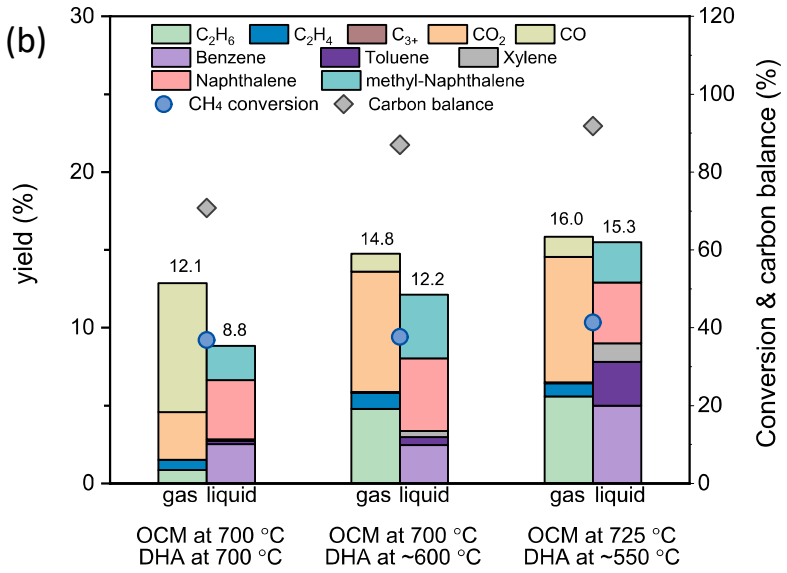

Figure 105. (a) Effect of reaction temperature for OCM reaction. (OCM catalyst: 5%Li_2CO_3/LPO catalyst, pressure= 1 bar, flow rate= 25 mL/min, reduction: 80vol%CH_4/20vol%Ar, oxidation 10vol%O_2/90vol%Ar). (b)Effect of reaction temperatures for OCM+DHA (OCM catalyst: 5%Li_2CO_3/LPO catalyst, DHA catalyst: HGaAlMFI catalyst, pressure= 1 bar, flow rate= 25 mL/min, 80vol%CH_4/20vol%Ar).

Based on the result of the wet C_2H_4-DHA and wet C_2H_6-DHA reactions reported in Figure 105, the HGaAlMFI catalysts exhibited a higher conversion and a better yield towards aromatics for C_2H_4-DHA. Therefore, it would be beneficial for higher C_2H_4 yield and a lower C_2H_6 yield is achieved from the OCM reaction. The effect of the temperature was investigated for the OCM reaction, as shown in Figure 105a. By increasing the temperature, a higher conversion and higher C_2H_4 yield can be achieved. Generally, the methane conversion reached 24.5% at 700 °C, with a C_2H_6 selectivity of 35.0% and a C_2H_4 selectivity of 38.9%. When the temperature was at 725 °C, the methane conversion reached 32.8% at 700 °C, with a C_2H_6 selectivity of 23.9% and a C_2H_4 selectivity of 46.1%. The yield of C_2H_4 increased from 9.5% to 15.3%. Thus the downstream of the OCM reactor favors the formation of aromatic in DHA reaction due to the higher reactivity of C_2H_4-DHA reaction.

The OCM+DHA reaction was conducted by setting two reactors to different temperatures, as shown in Figure 105b. For the fresh catalyst testing, both reactors were set at 700 °C with a gas yield was 12.1 % and the aromatic yield of 8.8% obtained along with a methane conversion of 36.9%. For OCM at 700 °C and DHA at 600 °C, the gas yield was 14.8% and the aromatic yield

was 12.2%, with a methane yield of 37.4%. For OCM at 725 °C and DHA at 600 °C, the gas yield was 16.0% and the aromatic yield was 15.3%, with a methane yield of 42.1%. For OCM at 725 °C and DHA at 550 °C, the CH_4 conversion was higher than the other two conditions. There was almost no C_2H_6 (0.5% yield) at OCM+DHA at 700 °C, but a significant amount of C_2H_6 can be observed for the other two conditions with only 4.7% for OCM at 700 °C+DHA at 600 °C and 5.0% for OCM at 725 °C+DHA at 550 °C. This is consistent with C_2H_6-DHA not being favorable at low temperatures. The carbon balance for the OCM+DHA at 700 °C was about 72% and the carbon balance for the OCM at 700 °C + DHA at 600 °C was about 87%. The carbon balance for the OCM at 725 °C + DHA at 550 °C was about 92%. The higher carbon balance is attributable to less carbon deposition occurring when the DHA reactor is set at a lower temperature. Therefore, it can be seen that varying the two reactor temperatures can change the product distribution between the desired aromatic and the undesired gas and coke. In this way, the 15% single-pass aromatic yield is achieved for the methane conversion to aromatic.

As shown in Figure 106, we conducted the cycling experiments for the optimized OCM+DHA reaction setup, with OCM reactor at 700 °C and DHA reactor at 550 °C. For the first reduction cycle in 80vol%CH_4/20vol%Ar, the gas product yield reached 16.1% and the aromatic yield reached 15.3%, with methane conversion of 42.1%. After the first cycle reduction, the catalyst reactors were flushed in Ar and then oxidized in 20%O_2/80%Ar to remove the carbon deposition and regenerate the catalysts. The 2nd cycle had the gas product yield of 16.4% and aromatic yield of 9.3%, with methane conversion of 38.9%. For the following cycles, the methane conversion further decreased from 37.4% for the 3rd cycle to 33.6% for the 5th cycle, and the aromatic decreased significantly from 5.5% for the 3rd cycle to 1.5% for the 5th cycle, whereas the gas product yield increased significantly from 18.9% for the 3rd cycle to 24.2% for the 5th cycle. While the conversion deactivation was within 20% relatively, we observed the product distribution was strongly affected during the cycling, a smaller fraction of aromatic products achieved. For the binary catalyst system, the OCM catalyst first converts methane into C_2 and C_{3+}, and the following DHA catalyst converts C_2 and C_{3+} into aromatic products. The increase in gaseous product yield and decrease in aromatic yield may result from deactivation of the DHA catalyst. Our previous cycling result showed the OCM can undergo the 50-cycle test without significant deactivation. While some loss in methane conversion is observed, this decrease is small compared to the decrease in aromatic yield. The DHA catalyst, on the other hand, may suffer from deactivation,

such as oxidation by H_2O, CO_2 or deactivation by CO, or carbon deposition, and thus gradually loses its capacity to convert the light C_2 and C_{3+} species into the aromatics.

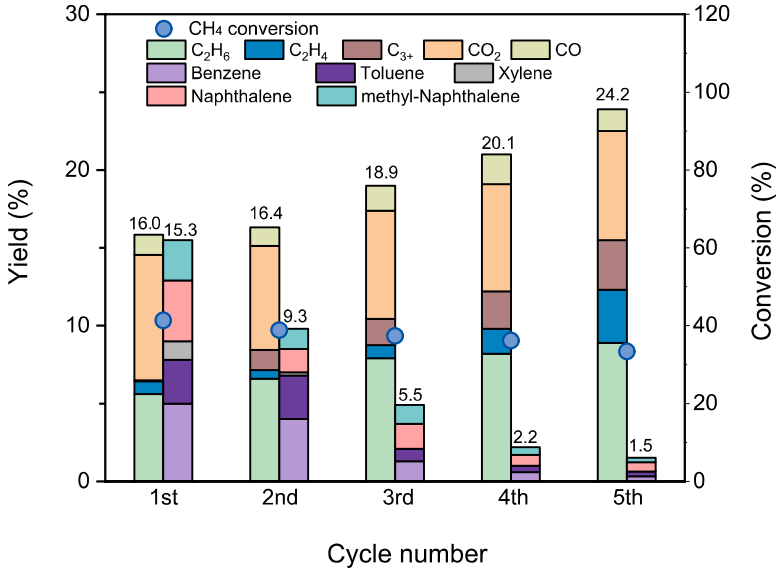

Figure 106. Stability test of the OCM+DHA reaction setup: OCM: 2g 5%Li_2CO_3/$LaPrO_{3+x}$ catalyst at 700 °C, DHA catalyst: 0.1 g HGaAlMFI catalyst at 550 °C, pressure= 1 bar, flow rate= 25 mL/min, reduction: 5-min 80vol%CH_4/20vol%Ar, internal flush: 5-min Ar, oxidation: 5-min 20vol% O_2/80vol%Ar).

As the OCM oxide catalyst requires O_2-oxidation to recover its lattice oxygen, the reaction of OCM+DHA reaction setups will have the regeneration step to use O_2 to recover the activity of the OCM, which can also aid in the removal of coke deposited on the C_2-DHA catalysts. However, our results indicate that O_2 is unable to recover the activity of the C_2-DHA catalyst as the quick deactivation cause is likely not carbon deposition. Instead, H_2 can effectively regenerate the C_2-DHA catalyst and recover 99% of its activity. Therefore, we upgraded the reactor setup and modified the gas feeding system to enable O_2-regeneration for OCM-reactor and H_2-regeneration for the DHA-reactor. As shown in Figure 107a, this modified setup enables CH_4/Ar to enter the OCM reactor first after which it flows into the DHA reactor along with the OCM products (C_2H_6, C_2H_4, H_2O, etc) during the reaction step. As for the regeneration step, the O_2/Ar enters the OCM reactor to replenish lattice oxygen vacancies of the reduced OCM catalyst, but not enters the DHA reactor. H_2/Ar enters the DHA reactor to recover the DHA catalyst and reverse the deactivation effect of H_2O on DHA catalyst.

Cycling experiments were conducted to evaluate the newly upgraded reaction setups for OCM+DHA reactions, as shown in Figure 107b. For the first cycle, the methane conversion reached 33.1% and the overall aromatic yield reached 14.5%, with benzene yield at 4.6 %, toluene yield at 2.7%, and xylene yield at 1.6%. For the fifth cycle, the methane conversion reached 31.4% and the overall aromatic yield reached 14.7%, with benzene yield at 4.4 %, toluene yield at 2.9%, and xylene yield at 1.8%. For the 8^{th} cycle, the methane conversion reached 31.5% and the total aromatic yield reached 14.3%. The average methane conversion reached 32.0 ± 0.9 % and average aromatic yield reached 14.2 ± 0.3 %. As a consequence, 0% relative aromatic yield loss can be achieved for the upgraded reaction setup (O_2-oxidation for OCM catalyst and H_2-reduction for DHA catalyst) as compared to 90% aromatic yield loss (relative) for the O_2-oxidation only for both OCM and DHA catalysts. Therefore, stable running can be achieved by upgrading the regeneration process. The side product of H_2O from the OCM reaction can strongly deactivate the DHA catalysts and the H_2-reduction can effectively recover the DHA catalyst. The upgraded setup enables the O_2-oxidation for the OCM catalyst and H_2-reduction for the DHA catalyst and significantly improves the stability of the combined OCM and DHA reaction with stable 14-15% single pass aromatic yield from methane. However, we observed the pressure increase during the reaction-regeneration step and the final pressure increase to ~24 psia.

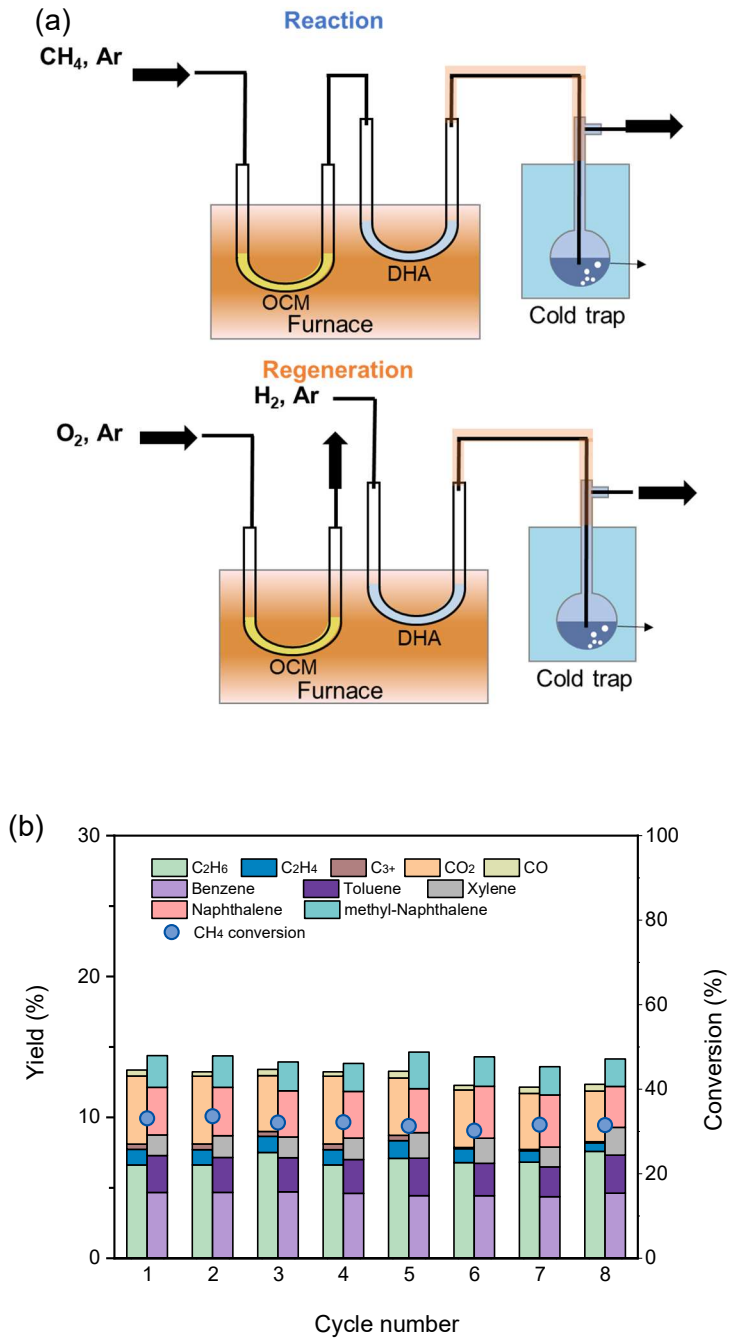

Figure 107. (a) Schemes of the upgraded setup for reaction step (CH_4/Ar enters OCM and DHA reactor) and regeneration step (O_2/Ar enters OCM reactor and H_2/Ar enters the DHA reactor separately) (b)Stability test of the OCM+DHA reaction setup: OCM: 2g 5%Li_2CO_3/$LaPrO_{3+x}$ catalyst at 725 °C, DHA catalyst: 0.1 g HGaAlMFI catalyst at 550 °C, pressure= 1 bar, flow rate= 25 mL/min, reduction: 5-min 80vol%CH_4/20vol%Ar, internal flush: 5-min Ar, regeneration: 10-min 20vol% O_2/80vol%Ar for OCM, 10-min 20vol% H_2/80vol%Ar for DHA,).

In order to solve the pressure problem, we further revisited the pressure drop increase and determined the increase resulted from the OCM catalyst when we tested the inlet pressure of the spent catalyst reactor individually. The inlet pressure of the OCM reactor was ~24 psia at 725 °C and the inlet pressure of the DHA reactor was ~15 psia at 550 °C with the same flow rate of 25 mL/min Ar. That indicates the OCM catalyst sintered gradually during the reaction-regeneration process. The following experiments were conducted as shown in Figure 108. Pressure drop increase were observed for both two OCM reactors with 5-minute reduction time or 3-minute reduction time. For 5-minute reduction one, the inlet pressure increased from 15.3 psia at 1st cycle to 22.3 psia at 5th cycle. For 3-minute reduction one, the inlet pressure increased from 14.8 psia at 1st cycle to 19.3 psia at 20th cycle. These indicated the extent of the reduction process can be an important factor of the catalyst sintering when considering a total 25-mintute reduction (5 cycle 5-minute) and a 60-minute reduction time (20 cycle 3-minute).

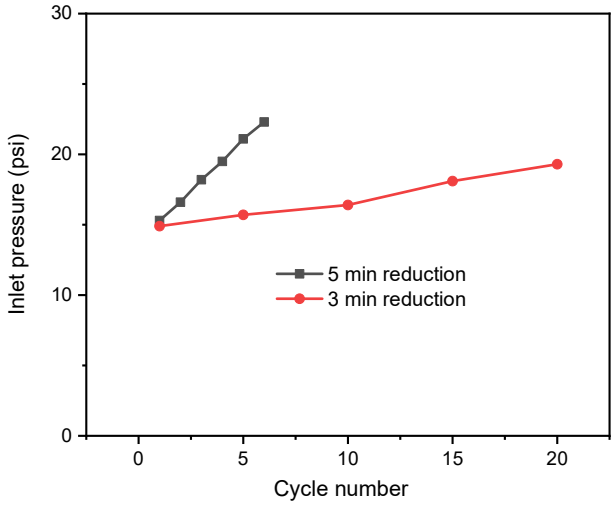

Figure 108. Inlet pressure of the OCM reactor: 2g 5%Li_2CO_3/$LaPrO_{3+x}$ catalyst at 725 °C, pressure= 1 bar, flow rate= 25 mL/min, reduction: 3-min or 5-min 80vol%CH_4/20vol%Ar, internal flush: 5-min Ar, regeneration: 5-min 20vol% O_2/80vol%Ar.

As shown in Figure 109, 20 cycles of OCM+DHA reactions were conducted with the 3-minute reaction time. For the 1st cycle, the methane conversion reached 28.9% and the total aromatic yield reached 14.8%. For the 10th cycle, the methane conversion reached 29.3% and the total aromatic yield reached 15.3%. For the 20th cycle, the methane conversion reached 28.3% and the total aromatic yield reached 14.5%. The average methane conversion reached 29.2 ± 0.6 % and

the average aromatic yield reached 14.7 ± 0.5 %. This result also indicated no activity or yield loss during the 20-cycle reaction-regeneration step. In conclusion, we successfully achieved 20-cycle ~15% single aromatic yield without deactivation.

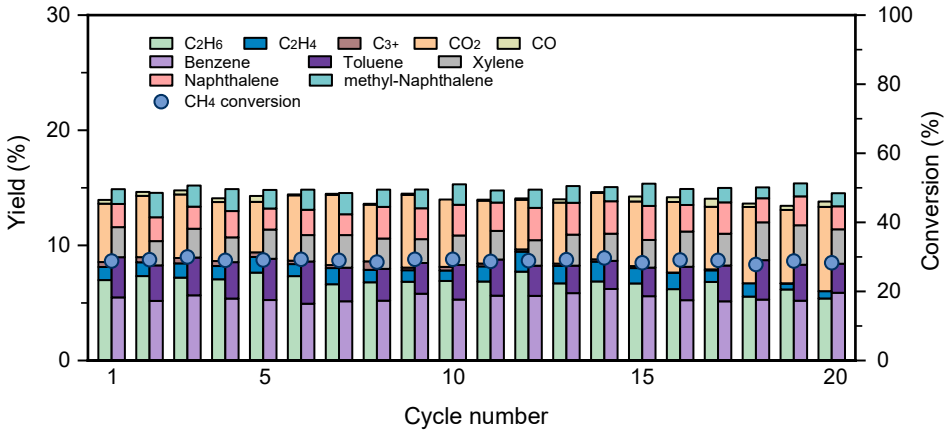

Figure 109. Stability test of the OCM+DHA reaction setup: OCM: 2g 5%Li_2CO_3/$LaPrO_{3+x}$ catalyst at 725 °C, DHA catalyst: 0.1 g HGaAlMFI catalyst at 550 °C, pressure= 1 bar, flow rate= 25 mL/min, reduction: 3-min 80vol%CH_4/20vol%Ar, internal flush: 5-min Ar, regeneration: 10-min 20vol% O_2/80vol%Ar for OCM, 10-min 20vol% H_2/80vol%Ar for DHA,).

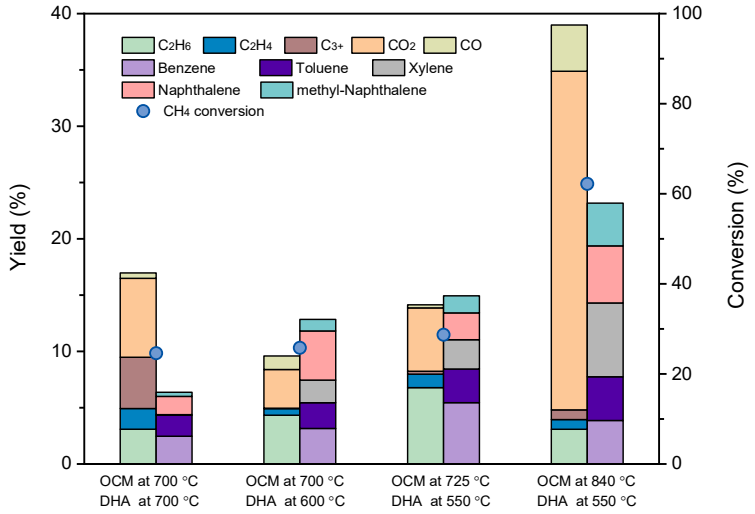

Figure 110. Comparison of the OCM+DHA with different catalyst combinations: For the first three cases, we used 2.0g of Pr based catalyst +0.1g HGaAlMFI catalyst, OCM at 700-725 °C, DHA at 550-600 °C, reaction: 5-min 80 vol%CH_4/20vol%Ar, internal flush: 5-min Ar, regeneration: 5-min 20vol% O_2/80vol%Ar. For the last condition, we use a second generation OCM catalyst (0.43 g) +0.2 g HGaAlMFI, OCM at 840 °C, DHA at 550 °C, reaction: 15s 80vol%CH_4/20vol%Ar, internal flush: 5-min Ar, regeneration: 10-min 20vol% O_2/80vol%Ar.

This OCM catalyst was tested for the integrated setup of OCM+DHA. For the OCM reaction, 0.43 grams of the $MnLi_aMg_bB_cO_x$ catalyst were employed at the temperature of 840°C. Concurrently, the DHA reaction was facilitated by 0.2 grams of the HGaAlMFI catalyst, operating at 550°C. The entire reaction was conducted at a constant pressure of 1 bar (absolute), with a flow rate of 25 mL/min. The reduction phase involved a 15-second injection of a gaseous mixture comprised of 80% methane and 20% argon in the OCM reactor, and the product of the OCM reactor was routed to DHA reactor set up for conversion into aromatics. This was subsequently followed by an internal flushing procedure using argon for a duration of 5 minutes. Finally, the regeneration was carried out for 10 minutes, utilizing a gas composition of 20% oxygen and 80% argon. Figure 111 shows the performance comparison using the $MnLi_aMg_bB_cO_x$ + HGaAlMFI catalyst, in comparison to the previously developed $LaPrO_{3+x}$@Li_2CO_3 OCM catalyst +DHA catalyst for OCM+DHA reaction setup. For OCM+DHA setup using $MnLi_aMg_bB_cO_x$ + HGaAlMFI catalyst, the methane conversion was 62.2% and the total aromatics yield was 23.2%. We observe that there were more xylene (6.5%) and naphthalene (5%) for the $MnLi_aMg_bB_cO_x$ + HGaAlMFI reaction setup which may possibly be ascribed to the different product distribution of the OCM reaction. The higher aromatic yield could be promising in converting methane into aromatics. Furthermore, the $MnLi_aMg_bB_cO_x$ catalyst has been shown to be highly robust and is likely to be a promising catalyst for long term OCM-DHA applications.

Subtask 5.2: Catalyst Synthesis Scale-up

As we usually use the OCM redox catalyst with 2.0g and the DHA catalyst with 0.1g for the OCM+DHA test, the scale-up production of the OCM redox catalyst became a concern. The scale-up production of OCM 5%Li_2CO_3/$LaPrO_{3+x}$ catalyst was conducted from the base 5g/batch to 20g/batch via the sol-gel method. As the 5g/batch catalyst was conducted in a 200mL beaker, the precursor amount was doubled and a 500 mL beaker was applied for the 10g/batch catalyst preparation. And the precursor amount was then increase to 4 times and a 2L beaker was applied. The generated gel was then collected, dried in oven, and calcined in the tube furnace. As shown in Figure 111, the catalytic performance for OCM reaction was tested for different catalysts. The methane conversion for OCM catalyst at 5g/batch was about 30.2%. For 10g/batch catalyst, the methane conversion was about 32.5%. And the conversion for 20g/batch catalyst was 30.8%, 32.3%, and 28.2%. As for the C2+ yield, the 5g/batch OCM catalyst had the yield at 23.3%, which is higher than the 22.8% for 10g/batch OCM catalyst and 21.2%, 20.2% and 20.1% for the 20g/batch OCM catalyst. The difference in OCM methane conversion and yield may result from the CO_2 selectivity. It was observed that the 20g/batch catalysts had higher CO_2 selectivity at 24-32% as compared to the 17% CO_2 selectivity for the 5g/batch OCM cataltyst.

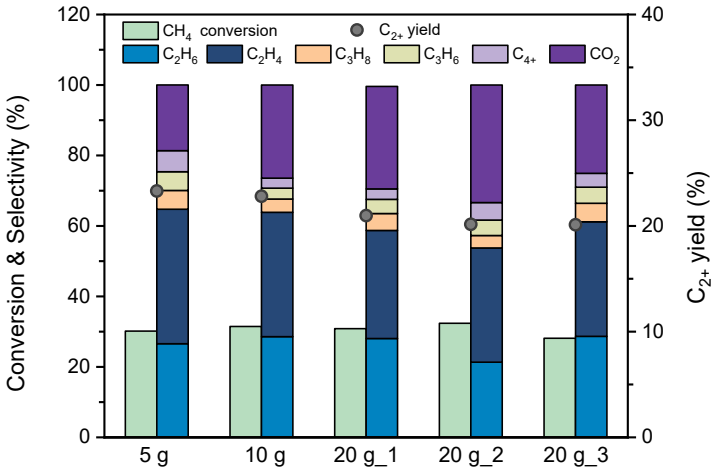

Figure 111. OCM reaction performance with different catalyst preparation batch for 5g/batch, 10g/batch and three 20g/batch. Reaction: 2g 5%Li_2CO_3/$LaPrO_{3+x}$ catalyst at 700 °C, pressure= 1 bar, flow rate= 25 mL/min, reduction: 3-min or 5-min 80vol%CH_4/20vol%Ar, internal flush: 5-min Ar, regeneration: 5-min 20vol% O_2/80vol%Ar.

Task 6: Long term demonstration of OAS

Subtask 6.1:Reactor design and fabrication

Setup and commissioning of OCM+DHA reactor system unit (NCSU)

In this quarter, the modular test unit is being designed by the NCSU. The design of the modular testbed is shown in Figure 112. The reactor is a packed bed reactor with >150 cm^3 catalyst bed space. The reactor will be a packed bed reactor with the capacity of holding > 50 cm^3 catalyst. The catalysts will be placed in the reactor and the heat supply of the OCM+DHA reaction is done by a furnace with a constant temperature area > 20 cm. Some K-type thermocouples will be placed around the reactor area and applied to measure and adjust the furnace output. The mass flow controllers and pneumatic valves are designed to control the reactant feedstock. This system unit will produce 50 mL of aromatic products per day, including benzene, toluene, xylene, and naphthalene. As shown in Figure 113, the current reactor unit was well established and will be tested for safety test and initial reaction test in the future. For the reactor part, the 3-zone furnace together with the 3-zone controller will provide the suitable temperature zones for the OCM reaction and DHA reaction, which enable the optimal reaction performance. The following separation system consists of one condenser with an observation tube, one side liquid collection tank, and one air separator. This separation system will cool down the downstream flow from the reactor part and separate the gas product (methane and light hydrocarbon product) and the liquid product (aromatic). The collected gas sample will be analyzed by the mass spec or gas chromatography. The collected liquid sample will be analyzed by gas chromatography.

However, we developed the regeneration step for the DHA catalyst and made modifications on the previous milestone. This catalyst system design in Figure 112 can work well for the common tandem catalysis system but may not work well for our OCM+DHA catalytic system design. We

further work on our benchtop catalyst system and focus on the catalyst development for common reactor system.

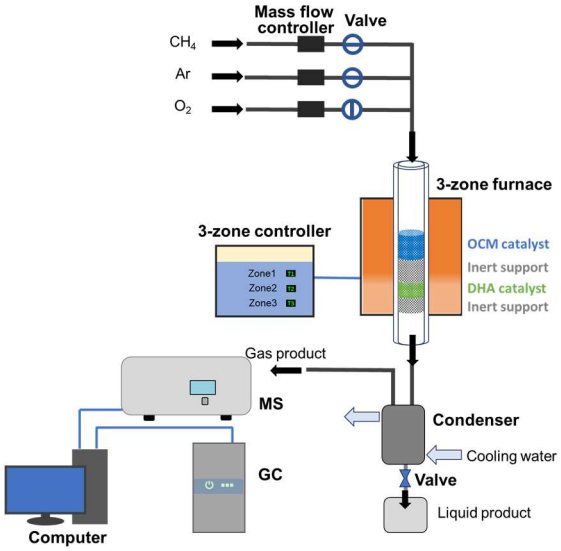

Figure 112. Scheme of the reaction setup including reactant feedstock, the reactor, the separation unit, and the analysis instrument.

Figure 113. Photo of the current large scale reactor (a) Overall outlook (b) Reactor part with (b1) the reactor, (b2) 3-zone furnace (b3) 3-zone controller; (c) Product separation unit with the (c1) liquid condenser and (c2) the air separator; (d) Analysis part with the (d1) gas chromatography for liquid product, (d2) gas chromatography for gas product and (d3) mass spec for gas product.

Subtask 6.2: Long-Term Testing

We conducted a cycling OCM+DHA reaction test with ~15% single-pass aromatic yield using an improved regeneration procedure for a 105-h long-term reaction test. With the improved regeneration procedure, we could achieve the recovery of Ga-H active sites during the regeneration step and thus maintain the activity and stability of the DHA catalyst by H_2 reductionAs shown in Figure 114a, we continued to conduct the OCM+DHA for an additional 30 cycles under the same conditions as the previous 20 cycles. For cycles 1-20, the average methane conversion was 29.2 ± 0.6 % and the average aromatic yield was 14.7 ± 0.5 %. For the cycles 21-30, the average methane conversion was 28.3 ± 0.6 % and the average aromatic yield was 14.1 ± 0.5 %. For the cycles 31-40, the average methane conversion was 27.2 ± 0.7 % and the average aromatic yield was 13.8 ±

0.5 %. For the cycles 41-50, the average methane conversion was 26.4 ± 0.6 % and the average aromatic yield was 12.9 ± 0.7 %. During the 50-cycle reaction, we could observe a slight, gradual deactivation. The 50-cycle OCM+DHA led to a ~12% relative decrease in the aromatic yield, which is still much better than the traditional methane-to-aromatic catalyst which generally shows ~8% maximum single-pass yield. We also observed the gradual inlet pressure increase from ~15 psia to ~24 psia. The pressure increase is attributable to the OCM reactor. The reactor pressures can be monitored separately during the regeneration step for the reactors, with the OCM reactor giving an inlet pressure of ~25 psia and the DHA reactor giving a pressure of ~15 psia. The pressure increase is consistent with sintering of the OCM catalyst, as we mentioned in our previous report. Sintered OCM bed not only blocks the flow path but may decrease the exposed area and cause bypass of the bed, which were considered potential mechanisms of activity loss. To keep the reaction working at a suitable pressure, we stopped the reaction after 50 cycles, and used a thin steel tube to loosen the sintered OCM catalyst before resuming operations. After adjustment the inlet pressure decreased from ~25 to ~19 psia.

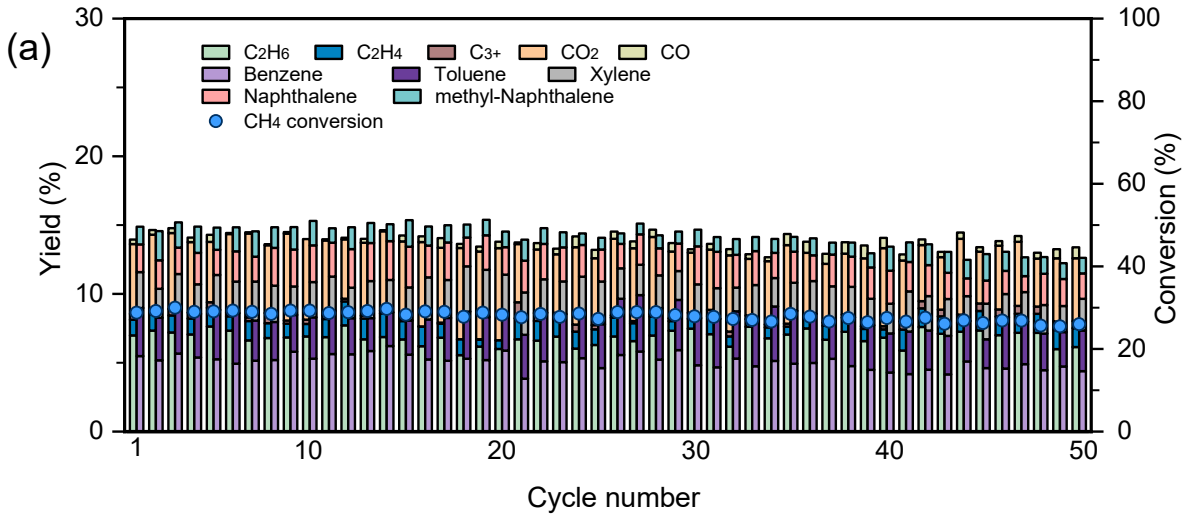

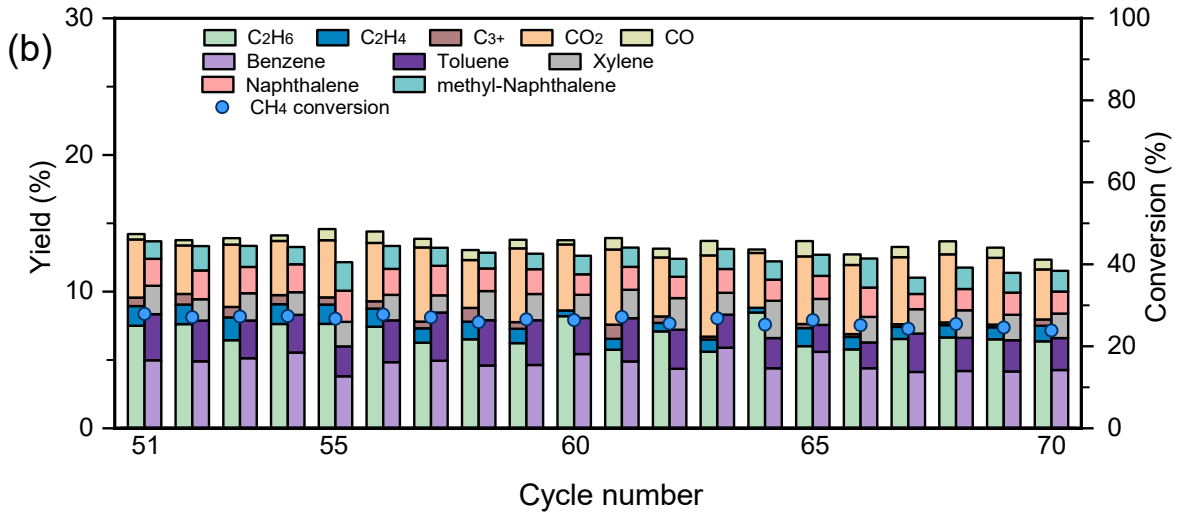

Figure 114. Long-term stability test of the OCM+DHA reaction setup: OCM: 2g 5%Li_2CO_3/$LaPrO_{3+x}$ catalyst at 725 °C, DHA catalyst: 0.1 g HGaAlMFI catalyst at 550 °C, flow rate= 25 mL/min. reduction: 3-min 80vol%CH_4/20vol%Ar, internal flush: 21-min Ar, regeneration: 15-min 20vol% O_2/80vol%Ar for OCM, 20vol% H_2/80vol%Ar for DHA. (a) Cycles 1-50, (b) Cycles 51-55, cycles 56-60, cycles 61-70. catalyst-recovery treatments conducted before cycle 51, cycle 56, and cycle 61: 15-h 10vol% O_2/90vol%Ar for OCM catalyst at 525 °C, 10-h 10vol% O_2/90vol%Ar +5h 10vol% H_2/90vol%Ar for DHA catalyst at 350 °C.

After loosening of the bed, another regeneration pretreatment step at a lower temperature was conducted, with the OCM reactor at 525 °C and the DHA reactor at 350 °C. During this regeneration, the OCM reactor was treated with O_2, and the DHA reactor was treated with O_2/Ar first and then H_2/Ar to remove the carbon deposition. This non-cyclic regeneration pretreatment was conducted before cycle 51, cycle 56, and cycle 61. For cycles 51-55, the average methane conversion was 27.3 ± 0.4 % and the average aromatic yield was 13.2 ± 0.5 %. For cycles 56-60, the average methane conversion was 26.7 ± 0.6 % and the average aromatic yield was 13.0 ± 0.3 %. For cycles 61-65, the average methane conversion was 26.3 ± 0.7 % and the average aromatic yield was 12.7 ± 0.4 %. For cycles 65-70, the average methane conversion was 24.7 ± 0.6 % and the average aromatic yield was 11.6 ± 0.5 %. Simultaneously, the inlet pressure continued to

gradually increase, as high as ~26 psia at cycle 70. The bypass from the catalyst bed sintering may account for the decreasing methane conversion and thus the aromatic yield.

In summary, we conducted a total of 105 hours of reaction testing with the improved regeneration setup and achieved an average methane conversion of 27.4 ± 1.5 % and an average single-pass aromatic yield of 13.8 ± 1.1 %. The H_2-reduction greatly recovered the Ga-H sites for the DHA reaction, as compared to ~90% activity loss in 5 cycles without the H_2-reduction. We also observed the sintering phenomena of the OCM catalyst. This highlights the importance of the OCM catalyst improvement.

Subtask 6.3: Post-Test Characterization

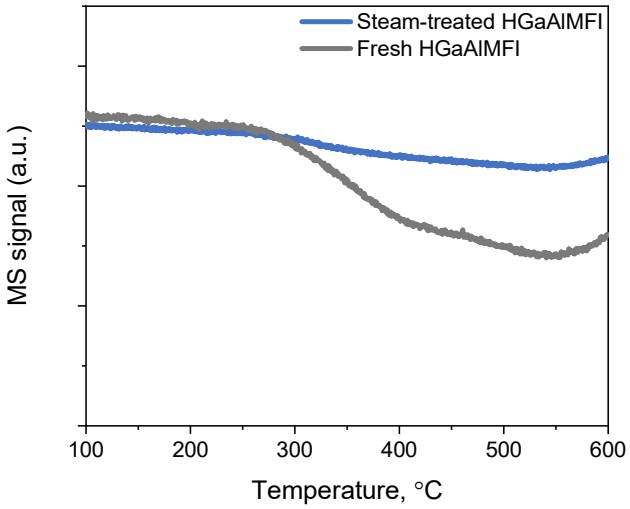

Figure 115. C_2H_4-TPSR for the steam-treated HGaAlMFI catalyst and fresh HGaAlMFI catalysts. Catalyst: 0.03 g, Flow: 100mL/min 10vol%C_2H_4/90vol%Ar, Ramping rate: 10 °C/min.

Temperature-programmed surface reaction in 10 vol% C_2H_4/90 vol% Ar was conducted to examine the steam-treated HGaAlMFI catalysts. As there was about 15% to 30% percent (by volume) H_2O in the OCM downstream, the effect of water need to be investigated. The HGaAlMFI catalyst was treated in 10 vol% H_2O(g)/90 vol% Ar at 500°C for 1h to represent the spent catalyst after water poisoning. In Figure 115, the behavior of fresh DHA catalyst and steam-treated DHA catalyst are compared for the C_2H_4-TPSR in 100mL/min 10vol%C_2H_4/90vol%Ar from 100 to

600 °C. The fresh DHA catalyst had an initial conversion temperature of 260 °C. The team-treated DHA catalyst has a much lower activity and an onset of conversion at a temperature of 300 °C, indicating that the H_2O may affect the Ga-H sites, which are considered the activation sites of the C2-DHA reaction. The fresh catalyst had a conversion at ~45% at 500 °C whereas the steam-treated DHA catalyst had a conversion at ~10%. The lower conversion of the steam-treated DHA catalyst in C_2H_4-TPSR indicated that the H_2O might oxidize the Ga-H sites and convert to other oxidized Ga species.

Task 7: Final TEA

Introduction

Susteon performed a techno-economic analysis (TEA) for the production of 520 bbl./day of liquid aromatics using the oxidative aromatization system (OAS) developed under DE-FE0031869. This report aims to evaluate the technical and economic feasibility of the process with a goal to provide a preliminary assessment of its viability, guiding further research and development. This TEA involves the estimation of capital and operational costs, production cost of the aromatics ($/bbl.) and key performance metrics using simplified models and assumptions based on available experimental data, analogous processes, and scaling factors. The TEA is conducted using the framework outlined by the U.S. Department of Energy (DOE) in the document "QGESS Cost Estimation Methodology for NETL Assessments of Power Plant Performance" (September 2019).[18]

- **Class of Estimate**: Class V cost estimate for the purposes of concept screening
    - establishing feasibility of a novel technology with respect to technical soundness, operational flexibility, and economic viability. No focus on detailed design/optimization.
- **Typical error ranges at this stage of technology development**:
    - Capital Cost Estimates: ±30% to ±50%
    - Operational Cost Estimates: ±20% to ±40%
    - Revenue Estimates: ±20% to ±40%
    - Key Performance Metrics (e.g., efficiency, yield): ±10% to ±30%.

The TEA shows the feasibility of this process to produce liquid aromatics at a production cost of $1.92/gal., assuming the aromatic products have an economic value equal to that of benzene. The current benzene prices are in the range of $2.9 – 3.3/gal. **The estimated total overnight capital cost is $104 million, to produce 885 bbl./day of aromatic liquids. This is equivalent to a capital intensity of roughly $117,500/bbl./day of product**. In comparison, the Fischer Tropsch (FT)-based gas-to-liquid fuel processes cost in the range of $100,000-120,000/bbl./day of liquid fuel. With further development and de-risking, this cost can be driven down.

Process Model

Base Case Process Model

The base case of methane dehydro-aromatization (DHA) involves a typical non-oxidative approach. The modular scale (<1000 bbl. aromatics/day) would not be suitable for *non-oxidative* DHA - the principal reason for this being the difficulty of H_2/CH_4 separation at modular scale. Accordingly, the base case DHA process model was developed at a larger scale (15,000 bbl./day), representing aromatics production in a centralized facility fed by natural gas delivered at pipeline conditions. The base case was modeled after the work of Huang *et al*. (2019)[17], the most complete representation of industrial-scale non-oxidative DHA in the literature. There is currently no industrially practiced version of methane DHA, but Huang and coworkers provide a detailed framework and reasonable technoeconomic analysis for what non-oxidative DHA could look like at scale.

Figure 116 depicts the scheme laid out in Huang et al. Beginning at left, fresh natural gas and a recycle stream are mixed and enter the catalytic DHA reactor (R-1). Feed pre-heating and reactor heating requirements are met by firing natural gas with air. The exiting hot stream is used to superheat steam for power generation to offset electricity needs elsewhere in the process (E-1). The cooled product stream then goes through a series of compressors (C-n) and flash vessels (F-1 to F-5) to incrementally separate heavier aromatics (toluene, naphthalene) from the lighter gases, before entering cryogenic separation (E-n, F-6 to F-9), which removes the bulk of benzene and separates high-purity hydrogen from methane. H_2 leaves as a product stream and a CH_4-rich heavy stream is recycled to the reactor, containing residual H_2, C_6H_6, and other compounds. Several distillation columns (D-1 to D-3) handle the separation of (1) C_1 from C_2, (2) naphthalene from single-ring aromatics, and (3) toluene from benzene. This base case was simulated by Susteon using AspenPlus™, as illustrated in Figure 117 (upstream) and Figure 118 (downstream).

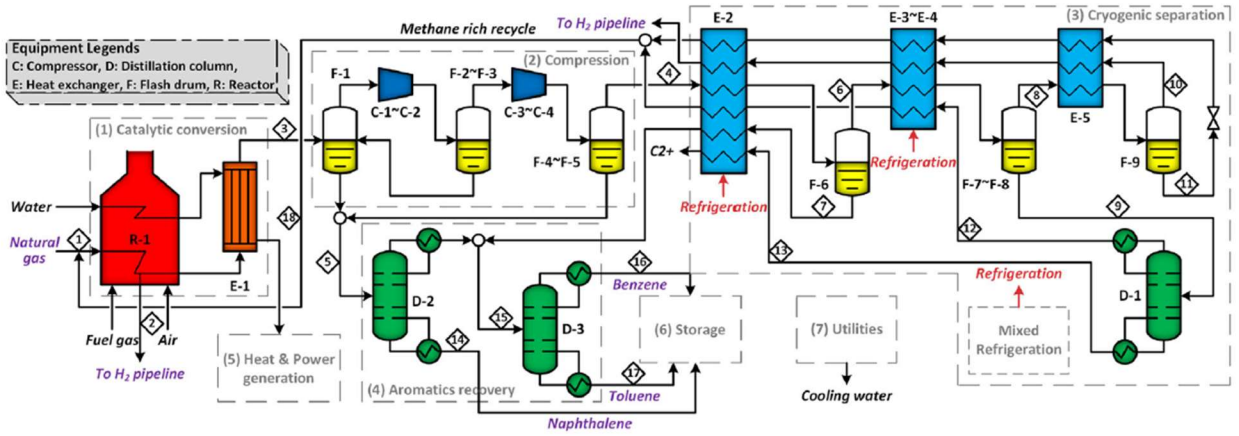

Figure 116. Process scheme for non-oxidative methane dehydroaromatization (DHA) at a scale of 5.0 MMSCF/h natural gas feed flowrate, from Huang *et al*. [17]. This model has been recreated by Susteon and used as the base case against which OAS is compared.

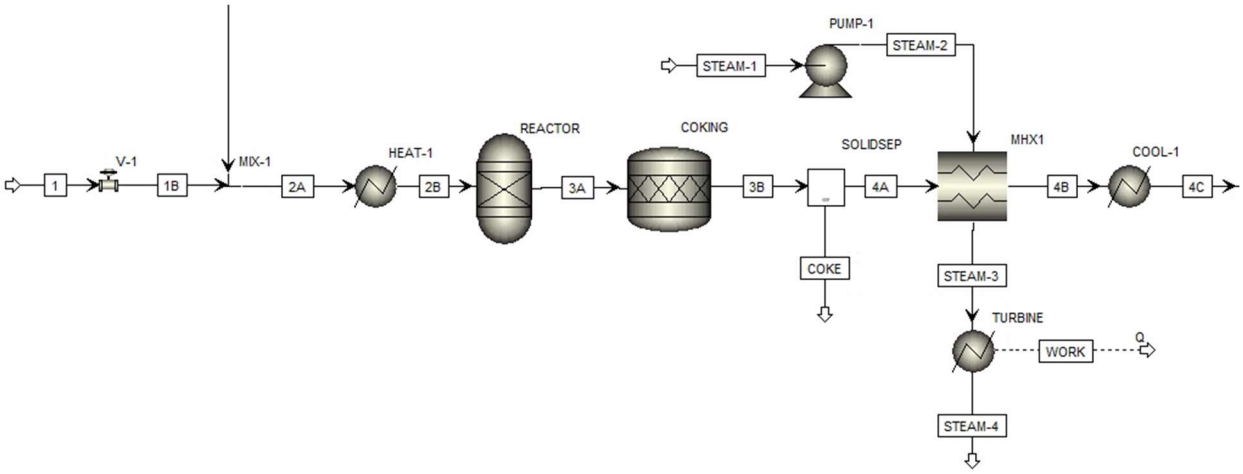

Figure 117. Recreation of the non-oxidative DHA process model built in AspenPlus™. The upstream section is shown, including the feed mixing and pre-heating, catalytic reactor, and heat recovery steam generation systems.

Fresh natural gas at pipeline specifications (25°C, 31 bar), consisting of 95.3% CH_4 with small amounts of ethane, propane, and *n*-butane, is throttled and mixed with a recycle stream containing primarily methane. The feed is pre-heated and sent to the DHA reactor, which is modeled as two blocks, one which handles the gaseous reactions (REACTOR, an R-Gibbs block) and one which simulates coke deposition (COKING, an R-Stoic block). The coke is removed (SOLIDSEP) and the stream passes through a heat recovery unit, which superheats steam at 30 bar and cools the process stream to 120°C. A final cooler brings the stream to 30°C. The cooled product stream

enters the compression and flash separation section (Figure 118, left side), where a series of flash vessels at 30°C remove most of the toluene and all the naphthalene at increasing pressure. The pressurized stream (at 36 bar), still containing most of the benzene, then enters the cryogenic separation system, where the benzene is removed at -72°C. The remaining flash units and coolers are for the separation of H_2 and CH_4, which requires a final temperature of -167°C. The vapor H_2 exits as a pure product stream (>97% purity), while the liquid methane is heat exchanged with other streams to return to vapor phase and join the distillate of column D-1 to create the reactor recycle stream, which is roughly six times greater than the fresh feed rate due to the low conversion of the DHA reactor.

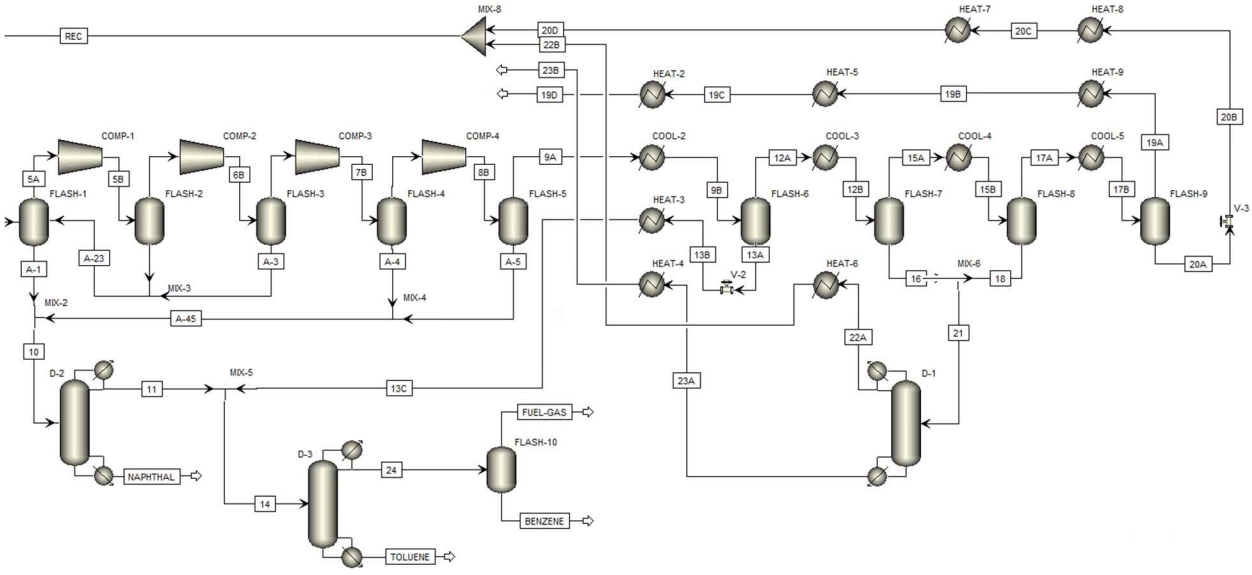

Figure 118. Recreation of the non-oxidative DHA process model built in AspenPlus™. The downstream section is shown, including the compression, flash separation, cryogenic separation, and distillation sections.

Distillation column D-1 handles a CH_4-rich stream which contains some H_2 and all of the C_{2+} compounds (which includes any remaining natural gas liquids as well as ethylene, propylene, and butenes). These exit as bottoms from D-1 and leave the system (stream 23) in a mixture without further purification. Columns D-2 and D-3 handle aromatics purification, with D-2 separating naphthalene from the single-ring aromatics and D-3 separating toluene from benzene. A final flash vessel is added to the Huang model to remove CH_4 from the D-3 distillate, which contains the product benzene; this stream is treated as fuel gas and can be used as an offset later when the TEA is refined.

OAS Process Model

A process model, utilizing 7 ton/hr. of methane, using the oxidative aromatization system (OAS), which includes the selective hydrogen combustion (SHC) component, was developed in AspenPlus™. Depending on the OAS case, the total aromatics (benzene, toluene, p-xylene, methylated and non-methylated naphthalene) account for 520-885 bbl./day. This model (shown in Figure 4 below) uses the experimental data obtained at NCSU. The detailed breakdown of each process section with corresponding stream information is provided in the Appendix. The process consists of three main sections, listed below:

Upstream OAS: This section includes the OAS reactors (reducing and regeneration reactors), which operate at 700^{o}C, 1-2 bar. The feed is primarily methane (assumed pure in the simulation) and a recycle stream, which contains unreacted methane and a portion of the light hydrocarbons like ethane and ethylene. The reactor has been assumed to have three parts, modeled as stoichiometric reactors in series:

OAS 1 – ethane + ethylene to aromatics: which assists in consuming these by-products present in the *recycle stream*. This is obtained from experimental data. This is used in the simulation to account for the consumption of the C2 compounds towards formation of the aromatics.

OAS 2 – a lumped methane OCM-DHA to aromatics: which incorporates the experimental data

SHC – by-product H_2 from the above two parts is selectively combusted to water.

The product distribution is shown in Table 39. MnO_2 → Mn_2O_3 transition has been assumed as the redox loop for OAS. This is a surrogate metal oxide, to represent the actual metal oxide-based redox catalyst. There are two cases shown: Case 1 (which has a lower methane conversion, but high aromatic selectivity) and Case 2 (which has a high methane conversion with lower aromatic selectivity, on a carbon basis).

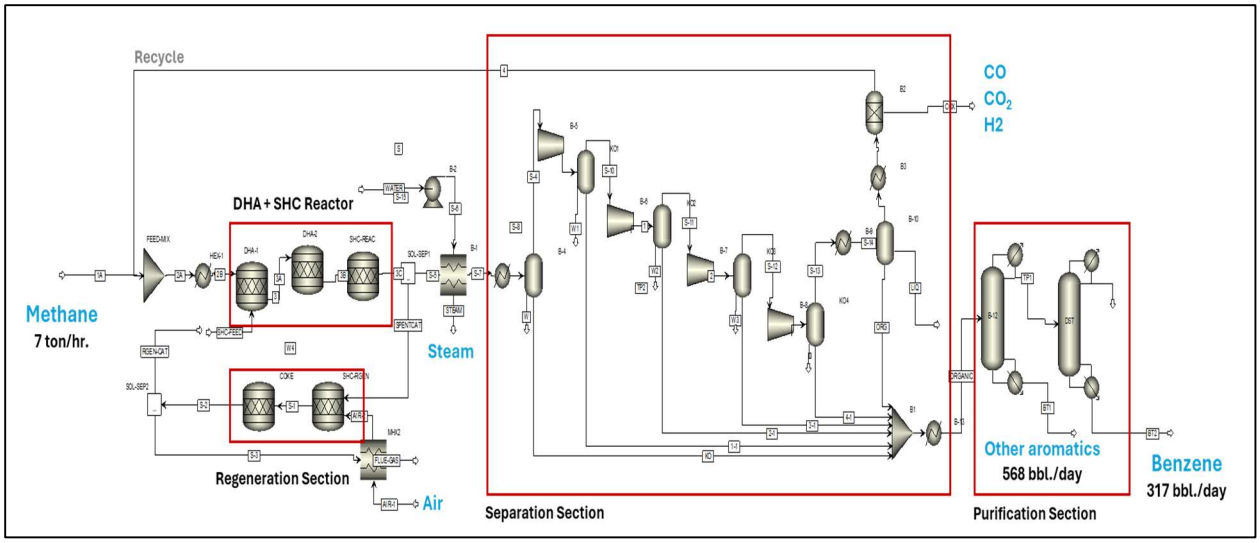

Figure 119. AspenPlus™ simulation of the OAS process (DHA + SHC) to produce 885 bbl./day of total aromatic liquids. Detailed sections and corresponding stream information are shown in the Appendix (focused on Case 1).

Table 39. Experimentally obtained product distribution (single pass for OAS 2)

Product		Product Yield (% carbon basis)	
		(Case 1) methane feed	(Case 2) methane feed
CH_4	Methane		-
C_2H_6	Ethane	6.2	3.1
C_2H_4	Ethylene	0.5	0.9
C_3H_6	Propylene	0.02	0.9
C_6H_6	**Benzene**	**5.2**	**3.9**
C_7H_8	**Toluene**	**3.1**	**3.9**
C_8H_{10}	**Xylene**	**3.4**	**6.6**
C_9H_{12}	**Isopropyl Benzene**	**-**	**-**
$C_{10}H_{18}$	**Naphthalene**	**2.5**	**5.1**
$C_{11}H_{10}$	**Methyl Naphthalene**	**1.1**	**3.8**
$C_{12}H_{12}$	**Dimethyl Naphthalene**	**-**	**-**
C	Coke	-	-
CO	Carbon Monoxide	0.4	4.1
CO_2	Carbon Dioxide	6.4	30.1
Observed Conversion		**28.82**	**62.4**
Methane-to-Aromatics Yield		**15.3**	**23.3**

Table 40. AspenPlus™ assumptions used in the simulation

Stream Class	MIXCLSD
Databank	PURE, AQUEOUS, SOLIDS, INORGANIC
Solid Components	MnO, C(s), Mn_2O_3
Property Method	RK-SOAVE and STEAM-TA for steam cycles

OAS Reactors	RStoic block, with defined product yields
Compressors	COMPR block
Heat Exchangers	Heater and MHEATX blocks
Distillations Columns	DSTWU (shortcut distillation block)
Separators/Flash Columns	SEP and FLASH2 blocks
CO_2 Separator (PSA) + Membrane separation of CH_4/H_2 mixture	SEP block, with defined recovery

Table 41. RStoic reactions used for the OAS section (shown for Case 1 and 2 along with C2 consumption path)

Step	Reaction	Yield per pass (C basis, except SHC)			
		OAS Case 1		OAS Case 2	
OAS 1 (from C_2)	$C_2H_4 + H_2 \rightarrow 2CH_4$	12% of C_2H_4	37% of total C2 to aromatics	12% of C_2H_4	37% of total C2 to aromatics
	$3C_2H_4 \rightarrow 2C_3H_6$	1% of C_2H_4		1% of C_2H_4	
	$3C_2H_4 \rightarrow C_6H_6 + 3H_2$	**16.9% of C_2H_4**		**16.9% of C_2H_4**	
	$3.5C_2H_4 \rightarrow C_7H_8 + 3H_2$	**4% of C_2H_4**		**4% of C_2H_4**	
	$4C_2H_4 \rightarrow C_8H_{10} + 3H_2$	**0% of C_2H_4**		**0% of C_2H_4**	
	$9C_2H_4 \rightarrow 2C_9H_{12} + 6H_2$	**1% of C_2H_4**		**1% of C_2H_4**	
	$5C_2H_4 \rightarrow C_{10}H_8 + 6H_2$	**7% of C_2H_4**		**7% of C_2H_4**	
	$6C_2H_4 \rightarrow C_{12}H_{12} + 6H_2$	**9% of C_2H_4**		**9% of C_2H_4**	
	$C_2H_4 + 8MnO_2 \rightarrow 2CO_2 + 4Mn_2O_3 + 2H_2O$	2% of C_2H_4		2% of C_2H_4	
	$C_2H_4 \rightarrow 2C_{(s)} + 2H_2$	5% of C_2H_4		5% of C_2H_4	
	$C_2H_6 \rightarrow C_2H_4 + H_2$	4.9% of C_2H_6		4.9% of C_2H_6	
	$C_2H_6 + H_2 \rightarrow 2CH_4$	12% of C_2H_6		12% of C_2H_6	
	$3C_2H_6 \rightarrow 2C_3H_6 + 3H_2$	0.6% of C_2H_6		0.6% of C_2H_6	
	$3C_2H_6 \rightarrow C_6H_6 + 6H_2$	**15.4% of C_2H_6**		**15.4% of C_2H_6**	
	$7C_2H_6 \rightarrow 2C_7H_8 + 13H_2$	**4.1% of C_2H_6**		**4.1% of C_2H_6**	
	$4C_2H_6 \rightarrow C_8H_{10} + 7H_2$	**0.2% of C_2H_6**		**0.2% of C_2H_6**	
	$9C_2H_6 \rightarrow 2C_9H_{12} + 15H_2$	**1.1% of C_2H_6**		**1.1% of C_2H_6**	
	$5C_2H_6 \rightarrow C_{10}H_8 + 11H_2$	**6.4% of C_2H_6**		**6.4% of C_2H_6**	
	$6C_2H_6 \rightarrow C_{12}H_{12} + 12H_2$	**9% of C_2H_6**		**9% of C_2H_6**	
	$C_2H_6 + 10MnO_2 \rightarrow 2CO_2 + 5Mn_2O_3 + 3H_2O$	2% of C_2H_6		2% of C_2H_6	
	$C_2H_6 \rightarrow 2C_{(s)} + 3H_2$	4.9% of C_2H_6		4.9% of C_2H_6	

OAS 2	$2CH_4 \rightarrow C_2H_6 + H_2$	6.2% of CH_4	15.3% to aromatics	3.1% of CH_4	23.2% to aromatics
	$2CH_4 \rightarrow C_2H_4 + 2H_2$	0.5% of CH_4		0.9% of CH_4	
	$3CH_4 \rightarrow C_3H_6 + 3H_2$	0.022% of CH_4		0.9% of CH_4	
	$6CH_4 \rightarrow C_6H_6 + H_2$	**5.2% of CH_4**		**3.9% of CH_4**	
	$7CH_4 \rightarrow C_7H_8 + 10H_2$	**3.1% of CH_4**		**3.9% of CH_4**	
	$8CH_4 \rightarrow C_8H_{10} + 11H_2$	**3.4% of CH_4**		**6.6% of CH_4**	
	$10CH_4 \rightarrow C_{10}H_8 + 16H_2$	**2.5% of CH_4**		**5.1% of CH_4**	
	$11CH_4 \rightarrow C_{11}H_{10} + 17H_2$	**1.1% of CH_4**		**3.8% of CH_4**	
	$CH_4 + 4MnO_2 \rightarrow CO_2 + 2Mn_2O_3 + 2H_2$	6.4% of CH_4		30.1% of CH_4	
	$CH_4 + 2MnO_2 \rightarrow CO + Mn_2O_3 + 2H_2$	0.4% of CH_4		4.1% of CH_4	
SHC	$H_2 + Mn_2O_3 \rightarrow H_2O + 2MnO_2$	43% of H_2		70% of H_2	

Separation Section: This section primarily involves the separation of the heavy aromatics from water and other light hydrocarbons, CO_x and H_2. As shown in Figure 119 (Case 1), this includes sequential compression + flash units to separate the valuable aromatics, listed in Table 39, from the rest. Initially, the product gas from the OAS section is cooled and the heat is utilized to generate saturated steam (320°C, 120 bar). The recycle stream contains the inert CO, CO_2 and H_2, along with CH_4 and other light alkanes, which need to be separated before recycling. CO_2 + CO can be first separated using a CO_2 pressure swing adsorption (PSA) unit, since the mixture is at 20 bar. H_2 is then separated from a predominant H_2 + CH_4 mixture using a commercial membrane system. The recycle stream then contains unreacted methane, which helps increase the overall C-to-C conversion in the process.

Aromatics Purification Section: This section involves sequential separation of benzene, other aromatics, and propylene, with a small amount of remnant CO_2. The first distillation column separates heavy aromatics (toluene, xylene, naphthalenes) from benzene + propylene. Benzene is then purified to 99 wt.% in a following distillation column. **The overall methane-to-aromatic yield is 72% (Case 1) (Table 41).**

Table 42 summarizes the process energy balances for the Base Case, and OAS Case 1 and 2. In the **Base Case**, which is based upon the non-oxidative methane DHA process described by Huang *et al*. [17], a net energy input of **1659.2 MW** is required to produce aromatics at a rate of 18.8 kg/s, which equates to an energy demand of **88.3 MJ/kg** aromatics. This calculation assumes that all H_2

produced during the process is directly used as a fuel gas to meet process heat requirements, which is not assumed in the reference. Overall, the OAS Case 1 and 2 require a specific energy demand of 31.5 and 44.7 MJ/kg aromatics, equating to an energy reduction of roughly 64% and 50% respectively, over the base case.

Table 42: Simplified mass balance across each reactor and across the entire process

OAS Case 1 Component	**Fresh methane** (kmol C/hr.)	**Reactant to OAS** (kmol C/hr.)	**OAS 1 Output** (kmol C/hr.)	**OAS 2 Output** (kmol C/hr.)
CH_4	**435**	**1560**	**1580.7**	**1125**
C2	**-**	**189**	**84.0**	**190**
C3-C5	-	-	1.2	1.2
COx	-	-	13.1	121
Aromatics	**-**	**-**	**70**	**312**
TOTAL	**435**	**1749**	**1749**	**1749**
		C2 to aromatics = 37% yield		
			C1 to aromatics = 15.3% yield	
	Overall fresh C1 to aromatics yield = 72%			

OAS Case 2 Component	**Fresh methane** (kmol C/hr.)	**Reactant to OAS** (kmol C/hr.)	**OAS 1 Output** (kmol C/hr.)	**OAS 2 Output** (kmol C/hr.)
CH_4	**435**	**700**	**705.7**	**265.0**
C2	**-**	**50**	**21.8**	**50.0**
C3-C5	-	-	0.5	6.0
COx	-	-	3.5	246
Aromatics	**-**	**-**	**18.5**	**183**
TOTAL	**435**	**750**	**750**	**750**
		C2 to aromatics = 37% yield		
			C1 to aromatics = 23.2% yield	
	Overall fresh C1 to aromatics yield = 42%			

Table 43: Simplified energy balance across the overall process – comparing Case 1 and 2 with the base case

Values in MW (unless otherwise noted)	**Base Case**	**OAS Case 1**	**OAS Case 2**
Aromatics Production Rate (kg/s)	18.8	1.13	0.68
INLET: Natural Gas (Feed Stream) (A)	**1400.0**	**93.1**	**93.1**

OUTLET Total (B)	**1528**	**72.5**	**43.3**
Benzene	334.5	16.4	5.7
Other aromatics	471.9	29.4	21.9
C2+	14.4	0.2	1.3
Fuel Gas	707.2	26.5	14.4
Net Heat Required	**679.1**	**22.6**	**11.0**
Exotherm from SHC (C1)	**-**	**-24.2**	**-46.3**
Compression	353.8	9.4	10.4
Generation (HRSG, Regen, etc.)	-91.6	-8.8	-6.9
Net Work Required	**262.2**	**0.6**	**3.44**
Totals			
NG for Heat (60% eff.) (C2)	**1131.8**	**37.7**	**18.3**
NG for Electricity (40% eff.) (D)	**655.5**	**1.5**	**8.6**
Net Energy Demand (A – B + C1 + C2 + D)	**1659.2**	**35.6**	**30.4**
Specific Net Energy Demand (MJ/kg aromatics)	**88.3**	**31.5**	**44.7**
% Reduction in Energy Demand	**--**	**64.3**	**49.4**

60% efficiency penalty applied to *in situ* heat generation from selective H_2 combustion reaction.
40% efficiency penalty applied to electricity from heat recovery steam generator / steam heated by regeneration.
"Net Energy Demand (Energy Lost)" is defined as all input energy (Natural Gas Feed and Natural Gas for Fuel) minus that energy which exits the system as valuable products (Benzene, Toluene, Naphthalene, and C2+; the latter is primarily ethylene, ethane, and propylene). Losses go to process heat/work requirements and undesired products.

Net CO_2 Emissions

The net CO_2 emissions for OAS Case 1 and 2 are roughly 1.6-1.7 kg CO_2/kg aromatics, which shows >40% reduction compared to the existing reported values (2-3 kg CO_2/kg aromatics) for methane DHA processes. Conventional aromatic production leads to 4-5 kg CO_2/kg aromatics.

Table 44. Net CO_2 emissions for OAS Case 1 and 2

Component	**Case 1**	**Case 2**	**Comments/Assumptions**
	CO_2 flow (kg/s)		
Reaction by-product	1.23	2.58	from the product distribution
Heat source	2.16	1.05	natural gas combusted for energy/heat
Power demand	0.02	0.1	renewable electricity:100 kg CO_2/MWh
Credit	-1.51	-2.65	avoidance of natural gas combustion with exotherm
Net CO_2 Emissions	**1.9**	**1.08**	
Normalized Emissions	**1.7 kg/kg**	**1.6 kg/kg**	**aromatic product flow** **Case 1: 1.13 kg/s and Case 2: 0.68 kg/s**

Techno-Economic Analysis (TEA)

Assumptions

Since the OAS Case 1 has shown significant energy savings and higher aromatic yields per kg of methane feed, compared to the base case and Case 2, the TEA is performed for Case 1. For this TEA, Susteon implements the levels of capital costs outlined by the U.S. Department of Energy (DOE) in the document "QGESS Cost Estimation Methodology for NETL Assessments of Power Plant Performance" (September 2019) [18]. The four categories are detailed below.

Bare Erected Costs (BEC) = Process Equipment Cost (PEC) + On-site facilities and infrastructure to support the plant, as well as direct and indirect labor expenses for construction.

Engineering, Procurement, and Construction Cost (EPCC) = BEC + [Costs of engineering services which includes detailed design, contractor permitting, and project/construction management costs.]

Total Plant Cost (TPC) = EPCC + [Process and Project Contingencies.]

Total Overnight Cost (TOC) = TPC + [Pre-production costs, inventory capital, financing costs and other owner costs, management reserve is excluded.]

- Following the calculation of all upfront capital costs, an annual capital charge is determined by multiplying the individual capital costs by the discount rate. This annual capital charge can then be added to the annual operating costs (fixed, direct, and utilities) to determine the average annual costs for operation of the facility and repayment of loan/equity for capital expenditures.
- To generate a BEC for the novel reactor system from the PEC, an installation factor of 3.47, per the NTNU report [Ref], was multiplied to the total scaled purchased equipment cost.
- An additional 15% was added to the BEC for engineering services, construction supervision to generate the EPCC.
- Per DOE guidelines [1], 50% process contingency was added to the BEC of the novel reactor as it is a "new concept with limited data." All other process equipment is proven and commercial, so only a 10% process contingency was added for other units.
- A 15% project contingency was selected from the recommended range of 15%-30% per the DOE due to the current uncertainty level, then added to the TPC.
- Owners' cost was added to the TPC: additional 22%.

- 1 acre of land is assumed to be required, at a cost of $36,000/acre.
- Plant operational life is 20 years, with a capital recovery factor of 12.4%/year.
- Plant on-stream capacity is 90%.
- The cost of electricity is $0.06/kWh, cost of natural gas is $3/MMBTU, cost of catalyst is assumed to be $30/kg, annual O&M cost is 5% of BEC, catalyst replacement is 3 changes in 20 years, cost of steam (exported) is $10/ton.

Table 45. Cost of the various equipment, based on AspenPlus™ Economics package, Perry's Handbook [19], vendor quotes, communication with the industry, scaling factors, and Ulrich's Chemical Engineering Process Design and Economics Textbook[20].

Block ID (Figure 119)	Unit Category	Case 1	Description
		PEC	
OAS Reactors	Packed Bed Reactor (3)	$7,920,000	described in #1 below
B2	CO_2 separator	$ 1,083,000	described in #2 below
HEX-1	Feed Heater	$ 620,000	described in #3 below
B3	Recycle heater	$ 103,000	from AspenPlus™ Economics
B-3	Product Cooler	$ 87,800	from AspenPlus™ Economics
B-6	Compressor	$ 2,715,000	assuming $750/hp of power
B-8	Compressor	$ 1,709,100	assuming $750/hp of power
B-1	Product Heat Exchanger	$ 500,000	from AspenPlus™ Economics
DST	Distillation Column	$ 33,400	from AspenPlus™ Economics
B-7	Compressor	$ 1,206,000	assuming $750/hp of power
KO4	Knock-out Flash Column	$ 22,300	from AspenPlus™ Economics
KO2	Knock-out Flash Column	$ 20,600	from AspenPlus™ Economics
KO1	Knock-out Flash Column	$ 25,700	from AspenPlus™ Economics
B-10	Flash Column	$ 26,600	from AspenPlus™ Economics
MHX2	Air Preheater	$ 362,000	described in #3 below
B-5	Compressor	$ 1,300,000	assuming $750/hp of power
B-2	Water pump	$ 120,000	from AspenPlus™ Economics
KO3	Knock-out Flash Column	$ 19,500	from AspenPlus™ Economics
B-4	Flash Column	$ 31,700	from AspenPlus™ Economics
B-9	Cooler	$ 56,800	described in #3 below
B-12	Distillation Column	$ 133,300	from AspenPlus™ Economics
B-13	Heater	$ 56,800	described in #3 below
TOTAL PEC		**$18,152,600**	

[1] OAS Reactor Cost Estimation

- This assumes a packed reactor configuration, with gas cycling, to operate both in reducing and regeneration mode.
- Three reactors have been assumed: one will carry out the DHA + SHC step, one will be in regeneration mode with air feed, and one as an auxiliary back-up reactor, in case of maintenance requirements.
- With recycling, this assumes a methane flow of 1730 kmol/hr. to the reactor, at 1 bar, and 700°C.
- The steam methane reforming (SMR) and Fischer Tropsch (FT) reactors have been assumed as a reference. Typical weight hourly space velocities (WHSV) for SMR//FT are in the range of 0.5 - 3 hr^{-1} (kg/hr. of feed flow rate per kg of catalyst). A value of 1 hr^{-1} has been assumed.
- With 27,680 kg/hr. mass flowrate, the amount of catalyst required is roughly 28 tons.
- Cost of the reactor ($) = A ($) x (Reactor Volume) ^{n}
    - A conservative reference cost (A) of a 10 m^3 packed bed reactor is $750,000.
    - Scaling factor, n, is assumed to be 0.7.
    - Gas Hourly Space Velocity (GHSV) is assumed to be 2,000 hr^{-1} for calculation purposes.
    - Volumetric feed flowrate is 70,000 m^3/hr., leading to a reactor volume of 35 m^3. Assuming a 20% open volume in the reactor, a catalyst occupies 29 m^3.
    - Estimated catalyst density is 28 tons/29 m^3 = 0.97 g/mL.
- **The cost of the reactor is $750,000 x $(35/10)^{0.7}$ = $1,800,000**
- The cost of the initial loading of the catalyst = $840,000. Operating/replacement cost of the catalyst is $126,000/year.

[2] CO_2 Separation using a Pressure Swing Adsorption (PSA) System

This involves considering various factors such as feed flow rate, feed composition, separation efficiency, and feed pressure.

- Feed flowrate: 28,000 kg/hr., CO_2 in feed: 20% by mass, methane flowrate: 5,600 kg/hr.
- Separation efficiency: 90%, feed pressure: 20 bar.
- A reference cost (A, $) of $1,000,000 for a CO_2 PSA system handling 5 ton/hr. CO_2.
- The scaling factor n is 0.7.
- **The estimated cost of the CO_2 PSA = $1,083,000.**

[3] Estimating the Heater Cost

- The heater to heat 4150 kg/hr. of a liquid mixture of benzene, toluene, and xylene from 15°C to 100°C has a duty of 120 kW.
- A 1000 kW heater (or heat exchanger) is assumed to cost $100,000.
- Cost of the heater ($) = A ($) x $(Q/Q_o)^n$
    - Qo is the reference heat duty (kW). Assuming, the reference heater, with 100 kW duty costs $50,000. Scaling factor, n, is assumed to be 0.7.
- **The cost of the required heater = 50,000 x $(72/100)^{0.7}$ = $56,800.**

The total overnight cost (TOC) for 317 bbl./day benzene production, from methane, is $104 million (MM). The BEC is **$60MM**, the EPCC is **$9MM**, process and project contingencies are **$5MM** and **$11MM** respectively, while the owners' and land costs are **$19MM**. The distribution of the annual costs is shown in Table 46 below.

Table 46. Estimated annual ($/year) and normalized cost ($/gal.) of aromatic liquid production from methane. This assumes a total of 885 bbl./day production of aromatics – 36% benzene, 64% rest. All the aromatics are assumed to be of the same economic value as benzene.

Cost Component	Annual Cost	Normalized Cost	Comments
Capital Cost	$12.89 MM	$1.06/gal.	recovery factor of 12.4% on TOC
Feedstock (methane)	$7.68 MM	$0.63/gal.	7 ton/hr., $3/MMBTU
Power	$2.18 MM	$0.18/gal.	6.9MW, $0.04/kWh
Steam (exported)	- $2.29 MM	-$0.19/gal.	29 ton/hr., $10/ton
O&M	$3.00 MM	$0.25/gal.	5% of the BEC
TOTAL	**$23.47 MM**	**$1.92/gal.**	**Market price is $2.9-3.3/gal. [Figure 120]**

Table 46 below, shows the return on investment (ROI) achievable with the above market price of benzene, which is projected to slightly rise in the coming years.

$$\text{ROI}\ (\%) = \frac{(\text{Selling price}, \$/\text{gal.}) - (\text{Production cost}, \$/\text{gal.})}{(\text{Production cost}, \$/\text{gal.})} \text{ x } 100$$

Table 47 ROI achievable with reduced production cost and higher market selling price of the aromatics

	Selling Price → / Production Cost ↓	$2.5/gal.	$2.9/gal.	$3.1/gal.	$3.3/gal.	$3.5/gal.
Described above	$1.92/gal.	30.2%	51.0%	61.5%	71.9%	82.3%
25% reduction in reactor cost	$1.77/gal.	41.2%	63.8%	75.1%	86.4%	97.7%
Process contingency lowered to 10%	$1.55/gal.	61.3%	87.1%	100.0%	112.9%	125.8%

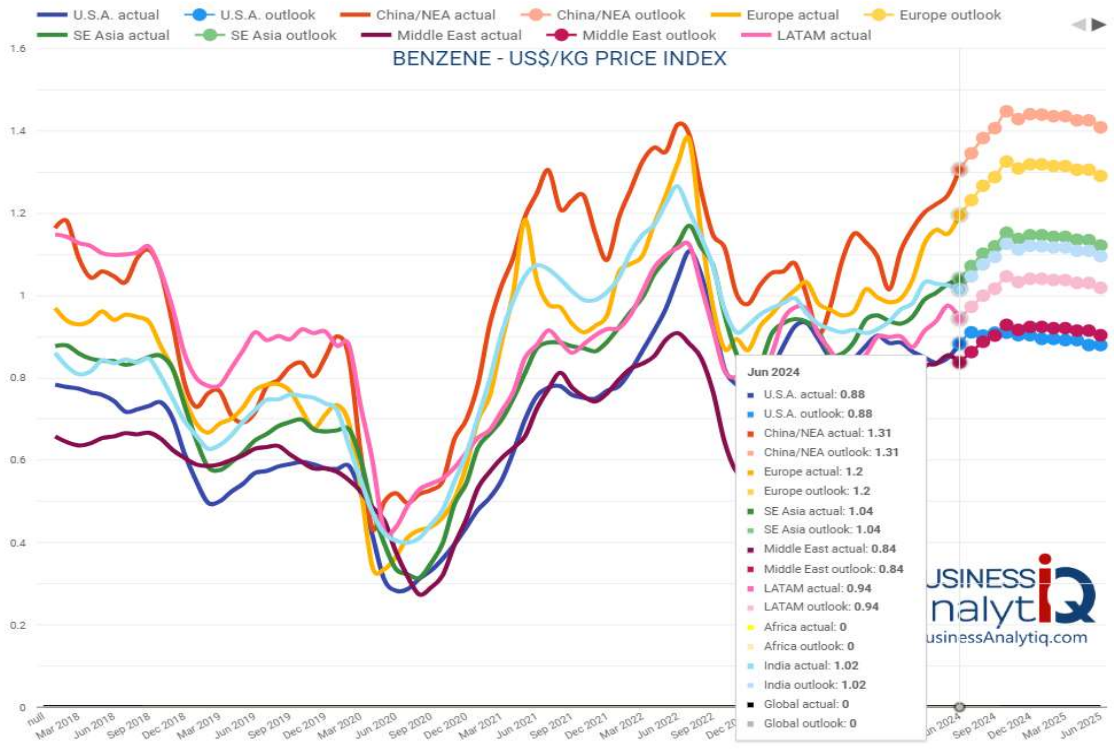

Figure 120. Benzene prices – past, present, and projections – in $/kg[21]. Assuming a density of 876 kg/m3 at ambient conditions, a price range of $0.88-1/kg is equivalent to $2.9 – 3.3/gal.

Key Takeaways

[1] Both Cases 1 and 2 showed much higher single pass aromatic yields than state of the art DHA systems (~8%). While Case 2 single pass yield (23.3%) was much higher than that from Case 1 (15.3%), the lower product selectivity negatively affected its overall energy savings and economic attractiveness. Despite that, Case 2 still showed advantage compared to state-of-the-art DHA technology. The TEA results highlight the importance of a balance between high single pass yield and high product selectivity;

[2] The estimated total overnight capital cost of the **OAS (Case 1) system is $104 million**, for a combined production of **885 bbl./day (OR 1.13 kg/s) of aromatic liquids**.

[3] This shows a **capital intensity of $117,500/bbl./day of aromatic liquids**. The production of liquid fuels like gasoline, diesel and/or jet fuel from crude oil, costs in the range of $100,000-$120,000/bbl./day.

[4] The estimated **cost of aromatic liquid production is $1.92/gal**. Assuming a benzene density of 876 kg/m^3 in ambient conditions, the current market price range for benzene is $0.88-1/kg, which is equivalent to $2.9 – 3.3/gal. **This shows the potential of the OAS to produce aromatics at >67% of the current market price.**

[5] The analysis shows the ability of OAS (Case 1) to produce aromatics from methane with a return of investment of >25% even with conservative assumptions at an early stage of the technology.

Technology Commercialization Roadmap

To develop a commercialization roadmap for this OAS Case 1 process with a 72% overall aromatic yield, an aromatic production cost of $1.92/gal, and a return on investment (ROI) of over 25%, we need to follow a structured approach. This roadmap (outlined in Table 48 with details in Figure 121) will cover the stages from early-stage technology development to market entry and scale-up.

Table 48. Technology roadmap with broad categories of development

Technology Development and Validation	▪ Proof of Concept ▪ Bench-Unit + Pilot Unit Design and Testing
Feasibility and Market Analysis	▪ Detailed Techno-Economic Analysis (TEA) ▪ Market Analysis and Competitive Benchmarking
Demonstration and Scale-Up	▪ Demonstration Plant Construction ▪ Regulatory Approvals and Safety Compliance
Commercialization and Market Entry	▪ Full-Scale Plant Design and Financing ▪ Commercial Plant Construction and Commissioning
Post-Commercialization and Expansion	▪ Continuous Improvement and Cost Optimization ▪ Diversification and New Applications

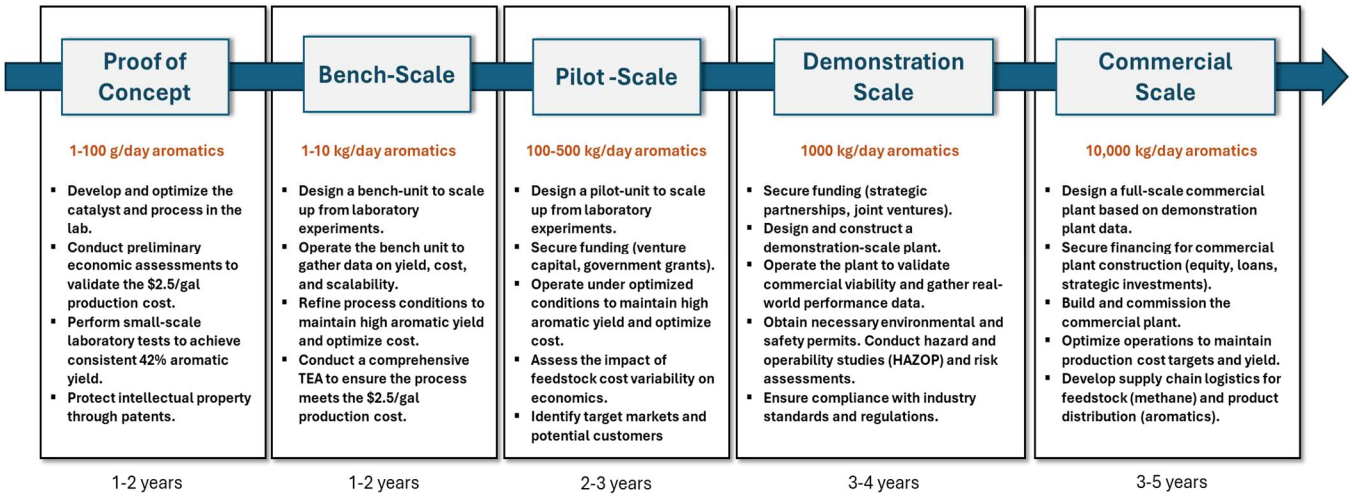

Figure 121: Commercialization roadmap

Appendix (AspenPlus™ flowsheets and stream information)

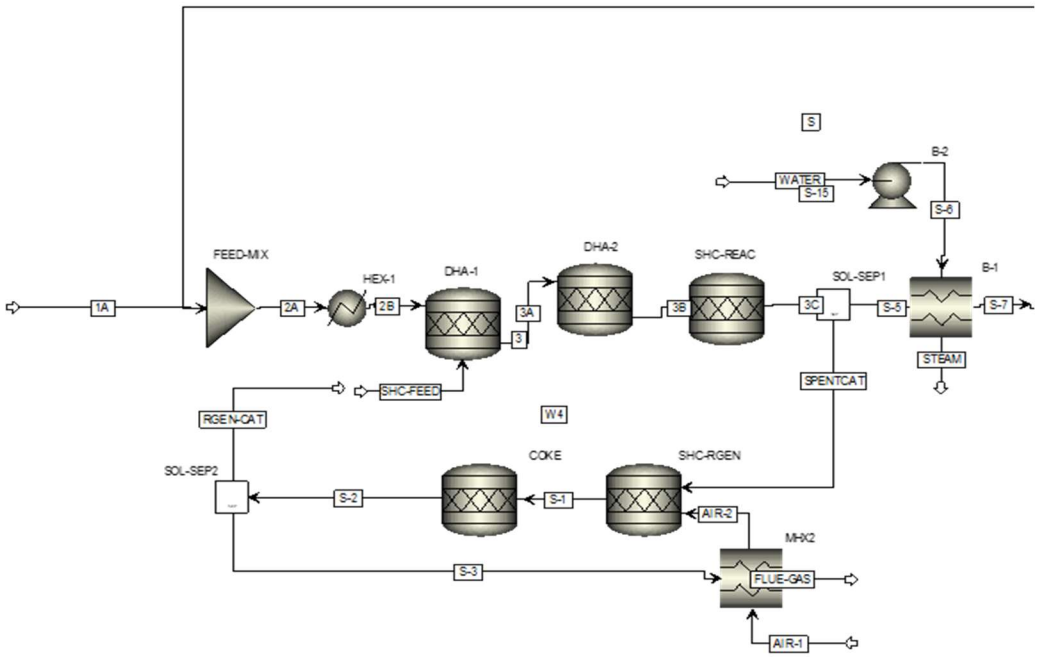

Figure 122. Upstream OAS reactor sections of the process model (885 bbl./day of liquid aromatics)

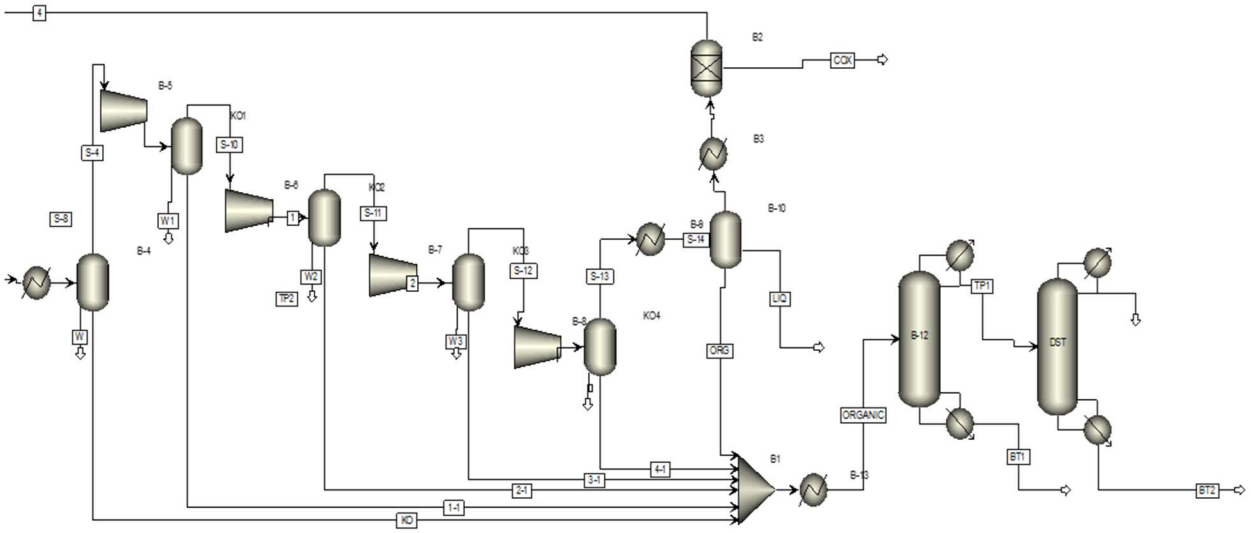

Figure 123. Separation and purification section of the process model (885 bbl./day of liquid aromatics)

Table 49. Key information of the streams (refer to Figure 119, Figure 122 and 123)

	Units	AIR-1	AIR-2	BT1	BT2	COX	FLUE-GAS	KO	LIQ	ORG	ORGANIC	RGEN-CAT	S
Temperature	C	25.0	514.2	**258.5**	**175.4**	30.0	120.0	25.0	-15.0	-15.0	75.0	700.0	30.0
Pressure	bar	1	1	**10**	**10**	20	1	1	20	20	10	1	20
Molar Vapor Fraction		1.0	1.0	**0.0**	**0.0**	1.0	1.0	0.0	0.0	0.0	0.0	0.0	1.0
Mass Density	kg/cum	1.2	0.4	**693.2**	**698.2**	8.8	0.9	961.5	998.6	879.7	806.1	2897.9	12.6
Average MW		28.9	28.9	**111.8**	**76.3**	11.2	28.1	118.8	18.0	71.4	92.9	86.9	15.6
Mole Flows	**kmol/hr**	**1534**	**1534**	**23**	**19**	**492**	**1275**	**13**	**0**	**2**	**45**	**1200**	**1787**
Mole Fractions													
CH4		0.00	0.00	**0.00**	**0.00**	0.00	0.00	0.00	0.00	0.04	0.01	0.00	0.63
H2		0.00	0.00	**0.00**	**0.00**	0.77	0.00	0.00	0.00	0.00	0.00	0.00	0.24
CO		0.00	0.00	**0.00**	**0.00**	0.02	0.00	0.00	0.00	0.00	0.00	0.00	0.01
CO2		0.00	0.00	**0.00**	**0.00**	0.21	0.00	0.00	0.00	0.03	0.01	0.00	0.06
C(s)		0.00	0.00	**0.00**	**0.00**	0.00	0.01	0.00	0.00	0.00	0.00	0.00	0.00
H2O		0.00	0.00	**0.00**	**0.03**	0.00	0.00	0.01	1.00	0.01	0.01	0.00	0.00
C2H6		0.00	0.00	**0.00**	**0.00**	0.00	0.00	0.00	0.00	0.03	0.01	0.00	0.05
C2H4		0.00	0.00	**0.00**	**0.00**	0.00	0.00	0.00	0.00	0.00	0.00	0.00	0.01
C3H6		0.00	0.00	**0.00**	**0.00**	0.00	0.00	0.00	0.00	0.04	0.01	0.00	0.01
C6H6		0.00	0.00	**0.00**	**0.97**	0.00	0.00	0.08	0.00	0.81	0.42	0.00	0.00
C7H8		0.00	0.00	**0.35**	**0.00**	0.00	0.00	0.10	0.00	0.04	0.18	0.00	0.00
C10H18		0.00	0.00	**0.22**	**0.00**	0.00	0.00	0.37	0.00	0.00	0.12	0.00	0.00
N2		0.79	0.79	**0.00**	**0.00**	0.00	0.95	0.00	0.00	0.00	0.00	0.00	0.00
O2		0.21	0.21	**0.00**	**0.00**	0.00	0.04	0.00	0.00	0.00	0.00	0.00	0.00
MnO2 (s)		0.00	0.00	**0.00**	**0.00**	0.00	0.00	0.00	0.00	0.00	0.00	1.00	0.00
Mn2O3 (s)		0.00	0.00	**0.00**	**0.00**	0.00	0.00	0.00	0.00	0.00	0.00	0.00	0.00
C9H12		0.00	0.00	**0.01**	**0.00**	0.00	0.00	0.01	0.00	0.00	0.01	0.00	0.00
C8H10		0.00	0.00	**0.29**	**0.00**	0.00	0.00	0.19	0.00	0.00	0.15	0.00	0.00
C12H12		0.00	0.00	**0.06**	**0.00**	0.00	0.00	0.11	0.00	0.00	0.03	0.00	0.00
C11H12		0.00	0.00	**0.07**	**0.00**	0.00	0.00	0.12	0.00	0.00	0.04	0.00	0.00

	Units	1	1.1	1A	2	2.1	2A	2B	3	3.1	3A	3B	3C	4	4.1
Temperature	C	149.0	10.0	25.0	97.7	7.0	18.8	700.0	72.9	5.0	700.0	700.0	700.0	30.0	3.0
Pressure	bar	8	2	31	20	8	2	2	40	20	1	1	1	20	40
Molar Vapor Fraction		1.0	0.0	1.0	1.0	0.0	1.0	1.0	1.0	0.0	0.6	0.7	0.8	1.0	0.0
Mass Density	kg/cum	3.7	879.5	21.1	10.4	874.2	1.4	0.4	22.2	866.3	0.9	0.8	0.8	14.3	847.2
Average MW		16.4	92.7	16.0	15.9	81.4	17.0	17.0	15.7	74.8	44.8	42.5	47.3	17.3	69.2
Mole Flows	**kmol/hr**	1813	8	435	1796	14	1730	1730	1791	5	2988	3146	2827	1295	2
Mole Fractions															
CH4		0.62	0.00	1.00	0.63	0.01	0.90	0.90	0.63	0.04	0.53	0.36	0.40	0.87	0.07
H2		0.23	0.00	0.00	0.24	0.00	0.02	0.02	0.24	0.00	0.04	0.24	0.15	0.03	0.00
CO		0.01	0.00	0.00	0.01	0.00	0.00	0.00	0.01	0.00	0.00	0.00	0.00	0.00	0.00
CO2		0.06	0.00	0.00	0.06	0.01	0.01	0.01	0.06	0.02	0.00	0.04	0.04	0.01	0.04
C(s)		0.00	0.00	0.00	0.00	0.00	0.00	0.00	0.00	0.00	0.00	0.00	0.00	0.00	0.00
H2O		0.00	0.01	0.00	0.00	0.01	0.00	0.00	0.00	0.01	0.00	0.00	0.11	0.00	0.01
C2H6		0.04	0.00	0.00	0.05	0.01	0.05	0.05	0.05	0.02	0.01	0.03	0.03	0.06	0.04
C2H4		0.01	0.00	0.00	0.01	0.00	0.01	0.01	0.01	0.00	0.00	0.00	0.00	0.01	0.00
C3H6		0.01	0.00	0.00	0.01	0.01	0.01	0.01	0.01	0.02	0.01	0.01	0.01	0.01	0.04
C6H6		0.01	0.29	0.00	0.00	0.60	0.00	0.00	0.00	0.74	0.00	0.01	0.01	0.00	0.73
C7H8		0.00	0.30	0.00	0.00	0.25	0.00	0.00	0.00	0.13	0.00	0.00	0.00	0.00	0.07
C10H18		0.00	0.03	0.00	0.00	0.00	0.00	0.00	0.00	0.00	0.00	0.00	0.00	0.00	0.00
N2		0.00	0.00	0.00	0.00	0.00	0.00	0.00	0.00	0.00	0.00	0.00	0.00	0.00	0.00
O2		0.00	0.00	0.00	0.00	0.00	0.00	0.00	0.00	0.00	0.00	0.00	0.00	0.00	0.00
MnO2 (s)		0.00	0.00	0.00	0.00	0.00	0.00	0.00	0.00	0.00	0.40	0.24	0.04	0.00	0.00
Mn2O3 (s)		0.00	0.00	0.00	0.00	0.00	0.00	0.00	0.00	0.00	0.00	0.07	0.19	0.00	0.00
C9H12		0.00	0.01	0.00	0.00	0.00	0.00	0.00	0.00	0.00	0.00	0.00	0.00	0.00	0.00
C8H10		0.00	0.34	0.00	0.00	0.09	0.00	0.00	0.00	0.02	0.00	0.00	0.00	0.00	0.00
C12H12		0.00	0.00	0.00	0.00	0.00	0.00	0.00	0.00	0.00	0.00	0.00	0.00	0.00	0.00
C11H12		0.00	0.00	0.00	0.00	0.00	0.00	0.00	0.00	0.00	0.00	0.00	0.00	0.00	0.00

	Units	S-1	S-2	S-3	S-4	S-5	S-6	S-7	S-8	S-9	S-10	S-11	S-12	S-13	S-14
Temperature	C	700.0	700.0	700.0	25.0	700.0	26.8	48.5	25.0	93.5	10.0	7.0	5.0	3.0	-50.0
Pressure	bar	1	1	1	1	1	120	1	1	2	2	8	20	40	60
Molar Vapor Fraction		0.5	0.5	1.0	1.0	1.0	0.0	0.9	0.8	1.0	1.0	1.0	1.0	1.0	1.0
Mass Density	kg/cum	1.4	1.4	0.3	0.7	0.2	992.2	0.7	0.8	1.1	1.4	5.5	14.0	28.9	63.1
Average MW		56.6	56.6	28.1	16.8	17.6	18.0	17.6	17.6	16.8	16.4	15.9	15.7	15.7	15.7
Mole Flows	**kmol/hr**	**2475**	**2475**	**1275**	**1830**	**2155**	**1601**	**2155**	**2155**	**1830**	**1813**	**1796**	**1791**	**1789**	**1789**
Mole Fractions															
CH4		0.00	0.00	0.00	0.61	0.52	0.00	0.52	0.52	0.61	0.62	0.63	0.63	0.63	0.63
H2		0.00	0.00	0.00	0.23	0.20	0.00	0.20	0.20	0.23	0.23	0.24	0.24	0.24	0.24
CO		0.00	0.00	0.00	0.01	0.01	0.00	0.01	0.01	0.01	0.01	0.01	0.01	0.01	0.01
CO2		0.00	0.00	0.00	0.06	0.05	0.00	0.05	0.05	0.06	0.06	0.06	0.06	0.06	0.06
C(s)		0.00	0.00	0.01	0.00	0.00	0.00	0.00	0.00	0.00	0.00	0.00	0.00	0.00	0.00
H2O		0.00	0.00	0.00	0.01	0.15	1.00	0.15	0.15	0.01	0.00	0.00	0.00	0.00	0.00
C2H6		0.00	0.00	0.00	0.04	0.04	0.00	0.04	0.04	0.04	0.04	0.05	0.05	0.05	0.05
C2H4		0.00	0.00	0.00	0.01	0.01	0.00	0.01	0.01	0.01	0.01	0.01	0.01	0.01	0.01
C3H6		0.00	0.00	0.00	0.01	0.01	0.00	0.01	0.01	0.01	0.01	0.01	0.01	0.01	0.01
C6H6		0.00	0.00	0.00	0.01	0.01	0.00	0.01	0.01	0.01	0.01	0.00	0.00	0.00	0.00
C7H8		0.00	0.00	0.00	0.00	0.00	0.00	0.00	0.00	0.00	0.00	0.00	0.00	0.00	0.00
C10H18		0.00	0.00	0.00	0.00	0.00	0.00	0.00	0.00	0.00	0.00	0.00	0.00	0.00	0.00
N2		0.49	0.49	0.95	0.00	0.00	0.00	0.00	0.00	0.00	0.00	0.00	0.00	0.00	0.00
O2		0.02	0.02	0.04	0.00	0.00	0.00	0.00	0.00	0.00	0.00	0.00	0.00	0.00	0.00
MnO2 (s)		0.48	0.48	0.00	0.00	0.00	0.00	0.00	0.00	0.00	0.00	0.00	0.00	0.00	0.00
Mn2O3 (s)		0.00	0.00	0.00	0.00	0.00	0.00	0.00	0.00	0.00	0.00	0.00	0.00	0.00	0.00
C9H12		0.00	0.00	0.00	0.00	0.00	0.00	0.00	0.00	0.00	0.00	0.00	0.00	0.00	0.00
C8H10		0.00	0.00	0.00	0.00	0.00	0.00	0.00	0.00	0.00	0.00	0.00	0.00	0.00	0.00
C12H12		0.00	0.00	0.00	0.00	0.00	0.00	0.00	0.00	0.00	0.00	0.00	0.00	0.00	0.00
C11H12		0.00	0.00	0.00	0.00	0.00	0.00	0.00	0.00	0.00	0.00	0.00	0.00	0.00	0.00

	Units	S-15	S-17	SHC-FEED	SPENTCAT	STEAM	TP1	TP2	W	WATER
Temperature	C	-15.0	13.2	700.0	700.0	324.6	153.0	-213.7	25.0	25.0
Pressure	bar	20	10	1	1	120	7	7	1	1
Molar Vapor Fraction		1.0	0.0	0.0	0.0	1.0	1.0	0.0	0.0	0.0
Mass Density	kg/cum	15.1	901.8	2897.9	4806.1	64.1	15.9	783.0	997.2	994.0
Average MW		15.6	92.9	86.9	142.5	18.0	72.1	30.3	18.0	18.0
Mole Flows	**kmol/hr**	**1787**	**45**	**1200**	**672**	**1601**	**21**	**2**	**312**	**1601**
Mole Fractions										
CH4		0.63	0.01	0.00	0.00	0.00	0.03	0.34	0.00	0.00
H2		0.24	0.00	0.00	0.00	0.00	0.00	0.01	0.00	0.00
CO		0.01	0.00	0.00	0.00	0.00	0.00	0.00	0.00	0.00
CO2		0.06	0.01	0.00	0.00	0.00	0.02	0.20	0.00	0.00
C(s)		0.00	0.00	0.00	0.01	0.00	0.00	0.00	0.00	0.00
H2O		0.00	0.01	0.00	0.00	1.00	0.03	0.00	1.00	1.00
C2H6		0.05	0.01	0.00	0.00	0.00	0.02	0.20	0.00	0.00
C2H4		0.01	0.00	0.00	0.00	0.00	0.00	0.02	0.00	0.00
C3H6		0.01	0.01	0.00	0.00	0.00	0.02	0.21	0.00	0.00
C6H6		0.00	0.42	0.00	0.00	0.00	0.88	0.00	0.00	0.00
C7H8		0.00	0.18	0.00	0.00	0.00	0.00	0.00	0.00	0.00
C10H18		0.00	0.12	0.00	0.00	0.00	0.00	0.00	0.00	0.00
N2		0.00	0.00	0.00	0.00	0.00	0.00	0.00	0.00	0.00
O2		0.00	0.00	0.00	0.00	0.00	0.00	0.00	0.00	0.00
MnO2 (s)		0.00	0.00	1.00	0.19	0.00	0.00	0.00	0.00	0.00
Mn2O3 (s)		0.00	0.00	0.00	0.80	0.00	0.00	0.00	0.00	0.00
C9H12		0.00	0.01	0.00	0.00	0.00	0.00	0.00	0.00	0.00
C8H10		0.00	0.15	0.00	0.00	0.00	0.00	0.00	0.00	0.00
C12H12		0.00	0.03	0.00	0.00	0.00	0.00	0.00	0.00	0.00
C11H12		0.00	0.04	0.00	0.00	0.00	0.00	0.00	0.00	0.00

	Units	1	1.1	1A	2	2.1	2A	2B	3	3.1	3A	3B	3C	4	4.1
Temperature	C	149.0	10.0	25.0	97.7	7.0	18.8	700.0	72.9	5.0	700.0	700.0	700.0	30.0	3.0
Pressure	bar	8	2	31	20	8	2	2	40	20	1	1	1	20	40
Molar Vapor Fraction		1.0	0.0	1.0	1.0	0.0	1.0	1.0	1.0	0.0	0.6	0.7	0.8	1.0	0.0
Mass Density	kg/cum	3.7	879.5	21.1	10.4	874.2	1.4	0.4	22.2	866.3	0.9	0.8	0.8	14.3	847.2
Average MW		16.4	92.7	16.0	15.9	81.4	17.0	17.0	15.7	74.8	44.8	42.5	47.3	17.3	69.2
Mass Flows	**kg/hr**	29778	754	6979	28562	1163	29402	29402	28185	369	133726	133726	133726	22423	138
CH4	kg/hr	18054	1	6979	18051	3	25023	25023	18048	3	25358	18055	18055	18045	2
H2	kg/hr	853	0	0	853	0	85	85	853	0	228	1496	853	85	0
CO	kg/hr	314	0	0	314	0	31	31	314	0	137	314	314	31	0
CO2	kg/hr	4943	1	0	4938	5	493	493	4934	4	493	4945	4945	493	3
C(s)	kg/hr	0	0	0	0	0	0	0	0	0	112	112	112	0	0
H2O	kg/hr	71	2	0	15	3	2	2	6	1	99	99	5848	2	0
C2H6	kg/hr	2451	1	0	2447	4	2440	2440	2444	3	978	2452	2452	2440	2
C2H4	kg/hr	376	0	0	376	0	375	375	375	0	265	376	376	375	0
C3H6	kg/hr	827	1	0	821	6	811	811	817	4	828	828	828	811	3
C6H6	kg/hr	1328	185	0	656	672	139	139	372	283	528	1598	1598	139	113
C7H8	kg/hr	403	222	0	81	323	2	2	21	60	103	748	748	2	13
C10H18	kg/hr	0	31	0	0	0	0	0	0	0	159	666	666	0	0
N2	kg/hr	0	0	0	0	0	0	0	0	0	0	0	0	0	0
O2	kg/hr	0	0	0	0	0	0	0	0	0	0	0	0	0	0
MnO2 (s)	kg/hr	0	0	0	0	0	0	0	0	0	102727	66449	10970	0	0
Mn2O3 (s)	kg/hr	0	0	0	0	0	0	0	0	0	1450	34390	84764	0	0
C9H12	kg/hr	3	12	0	0	3	0	0	0	0	30	30	30	0	0
C8H10	kg/hr	153	295	0	10	142	0	0	1	9	4	718	718	0	1
C12H12	kg/hr	0	1	0	0	0	0	0	0	0	225	225	225	0	0
C11H12	kg/hr	0	3	0	0	0	0	0	0	0	0	225	225	0	0
Volume Flow (bbl./day)	**bbl/day**		129			201				64					25

	Units	AIR-1	AIR-2	BT1	BT2	COX	FLUE-GAS	KO	LIQ	ORG	ORGANIC	RGEN-CAT	S
Temperature	C	25.0	514.2	**258.5**	**175.4**	30.0	120.0	25.0	-15.0	-15.0	75.0	700.0	30.0
Pressure	bar	1	1	**10**	**10**	20	1	1	20	20	10	1	20
Molar Vapor Fraction		1.0	1.0	**0.0**	**0.0**	1.0	1.0	0.0	0.0	0.0	0.0	0.0	1.0
Mass Density	kg/cum	1.2	0.4	**693.2**	**698.2**	8.8	0.9	961.5	998.6	879.7	806.1	2897.9	12.6
Average MW		28.9	28.9	**111.8**	**76.3**	11.2	28.1	118.8	18.0	71.4	92.9	86.9	15.6
Mass Flows	**kg. /hr**	44257	44257	**2611**	**1468**	5485	35778	1578	1	135	4137	104324	27909
CH4		0	0	**0**	**0**	0	0	0	0	1	11	0	18045
H2		0	0	**0**	**0**	767	0	0	0	0	0	0	853
CO		0	0	**0**	**0**	283	0	0	0	0	0	0	314
CO2		0	0	**0**	**0**	4435	0	1	0	2	17	0	4928
C(s)		0	0	**0**	**0**	0	112	0	0	0	0	0	0
H2O		0	0	**0**	**11**	0	0	3	1	0	11	0	2
C2H6		0	0	**0**	**0**	0	0	0	0	2	12	0	2440
C2H4		0	0	**0**	**0**	0	0	0	0	0	1	0	375
C3H6		0	0	**0**	**0**	0	0	0	0	3	17	0	811
C6H6		0	0	**1**	**1457**	0	0	86	0	120	1459	0	139
C7H8		0	0	**747**	**0**	0	0	123	0	6	747	0	2
C10H18		0	0	**666**	**0**	0	0	634	0	0	666	0	0
N2		33949	33949	**0**	**0**	0	33949	0	0	0	0	0	0
O2		10308	10308	**0**	**0**	0	1718	0	0	0	0	0	0
MnO2 (s)		0	0	**0**	**0**	0	0	0	0	0	0	104324	0
Mn2O3 (s)		0	0	**0**	**0**	0	0	0	0	0	0	0	0
C9H12		0	0	**30**	**0**	0	0	15	0	0	30	0	0
C8H10		0	0	**718**	**0**	0	0	270	0	0	718	0	0
C12H12		0	0	**225**	**0**	0	0	224	0	0	225	0	0
C11H12		0	0	**225**	**0**	0	0	222	0	0	225	0	0
Volume Flow (bbl./day)				**568**	**317**			248		23	775	5434	

	Units	S-1	S-2	S-3	S-4	S-5	S-6	S-7	S-8	S-9	S-10	S-11	S-12	S-13	S-14
Temperature	C	700.0	700.0	700.0	25.0	700.0	26.8	48.5	25.0	93.5	10.0	7.0	5.0	3.0	-50.0
Pressure	bar	1	1	1	1	1	120	1	1	2	2	8	20	40	60
Molar Vapor Fraction		0.5	0.5	1.0	1.0	1.0	0.0	0.9	0.8	1.0	1.0	1.0	1.0	1.0	1.0
Mass Density	kg/cum	1.4	1.4	0.3	0.7	0.2	992.2	0.7	0.8	1.1	1.4	5.5	14.0	28.9	63.1
Average MW		56.6	56.6	28.1	16.8	17.6	18.0	17.6	17.6	16.8	16.4	15.9	15.7	15.7	15.7
Mass Flows	**kmol/hr**	140103	140103	35778	30688	37881	28842	37881	37881	30688	29778	28562	28185	28045	28045
CH4		0	0	0	18055	18055	0	18055	18055	18055	18054	18051	18048	18046	18046
H2		0	0	0	853	853	0	853	853	853	853	853	853	853	853
CO		0	0	0	314	314	0	314	314	314	314	314	314	314	314
CO2		0	0	0	4944	4945	0	4945	4945	4944	4943	4938	4934	4930	4930
C(s)		112	112	112	0	0	0	0	0	0	0	0	0	0	0
H2O		0	0	0	229	5848	28842	5848	5848	229	71	15	6	4	4
C2H6		0	0	0	2452	2452	0	2452	2452	2452	2451	2447	2444	2442	2442
C2H4		0	0	0	376	376	0	376	376	376	376	376	375	375	375
C3H6		0	0	0	828	828	0	828	828	828	827	821	817	814	814
C6H6		0	0	0	1513	1598	0	1598	1598	1513	1328	656	372	259	259
C7H8		0	0	0	626	748	0	748	748	626	403	81	21	8	8
C10H18		0	0	0	31	666	0	666	666	31	0	0	0	0	0
N2		33949	33949	33949	0	0	0	0	0	0	0	0	0	0	0
O2		1718	1718	1718	0	0	0	0	0	0	0	0	0	0	0
MnO2 (s)		104324	104324	0	0	0	0	0	0	0	0	0	0	0	0
Mn2O3 (s)		0	0	0	0	0	0	0	0	0	0	0	0	0	0
C9H12		0	0	0	15	30	0	30	30	15	3	0	0	0	0
C8H10		0	0	0	448	718	0	718	718	448	153	10	1	0	0
C12H12		0	0	0	1	225	0	225	225	1	0	0	0	0	0
C11H12		0	0	0	3	225	0	225	225	3	0	0	0	0	0

	Units	S-15	S-17	SHC-FEED	SPENTCAT	STEAM	TP1	TP2	W	WATER
Temperature	C	-15.0	13.2	700.0	700.0	324.6	153.0	-213.7	25.0	25.0
Pressure	bar	20	10	1	1	120	7	7	1	1
Molar Vapor Fraction		1.0	0.0	0.0	0.0	1.0	1.0	0.0	0.0	0.0
Mass Density	kg/cum	15.1	901.8	2897.9	4806.1	64.1	15.9	783.0	997.2	994.0
Average MW		15.6	92.9	86.9	142.5	18.0	72.1	30.3	18.0	18.0
Mass Flows	**kmol/hr**	27909	4137	104324	95846	28842	1526	58	5615	28842
CH4		18045	11	0	0	0	11	11	0	0
H2		853	0	0	0	0	0	0	0	0
CO		314	0	0	0	0	0	0	0	0
CO2		4928	17	0	0	0	17	17	0	0
C(s)		0	0	0	112	0	0	0	0	0
H2O		2	11	0	0	28842	11	0	5615	28842
C2H6		2440	12	0	0	0	12	12	0	0
C2H4		375	1	0	0	0	1	1	0	0
C3H6		811	17	0	0	0	17	17	0	0
C6H6		139	1459	0	0	0	1457	0	0	0
C7H8		2	747	0	0	0	0	0	0	0
C10H18		0	666	0	0	0	0	0	0	0
N2		0	0	0	0	0	0	0	0	0
O2		0	0	0	0	0	0	0	0	0
MnO2 (s)		0	0	104324	10970	0	0	0	0	0
Mn2O3 (s)		0	0	0	84764	0	0	0	0	0
C9H12		0	30	0	0	0	0	0	0	0
C8H10		0	718	0	0	0	0	0	0	0
C12H12		0	225	0	0	0	0	0	0	0
C11H12		0	225	0	0	0	0	0	0	0
Volume Flow (bbl./day)			692	5434	3010			11	850	4380

Conclusion

The project goals were met successfully i.e., 1) the development, characterization, and testing of the redox SHC and OCM materials were successful in terms of their redox performance and methane activity 2) the development, characterization and regeneration study of the zeolite catalysts were conducted, and proven effective convert the hydrocarbons into aromatics; 3) the OCM+DHA catalyst strategy was shown to be stable over long periods at 105-h of operation with ~15% aromatic yield with the developed a new regeneration method although the incompatibility of SHC+DHA; 4) TEA models were successfully conducted to evaluate the economic benefits of liquefaction of methane into the aromatics with the OCM+DHA strategy. For further scale-up of the reaction system, it is recommended that the catalysts to be further optimized on sintering and water-resistance.

Peer-reviewed publications

Baitang Jin, Ibrahim Sultan, Xin Li, Ashley Caiola, Bar Mosevitzky Lis, Isreal E. Wachs, John Hu, Fanxing Li, Natural gas liquefaction into aromatics via the integrated chemical looping oxidative coupling of methane and dehydroaromatization reactions. (In progress)

Methods

Catalyst preparation

SHC Redox Catalyst preparation

Take the Na_2WO_4-promoted $CaMnO_3$ as an example. Perovskite-structured $CaMnO_3$ was synthesized using a SSR method. Stoichiometric amounts of powdered $CaCO_3$ (Noah) and MnO_2 (Materion) were physically blended in a ceramic jar and mixed for 24 h at 250 rpm in a planetary ball mill. The powder mixture was heated up to 1200 °C under air flow at 5 °C min^{-1} in a tube furnace and calcined for 12 h. In addition to the base $CaMnO_3$ redox catalyst, Na_2WO_4-promoted $CaMnO_3$ ($Na_2WO_4/CaMnO_3$) was prepared via wet impregnation. Sodium tungstate dihydrate ($Na_2WO4{\cdot}2H_2O$, Sigma-Aldrich) was dissolved in a small amount of water and added dropwise to the as-prepared $CaMnO_3$ sample. The resulting wet powder was alternately hand-stirred and dried at 90 °C until water had evaporated, then kept at 90 °C overnight. Finally, the $Na_2WO_4/CaMnO_3$ sample was heated at 5 °C min^{-1} to 900 °C and calcined for 8 h in a muffle furnace.

OCM catalyst preparation

For synthesis of $LaPrO_3$, 21.651 g $La(NO_3)_3{\cdot}6H_2O$ (Sigma-Aldrich) and 21.751 g $Pr(NO_3)_3{\cdot}6H_2O$ (Sigma-Aldrich) were dissolved in 200 mL of deionized water and stirred for 30 min. Citric acid (99.5%, Sigma-Aldrich) was then added into the solution at a molar ratio of 3:1 to metal ions (La^{3+} and Pr^{3+}). The solution was kept stirring at 500 rpm for 30 min. Afterwards, ethylene glycol (99.8%, Sigma-Aldrich) in a molar ratio of 2:1 to citric acid was introduced to the mixture to promote gel formation. The solution was heated to 80 ºC with continuous stirring until a viscous gel formed, then the beaker was placed in an oven for drying overnight at 130 ºC. The dried precursor was first pre-treated in a muffle furnace at 450 ºC for 1 h to burn off nitrates, and then calcined in a tube furnace at 950 ºC for 10 h under an airflow at of approximately 100 mL/min. 5 wt. % Li_2CO_3 were loaded the resultant of $LaPrO_3$ using the wet impregnation method. After being stirred for 1 h, it was kept overnight at 80 ºC in an oven. Finally, the promoted samples, namely $LaPrO_3$@ Li_2CO_3. $LaPrO_3$@ Li_2CO_3 were calcined at 800 ºC for 2 h. All catalysts were ground and sieved into the size range of 250-400 μm for reaction testing.

Zeolite catalyst with the solid-state crystallization method

Solid-state crystallization synthesis begins by mixing tetrapropyl ammonium hydroxide (TPAOH, 1 M in H_2O), sodium aluminate ($NaAlO_2$), tetraethylorthosilicate (TEOS), and water with a particular molar ratio of 0.25 TPAOH: 0.03 Al_2O_3: 1 SiO_2: 80 H_2O. The water was added first to the Teflon insert of the autoclave and a stir bar was dropped in to begin stirring on a hot plate at room temperature. The TPAOH and the $NaAlO_2$ were dissolved in the water while stirring continuously. Lastly, TEOS was added slowly dropwise under the strong agitation of the stirring. The solution was kept stirring for 4 hours before being placed in an oven at 80°C for 12 hours. The clear solution obtained was dried and the dry gel collected was ground into a powder. The dry powder aluminosilicate nanogels were then transferred into the Teflon-lined autoclave for crystallization in the oven at 160°C for 24 hours. After crystallization, the powder was washed using deionized water and then dried at 120°C for 12 hours. Finally, the powder was calcined in a muffle furnace and slowly heated to 550°C and held for 6 hours.

Zeolite catalyst with the conventional hydrothermal method

Tetrapropyl ammonium hydroxide (TPAOH, 1 M in H_2O), sodium aluminate ($NaAlO_2$), tetraethylorthosilicate (TEOS), and water, were used as the precursors for the conventional hydrothermal synthesis with ratio of 0.25 TPAOH: 0.03 Al_2O_3: 1 SiO_2: 40 H_2O. The solution was also stirred for 4 hours until being placed in the oven at 160°C for 4 days (96 hours). Once crystallization was complete, the precipitate was separated from the liquid using a centrifuge (5,000 rpm for 5 min) and washed with deionized water. The precipitate was then dried in an oven at 120°C for 12 hours. Finally, the powder was calcined in a muffle furnace and slowly heated to 550°C and held for 6 hours. Both methods considered here are preformed over the course of 5-7 days. During the optimization of the procedure, the synthesized zeolites were characterized using X-ray diffraction (XRD) to distinguish if the product had the characteristic peaks of ZSM-5. The first few attempts showed poor intensity of the unique peaks, so the crystallization step for each method was adjusted in both temperature and time. The final procedures were as stated above; each showed good intensity in the XRD spectrum and clearly showed the characteristic peaks of ZSM-5, seen below in Figure 20. After the synthesis methods showed satisfactory XRD patterns and intensity, a surface area analysis was completed on each zeolite produced. Each of the synthesis methods was designed to produce ZSM-5 zeolite with a silica/alumina ratio (SAR) of approximately 33.

Zeolite catalyst with the microwave method

Tetrapropyl ammonium hydroxide (TPAOH, 1 M in H_2O), sodium aluminate ($NaAlO_2$), tetraethylorthosilicate (TEOS), and water, were used as the precursors. The precursor ratio of 0.25 TPAOH: 0.03 Al_2O_3: 1 SiO_2: 40 H_2O was used for the synthesis of these zeolites with a SAR of 33. The solutions were also stirred for 4 hours prior to being loaded into the reaction vessels.

The synthesis was conducted in the new CEM MW unit at 160- 200°C for 30~ 90 mins. Solutions were stirred for 4 hours and placed into two vessels with small stir bars which stir the solution while in the CEM unit. The CEM was set to ramp for 30 mins to the reaction temperature while followed by a hold step for either 30, 60, or 90 mins. Following the hold step the reactions were allowed to cool and depressurize within the CEM until the next day. Once the vessels were cooled enough the precipitate and the solution were collected, separated, washed, and dried. A centrifuge was used to separate the precipitate out of the solution. The samples were centrifuged three times for 10 minutes and 8000 rpm, pouring off the liquid each time and washing with deionized water between each centrifuge. Following the separation and washing the precipitate was dries in an oven at 100°C overnight. Finally, the powder was calcined in a muffle furnace and slowly heated to 550°C and held for 6 hours.

HGaAlMFI Zeolite catalyst with conventional hydrothermal method

To a solution of 2.55 g TPAOH (40 wt%), 0.05 g NaOH (s), and 7.07 g DI water was added 2.50 g TEOS, 0.25 g sodium aluminate, and 0.50 g gallium nitrate. The mixture was aged at room temperature for 24 h under continuous stirring. The growth solution was then placed in a Teflon-lined stainless steel acid digestion bomb (Parr Instruments) and heated at 170°C and autogenous pressure in a oven. The autoclave was removed from the oven after 3 days and immediately cooled to room temperature by quenching. The solid was isolated from the supernatant by three cycles of centrifugation and washing using a high-speed centrifuge. The solid product was then dried at room temperature in air. The sample was calcined in flowing dried air (100 ml min^{-1}) at 550°C using heating and cooling rates of 1 °C min^{-1} for a total of 5 h to remove occluded organics. Ion exchange for catalyst preparation was performed three times using a 1 M NH_4NO_3 solution containing 2 wt% of calcined zeolite sample. This solution was heated at 80°C under continuous

stirring for 2 h. The exchanged samples were dried and calcined in flowing dried air (100 ml min^{-1}) at 550°C.

HGaAlMFI Zeolite catalyst with the microwave method

To a solution of 2.55 g TPAOH (40 wt%), 0.05 g NaOH (s), and 7.07 g DI water was added 2.50 g TEOS, 0.25 g sodium aluminate, and 0.50 g gallium nitrate. The synthesis temperature was increased to 220°C and only 30 mins of synthesis time in the microwave equipment. This decrease in synthesis time increases the product efficacy of the synthesis because from 2 vessels, same solution prep, the microwave synthesized ~8 grams of the HGaAlMFI catalyst in less time than conventionally. The solid was isolated from the supernatant by three cycles of centrifugation and washing using a high-speed centrifuge. The solid product was then dried at room temperature in air. The sample was calcined in flowing dried air (100 ml min^{-1}) at 550°C using heating and cooling rates of 1 °C min^{-1} for a total of 5 h to remove occluded organics.

Catalyst test

OCM reaction

Reactivity tests were conducted in a fixed bed quartz U-tube reactor with ID of 1/8 inches or 3.18 mm. Approximately 2 g of catalyst was loaded at the bottom of the U-tube reactor with quartz wool placed on both sides of the reactor to keep the catalysts in place. Typically, the OCM reaction was conducted at 700 °C, a mixture of methane (20–100%, balance Ar) was injected into the reactor for 1-5 min. After the OCM step, Ar was introduced to purge the reactor for some min and then 10% oxygen (25 mL/min, balance Ar) was introduced for the oxidation step for 5 min. A gas bag was used to collect all the gas product over the entire OCM step. The obtained gaseous products collected were detected by gas chromatography (Agilent 7890 B). The catalyst OCM activity are calculated based on the average products across the OCM step obtained in the gas bag.

DHA reaction

Reactivity tests for DHA were conducted in a fixed bed quartz U-tube reactor with ID of 1/8 inches or 3.18 mm. 0.1-1 g of catalyst was loaded at the bottom of the U-tube reactor with quartz wool placed on both sides of the reactor to keep the catalysts in place. The reactant gas CH_4, C_2H_4, or C_2H_6 enters the gas reaction with its concentration at 10-100% with Ar balance. Typically, the

DHA reaction was conducted at 400-700 °C. The gas sample and liquid sample are collected every 5-15 minutes and Ar is used to flush the system during the sample collection. A gas bag was used to collect all the gas product. The obtained gaseous products collected were detected by gas chromatography (Agilent 7890 B). The liquid product undergoes a cold trap with dodecane with outside iced water. The dodecane containing the liquid product is analyzed by the gas chromatography (Agilent 7890 A).

OCM+DHA reaction

Reactivity tests for OCM+DHA were conducted in two fixed bed quartz U-tube reactor with ID of 1/8 inches or 3.18 mm. 2g OCM catalyst was loaded at the bottom of the OCM U-tube reactor and 0.1g DHA catalyst was loaded at the bottom of the DHA U-tube reactor with quartz wool placed on both sides of the reactor to keep the catalysts in place. The reactant gas CH_4 enters the gas reaction with its concentration at 80% with Ar balance at 25 mL/min. Typically, the OCM reactor was at 700-725 °C and the DHA reactor was conducted at 500-600 °C. During the flushing, 25mL/min Ar was used to flush to reactor system. During the regeneration, 20vol% O_2/80vol%Ar was used for OCM catalyst regeneration and 20vol% H_2/80vol%Ar was used for DHA catalyst regeneration at 25mL/min. The gas sample and liquid sample are collected every cycle and Ar is used to flush the system during the sample collection. A gas bag was used to collect all the gas product. The obtained gaseous products collected were detected by gas chromatography (Agilent 7890 B). The liquid product undergoes a cold trap with dodecane with outside iced water. The dodecane containing the liquid product is analyzed by the gas chromatography (Agilent 7890 A).

References

[1] R.B. Dudek, Y. Gao, J. Zhang, F. Li, Manganese‐containing redox catalysts for selective hydrogen combustion under a cyclic redox scheme, AICHE journal, 64 (2018) 3141-3150.
[2] S. Yusuf, L. Neal, Z. Bao, Z. Wu, F. Li, Effects of sodium and tungsten promoters on Mg6MnO8-based core–shell redox catalysts for chemical looping—Oxidative dehydrogenation of ethane, ACS Catalysis, 9 (2019) 3174-3186.
[3] https://tradingeconomics.com/commodity/heating-oil. Accessed on July 28th, 2019. .
[4] J. Gao, Y. Zheng, G.B. Fitzgerald, J. De Joannis, Y. Tang, I.E. Wachs, S.G. Podkolzin, Structure of Mo_2C_x and Mo_4C_x molybdenum carbide nanoparticles and their anchoring sites on ZSM-5 zeolites, The Journal of Physical Chemistry C, 118 (2014) 4670-4679.
[5] S.H. Morejudo, R. Zanón, S. Escolástico, I. Yuste-Tirados, H. Malerød-Fjeld, P.K. Vestre, W.G. Coors, A. Martínez, T. Norby, J.M. Serra, Direct conversion of methane to aromatics in a catalytic co-ionic membrane reactor, Science, 353 (2016) 563-566.
[6] Y. Gao, L.M. Neal, F. Li, Li-Promoted $La_xSr_{2-x}FeO_{4-\delta}$ Core–Shell Redox Catalysts for Oxidative Dehydrogenation of Ethane under a Cyclic Redox Scheme, ACS Catalysis, 6 (2016) 7293-7302.
[7] B. Robinson, X. Bai, A. Samanta, V. Abdelsayed, D. Shekhawat, J. Hu, Stability of Fe-and Zn-promoted Mo/ZSM-5 catalysts for ethane dehydroaromatization in cyclic operation mode, Energy & Fuels, 32 (2018) 7810-7819.
[8] X. Guo, G. Fang, G. Li, H. Ma, H. Fan, L. Yu, C. Ma, X. Wu, D. Deng, M. Wei, Direct, nonoxidative conversion of methane to ethylene, aromatics, and hydrogen, science, 344 (2014) 616-619.
[9] X. Bai, A. Samanta, B. Robinson, L. Li, J. Hu, Deactivation mechanism and regeneration study of Ga–Pt promoted HZSM-5 catalyst in ethane dehydroaromatization, Industrial & Engineering Chemistry Research, 57 (2018) 4505-4513.
[10] R.B. Dudek, X. Tian, M. Blivin, L.M. Neal, H. Zhao, F. Li, Perovskite oxides for redox oxidative cracking of n-hexane under a cyclic redox scheme, Applied Catalysis B: Environmental, 246 (2019) 30-40.
[11] L.M. Neal, V.P. Haribal, F. Li, Intensified ethylene production via chemical looping through an exergetically efficient redox scheme, Iscience, 19 (2019) 894-904.
[12] Y. Tian, R.B. Dudek, P.R. Westmoreland, F. Li, Effect of sodium tungstate promoter on the reduction kinetics of $CaMn_{0.9}Fe_{0.1}O_3$ for chemical looping–oxidative dehydrogenation of ethane, Chemical Engineering Journal, 398 (2020) 125583.
[13] Y. Zhou, H. Thirumalai, S.K. Smith, K.H. Whitmire, J. Liu, A.I. Frenkel, L.C. Grabow, J.D. Rimer, Ethylene dehydroaromatization over Ga‐ZSM‐5 catalysts: nature and role of gallium speciation, Angewandte Chemie International Edition, 59 (2020) 19592-19601.
[14] C. Wang, X. Zhao, M. Hu, G. Qi, Q. Wang, S. Li, J. Xu, F. Deng, Unraveling Hydrocarbon Pool Boosted Propane Aromatization on Gallium/ZSM-5 Zeolite by Solid-State Nuclear Magnetic Resonance Spectroscopy, Angewandte Chemie International Edition, 60 (2021) 23630-23634.
[15] A. Samanta, X. Bai, B. Robinson, H. Chen, J. Hu, Conversion of Light Alkane to Value-Added Chemicals over ZSM-5/Metal Promoted Catalysts, Industrial & Engineering Chemistry Research, 56 (2017) 11006-11012.
[16] Y. Zhang, H. Jiang, A novel route to improve methane aromatization by using a simple composite catalyst, Chem. Commun., 54 (2018) 10343-10346.

[17] K. Huang, C.T. Maravelias, Synthesis and analysis of nonoxidative methane aromatization strategies, Energy Technology, 8 (2020) 1900650.
[18] QGESS: cost estimation methodology for NETL assessments of power plant performance, National Energy Technology Laboratory, USDOE, (2019).
[19] J.O. Maloney, Perry Chemical Engineers Handbook, The McGraw-Hill Companies, Inc2008.
[20] G.D. Ulrich, A guide to chemical engineering process design and economics, Wiley New York1984.
[21] H.Y. Kim, H.M. Lee, J.-N. Park, Bifunctional mechanism of CO_2 methanation on Pd-MgO/SiO_2 catalyst: independent roles of MgO and Pd on CO_2 methanation, J. Phys. Chem. C, 114 (2010) 7128-7131.